Small-signal Analysis of Active Loads and Large-signal Analysis of Faults in Inverter Interfaced Microgrid Applications

Nathaniel Bottrell

M.Eng(Hons)

Submitted in part fulfilment of the requirements for the degree of

Doctor of Philosophy in Electrical Engineering of

Imperial College London and the Diploma of Imperial College London

Control and Power Group

Department of Electrical and Electronic Engineering

Imperial College London

1st March 2014

Abstract

Rectifiers and voltage regulators that have characteristics of constant power loads may form a significant percentage of a microgrid's total loads. The real part of the input impedance of a constant power load is negative and it may have control loop dynamics in a similar frequency range to the inverters that are supplying the microgrid. This thesis examines the interactions between an active constant power load and a microgrid for the impact on stability. Participation analysis of the eigenvalues that result from the model of the combined microgrid and active load identified that the low-frequency modes are associated with the voltage controller of the active rectifier and the droop-controllers of the inverters. The analysis also revealed that when the active load dc-voltage controller is designed with large gains, the voltage controller of the inverter becomes unstable but the low frequency modes associated with the droop controller of the inverter remain stable.

The transient stability of a microgrid may require that the inverter-interfaced generation remain connected during a fault and return to normal power export once a fault is cleared. For an inverter to supply fault current, the controller of the inverter must current-limit the output and the fault strategy chosen must ensure that the current and voltage limiter do not latch-up and that the controller integrators do not wind-up. This thesis analyses different limiting and reset strategies and concluded that that it is not possible to successfully reset a limiter when using a reset signal from a closed-loop controller within the inverter. In a system where there are cascaded limiters, successful operation is obtained when the inner limit is a saturation limiter and the output limiter is a set-reset limiter.

It was found that the transient stability of an inverter interfaced microgrid using a droop control algorithm is dependent on the current limiter and inductance of the network.

Acknowledgements

There are many people who have made my time at Imperial a unique experience and one that I will certainly never forget. I have enjoyed many years which made me the person that I am today.

I would first like to thank my PhD supervisor, Professor Timothy C. Green, for his patience, understanding, flexibility and most important, his guidance. A special thanks goes to Dr. Milan Prodanović for providing much support during my first year, teaching me how to conduct experimental work and for participating in lengthy discussions which allowed a greater understanding of the subject. Thank you to Dr Richard Silversides for proving support with the hardware and software of the laboratory.

If it was not for all the staff and students who I met during the many year I participated in Imperial College Union, my time at Imperial would not have been as rich and fulfilled. Notably, thank you to Phil Power, Rebecca Coxhead, Alex McKee, Kris Rajamanikam, Joe Cooper, Paul Beaumont, Ashley Brown and all who I met through the Imperial College Union Trustee Board. I would like to thank the members of the RCC, Fellwanderers and ICU Cinema for providing me with the opportunity to chair committees and lead societies. A defining moment during my PhD was the summer of 2011 where I spent five weeks on an expedition in Svalbard. For this I would like to thank my supervisor for allowing me to take this time out of my PhD and most importantly Dr. Lorraine Craig and the Exploration Board for providing funding and extensive support. If it was not for our expedition group, the expedition may not have been a success. I would like to thank Alex Kendall, Sietse Braakman, Heather Jones, Andrew Elliott and Ally Cott for enabling the expedition to be the adventure that it was.

Thank you to all that I have worked with in the Control and Power Research Group and Smart Energy Laboratory for providing an excellent working environment. I have met many great people and must mention Phil, Jeff, Cees, Dan, Mark, Paul, Geraint, Caitríona and Alwyn from the laboratory and Thulasi, Kameswarie, Stefanie, Adrià and Jaehwa from the office.

During my PhD I have lived in many houses and had the opportunity to share PhD life with Chris, Rachel, Katharina, Judith, Anthony, Anton and Florian. Thank you for all the support during the PhD highs and lows.

I would like to acknowledge the financial support provided by the Power Networks Research Academy (PNRA) under EPSRC grant EP/F037686/1 and the technical suggestions provided by the industrial contacts within the PNRA.

To all my friends and family (Mum, Dad, Heidi, Dominic, Auntie Elaine and Uncle Joe) and especially my partner, Charlotte Staples. Thank you for supporting me throughout my PhD.

Contents

Declaration of Originality

I, Nathaniel Bottrell, confirm that all work presented in this thesis is my own and all work undertaken by other authors is appropriately referenced within the text. All of my work is original and has not been published before by a different author. All work that has been published by myself is clearly indicated within the introduction of the relevant chapter.

Copyright Declaration

List of Figures

List of Tables

List of Symbols

A	State matrix of a linear state-space system (any subscript will be defined in the thesis)
B	Input matrix of a linear state-space system (any subscript will be defined in the thesis)
C	Output matrix of a linear state-space system (any subscript will be defined in the thesis)
C_{dc}	dc-bus Capacitor [Farad (F)]
C_f	Filter capacitor [F]
D	Feed-forward matrix of a linear state-space system (any subscript will be defined in the thesis)
DQ	Direct and quadrature axis of the common reference frame (generally used as subscripts)
dq	Direct and quadrature axis of the local reference frame (generally used as subscripts)
f_{DQ}	Frequency of the common dq reference frame [Hz]
f_{dq}	Frequency of the local dq reference frame [Hz]
i_{conv}	Current loop from the dc-side of the inverter bridge to the DC capacitor [A]
i_{dc}	Current loop from the DC capacitor to the DC load [A]
$i_{g,abc}$	Current from the LCL Capacitor to the grid (inverter export current) in abc coordinates [A]
$i_{g,dq}$	Current from the LCL Capacitor to the grid in dq coordinates [A]
I_s	RMS current at the sending end of a transmission line [A]
$i_{l,abc}$	Current from the ac-side of the inverter to the LCL capacitor (inverter filter current) in abc coordinates [A]
$i^*_{l,abc}$	Reference current from the ac-side of the inverter to the LCL capacitor in abc coordinates [A]
$i_{l,dq}$	Current from the ac-side of the inverter to the LCL capacitor in dq coordinates [A]
$i^*_{l,dq}$	Reference current from the ac-side of the inverter to the LCL capacitor in dq coordinates [A]

K_{ic}	Integral gain of the current controller
K_{pc}	Proportional gain of the current controller
K_{iv}	Integral gain of the voltage controller
K_{pv}	Proportional gain of the voltage controller
L	An arbitrary inductance [Henry (H)]
L_c	Coupling inductor [H]
L_f	Filter inductance [H]
P_S	Real power at the sending end of a transmission line [Watt (W)]
Q_S	Reactive power at the sending end of a transmission line [Volt Ampere Reactive (VAr)]
R_{load}	Resistance of the DC load [Ohm (Ω)]
r_c	Resistance of the coupling inductor [Ω]
r_f	Resistance of the filter inductance [Ω]
T_R	Reference frame transformation matrix
$v_{c,abc}$	Voltage of the capacitor in the LCL filter in abc coordinates [Volts (V)]
$v_{c,dq}$	Voltage of the capacitor in the LCL filter in dq coordinates [V]
v_{dc}	dc-bus voltage and voltage of the DC capacitor [V]
v_{dc}^*	Reference voltage of the dc-bus [V]
$v_{g,abc}$	Grid voltage (the voltage at the output of the inverter) in abc coordinates [V]
$v_{g,dq}$	Grid voltage in dq coordinates [V]
$v_{i,abc}$	Voltage at the ac-side of inverter bridge (and input to the LCL filter) in abc coordinates [V]
$v_{i,abc}^*$	Reference voltage at the ac-side of inverter bridge (and input to the LCL filter) in abc coordinates [V]
$v_{i,dq}$	Voltage at the ac-side of inverter bridge in dq coordinates [V]
$v_{i,dq}^*$	Reference voltage at the ac-side of inverter bridge in dq coordinates [V]
V_R	RMS Voltage at the receiving end of a transmission line [V]
V_S	RMS Voltage at the sending end of a transmission line [V]
X	An arbitrary reactance [Ω]
Δ	Denotes small-signal when the prefix of any variable
δ	The angle between two arbitrary reference frames
δ_i	The angle between the common reference frame the the ith local reference frame
ω	Arbitrary frequency [Radian (rad)/Second (s)]
ω_0	Initial frequency [rad/s]
ω_{com}	Common reference frame frequency [rad/s]
ω_n	Nominal frequency [rad/s]

List of Abbreviations

Ω Ohm.

A Ampere.

AC Alternating Current.

D/A Digital-to-Analogue.

DC Direct Current.

DFIG Doubly Fed Induction Machine.

DG Distributed Generation.

DNO Distribution Network Operator.

DQ Direct Quadrature.

EMS Energy Management System.

F Farad.

H Henry.

Hz Hertz.

IEEE Institute of Electrical and Electronic Engineers.

kV Kilovolts.

kVA Kilovolt Ampere.

kVAr Kilovolt Ampere Reactive.

kW Kilowatt.

LCL Inductor-Capacitor-Inductor.

LoM Loss of Mains.

MW Megawatt.

PCC Point of Common Coupling.

PI Proportional Integral.

PLL Phase Locked Loop.

PQ Real and Reactive Power.

PR Proportional Resonate.

PV Photovoltaic.

rad Radian.

RMS Root Mean Square.

s Second.

UK United Kingdom.

UPS Uninterruptible Power Supply.

V Volts.

VAr Volt Ampere Reactive.

Vf Voltage and Frequency.

W Watt.

Chapter 1

Introduction

Reducing CO_2 emissions is a target for many countries and the UK in particular is committed to reducing greenhouse gas emissions by 80 % by 2050 [1]. To achieve this, the UK aims to move to a low-carbon economy [2]. This means less reliance on fossil fuels, more renewable generation and reducing demand for energy from industry, business and the public sector [3].

Renewable energy as defined by the Energy Saving Trust [4] is energy from any source that is naturally replenished in a short period of time. This includes energy from wind, solar, hydro, tidal, geothermal or biomass and does not include energy or waste products from fossil fuels.

Electricity from fossil fuels is traditionally generated in large power plants by burning coal, gas or oil in a boiler to generate steam. Steam is then used to rotate large turbines which in turn is used to rotate large synchronous machines. These machines are typically capable of exporting 500 Megawatt (MW) of power. In a synchronous machine, the rotor operates at the same frequency as the stator and the frequency of the generator is controlled using a governor. In Great Britain (as in all of Europe) the nominal frequency is 50 Hz. Generation by synchronous machines is connected to the electrical network without the requirement for any frequency conversion.

Generation by renewable sources may not be 50 Hz and if it is not 50 Hz then the use of a converter is required. Frequency conversion allows the renewable source to interface

with electrical network which is operating at 50 Hz. Wind turbines generate at a frequency which is dependent on the speed of the wind [5]. These sources are either connected by the use of a partial converter topology such as the Doubly Fed Induction Machine (DFIG) or a full converter topology [6]. A full converter converts the rotation of the wind turbine to Direct Current (DC) and then the DC is converted back to the frequency of the electricity network. Solar Photovoltaic (PV) only generates at DC and requires a full-converter to export power [7]. An inverter is typically used as the full-converter to convert DC to Alternating Current (AC) [8].

Renewable sources have a much lower unit energy extraction capacity and a lower energy density than conventional fossil fuel power stations. Renewable sources are often connected to the electricity network at a lower voltage than fossil fuel power stations. Often a large number of renewable sources are required to generate a significant amount of energy. The large number of sources may have their own network which collects the electricity and supplies the power to the electricity network at a bulk supply point [9]. This is typically used for a wind farm. Alternatively, each source is connected individually to the electricity network and the sources are distributed over a large geographic area. This is typically how roof-top solar PV panels are connected and this method of connection has been defined as Distributed Generation (DG).

The amount of renewable generation connected to the electrical network is continually increasing and Figure 1.1 shows the increase from 2010 to the beginning of 2013. Wind and solar PV are increasingly playing an important part of the UK generation mix. The effect of the inverter technology that connects wind and solar PV to the electricity network requires an understand of its operation in both normal operating conditions and abnormal operating conditions. This thesis aims to continue the understanding of inverter-based generation technologies in order to facilitate the continual increase of inverter generation.

1.1 Distributed Generation

Throughout this thesis the term DG will be used. However, in the literature a multitude of terms are used to describe the same concept. DG is also referred to as ‘embedded generation’ (Anglo-American), ‘dispersed generation’ (North American) and ‘decentralised generation’ (Europe &

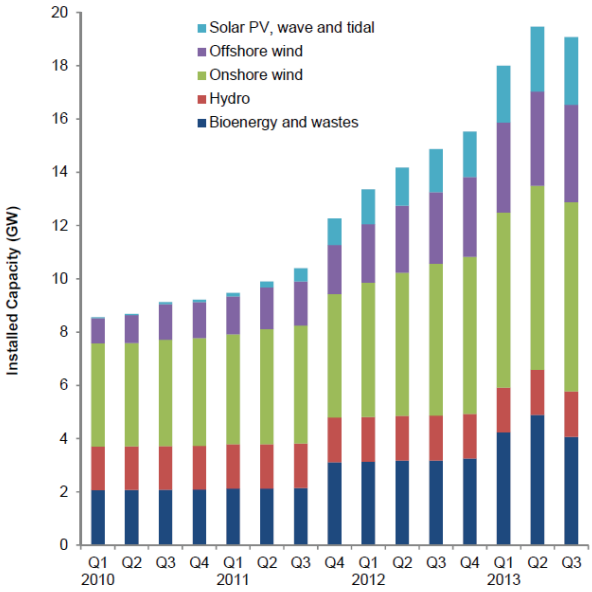

Figure 1.1: The installed renewable generation in the UK electrical network. Data is from the Department of Energy and Climate Change, UK Government. Title of publication is "Energy trends section 6: renewables" and was published on 20 December 2012

Asia). It must be stated that DG is not necessarily from a renewable source and equally renewable generation is not always DG. This section will define distributed generation and discuss the advantages and disadvantages of integrating DG. The next section applies to both renewable and non-renewable DG.

1.1.1 Definition of DG

The exact definition of DG is not clear in the literature and many definitions exist both from a legal and technical point of view. This thesis will use the definition presented in [10] where DG is defined in terms of the point of connection rather than the generation technology, primary energy source, power rating, voltage level, purpose, mode of operation, dispatch, environmental impact or ownership. The definition in [10] is:

> "Distributed generation is an electric power source connected directly to the distribution network or on the customer side of the meter"

Distributed generators are typically not centrally dispatched or centrally planned, and they do not participate in voltage or frequency regulation. The voltage level which a DG will

Category	Power Rating	UK Voltage Level
Micro	1 W – 5 Kilowatt (kW)	400 V
Small	5 kW – 5 MW	400 V – 11 Kilovolts (kV)
Medium	5 MW – 50 MW	11 kV – 33 kV
Large	50 MW – 300 MW	33 kV – 132 kV

Table 1.1: Distributed generation power rating categories

connect to often depends on the maximum power export of the DG. Typical connection voltages are shown in Table 1.1.

1.1.2 DG technologies

Technologies used for DG include internal combustion engines, gas turbines, micro-turbines, PV cells, fuel cells, and wind turbines. The thermal based DG tend to connect to the distribution network using synchronous machines, the same technology as conventional generation. Renewable technologies, namely PV cells and wind turbines, tend not to be natural 50 Hz sources, hence these are commonly interfaced using an inverter [11] [12]. It is well known that inverters have different characteristics to synchronous machines, they have a low tolerance of over-current [13] and a reliance on fast acting control. When inverters are a small percentage of the power export on the network, knowledge of their detailed characteristic is not vital but will become so as penetration increases and security partially rests on that generation. Much is known about synchronous machines connecting to networks, however there is a lack of analysis of inverters from the point of view of power system operation and protection. In particular, there are insufficient tools to allow those calculations that are standard for conventional generation to be extended to inverters. Thus, this work will concentrate on inverter based distributed generation.

1.1.3 Typical DG control algorithms

There are three main control algorithms available for power export. The first method is Voltage and Frequency (Vf) control, the second is Real and Reactive Power (PQ) control, and the third is droop control.

Voltage and frequency control

Voltage and frequency control regulates the output voltage, phase angle and frequency of the inverter [14]. If multiple inverters use voltage and frequency control, a fast communication system is required to ensure all sources stay in-phase with each other. Controlling the voltage magnitude and angle between all sources will control the share of real and reactive power export [15]. If a communication system is not in place then only one source is able to use voltage and frequency control and others would require PQ or droop control to ensure the absence of out-of-phase generation.

Real and reactive power (PQ) control

PQ control is common for small DG; export normally depends on maximum available power. Such a control scheme is described in [16] and [17]. For example, on a windy day an inverter connected to a small turbine would export more than on a calm day. An island with many PQ inverters will require a communication system to curtail generation if demand is low, and curtail load if generation is low. Alternatively a storage system could be used to balance the system. PQ controllers generally use a PLL as in [18] to lock to the system frequency.

Droop control

A droop controller will change the power export based on the system frequency or change the local frequency of the inverter as the power export of the inverter changes. Droop controllers enable autonomous operation of an island [19] [20]. The droop controllers in an inverter based network have the least damping and present small-signal stability issues [20]. When using droop controllers, it is critical that their stability is studied.

1.1.4 Benefits of DG

There is much in the literature about the benefits that DG offers over traditional large power plants that supply power through the transmission and distribution system. The following five

sub-sections will briefly summarise the key advantages that DG offers. The list is not exhaustive and is included to demonstrate that research in DG is important because of the possibility to utilise the benefits that DG presents.

Integrating renewable technologies

Renewable sources have a low energy density and in order to generate a modest amount of power, a large area is required. One solution for integrating more renewable technology is to use DG [21] and connect a large area of small-scale renewable generation to the distribution network. By using renewable sources, the UK is able to provide clean energy, decrease the dependence on oil and natural gas stocks and meet the greenhouse gas emission targets that were set out in the beginning of this chapter [22].

Utilising generation by-products

As stated in the definition of DG, distributed generation is connected close to load centres. Some load centres, namely residential and industrial, will have a heat demand as well as an electricity demand. Technology like micro turbines and biomass engines produce heat as a by-product. This waste heat can be used to supply all or part of the residential and industrial customers heat demand [23] [24].

Generation reliability

A conventional generator may be generating 500 MW of power whereas a DG unit may only be generating 1 MW of power. If the 500 MW generator were to fail, the system would be required to either produce an extra 500 MW of power or shed 500 MW of load in order to maintain the system balance. A loss of a 1 MW is more manageable. Also, if the 500 MW of generation is spread over 500 different small generation units the probability of all 500 small generation units failing is less than the probability of one 500 MW unit failing. To summarise, many generation units present less risk for failure compared to one large generation unit.

Transportation losses

Connecting generation at the lower voltage levels, where the demand is, will reduce the transportation losses. Electricity from a large power station may be transported over long transmission lines and through a number of transformers. Each kilometre of transmission line and each transformer between the generation and the load reduces the efficiency because of resistive and inductive losses. By reducing the amount of generation required to be transported over long transmission networks, the amount of loss is lowered and the efficiency of the network is increased. A study in [25] analyses the reduction of losses from integrating DG.

Reducing feeder capacity

Each feeder of a distribution network has a demand profile that ranges between an average minimum and an average maximum. During peak demand, there is a possibility that DG will reduce the feeder peak [26]. Having the ability to reduce the peak may allow for more generation to be connected to that feeder without having to re-enforce the feeder with a larger transformer or larger cable. To connect more load to a feeder, it may be more economical to introduce DG than to upgrade the section of network that the load is connected to.

1.1.5 Difficulties of DG

Before the benefits of DG are utilised, the issues that DG present to the network must be solved. Work in [27] identifies and reviews the issues that DG will present to the UK grid, these are stability, protection discrimination, islands, Loss of Mains (LoM), power quality impact in protection and generator ride-through.

Stability

The addition of DG into the distribution network presents a number of stability issues. These are small-signal instability, voltage instability and transient instability. Small-signal instability may be caused by the dynamic characteristics of DG, the improper tuning of the controllers [28],

the dynamic characteristics of the loads interacting with the DG units [29] and the parameters of droop controllers [20], if used within the DG design. Voltage instability may be more prevalent when power is exported into a network which has a high resistance to inductance ratio [30]. Voltage limits may be breached in the distribution network when there are a lot of DG on a feeder that are all exporting power. Transient instability may be caused by the inverter loosing synchronism after a fault has occurred. This may happen if a PLL fails to follow the frequency after a frequency disturbance or if a standalone network fails to reach a new steady-state operating point after a fault has been cleared.

Protection discrimination

Protection discrimination is the ability for the protection in a network to detect, and then isolate the faulted section without disconnecting any loads that have a healthy supply. Only the breaker closest to the fault should trip in a correctly discriminated network. If a fault at the end of a feeder causes a breaker which is two breakers away from the fault to trip then the network is not correctly discriminated.

Adding DG to a feeder may cause standard time graded over-current protection to lose protection discrimination and the setting of such a device will require adjustment. The presence of DG on a feeder causes the clearing time of protection devices on the network to increase [31]. If DG causes a protection device to operation that is not the protection device closest to the fault, then protection discrimination is lost. If there is a difference in fault current then there is a margin available for the coordination to remain valid [32].

Fault level contribution from DG

Fault current availability is dependent on the technology of the generator. Synchronous machine generation typically contributes a high fault current whereas inverter-based generation is fault constrained and typically is only able to export twice its nominal current for faults [33] [34]. This causes complications when planing new generator connections and maintaining existing network protection.

The distribution network is often fault constraint and the fault contribution from generation may increase the fault current to beyond safe operating levels. Therefore in some networks, the fault contribution from DG may be required to be very small. To achieve this, DG may be required to trip or export a low current when a fault has been detected.

Generator ride-through

Large generators are required by the grid code to ride through faults. This allows the protection to operate correctly and isolate the fault. Once the fault has been cleared the network may return to normal. Small generators, namely DG, are required to disconnect from a faulted network. In an area with a significant amount of DG, cascaded tripping of DG units may result in local voltage collapse [35]. Therefore, controllers need to be developed to improve the fault ride-though capability of DG that allows them to maintain connection during faults.

Loss of mains

LoM protection will trip the DG when the logic in the protection device has calculated that a LoM event has occurred. The sensitivity of LoM is compromised when the generation closely matches the load and LoM may also cause nuisance trips.

It is acknowledged that LoM is one of the most challenging aspects of integrating DG into the distribution network [36]. As such there has been much research in this topic with many published papers investigating solutions to detect LoM and minimise nuisance trips. Solutions include using rate of change of power [37], using the variation of the voltage magnitude [38], using an elliptical trajectory technique [39], using rate of change of voltage and power factor [40], using rate of change of frequency [41] [42], using a small disturbance in the voltage controller and AC-filter [43], using a measurement of system impedance [44], using frequency oscillations and the damping of these oscillations [45], using communications by power line carrier [46], using active frequency drift [47] and using active and reactive power controllers [48].

Unintentional Islands

Islanding is where a section of grid disconnects from the main network. This can either be intentional, as in the microgrid case, or unintentional. Unintentional islands may be the size of a country, for example, where a major event happens in the transmission network that disconnects England from Scotland. At the distribution network level, one rural feeder can disconnect and leave several houses connected to a DG source that continues to supply power. Islands at the distribution network level have both advantages and disadvantages.

Islands may go unnoticed because a typical DNOs network status knowledge stops at the 11 kV substation, this leaves the 400 V network unmonitored. If an island forms and goes unnoticed to the distribution controller or maintenance engineer, problems may arise:

- The island may exceed the acceptable limits, of voltage tolerance for example, which are specified in the regulations [49].
- The network may have large uncontrollable voltage swings due to the source dynamics, or have poor power quality where the voltage waveform is no longer a pure sinusoidal waveform.
- Islands may be running with un-cleared earth and phase faults present. This may go unnoticed due to low short-circuit capacity or unearthed operation and is potentially very dangerous.
- An attempt may be made to reconnect an unknown island to the distribution network, either by an operator or an auto re-closer, when the two networks are out-of-phase. The existing equipment may not be able to cope with an out-of-phase connection and breakers should only be closed when the phase, frequency and voltage are aligned. Closing two unaligned networks will cause high transient inrush currents. These high currents are an effect of the two parts of the networks attempting to re-synchronise.

Usually, these hazards are restricted by the tripping limits of protective relays (voltage and frequency) implemented at generator sites. Allowing unintentional islands to form may lead to equipment damage or present a danger to human life. These risks are against the

safety obligations set by the distribution contract and hence, in most cases DNOs do not allow islanding. Not allowing islanding requires all DG to disconnect on the detection of loss-of-mains.

Assuming the risks can be mitigated, islanding has advantages. By forming an island after a network event, supplies within the island are maintained which may be critical for some customers. Also, islanding could be allowed in areas where supply reliability is an issue or when maintenance is required. To improve the reliability of supply, planned islanding is being investigated on some rural feeders in Canada [50].

Unintentional islanding presents several difficulties for the Distribution Network Operator (DNO). The DNO must know if an island will occur after a network event and which section of the network will island. If an island occurs and is permitted to run it needs to maintain a stable voltage and frequency, and be able to clear faults.

1.2 Inverter based generation

Inverter based generation is used to connect non 50 Hz sources to the electricity network. Renewable generation typically does not generate electricity at 50 Hz and the use of an inverter is required to export the generated power. As the amount of renewable generation that is integrated into the electricity network increases, the amount of inverters connected to the electricity network is also increasing.

Some examples of inverter-interfaced generation in the distribution network to demonstrate the flexibility of the technology are sources such as PV [51], wind turbines [52], battery storage [53], variable frequency micro-turbines [54] and high frequency flywheels [55]. Sources that generate in DC may be connected directly to the inverter and sources that generate a non 50 Hz AC voltage will use a rectifier to convert the non 50 Hz AC to DC and then the DC is converted to 50 Hz AC.

1.3 Microgrids

A microgrid is a small collection of loads and sources that together act as a single controllable network [56], shown in Figure 1.2. These networks are designed to provide power for small areas,

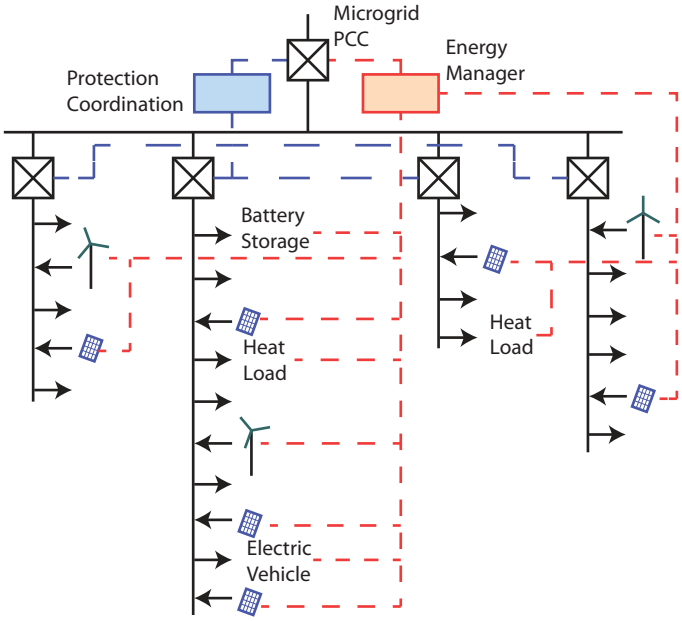

Figure 1.2: An example microgrid

such as an industrial site or small cluster of residential dwellings [57]. The microgrid would connect to the grid at the *of common coupling* (Point of Common Coupling (PCC)). The PCC would decide on the import / export power and whether the microgrid should remain connected to the grid or be operated in stand-alone (island). A feeder with a number of distributed energy resources (DER) is not a microgrid if the DER are connected to only export power and not exercise control over the network.

The concept of the microgrid may increase the reliability of supply to high priority loads by being able to disconnect from the grid. Disconnection would be made in the event of a grid fault or disturbance and would reconnected once the grid fault or disturbance is cleared.

Microgrids are thought to have many advantages over grid power in terms of security, power autonomy and the ability to incorporate distributed generation, including renewable energy [58]. Having many microgrids connected together could form an active distribution network and combine different forms of generation and loads within the distribution voltage level [59].

1.3.1 Inverter Microgrids

There are two methods used to control an inverter-based microgrid. The first is by using communication links between the inverters as demonstrated in [60] and the second is by using controllers that allow the inverters to operate autonomously [20].

If microgrids are to be established, they must be shown to be able to remain within safe operating limits for normal load perturbations and during abnormal fault operation. The operation of a microgrid for load perturbations is investigated using small-signal stability analysis and the operation during faults is investigated using large-signal stability analysis.

1.3.2 Microgrids and Load Models

There has been much work on the small-signal stability of droop-controlled microgrids and this is presented in Chapter 2. In general, the published literature either considers the modelling of such networks or the interactions between the inverters when connected to resistance-inductance loads. However, it has not considered the interactions between the droop controlled inverters and other types of load connected to the microgrid.

It is known that load dynamics interact with generation and influence the stability of the network [61]. Loads affect the system damping; constant impedance loads generally increase damping, whereas constant power loads tend to decrease damping [62]. To understand how a network responds to different generation technologies, in this case DG, the different load dynamics must also be studied. Using only static load models may produce misleading results [63].

There are two types of load model: load models using demand profiles [64] and load models that consider the load dynamics [65]. Both types of modelling are relevant and should be considered when determining network operation. Any change in demand should be matched by a change in generation output. The corresponding generation change could cause a voltage perturbation, which in turn might cause the load current to change. This interdependent relationship will either cause the network to enter a new steady state, enter an oscillatory mode or possibly collapse. Also, the load dynamics could interact with the generation dynamics and

two stable systems may be unstable when connected together. For the two reasons outlined, it is important that the effects of loads within the distribution network are studied.

1.3.3 Microgrids and Faults

The fault response of an inverter is well documented and is discussed in Chapter 2. However, there is a gap in the literature about the transition from exporting current into a fault and then returning to normal operation. This consideration may be extended to the case of a complete microgrid in which there are multiple inverter sources and all are required to ride-through the fault. After the fault has been removed from the network, the droop controllers of the various inverters may exhibit instabilities and prevent the network from recovering and returning to a new steady-state operating point.

1.4 Problem Statement and Thesis Outline

Inverters are a key component in the integration of renewable technologies in the distribution network. One possible mode of operation for inverters integrated into the distribution network is in the form of a microgrid. If the benefits of a microgrid are going to be realised then they must be fully understood under all network operation. Any microgrid operation must maintain stability for both small changes due to normal operation (small-signal) and large changes due to abnormal operation conditions (large-signal). There has been much work on the small-signal stability of inverters with passive loads, however, in a real microgrid there may be a significant amount of active loads.

The focus of this research is split into two sections. The first section investigates the small-signal stability of inverter based microgrids with active-loads. This work builds on existing literature and uses well documented modelling techniques that are discussed in Chapter 2. The key focus of the first section is not the modelling of the microgrid; instead the focus is on the modelling of the active load and the interactions between the microgrid and the active load. The second section investigates the large-signal stability of inverter based microgrids and focuses on the ability of a microgrid to ride-though a fault and for the droop controllers to return to a

post-fault steady-state operating point. Before investigating the large-signal stability, a study is needed of how inverters current-limit and, more importantly, to reset their current limit to ensure correct operation once the fault has been cleared.

Work to be described in this thesis is divided into the following chapters:

- Chapter 2 will discuss the background topics on power systems stability, inverter control and the current limiting of inverters when supplying fault current to faulted networks. Traditional power systems stability will be discussed and then related to inverter based microgrid applications. Existing small-signal and large-signal stability analysis for inverter based microgrids will be presented and discussed. A discussion on inverter control strategies is given to serve as a background for the development of strategies to reset an inverter from current limit.

- Chapter 3 discusses the modelling of active loads and presents a small signal model of an active load for use within a microgrid application. The standalone operation of the active load is discussed and the small-signal stability of the active load is analysed using techniques there are presented in Chapter 2. Conclusions from the small-signal analysis are verified using an experimental system. The model of the active load is connected to a microgrid at two different nodes alternately. The same small-signal techniques that are used for the standalone operation are used for the active load connected to a microgrid. Again, conclusions from the small-signal analysis are verified using an experimental microgrid. All experimental results presented are compared with the results from the small-signal models presented within Chapter 3. The chapter will consolidate the conclusions from each of the small-signal models and compare the active load in standalone with the active load connected to different parts of the microgrid.

- Chapter 4 investigates the resetting of current limiters within inverters. Different strategies for resetting the current limiters are presented and experimentally tested for three-phase and signal-phase faults applied to the output of the inverter. For each strategy, the inverter is operated in a standalone mode and connected to a passive load. Conclusions are drawn to the best method to ensure that the current limit resets once a network disturbance has been cleared and to ensure the fault ride-through of an inverter.

- Chapter 5 uses the knowledge obtained from Chapter 4 and investigates the large-signal stability of inverter-based microgrid networks. A two droop inverter network is analysed in order to understand the operation of the droop-controllers during the transition from supplying fault current to post-fault operation. The interactions between the droop controllers and the current limiters are investigated for different fault durations and different line impedances. Factors that affect the large-signal stability of the microgrid when subject to a fault are discussed and shown through the use of simulations.

- Chapter 6 draws the conclusions from the research presented in this thesis and discusses the contribution of this work to the research community. The chapter finishes with ideas for future work that will build on the results from this research.

Chapter 2

Background

This chapter discusses background information relevant to the research laid out in the subsequent chapters. To introduce the discussion, the classification of power systems stability which is commonly used for traditional generation and transmission systems is explained. Small-signal and large-signal analysis techniques of traditional generation systems are presented for general reference.

The background is narrowed to only consider inverters and inverter networks which is the focus of the thesis. Prior art of the application of small-signal and large-signal analyses to inverters and microgrid networks is discussed. An inverter would not function without a controller and the control algorithms for inverters that are used within this research are presented. If an inverter is to remain connected during a fault event, it must be able to limit the output. Techniques for the limiting of inverters for fault and over load operation is presented and the discussion also includes the limitations of such algorithms.

At the end of the chapter, there is a discussion on the modelling of loads. This is a side topic to background material but is important for Chapter 3 where the small-signal model an active load is analysed within an inverter-interfaced microgrid.

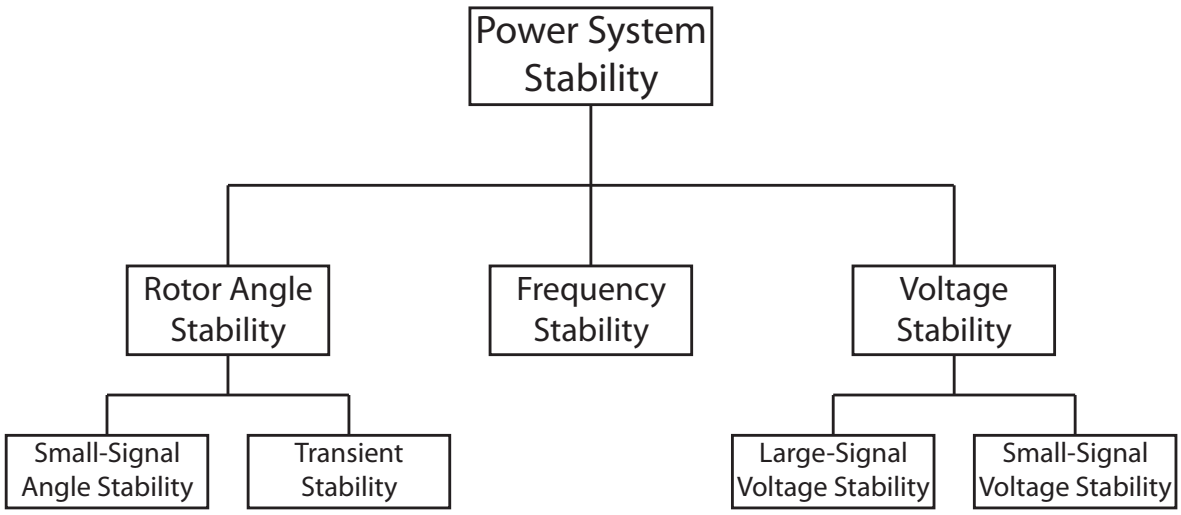

Figure 2.1: Classification of power system stability

2.1 Power system stability

Power system stability as defined in [66] and shown in Figure 2.1 is the ability of an electric power system, for a particular initial operating condition, to regain a state of operating equilibrium after being subjected to a physical disturbance, with most system variables bounded so that practically the entire system remains intact. Many books have been published and a few examples are referenced in [67, 68, 69]. Each category in Figure 2.1 is briefly explained below.

2.1.1 Rotor Angle stability

Rotor angle stability refers to the ability of synchronous machines within an interconnected power system to remain in synchronism after the power system is subject to a disturbance [66]. The system will return to a steady state if the equilibrium between the electromagnetic torque and the mechanical torque is maintained or restored. Instability may occur if the rotor oscillations after an event are not damped and continue to increase. This increase may lead to synchronous machines losing synchronism with other machines.

The power output of synchronous machines vary as their rotor angle changes. In steady state, the input mechanical torque and the output electromagnetic torque is in equilibrium.

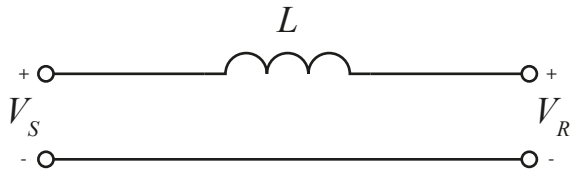

Figure 2.2: Voltage drop across an inductor

During a perturbation, the equilibrium is broken and this results in an acceleration or deceleration of the rotors. If a rotor accelerates, the angular position of that rotor with respect to the other rotors will advance. The increase in angle will cause this synchronous machine to supply more of the load. The increase in load will reduce the acceleration and hence reduce the angle separation. A measure of the effectiveness of the machine to return to steady-state is given by the synchronising power coefficient.

An increase in angle will only cause the machine loading to increase if the angle is within a pre-determined limit. Beyond this limit, an increase in angle will cause a decrease in power transfer. In this case there is no deceleration and the angle difference may continue to increase. The relationship between the synchronous machine loading and angle is governed by the power-angle relationship. Power systems tend to be largely reactive and a simplified power-angle relationship can be derived by considering an inductor with two voltages, as shown in Figure 2.2.

By considering the voltage drop across the inductor, the current through the inductor can be calculated.

$$I_S = \frac{V_S \angle \delta - V_R}{jX} = \frac{V_S \cos\delta - V_R + jV_S \sin\delta}{jX} \tag{2.1}$$

Where $X = \omega L$

The sending-end real and reactive powers are given by Equation (2.2).

$$P_S + jQ_S = V_S I_S = V_S \left(\cos\delta + j\sin\delta\right) \frac{V_S \cos\delta - V_R - jV_S \sin\delta}{-jX} \tag{2.2}$$

Equation (2.2) is simplified to Equation (2.3).

$$P_S + jQ_S = \frac{V_S V_R \sin\delta + j\left(V_S^2 - V_S V_R \cos\delta\right)}{X} \tag{2.3}$$

The real power at the sending-end is the real part of Equation (2.3).

$$P_S = \frac{V_S V_R}{X} \sin\delta \tag{2.4}$$

From Equation (2.4), the maximum power is when δ is 90 degrees. If δ is increased above 90 degrees, the power transmitted will decrease. This will lead to instability in the power system. To maintain angle stability, the angle must be lower than 90 degrees.

Instability results if the system cannot absorb the kinetic energy corresponding to these rotor speed differences. For any given situation, the stability of the system depends on whether or not the deviations in angular positions of the rotors result in sufficient restoring torques [68]. Loss of synchronism can occur between one machine and the rest of the system, or between groups of machines, with synchronism maintained within each group after separating from each other.

The change in electromagnetic torque of a synchronous machine following a perturbation can be resolved into two components, synchronising torque and damping torque. The synchronising torque component is in phase with the rotor angle deviation and is the torque that acts on the shaft of a synchronous machine with the rotational speed of the rotor deviates from the synchronous speed. Synchronising torque can be defined as the rate of change of electrical power per radian of electrical angle. The damping torque component is in phase with the speed deviation and prevents the synchronous machine from sustained oscillations. For the synchronous machine to remain stable both the synchronous torque and the damping torque must be positive.

Small-signal angle stability

Small-signal angle stability is the study of the power system when subject to a small disturbance. Small disturbances are usually from random small changes in loads and generation levels. These

small changes can cause large oscillations or gradual increases in angle in the power system which can cause system collapse.

The disturbances are considered to be sufficiently small that the system is assumed to be linear and analysis is undertaken around a particular operating point. Around this operating point, the system is represented as a state-space equation and non-linear components are usually linearised around the system operating point.

Transient stability

Transient stability is the study of the power system when subjected to large disturbances. Large disturbances are usually from faults, line trips or large load changes. When such disturbances occur large current and torques are produced which can cause violations of rotor angles. The purpose of transient stability is to determine whether the power system returns to steady-state after a large disturbance.

Steady-state angle stability

Steady-state stability is the study of the power system in equilibrium. Typically load-flow methods are used to calculate the voltages of nodes and the current flows between loads. The results of the load-flow allow for angle limits of the system to be checked. This ensures that there is no over loading of the equipment and transmission lines.

2.1.2 Frequency stability

Frequency stability is the ability of the power system to remain within the frequency limits during steady-state or following a disturbance. The frequency of a power system may increase when generation is greater than the load and may decrease when the generation is less than the load.

2.1.3 Voltage stability

Voltage stability is the ability of the voltage at every node in the system to remain stable and within voltage limits. The term voltage collapse is often used when a sequence of events leads to a blackout of abnormally low voltages. Voltage instability may be caused by loss of synchronism of generators, faults, sudden draw of power from loads or as a result of angle instability.

Large-signal voltage stability

Large-signal voltage stability refers to the systems ability to maintain steady voltages following large disturbances such as system faults or changes in reactive power flows. This is determined by the system and load characteristics, and the interactions of system control and protection. Determination of large-disturbance voltage stability requires the examination of the non-linear response of the power system over a period of time sufficient to capture the performance and interactions of such devices as reactive loads, motors, transformer tap changers, and generator field-current limiters. The study period of interest may extend from a few seconds to tens of minutes.

Small-signal voltage stability

Small-signal voltage stability refers to the system's ability to maintain steady voltages when subjected to small perturbations such as incremental changes in system load. This concept is useful in determining how the system voltages will respond to small system changes. With appropriate assumptions, system equations can be linearised for analysis thereby allowing computation of variable sensitivity information useful in identifying factors influencing stability. This linearisation, however, cannot account for non-linear effects such as tap changer controls (dead-bands, discrete tap steps, and time delays). Therefore, a combination of linear and non-linear analyses is used in a complementary manner.

2.2 Power system modelling techniques

2.2.1 Swing Equation

The swing equation describes the behaviour of the rotor dynamics of synchronous machines. It is used as a tool to access the transient stability of a synchronous machine after a large disturbance. If the system is found to be stable during the first swing, the system is assumed to be subsequently stable. In order to determine if a system is stable, the swing equation needs to be derived.

The swing equation is derived by first considering the shaft of a generator rotating freely and by considering Newton's second law where the inertia of the turbine and generator plus the losses due to windage and friction is equal to the difference between the mechanical torque and the electrical torque. Once the derivation is complete, the swing equation is presented as a function of angular momentum and power.

$$M_m \frac{d^2\delta_m}{dt^2} = P_m - P_e - D_m \frac{d\delta_m}{dt} \tag{2.5}$$

Where M_m is the angular momentum of the rotor at synchronous speed, D_m is the damping coefficient, P_m is the mechanical power going to the generator, P_e is the electrical power and δ_m is the rotor angle.

It is common to express the angular momentum of the rotor in terms of a normalized inertia constant. This allows for an easy comparison between generators regardless of their rating. The inertia constant is given the symbol H and defined as the stored kinetic energy in megajoules at synchronous speed divided by the machine rating S_n in megavolt-amperes.

$$H = \frac{0.5 J \omega_s m^2}{S_n} \tag{2.6}$$

and that,

$$M_m = \frac{2HS_n}{\omega_s m} \tag{2.7}$$

In effect, H quantifies the kinetic energy of the rotor at synchronous speed in terms of the number of seconds it would take the generator to provide an equivalent amount of electrical

energy when operating at a power output equal to its MVA rating.

2.2.2 Equal Area Criterion

The equal area criterion is a method for transient stability that analyses the angle of the rotor of a generator before, during and after a disturbance has occurred. The method uses the power angle curve to determine if angle stability will be breached.

When a fault occurs at t = 0, the electrical power output may decrease while the mechanical input power of the machine is unaltered. The difference in power must be accounted for by a rate of change of stored kinetic energy in the mass of the rotor. If the electrical output of the machine is less than the mechanical input, then the rotor will accelerate until the electrical power output is equal to the mechanical power input.

The time constant of the electrical system is in the order of milliseconds, whereas the time constant of the mechanical system is in the order of seconds. When analysing the equal area criterion, the mechanical power is assumed to not change over the period of interest and instead remain constant. The equal area criterion analyses the ability of the power system to recover from the fault and deliver the constant power from the turbine P_m at a new load angle δ.

A generator is delivering a power of P_m at a load angle of δ_1. After a network event, a circuit breaker opens and releases the load from the generator. This prevents the generator from exporting power and the electrical power delivered is reduced to zero. As already explained, the mechanical power remains constant. This causes the rotor mass to accelerate as governed by the swing Equation (2.5). The acceleration of the rotor causes the load angle to increase to δ_c and the power export will follow the fault impedance power curve. At this time the fault has cleared and the circuit breaker re-closes and the generator load is reconnected. If the electrical power drawn from the generator is greater than the mechanical power, the rotor will decelerate. During the deceleration, the inertia of the rotor will cause the angle to increase to δ_r where the power output follows the post-fault impedance power curve. For the generator to remain stable, the area due to the acceleration, A_1, must equal to the area due to the deceleration A_2. The graph in Figure 2.3 shows the points of interest.

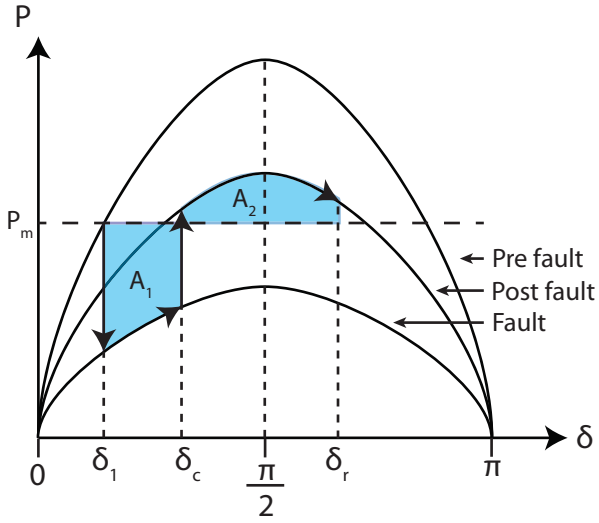

Figure 2.3: Equal Area Criterion

2.2.3 Linearisation

It is common practice that when analysing a non-linear system for small-signal stability studies, the system is modelled as a linear system at an equilibrium point (steady-state condition) of interest. The modelled linear-system is an approximation of the non-linear system model and is only valid for the equilibrium point which the non-linear system was linearised around. It is known from Lyapnuov's first method that if the linear system is stable then the non-linear system is also stable at the equilibrium point.

Linear systems represented by a set of first order differential equations may be shown as a state-space model with a constant A matrix. The state of the system, dynamics of the system and input to the system are represented by the variables x, A and u respectively. With knowledge of these variables the future state and output, y, of the system may be calculated. This model of the system is known as a state-space model and has two forms, homogeneous Equation (2.8) and non-homogeneous Equation (2.9).

$$\dot{x} - Ax = 0 \tag{2.8}$$

$$\dot{x} - Ax = Bu \tag{2.9}$$

Where,

$$\dot{x} = \frac{\mathrm{d}x}{\mathrm{d}t}, y = Cx + Du \tag{2.10}$$

Non-linear systems, as described in Equation (2.11) and Equation (2.12), may be linearised around an equilibrium point by using the Taylor series to form Equation (2.13) and Equation (2.14). The matrices $A = \frac{\partial F_1}{\partial x}, B = \frac{\partial F_2}{\partial u}, C = \frac{\partial F_3}{\partial x}, D = \frac{\partial F_4}{\partial u}$ are known as the Jacobi matrices calculated at the points X,U,Y [70].

$$\dot{x} = F_1(x) + F_2(u) \tag{2.11}$$

Where,

$$y = F_3(x) + F_4(u) \tag{2.12}$$

$$\Delta\dot{x} = A\Delta x + B\Delta u \tag{2.13}$$

$$y = C\Delta x + \Delta u \tag{2.14}$$

Where,

$$\Delta x = x - X, \Delta u = u - U, \Delta y = y - Y \tag{2.15}$$

2.2.4 Eigenvalues

Eigenvalues are the solution of the characteristic equation of a linear system's state matrix, which is matrix A [68]. An eigenvalue of a matrix is a scalar parameter λ for which there exists a non-zero solution to the Equation (2.16), where A is an $n \times n$ matrix and ϕ is an $n \times 1$ vector.

$$A\phi = \lambda\phi \tag{2.16}$$

The eigenvalues in Equation (2.16) are calculated by introducing an identity matrix I and writing Equation (2.16) as shown in Equation (2.17).

$$(A - \lambda I)\,\phi = 0 \tag{2.17}$$

For a non-zero solution, Equation (2.17) is written as Equation (2.18).

$$det\,(A - \lambda I) = 0 \tag{2.18}$$

The Equation (2.18) is known as the characteristic equation of A. The n solutions of $\lambda = \lambda_1, \lambda_2, \ldots, \lambda_n$ are the eigenvalues of the matrix A

Eigenvalues are either real or occur in complex conjugate pairs. A real eigenvalue where $\lambda = \alpha$ corresponds to a non-oscillatory mode and is known as an aperiodic mode. A negative real eigenvalue represents a decaying mode and a positive real eigenvalue represents an expanding mode. The larger the magnitude, the faster the decay or expansion. Due to the continual expanding mode of a positive real eigenvalue, these eigenvalues represent an instability within the system that the eigenvalues define.

Conjugate eigenvalue pairs correspond to oscillatory modes. The real component of a complex conjugate eigenvalue gives the damping and the imaginary component gives the frequency of oscillation and is defined in Equation (2.19). Synonymous to real eigenvalues, a negative real part represents a damped oscillation and a positive real part represents an oscillation of increasing amplitude. The frequency of the oscillation and the damping ratio of the oscillation are defined in Equation (2.20) and Equation (2.21) respectively.

$$\lambda = \sigma \pm j\omega \tag{2.19}$$

$$f = \frac{\omega}{2\pi} \tag{2.20}$$

$$\varsigma = \frac{-\sigma}{\sqrt{\sigma^2 + \omega^2}} \tag{2.21}$$

2.2.5 Eigenvectors

The term 'eigen' is defined from the Oxford dictionary as, 'proper; characteristic' and originates from the German word 'eigen' which means 'own' [71]. The term 'vector' is defined as a 'quantity having direction as well as magnitude, especially as determining the position of one point in space relative to another' [71]. An eigenvector is a characteristic vector of the state-space matrix A.

When a vector is multiplied by the state matrix A, the vector usually changes direction. Eigenvectors are a special sub-set of vectors. When eigenvalues are multiplied by the state matrix A, only the magnitude of the eigenvector changes. The quantity the eigenvector is scaled by is the eigenvalue, λ

The eigenvalue provides information as to whether the eigenvector is stretched, shrunk, reversed or not changed when the eigenvector is multiplied by the state matrix A. If the matrix A is the identity matrix I, all vectors are eigenvectors and all eigenvalues λ are 1. This is a special case and most n by n matrices have n eigenvector directions and n eigenvalue scaling.

Mathematically there are two types of eigenvector, left eigenvectors and right eigenvectors. For many problems, it is sufficient to only consider the right eigenvectors. When the term eigenvector is used without any prefix of left or right, it is understood that these are right eigenvectors [72].

Right Eigenvectors

A right eigenvector is a non-zero vector that satisfies Equation (2.22) where A is an n by n matrix. Each right eigenvector ϕ_R of A has an associated eigenvalue λ

$$A\phi_R = \lambda\phi_R \tag{2.22}$$

Left Eigenvectors

A left eigenvector, similar to a right eigenvector, is a non-zero vector that satisfies Equation (2.23) where A is an n by n matrix. Each left eigenvector ϕ_L of A has an associated eigenvalue λ

$$\phi_L A = \phi_L \lambda \tag{2.23}$$

In some texts, the left eigenvalue is denoted as ψ, in this thesis the left eigenvalue will be denoted as ϕ_L.

Left and Right Eigenvectors

The left eigenvectors of A are the right eigenvectors of the transpose of A, this is shown in Equation (2.24)

$$\phi_L A = A^T \phi_L = \phi_L \lambda \tag{2.24}$$

Left and right eigenvectors are orthogonal when they correspond to a different eigenvalue. This is shown in Equation (2.25) where the eigenvector ϕ_{Lj} corresponds to the eigenvalue λ_j and the eigenvector ϕ_{Ri} corresponds to the eigenvalue λ_i. The multiplication of the left and right eigenvector equals a non-zero constant when the eigenvector corresponds to the same eigenvalue. This is shown in Equation (2.26) where the eigenvector ϕ_{Li} and ϕ_{Ri} corresponds to the eigenvalue λ_j. In many applications, the left and right eigenvectors are normalised as shown in Equation (2.27).

$$\phi_{Lj}\phi_{Ri} = 0 \tag{2.25}$$

$$\phi_{Li}\phi_{Ri} = C_i \tag{2.26}$$

$$\phi_{Li}\phi_{Ri} = 1 \tag{2.27}$$

2.2.6 Modal Matrices

To represent the left eigenvectors, right eigenvectors and eigenvalues some matrices are defined. The left eigenvectors, right eigenvectors and eigenvalues are defined in the matrices ϕ_L, ϕ_R and Λ and shown in Equation (2.28), Equation (2.29) and Equation (2.30) respectively.

$$\phi_L = \begin{bmatrix} \phi_{L1} & \phi_{L2} & \cdots & \phi_{Ln} \end{bmatrix} = \begin{bmatrix} \begin{bmatrix} \phi_{L11} \\ \phi_{L21} \\ \vdots \\ \phi_{Ln1} \end{bmatrix} & \begin{bmatrix} \phi_{L12} \\ \phi_{L22} \\ \vdots \\ \phi_{Ln2} \end{bmatrix} & \cdots & \begin{bmatrix} \phi_{L1n} \\ \phi_{L2n} \\ \vdots \\ \phi_{Lnn} \end{bmatrix} \end{bmatrix} \tag{2.28}$$

$$\phi_R = \begin{bmatrix} \phi_{R1} \\ \phi_{R2} \\ \vdots \\ \phi_{Rn} \end{bmatrix} = \begin{bmatrix} \begin{bmatrix} \phi_{R11} & \phi_{R12} & \cdots & \phi_{R1n} \end{bmatrix} \\ \begin{bmatrix} \phi_{R21} & \phi_{R22} & \cdots & \phi_{R2n} \end{bmatrix} \\ \vdots \quad \vdots \quad \ddots \quad \vdots \\ \begin{bmatrix} \phi_{Rn1} & \phi_{Rn2} & \cdots & \phi_{Rnn} \end{bmatrix} \end{bmatrix} \tag{2.29}$$

$$\Lambda = \begin{bmatrix} \lambda_1 & 0 & \cdots & 0 \\ 0 & \lambda_2 & \cdots & 0 \\ \vdots & \vdots & \ddots & \vdots \\ 0 & 0 & \cdots & \lambda_n \end{bmatrix} \tag{2.30}$$

The matrices in Equations (2.28) – (2.30) have n by n elements. It is possible to expand Equation (2.22) and Equation (2.33).

$$A\phi_{R1} = \phi_R\Lambda \tag{2.31}$$

$$\phi_L\phi_R = I \tag{2.32}$$

$$\phi_L = \phi_R^{-1} \tag{2.33}$$

From Equation (2.22) and Equation (2.33), the modal matrix can be defined as Equation (2.34). The model matrix is the n by n matrix Λ which is calculated when the eigenvectors of A are formed in the matrix M and surround the matric M as shown in Equation (2.34).

$$\phi_R A \phi_R^{-1} = \Lambda \tag{2.34}$$

2.2.7 Using eigenvalues and eigenvectors to solve differential equations

An application of eigenvalues and eigenvectors is to solve matrix differential equations. Taking a homogeneous differential equation in the form of Equation (2.35) where x is a vector of the states. The states are derived from the physical system that the matrix differential equation represents.

$$\dot{x} = Ax \tag{2.35}$$

Equation (2.35) does not allow for much analysis of the physical system. This is because each state variable in Equation (2.35) is a linear combination of all of the state variables. The cross coupling between the states in Equation (2.35) does not allow the states to be identified that are most significant in influencing the physical system.

To solve the homogeneous differential equation in Equation (2.35) and to identify that states the are most significant in influencing the physical system, a new state vector z is defined. The state vector z is related to the state vector x by the transformation in Equation (2.36).

$$x = \phi_R z \tag{2.36}$$

Substituting Equation (2.35) into Equation (2.36), Equation (2.37) is formed. Rearranging Equation (2.37) into Equation (2.38) forms the new state space equation that uses the vector

z as the state vector. Equation (2.38) can be simplified into Equation (2.39) by the model matrix Equation (2.34)

$$\phi_R \dot{z} = A\phi_R z \tag{2.37}$$

$$\dot{z} = \phi_R^{-1} A\phi_R z \tag{2.38}$$

$$\dot{z} = \Lambda z \tag{2.39}$$

The difference between Equation (2.35) and Equation (2.39) is that the state vector z has a linear mapping and there is no cross-coupling between the states because Λ is a diagonal matrix.

$$z_i(t) = z_i(0)\, e^{\lambda_i t} \tag{2.40}$$

The solution with respect to time to the differential equation in Equation (2.39) is shown in Equation (2.40) where $z_i(0)$ is the initial value of z_i. The variable $z_i(t)$ can be transformed back to $x_i(t)$ with the use of the transform in Equation (2.36) and this transform can be used to produce Equation (2.41) and then Equation (2.42).

$$x(t) = \phi_R z_i(t) \tag{2.41}$$

$$x(t) = \begin{bmatrix} \phi_{R1} & \phi_{R2} & \cdots & \phi_{Rn} \end{bmatrix} \begin{bmatrix} z_1(t) \\ z_2(t) \\ \vdots \\ z_n(t) \end{bmatrix} \tag{2.42}$$

Manipulating Equation (2.42) by using the sequence shown in Equations (2.43) – (2.46), derives Equation (2.47). Substituting Equation (2.47) into Equation (2.41) removes the requirement to calculate the z state variable when providing a solution to the differential equation in Equation (2.35) from the initial conditions $x(0)$, the left eigenvectors ϕ_L and the eigenvalues λ. The substitution of Equation (2.47) into Equation (2.41) is shown in Equation (2.48)

$$x(t) = \sum_{i=1}^{n} \phi_{Ri} z_i(0) e^{\lambda_i t} \tag{2.43}$$

$$z(t) = \phi_R^{-1} x(t) \tag{2.44}$$

$$z(t) = \phi_L x(t) \tag{2.45}$$

$$z_i(t) = \phi_{Li} x(t) \tag{2.46}$$

$$z_i(0) = \phi_{Li} x(0) \tag{2.47}$$

$$x(t) = \sum_{i=1}^{n} \phi_{Ri} \phi_{Li} x(0) e^{\lambda_i t} \tag{2.48}$$

Equation (2.47) is a constant and to denote the scalar product $\phi_{Li} x(0)$ can be defined as c_i. This simplifies Equation (2.48) to Equation (2.49). From Equation (2.49), the time response of the ith state variable is given by Equation (2.50).

$$x(t) = \sum_{i=1}^{n} \phi_{Ri} c_i e^{\lambda_i t} \tag{2.49}$$

$$x_i(t) = \phi_{Ri1} c_1 e^{\lambda_1 t} + \phi_{Ri2} c_2 e^{\lambda_2 t} + \cdot + \phi_{Rin} c_n e^{\lambda_n t} \tag{2.50}$$

2.2.8 Sensitivity of modes to states

Section 2.2.7 introduced the state variables x and z and derived how they are related. The variables in the matrix x are chosen to represent the dynamics of the physical system being modelled. The variables in the matrix z are the transformed state variables and are only associated with one mode.

$$\begin{bmatrix} x_1(t) \\ x_2(t) \\ \vdots \\ x_n(t) \end{bmatrix} = \begin{bmatrix} \phi_{R1} & \phi_{R2} & \cdots & \phi_{Rn} \end{bmatrix} \begin{bmatrix} z_1(t) \\ z_2(t) \\ \vdots \\ z_n(t) \end{bmatrix} \tag{2.51}$$

$$\begin{bmatrix} z_1(t) \\ z_2(t) \\ \vdots \\ z_n(t) \end{bmatrix} = \begin{bmatrix} \phi_{L1} \\ \phi_{L2} \\ \vdots \\ \phi_{Ln} \end{bmatrix} \begin{bmatrix} x_1(t) \\ x_2(t) \\ \vdots \\ x_n(t) \end{bmatrix} \tag{2.52}$$

Equation 2.51 provides information about the influence of the state variable when a particular mode is excited. The influence of the state variable x_k in the ith mode is given by the element ϕ_{Rki} of the right eigenvector ϕ_R. Equation 2.52 provides information about the combination of the state variables in the ith mode.

2.2.9 Eigenvalue sensitivity

In a system where there are i eigenvalues and k states and where $i = k$, it is possible to quantify the sensitivity of the ith eigenvalue to the kth state. Through sensitivity analysis, if there are any unacceptable modes, the state variables that have the greatest participation can be determined. By knowing this information, gains within the system can be changed with the aim of changing the eigenvalues of the system to obtain a desirable response.

The sensitivity of eigenvalues to the elements of the state matrix is derived in Equations (2.53) – (2.55). The derivation starts with Equation (2.22) and differentiates this with respect to a_{ki} which is the element in the kth row and jth column of the matrix A.

$$\frac{\partial A}{\partial a_{ki}}\phi_{Ri} + A\frac{\partial \phi_{Ri}}{\partial a_{ki}} = \frac{\partial \lambda_i}{\partial a_{ki}}\phi_{Ri} + \lambda_i\frac{\partial \phi_{Ri}}{\partial a_{ki}} \tag{2.53}$$

Premultiplying by ϕ_L and using the properties that $\phi_{Li}\phi_{Ri}$ and $\phi_{Li}\left(A - \lambda_i I\right) = 0$, Equation (2.53) is simplified to Equation (2.54).

$$\phi_{Li}\frac{\partial A}{\partial a_{ki}}\phi_{Ri} = \frac{\partial \lambda_i}{\partial a_{ki}} \tag{2.54}$$

All elements of $\frac{\partial A}{\partial a_{ki}}$ are zero except for the element in the kth row and jth coloumn which equals one. The Equation (2.54) simplifies to Equation (2.55).

$$\frac{\partial \lambda_i}{\partial a_{ki}} = \phi_{Lik}\phi_{Rji} \tag{2.55}$$

This shows that the sensitivity of the eigenvalue λ_i to the element a_{ki} is the product of the left eigenvector element ϕ_{Lik} and right eigenvector element ϕ_{Rji}.

2.2.10 Participation of eigenvalues with respect to the system states

The participation matrix combines the right eigenvectors and left eigenvectors to measure the association between the state variables and the modes. The participation matrix is defined in Equation (2.56) – (2.57). The element ϕ_{Lik} is the element on the ith row and kth column of the modal matrix ϕ_L and the kth element of the left eigenvector ϕ_{Li}. The element ϕ_{Rki} is the element on the kth row and ith column of the modal matrix ϕ_R and the kth element of the right eigenvector ϕ_{Ri}.

$$P = \begin{bmatrix} p_1 & p_2 & \cdots & p_n \end{bmatrix} \tag{2.56}$$

$$p_i = \begin{bmatrix} p_1 i \\ p_2 i \\ \vdots \\ p_n i \end{bmatrix} = \begin{bmatrix} \phi_{Li1}\phi_{Ri1} \\ \phi_{Li2}\phi_{Ri2} \\ \vdots \\ \phi_{Lin}\phi_{Rin} \end{bmatrix} \tag{2.57}$$

The element $p_k i = \phi_{Lik}\phi_{Rki}$ is known as the participation factor. It a measure of the relative participation of the kth state in the ith mode and a relative measure of the ith mode in the kth state. If the eigenvectors are correctly normalised such that $\phi_{Li}\phi_{Ri} = 1$, then the sum of the participation factors associated with any mode or with any state variable is equal to one. This is shown in Equation (2.58) and Equation (2.59) respectively.

$$\sum_{i=1}^{n} p_{ki} = 1 \tag{2.58}$$

$$\sum_{k=1}^{n} p_{ki} = 1 \tag{2.59}$$

It can be seen from Equation (2.56) and Equation (2.55) that the participation factor p_{ki} is equal to the sensitivity of the eigenvalue λ_i to the diagonal element a_{kk} of the state matrix A. This is shown in Equation (2.60).

$$p_{ki} = \phi_L \phi_R = \frac{\delta \lambda_i}{\delta A_{kk}} \tag{2.60}$$

Participation factors and eigenvalues are extensively used in conventional power system stability analysis. Their applications have also been reported in DC-DC converter analysis [73].

2.3 Application of small and large signal stability for inverters

The application of stability for microgrid applications is discussed in [74] and the stability of an inverter based system can be linked to the categories presented in Figure 2.1. By taking each category in Figure 2.1 it is possible to discuss the equivalent for an inverter system. Rotor angle stability of a synchronous machine is comparable to the angle stability of a PLL used to connect the inverter to a distribution network or a droop function used to connect the inverter in a microgrid application. Frequency stability is comparable to the inverter maintaining the supply frequency when using a droop function. Although the frequency output of the inverter is determinable by the droop function used and there is no spinning rotor that may spin faster

or slower than the upper or lower frequency limits respectively. Voltage stability is comparable and more important in both grid-connected and standalone microgrid mode. In grid connected mode the presence of generation is likely to cause over-voltage when there is a lot of generation but a low level of load. In a microgrid application, the voltage output will decrease during a fault or overload when a current limit on an inverter is activated.

2.3.1 Small-signal stability

To analyse the small-signal stability of an inverter network, a linear model is developed and the eigenvalues are investigated. The technique for modelling non-linear systems as linear systems is discussed in Section 2.2.3 and the eigenvalue analysis is discussed in Section 2.2.4. By changing the controller gains and the system parameters, it is possible to determine how these affect the small-signal stability by observing the eigenvalues [75, 20].

The small-signal stability of a two inverter microgrid where a master inverter controls the AC voltage and a slave inverter is connected using a PQ controller is modelled in [76]. An example of a droop controlled microgrid is in [75, 20]. The advantage of using droop over a master-slave system is that communication links are not required and complicated power sharing algorithms are also not required as the droop algorithm will autonomously distribute the power between the available generation.

In a microgrid, the work on small-signal stability has shown that the low-frequency modes are highly sensitive to the network configuration and the parameters of the power sharing controller in the inverter sources [75, 20].

Droop controller developments

Previously discussed, the droop algorithm is the limiting factor for the small-signal stability of a microgrid. Therefore a method of improving the stability of a microgrid is to change the droop function. In [77] an arc-tan droop gradient is used instead of a linear droop gradient and this achieves a stability improvement and in [78] an additional derivative term is placed within the droop controller. To improve the voltage regulation a virtual impedance may be

added to the voltage reference which is the output of the droop controllers and input to the voltage controller [79]. The purpose of this extra loop is to correct the voltage reference so that there is an improvement of load sharing across the inverters. The controllers also induce a virtual impedance upon connection so that the current transients are minimised. Each of the enhancements show a stability improvement, however these are all computationally more intensive.

Microgrid modelling developments

Small-signal models of microgrids first considered two and three node microgrids. However, these microgrids may not be representative of a real microgrid that may have many more inverters, line and loads connected. The model presented in [75, 20] is detailed and uses many state variables. Although it is possible to scale this model to a larger microgrid, the process of modelling will require a very large matrix and be computationally intensive.

A small-signal model for a large microgrid which consists of a 69 bus radial system supplied by 20 generation units is presented in [80]. This model simplifies each element to only 4 states and hence reduces the computational intensity of large microgrids without a large decrease in modelling accuracy. This work only considers PQ and Vf controllers. In [81] a model reduction is presented where only the droop controller of each inverter source is modelled. The models assume that the internal controllers have a bandwidth of at least an order of magnitude greater than the bandwidth of the droop controllers and are therefore assumed to be ideal.

These methods are effective at reducing the computational intensity of a large microgrid. However, if there are any interactions between the inner controllers of the inverter then these interactions would not be modelled and would not be spotted during any analysis.

If the parameters of the microgrid are not known, then [82] presents a method in which an estimation of the parameters can be obtained from perturbing the microgrid. This is particularity useful if connecting a new load or generator to an existing microgrid. However, if the parameters are known, as is the case for a laboratory microgrid, a more accurate model can be formed by following the technique in [75, 20].

Microgrid system control

The use of an Energy Management System (EMS) has also been proposed to improve the stability or adjust the parameters to optimise the output of the microgrid while ensuring that the small-signal stability is maintained. An example of such work is in [83, 84] where an EMS is used to perform droop stability analysis, droop selection and generator dispatch. It was shown that the line and inverter coupling inductances had the largest effect on the range of droop-gain that could be selected by the EMS before the microgrid experienced stability constraints.

Microgrids with non-impedance loads

It is important to consider loads which may be connected to the microgrid that are not constant impedance loads. The effect of the impedance load angle was explored in [85]. It was observed that an increase in angle of the load decreases the stability, however an increase in magnitude does not affect the stability. When a constant power load was modelled in [86], it was concluded that the constant power load caused the microgrid to be unstable. However, the dynamic interactions between the load and the inverter sources were not investigated. The testing of a dynamic model of a constant power load is required before it can be concluded that constant power load cause microgrids to become unstable.

Small signal summary

Small-signal analysis is an important tool for assessing the stability of a microgrid or grid connected network. The literature discussed in Section 2.3.1 demonstrates a wide-range of applications. The papers all follow a similar procedure. The system is modelled as a linear system. The eigenvalues of the system matrix are calculated. Parameters are changed and the changes in eigenvalues are observed to understand the stability of the system. There is a lot of work published on microgrid networks which supply passive loads. However, this is not complete and the literature should be expanded to include other load types, for example active loads.

2.3.2 Large-signal stability

Transient stability of the microgrid is investigated in [87] through the use of PSCAD/EMTDC software simulations. The work demonstrates that the microgrid could become unstable due to a fault but did not investigate the specific cause within the inverter controllers that resulted in the microgrid becoming unstable. It was concluded that the transient stability could be improved by the use of a flywheel and by load-shedding measures on the motor loads. The flywheel was there to provide energy storage and inertia in the event of a fault and that by shedding the motor loads, the risk of voltage collapse can be minimised.

The size of the microgrid is increased in [88] to a 37 node distribution system. This work used simulation results to show that there was a critical clearing time of 0.274 seconds to guarantee the transient stability of the microgrid under study. It also showed that a droop controlled inverter exhibits better transient characteristics than a synchronous generator when supplying a three-phase-to-ground short-circuit fault in a distribution system.

A non-linear model is applied to the microgrid in [89] and this model is used to calculate if the microgrid will remain stable after a large disturbance. It was shown that the microgrid remained stable after a short disturbance of 0.2 seconds but the microgrid did not remain stable after a disturbance of 4 seconds.

From the work in [88] and [89] it can be concluded that the length of the disturbance affects the transient stability of the microgrid. However, these two papers have not considered the effect of a current-limiting circuit which may be required to operate if the currents required are larger than the physical operating limits of the inverters.

2.4 Control of inverters

2.4.1 Reference frames

Inverter sources can be controlled in the synchronous reference frame (DQ-frame), stationary reference frame ($\alpha\beta$-frame), or in the natural reference frame (ABC-frame).

Control in DQ

The DQ reference frame is known as the synchronous reference frame. The two perpendicular axes in this reference frame rotate at the fundamental frequency. The fundamental frequency is represented in the DQ reference frame as DC signals. There are many transformations used to convert between the ABC reference frame and the DQ reference frame. They are either power invariant or voltage invariant and either represent the D axis on the horizontal or vertical axis of an x-y plot. The transformation used in this thesis is a variant of the Park-Clark transformation as first proposed in 1929 by R. H. Park [90]. It is power invariant and the D axis is plotted on the horizontal axis of a two axis plot.

$$[T_{dq}] = \sqrt{\frac{2}{3}} \begin{bmatrix} \cos(\omega t + \theta) & \cos\left(\omega t + \theta - \frac{2\pi}{3}\right) & \cos\left(\omega t + \theta + \frac{2\pi}{3}\right) \\ -\sin(\omega t + \theta) & -\sin\left(\omega t + \theta - \frac{3}{2\pi}\right) & -\sin\left(\omega t + \theta + \frac{3}{2\pi}\right) \\ \frac{1}{\sqrt{2}} & \frac{1}{\sqrt{2}} & \frac{1}{\sqrt{2}} \end{bmatrix}. \tag{2.61}$$

The advantage of control in the synchronous reference frame is that it allows the use of a simple PI controller, shown and modelled in [91]. However, these controllers experience a degradation in performance when the load becomes unbalanced. DQ controllers are typically designed to be used with only positive sequence voltage and current measurements. When there is an unbalance in the load, the voltage and current measurements have positive and negative sequence components. The DQ measured currents and voltages become oscillatory unless a filter is used to separate the positive and negative components of the unbalanced voltage and current measurements. For control of unbalanced loads with DQ controllers, one solution is to implement a positive sequence DQ loop and a negative DQ loop. Other designs that enable DQ controllers to supply unbalanced loads are discussed in [92]. When DQ controllers experience an unbalanced fault, the inverter output experiences an over-voltage in the un-faulted phase or phases [93]. One solution to compensate the over-voltage is to emulate an output-impedance in parallel with the filter capacitor [94].

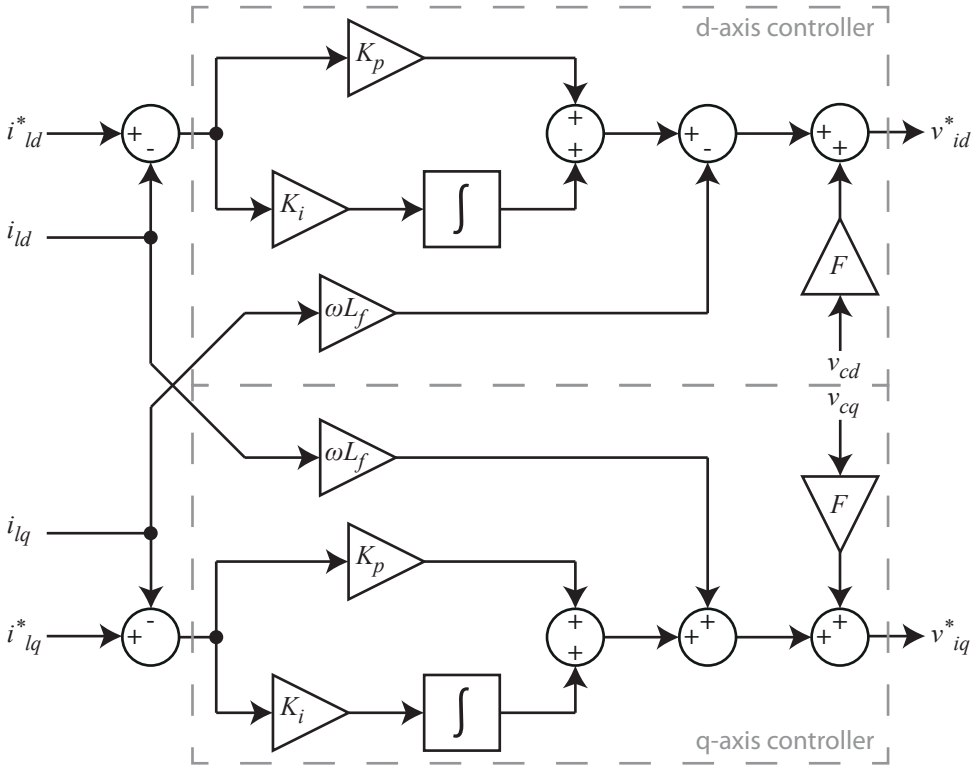

Figure 2.4: PI Control in the DQ reference-frame

Control in Alpha Beta

The Alpha-Beta ($\alpha\beta$) is known as the stationary reference frame. The axes in this reference frame do not rotate and are stationary. A three-phase signal is represented by a vector in the $\alpha\beta$ that completes a revolution at the same frequency as the fundamental frequency. A Clark transform is required to convert between the ABC reference frame and the $\alpha\beta$ reference frame.

Using the $\alpha\beta$ reference frame allows for the use of a less complex transform than that used for control in the DQ reference frame as only a Clarke transform is required instead of a Park-Clarke transform. The reference signals in $\alpha\beta$ retain the rotation of the fundamental frequency and require a more complex controller. A PR controller, as shown in [95], can be tuned to the nominal system frequency and is effective. Unlike DQ controllers, ($\alpha\beta$) control is able to compensate both positive and negative sequence components with only two phases and without loss of performance. However, if the zero sequence component is present (which may happen in 4-wire systems) then a third control signal is required which is known as the (λ) signal. Supplying a balanced fault current in $\alpha\beta$ requires a fault-current vector that is circular. For an

unbalanced fault current a more complex fault-current vector, that is elliptical, is required to prevent any over-voltages in the healthy phase or phases.

Control in ABC

The ABC reference frame is known as the natural reference frame. No transform is required and the signals are the same as if they were measured by voltage and current sensors. Control in the natural (ABC) reference frame also requires the use of PR controllers. The advantage is that ABC has independent control of each phase and is effectively three single phase controllers. The control of each phase allows for both positive and negative sequence components (and zero sequence in 4-wire systems) to be compensated simultaneously [96]. ABC control does not require the use of transformations that $\alpha\beta$ and DQ controllers require. Since ABC is effectively three single phase controllers, the same current limiting strategy can be used for single-phase and three-phase faults without causing over voltages in the un-faulted phase or phases, or without the requirement for different fault-current reference signals for three-phase and single-phase faults. For these reasons control in the (ABC) reference frame is chosen over control in the $\alpha\beta$ or DQ reference frames.

There are two types of PR controller, an ideal PR controller and a non-ideal PR controller. An ideal PR controller has an infinite gain at the resonance frequency however the bandwidth at the resonate frequency is very small. If the frequency of the control signals were to deviate from the resonance frequency, the resonator would have poor performance and the controller would be as effective as only a proportional controller. The non-ideal PR controller has a bandwidth that can be changed at the resonance frequency. Therefore this controller has good performance when the control signals deviate from the resonate frequency. However, the gain at the resonate frequency is finite. A finite gain at the resonance frequency is a good trade-off for a greater bandwidth as the resonance frequency. When the inverter is connected to a network, the frequency of the current and voltage may deviate from the fundamental frequency. For this reason a non-ideal PR controller is chosen over an ideal PR controller.

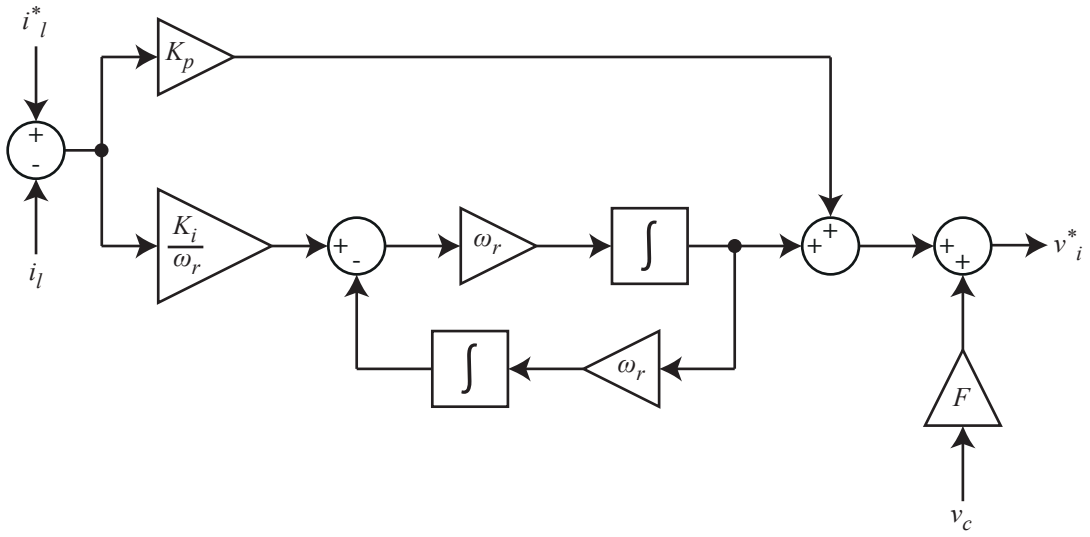

Figure 2.5: Ideal PR control in the ABC reference-frame

2.4.2 Droop Control

Power sharing of generators can be achieved through the use of droop characteristics. For synchronous generators, droop control is undertaken within the governor that controls the steam to the turbine or the fuel to the engine. For inverters, droop controller is mathematically emulated through the used of a droop function.

Droop control allows for the load connected to a network to be shared among the network generators without the requirement of a communications system or a centralised controller. In the presence of a droop characteristic for a synchronous machine, when there is an increase in load, the governor of a synchronous machine provides more steam to the turbine or more fuel to the engine. This causes the speed of the rotor and hence the frequency of the rotor to increase. The error between the electrical power load and the mechanical power from the turbine or the generator's engine is reduced. When the load is reduced, the droop characteristic causes less steam to the turbine or less fuel to the engine and the reverse happens.

During the process, the droop characteristic introduces a negative feedback error to regulate the speed of the rotor and this error is defined by the droop gain used. The error introduced causes a frequency error that depends on the total load connected to the generators. In this way, each generator varies its frequency until all the generators converge to a common frequency

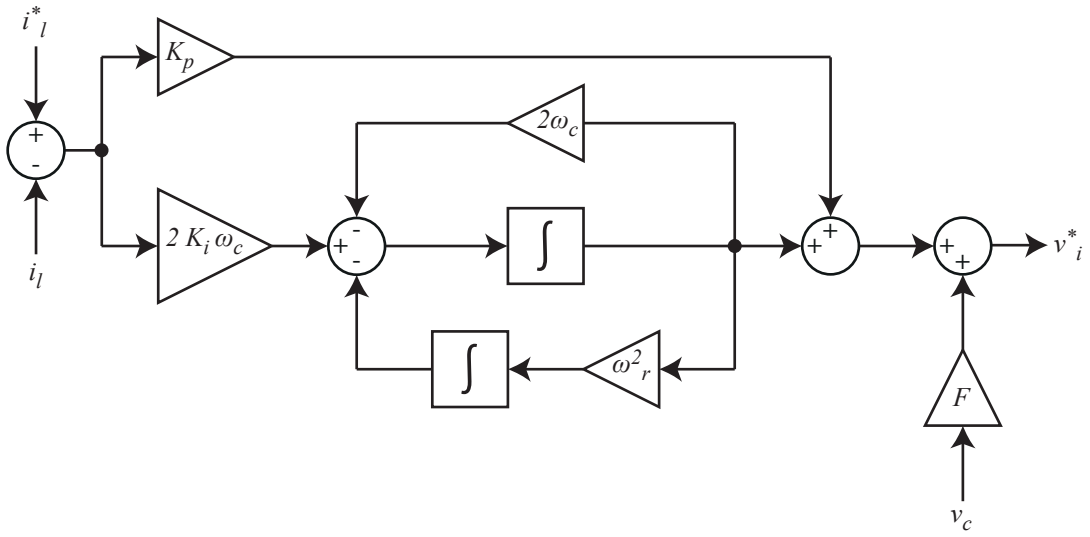

Figure 2.6: Non-ideal PR control in the ABC reference-frame

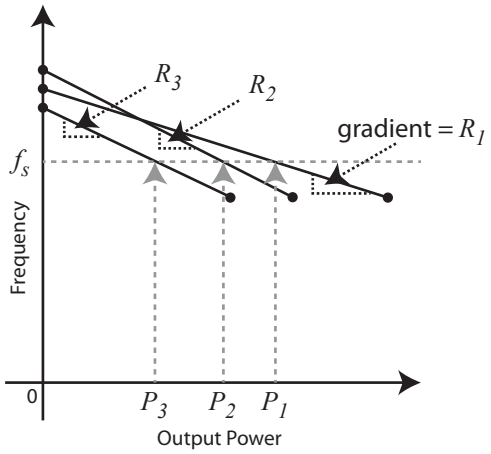

Figure 2.7: Load sharing by parallel generators with drooping governor characteristics

which is less than the nominal frequency. Figure 2.7 shows the solution of a three droop generator network when the total load on the system is equal to $P_1 + P_2 + P_3$.

2.5 Limiting of inverters

It is well known that the output current of an inverter should be limited to avoid damage to the semiconductors. As a protective measure, practical inverter applications may disconnect the inverter when a short-circuit current is detected in the inverter. One protection scheme for semiconductors is to use desaturation (desat) protection as explained in [97]. Desat protection

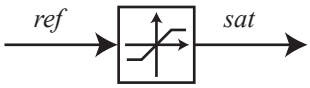

Figure 2.8: Instantaneous limits

measures the voltage across the semiconductor and if the voltage rises above a threshold when the gate signal is high, the gate drive circuit switches off the device. A second protection strategy is to use an i^2t limit which is calculated using the integral of the square of the current. This allows the inverter to supply a lower over-load current for time duration that is longer than if the inverter where supplying a higher fault-current. However, the i^2t trip does not limit the inverter output current. If the i^2t limit is exceeded, the inverter will trip and be disconnected from the network.

In the literature [98] – [103], inverters have used a software current limiting method to supply a fault-current and to ensure that the output current does not exceed the rating of the inverter. The software limit allows the inverter to remain connected for the duration of the fault. When using a software current limiting method, the fault-current of an inverter is determined by its controller [104].

2.5.1 Instantaneous limiting

Instantaneous saturation limits prevent a signal or output value increasing beyond a pre-determined value. They are simple to implement and provide an easy method to control signals within a controller. However, if the signal is sinusoidal, they clip the crest and the resulting magnitude is not pre-determinable.

2.5.2 Latch limiting

A latched limit measures the signal and when the signal is above a pre-determined threshold, the latch changes the signal flow to a limit that is determined. However, these limits require consideration on how the reset is operated.

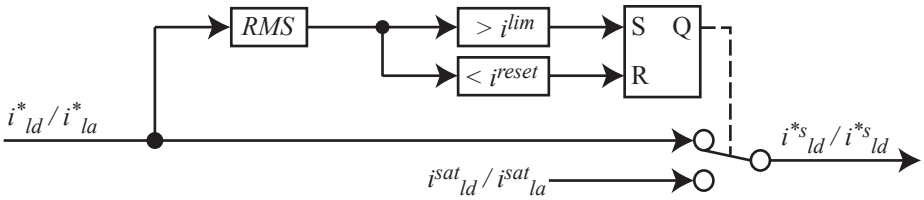

Figure 2.9: Latch limits also known as set and reset limits

2.5.3 Limiting of an inverter by changing the reference inputs

A proposal for current limiting in a static synchronous compensator is to calculate the controller set point with respect to the maximum current that the inverter can safely deliver [105] [106]. This strategy allows the device to naturally limit the current without exceeding the compensator's safe operating region and without producing a distorted current. In cases where it is desirable to provide a current limit that is different to the normal export current, a latched-limit design may be chosen. For this reason, it is important to study how these limits should be reset in order to ensure correct operation during fault ride-through.

2.6 Modelling loads

There are three basic methods to model the dynamics of loads as presented in the literature. The three methods are a component based model, a measurement based method and a composite load method. Much work on load modelling was done by Institute of Electrical and Electronic Engineers (IEEE) Task Force on Load Representation for Dynamic Performance [107] [108].

2.6.1 Component based models

Component based approach modelling requires detailed circuit and control algorithm information. The circuit design and parameters are used to construct an accurate representation. If many loads are aggregated, this approach often results in large models that are slow and cumbersome requiring large amounts of computing time.

When a more accurate model is required or the load circuit components to be modelled are known, it may be more appropriate to use a component-based method. Common loads in a distribution network will either be impedance loads, rotating machine loads, or rectifier loads.

Impedance Loads

An impedance load model is the simplest and mainly used for representing incandescent light bulbs and heating elements. For example, a domestic heater may be modelled as a resistor and an inductor in series [109].

Machine Loads

Much industrial and commercial equipment requires mechanical torque, for example pumps and fans. The mechanical torque is normally produced by an induction machine. Induction machine characteristics have been extensively researched and modelled. Literature published includes faults and transient behaviour for both standalone and network applications [110] [111]. Unlike impedance loads, induction machine characteristics depend on the mechanical system and may behave as a constant power load. Constant power loads are known to destabilise networks [62].

Rectifier Loads

Over the last three decades, the number of rectifiers in the distribution network has increased as more loads require a DC supply. Such loads are: high frequency switched fluorescent lighting, electronic loads, Uninterruptible Power Supply (UPS) loads, computers, DC motor loads and induction furnaces [112]. Most rectifier loads will have a DC voltage regulator keeping a constant voltage. This will cause the load to have constant power characteristics during a network transient, only if the equipment requiring the DC voltage has a steady current draw over the network transient.

2.6.2 Measurement Based

The measurement based technique involves installing a data logger at a substation to record measurements of load behaviour after a network disturbance. Measurements of the load provide

accurate parameter values for use in power stability simulations [107]. These parameters are easily obtained for any load or aggregation of loads. The complexity of the model will depend on the mathematical representation of the measured data and not the design of the circuit [113] [114].

Many estimation algorithms for parameter estimation exist, some proposed methods are, Ant Colony Search [115], Monte-Carlo Method [116], Probabilistic Collocation Method [116], Least Square Method [117] and Newton-Raphson Iterative Technique [118].

2.6.3 Composite Load Models

The composite based technique is a hybrid of the component based and measurement based load models. The idea is to match parameters from a standard component based model to a measured set of results. This processes enables transient-stability software libraries to have the same model for many different sets of measured load data. There are many different composite load models and parameter matching algorithms to use. Composite load models usually comprise an equivalent induction machine paralleled with a static impedance load and do not account for rectifier loads. [115].

Chapter 3

Modelling of Active Loads in Microgrids

This chapter is the start of the original work to be presented in this thesis and has been published in two conference proceedings and one journal proceeding. Specifically, Section 3.1 is published in [119], Section 3.2 is published partly in both [119] and [120], Section 3.4 is published in [120] and Section 3.6 is published in [121]. The work presented in Section 3.5 has not been published.

Historically, loads in electrical networks were predominantly resistive and inductive loads. Examples of these loads are incandescent lighting, heating loads and direct online motors. With the introduction of power electronics, more loads have an active rectifier. Examples of these loads are three-phase UPS and three-phase inverter controlled motor drives which examples include industrial air-conditioning, industrial refrigeration and building lift or crane motors.

A microgrid may be required to supply three-phase active loads. The dynamics of the active load may be similar to the dynamics of the inverter-based generation as the design and controllers used are similar. Typically, microgrid studies have focused on resistive loads. However it is important to consider active loads in microgrid applications and this is the focus of this chapter.

Section 3.1 presents a model of an active load which is analysed using eigenvalue and participation analysis in Section 3.2 and verified experimentally in Section 3.3. The active load

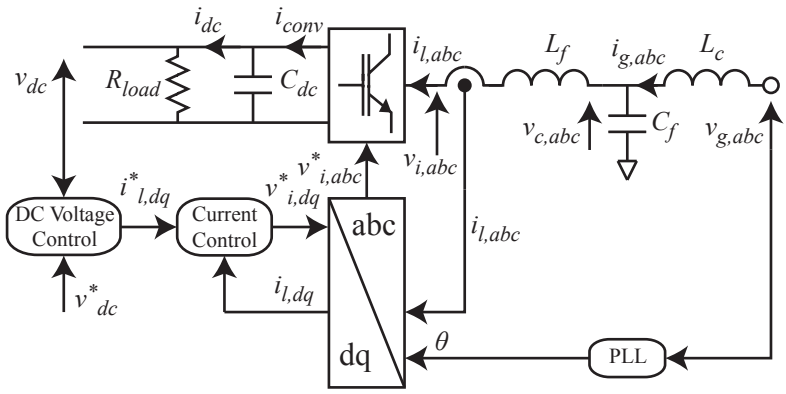

Figure 3.1: Active load circuit and control

is then connected to a microgrid model by the use of matrices in Section 3.4; this is intended to be general and does not attempt to present a set of equations for only one configuration of the microgrid. Two different microgrid circuits are modelled using the equations developed in Section 3.4 and subsequently analysed in sections 3.5 and 3.6. Both microgrids consist of three inverter sources, two lines, one active load and one passive load. The difference between the two circuits is the location of the active load and passive load. Eigenvalue and participation analysis is used to analyse and compare both circuits. The circuit in Section 3.6 is also experimentally verified in Section 3.7.

3.1 Active Load Small Signal Model

Figure 3.1 shows the circuit and control of the active load. Modelling of this system involves the formation of state-space models of the circuit and controllers. The control system of the active load can be divided into two sub sections. The first subsection is the outer dc-voltage controller which controls the dc-voltage across the dc-voltage capacitor labelled C_{dc} in Figure 3.1. The second subsection is the inner ac-current controller which controls the current through the inductor labelled L_f in Figure 3.1.

The active load is controlled in the DQ reference frame and not the ABC reference frame. The DQ reference frame was chosen instead of the ABC reference frame because the active load is a balanced three-phase load that only draws positive sequence current. Control in

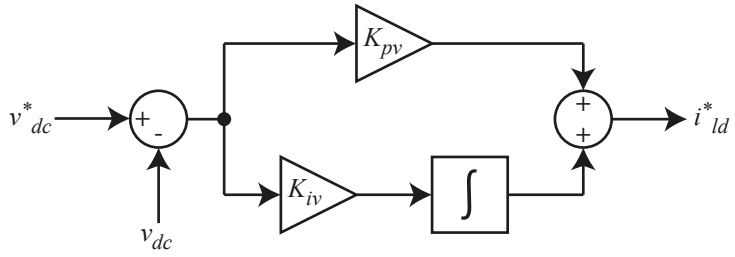

Figure 3.2: Active load dc-voltage controller

the ABC reference frame is more complex because resonant controllers are required to operate at the fundamental frequency, however it is a better solution when injecting unbalanced current. Inverters that draw balanced current are balanced loads and using the DQ reference frame is an effective controller. Inverters that supply current to a microgrid may be required to support unbalanced loads and the ABC reference frame is required. Since there is no envisaged unbalanced current being drawn by the active load, the DQ reference frame was used.

3.1.1 Small-signal model of the dc-voltage controller

The dc-voltage is controlled by using a standard PI controller which determines the reference input to the ac-current PI controller. When the dc-voltage decreases, the ac-current controller reference is increased, and when the DC-voltage increases the AC-current controller reference is decreased. This is because when a DC-load change occurs, the new load will either draw more or less current from the DC capacitor. The capacitor charge will then decrease or increase and this change in charge will cause the capacitor voltage to fall or rise. To restore the DC-voltage to the correct level, the DC-voltage controller must send a higher or lower set-point to the AC-current controller. If the control gains are tuned correctly, the DC-voltage will quickly return to steady-state after a disturbance.

The dc-voltage controller is shown in Figure 3.2. Equation (3.1) and Equation (3.2) represent the small-signal linearised state-space form of the dc-voltage controller. The integral term is denoted as ϕ and the subscript 'V' is used for the coefficients of the state-space equations of the dc-voltage controller.

$$\begin{bmatrix} \dot{\Delta\phi_{dc}} \end{bmatrix} = \begin{bmatrix} 0 \end{bmatrix} \begin{bmatrix} \Delta\phi_{dc} \end{bmatrix} + B_{V1} \begin{bmatrix} \Delta v_{dc}^{*} \\ \Delta i_{lq}^{*} \end{bmatrix} + B_{V2} \begin{bmatrix} \Delta v_{dc} \end{bmatrix}, \tag{3.1}$$

$$\begin{bmatrix} \Delta i_{ldq}^{*} \end{bmatrix} = C_V \begin{bmatrix} \Delta\phi_{dc} \end{bmatrix} + D_{V1} \begin{bmatrix} \Delta v_{dc}^{*} \\ \Delta i_{lq}^{*} \end{bmatrix} + D_{V2} \begin{bmatrix} \Delta v_{dc} \end{bmatrix}. \tag{3.2}$$

The variables of Equation (3.1) and Equation (3.2) are defined in Equations (3.3) – (3.5).

$$\int (v_{dc}^{*} - v_{dc})\, dt = \Delta\phi_{dc} \tag{3.3}$$

$$B_{V1} = \begin{bmatrix} 1 & 0 \end{bmatrix}, \; B_{V2} = \begin{bmatrix} -1 \end{bmatrix}, \tag{3.4}$$

$$C_V = \begin{bmatrix} K_{iv} \\ 0 \end{bmatrix}, \; D_{V1} = \begin{bmatrix} K_{pv} & 0 \\ 0 & 1 \end{bmatrix}, \; D_{V2} = \begin{bmatrix} -K_{pv} \\ 0 \end{bmatrix}. \tag{3.5}$$

3.1.2 Small-signal model of the ac-current controller

The ac-current controller, shown in Figure 3.3, controls the current through the inductor L_f (Inductor L_f couples the H-bridge to the filter capacitor C_f). The controller makes the use of feed-forward terms to decouple the measured inductor current d and q axis. The d and q axis are decoupled by multiplying the measured current with the nominal system frequency ω_n and inductance L_f.

To design the current controller of the active load, the direction of the nominal current flow is considered. As shown in Figure 3.1, positive current in the active load is defined as flowing from the grid connection to the switching bridge. This means that the controller equations are as stated in Equation (3.6) and Equation (3.7).

$$v_{id}^{*} = \omega_n L_f i_{lq} - K_{pc}\,(i_{ld}^{*} - i_{ld}) - K_{ic} \int (i_{ld}^{*} - i_{ld})\, dt \tag{3.6}$$

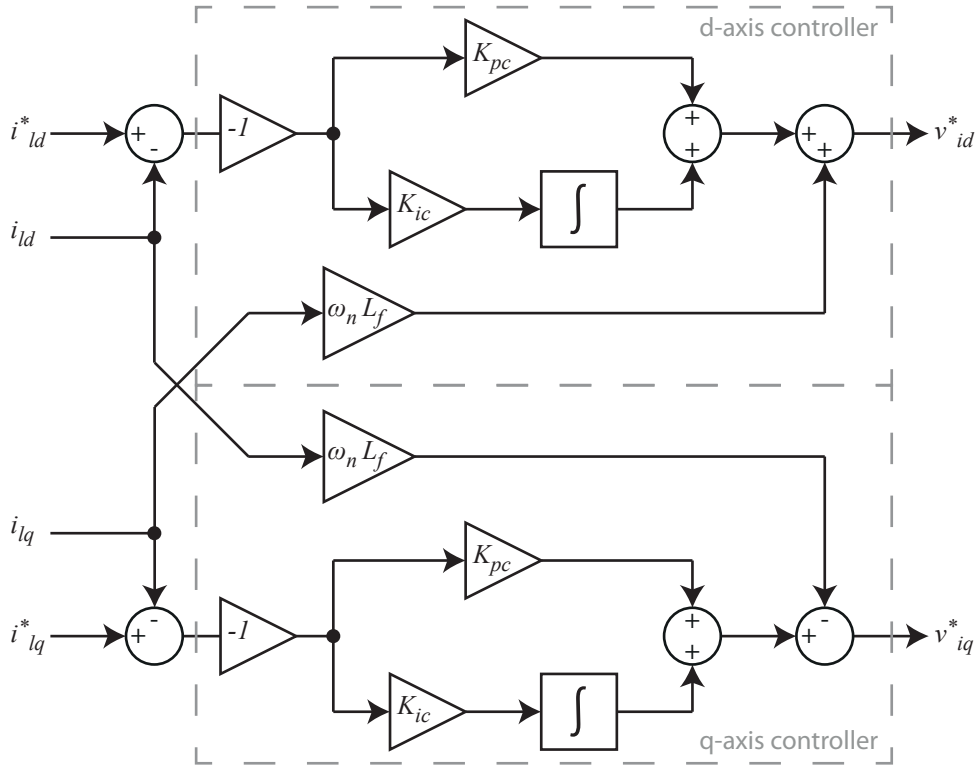

Figure 3.3: Active load ac-current controller

$$v^*_{iq} = -\omega_n L_f i_{ld} - K_{pc}\left(i^*_{lq} - i_{lq}\right) - K_{ic}\int\left(i^*_{lq} - i_{lq}\right)dt \tag{3.7}$$

To define the ac-current controller in state-space representation, the same procedure that was applied to the dc-voltage controller is applied to the current controller. The ac-current controller equations are presented in Equations (3.8) – (3.9) and the components of the matrices are presented in Equations (3.10) – (3.12). The integral term is denoted as γ and the coefficients of the state-space equations for the ac-current controller use the subscript 'C'.

$$\dot{\left[\Delta\gamma_{dq}\right]} = \left[0\right]\left[\Delta\gamma_{dq}\right] + B_{C1}\left[\Delta i^*_{ldq}\right] + B_{C2}\begin{bmatrix}\Delta i_{ldq}\\ \Delta v_{vdq}\\ \Delta i_{gdq}\end{bmatrix}, \tag{3.8}$$

$$\left[\Delta\gamma_{dq}\right] = C_C\left[\Delta\gamma_{dq}\right] + D_{C1}\left[\Delta i^*_{ldq}\right] + D_{C2}\begin{bmatrix}\Delta i_{ldq}\\ \Delta v_{cdq}\\ \Delta i_{gdq}\end{bmatrix}. \tag{3.9}$$

$$B_{C1} = \begin{bmatrix} 1 & 0 \\ 0 & 1 \end{bmatrix}, \; B_{C2} = \begin{bmatrix} -1 & 0 & 0 & 0 & 0 & 0 \\ 0 & -1 & 0 & 0 & 0 & 0 \end{bmatrix}, \tag{3.10}$$

$$C_C = \begin{bmatrix} -K_{ic} & 0 \\ 0 & -K_{ic} \end{bmatrix}, \tag{3.11}$$

$$D_{C1} = \begin{bmatrix} -K_{pc} & 0 \\ 0 & -K_{pc} \end{bmatrix}, \; D_{C2} = \begin{bmatrix} K_{pc} & \omega_n L_f & 0 & 0 & 0 & 0 \\ -\omega_n L_f & K_{pc} & 0 & 0 & 0 & 0 \end{bmatrix}. \tag{3.12}$$

3.1.3 Small-signal model of the switching bridge

Figure 3.1 includes the dc-capacitor circuit which is connected to the switching bridge. The corresponding equation for the dc-capacitor is written in Equation (3.13).

$$\frac{dv_{dc}}{dt} = \frac{1}{C_{dc}} i_{conv} - \frac{1}{C_{dc} i_{dc}} \tag{3.13}$$

The approach taken to model the switching bridge is to assume that the switching bridge is an ideal power converter where the internal power losses are negligible. An ideal power converter is a valid assumption providing the semi-conductor technology has low losses. The corresponding equation of the switching bridge where the input power equals the output power is written in Equation (3.14)

$$v_{id} i_{ld} + v_{iq} i_{lq} = i_{conv} v_{dc}. \tag{3.14}$$

By substituting Equation (3.14) into the equation of the dc-bus capacitor, a relationship that relates the ac-side to the dc-side of the switching bridge is formed in Equation (3.15)

$$\frac{dv_{dc}}{dt} = \frac{1}{C_{dc}} \frac{v_{id} i_{ld} + v_{iq} i_{lq}}{v_{dc}} - \frac{1}{C_{dc} i_{dc}} \tag{3.15}$$

Equation (3.16) is the small-signal representation of Equation (3.15) written in a state-space notation. Subscript 'SW' is used for the coefficients of the state-space equations of the switching bridge.

$$\left[\dot{\Delta v_{dc}}\right] = A_{SW}\left[\Delta v_{dc}\right] + B_{SW}\begin{bmatrix}\Delta i_{ldq}\\ \Delta v_{cdq}\\ \Delta i_{gdq}\end{bmatrix} + B_{SWu}\left[\Delta v_{idq}\right] + B_{SWdc}\left[\Delta i_{dc}\right]. \tag{3.16}$$

The variables of Equation (3.16) are defined in Equations (3.17) – (3.19).

$$A_{SW} = \left[-\frac{V_{id}I_{ld}+V_{iq}I_{lq}}{C_{dc}V_{dc}^2}\right], \tag{3.17}$$

$$B_{SW} = \begin{bmatrix}\frac{V_{id}}{C_{dc}V_{dc}} & \frac{V_{iq}}{C_{dc}V_{dc}} & 0 & 0 & 0 & 0\end{bmatrix}, \tag{3.18}$$

$$B_{SWu} = \begin{bmatrix}\frac{I_{ld}}{C_{dc}V_{dc}} & \frac{I_{lq}}{C_{dc}V_{dc}}\end{bmatrix},\ B_{SWdc} = \left[-\frac{1}{C_{dc}}\right]. \tag{3.19}$$

3.1.4 Small-signal model of the dc-load

The dc-load for the active load is a resistor. If a more complex load were to be used, the equations presented in this sub-section would need to be changed accordingly. For a resistive load with a current disturbance, the linearised state-space equations are presented in Equation (3.20) and Equation (3.21).

$$\left[\dot{\Delta i_{dc}}\right] = \overbrace{\left[0\right]}^{A_{DC}}\left[\Delta i_{dc}\right] + \overbrace{\left[0\right]}^{B_{DC}}\left[\Delta v_{dc}\right] + \overbrace{\left[0\right]}^{B_{DCdist}}\left[\Delta i_{dcdist}\right], \tag{3.20}$$

$$\left[\Delta i_{dc}\right] = \overbrace{\left[0\right]}^{C_{DC}}\left[\Delta i_{dc}\right] + \overbrace{\left[\frac{1}{R_{load}}\right]}^{D_{DC}}\left[\Delta v_{dc}\right] + \overbrace{\left[1\right]}^{D_{DCdist}}\left[\Delta i_{dcdist}\right]. \tag{3.21}$$

Subscript 'DC' is used for the coefficients of the state-space equations of the DC load.

3.1.5 Small-signal model of the ac-side LCL filter

To simplify the model, ideal switching is assumed where the output ac-voltage of the switching block is the same as the voltage reference from the current controller ($v_{idq} = v^*_{idq}$). From this assumption, the Inductor-Capacitor-Inductor (LCL) filter is modelled as having two known voltages at either end.

In a standard LCL inverter DQ model, the coupling terms are $-\omega i_{lq}$ for the D axis, and ωi_{ld} for the Q axis. This is not the case for the active load. In an inverter, the current is defined as flowing from the converter-side to the grid-side as it is normally exporting power to the grid. However, since the active load normally sinks power, the positive current is defined as travelling from the grid-side to the converter-side (current direction of the active load is shown in Figure 3.1). The change in definition of current direction changes the sign of the coupling terms from $-\omega_0 i_{lq}$ to $\omega_0 i_{lq}$ for the D axis, and from $\omega_0 i_{ld}$ to $-\omega_0 i_{ld}$ for the Q axis.

The state-space equation of the LCL filter is presented in Equation (3.22) and the variables of Equation (3.22) are defined in Equations (3.23) – (3.24). The subscript 'LCL' is used for the coefficients of the state-space equations of the LCL filter.

$$\begin{bmatrix} \dot{\Delta i_{ldq}} \\ \Delta v_{cdq} \\ \Delta i_{gdq} \end{bmatrix} = A_{LCL} \begin{bmatrix} \Delta i_{ldq} \\ \Delta v_{cdq} \\ \Delta i_{gdq} \end{bmatrix} + B_{LCLu} \left[\Delta v_{idq} \right] + B_{LCLv} \left[\Delta v_{gdq} \right] + B_{LCL\omega} \left[\Delta \omega_{COM} \right]. \quad (3.22)$$

$$A_{LCL} = \begin{bmatrix} -\frac{r_f}{L_f} & \omega_0 & \frac{1}{L_f} & 0 & 0 & 0 \\ -\omega_0 & -\frac{r_f}{L_f} & 0 & \frac{1}{L_f} & 0 & 0 \\ -\frac{1}{C_f} & 0 & 0 & \omega_0 & \frac{1}{C_f} & 0 \\ 0 & -\frac{1}{C_f} & -\omega_0 & 0 & 0 & \frac{1}{C_f} \\ 0 & 0 & -\frac{1}{L_c} & 0 & -\frac{r_c}{L_c} & \omega_0 \\ 0 & 0 & 0 & -\frac{1}{L_c} & -\omega_0 & -\frac{r_c}{L_c}, \end{bmatrix} \quad (3.23)$$

$$B_{LCLu} = \begin{bmatrix} -\frac{1}{L_f} & 0 \\ 0 & -\frac{1}{L_f} \\ 0 & 0 \\ 0 & 0 \\ 0 & 0 \\ 0 & 0 \end{bmatrix}, \; B_{LCLv} = \begin{bmatrix} 0 & 0 \\ 0 & 0 \\ 0 & 0 \\ 0 & 0 \\ \frac{1}{L_c} & 0 \\ 0 & \frac{1}{L_c} \end{bmatrix}, \; B_{LCL\omega} = \begin{bmatrix} I_{lq} \\ -I_{lq} \\ V_{cq} \\ -V_{cd} \\ I_{gq} \\ -I_{gd} \end{bmatrix}. \tag{3.24}$$

3.1.6 Reference frame used to connect the active load to a larger network

To connect multiple models together, all reference frames must be referred to a common reference frame. In this model the output variables of the active load are the grid currents represented as a vector Δi_{gDQ} and the input variable is the input voltage represented as a vector Δv_{gDQ}. The subscript 'DQ' is used for the common reference frame and the subscript 'dq' is used for the local reference frame.

By using the transformation technique mathematically described in Equation (3.25), the small-signal input voltage and output current are obtained. This is shown in Equation (3.27) and Equation (3.28) respectively.

$$\left[f_{DQ}\right] = \left[T_R\right]\left[f_{dq}\right] \tag{3.25}$$

Where T_R is the transform between the common reference frame and the local reference frame of the device and δ_i is the angle between these two reference frames of the ith device.

$$T_R = \begin{bmatrix} \cos(\delta_i) & -\sin(\delta_i) \\ \sin(\delta_i) & \cos(\delta_i) \end{bmatrix} \tag{3.26}$$

$$\left[\delta v_{gdq}\right] = \left[T_R\right]^{-1}\left[\delta v_{gDQ}\right] \tag{3.27}$$

$$\left[\delta i_{gDQ}\right] = \left[T_R\right]\left[\delta i_{gdq}\right] \tag{3.28}$$

3.1.7 Complete small-signal model of the active load

By combining the state-space models of the dc-voltage controller (Equation (3.1)), the ac-voltage controller (Equaiton (3.8)), the switching bridge (Equation (3.16)), the dc-load (Equation (3.20)), ac-side LCL filter (Equation (3.22)), and the reference frame coupling (Equation (3.25)) the complete rectifier model is formed. The complete model is shown in Equation (3.29), and has 10 states, 6 inputs and 3 outputs. All equations are shown with an i subscript to allow for N_i multiple rectifiers to be coupled to a larger circuit model. The subscript 'AL' is used for the coefficients of the state-space equations of the active load.

$$\begin{aligned}\begin{bmatrix}\dot{\Delta x_{ALi}}\end{bmatrix} = A_{ALi}\begin{bmatrix}\Delta x_{ALi}\end{bmatrix} + B_{ALui}\begin{bmatrix}\Delta v_{dc}^{*} \\ \Delta i_{lq}^{*}\end{bmatrix} + B_{ALvi}\begin{bmatrix}\Delta v_{gDQ}\end{bmatrix} \\ + B_{AL\omega i}\begin{bmatrix}\Delta \omega_{com}\end{bmatrix} + B_{ALdci}\begin{bmatrix}\Delta\ i_{dc}\end{bmatrix},\end{aligned} \tag{3.29}$$

$$\begin{aligned}\begin{bmatrix}\Delta i_{gDQi}\end{bmatrix} &= C_{ALci}\begin{bmatrix}\Delta x_{ALi}\end{bmatrix}, \\ \begin{bmatrix}\Delta v_{dci}\end{bmatrix} &= C_{ALdci}\begin{bmatrix}\Delta x_{ALi}\end{bmatrix}.\end{aligned} \tag{3.30}$$

The states of the active load Δx_{ALi} are shown in Equation (3.31), the inputs of the active load are shown in Equation (3.32) and the coefficients A_{ALi}, B_{ALui}, B_{ALvi}, $B_{AL\omega i}$, B_{ALdci}, C_{ALci}, C_{ALdci} are shown in Equations (3.33) – (3.37).

$$\Delta x_{ALi} = \begin{bmatrix}\Delta\phi_{dci} \mid & \Delta\gamma_{dqi} \mid & \Delta i_{ldqi} & \Delta v_{cdqi} & \Delta i_{gdqi} \mid & \Delta v_{dci}\end{bmatrix}^{T}. \tag{3.31}$$

$$\Delta u_{ALi} = \begin{bmatrix}\Delta v_{d}^{*}c \mid & \Delta i_{lq} \mid & \Delta i_{dcdist}\end{bmatrix}^{T}. \tag{3.32}$$

The matrices A_{ALi}, B_{ALui}, B_{ALvi}, $B_{AL\omega i}$, B_{ALdci}, C_{ALci}, C_{ALdci} form Equation (3.29) and Equation (3.30) are defined in Equations (3.33) – (3.37).

$$A_{ALi} = \begin{bmatrix} 0 & 0 & 0 & B_{V2} \\ B_{C1}C_V & 0 & B_{C2} & B_{C1}D_{V2} \\ B_{LCLu}D_{C1}C_V & B_{LCLu}C_C & A_{LCL} + B_{LCLu}D_{C2} & B_{LCLu}D_{C1}D_{V2} \\ B_{SWu}D_{C1}C_V & B_{SWu}C_C & B_{SW} + B_{LCLu}D_{C2} & \begin{pmatrix} A_{SW} \\ +B_{SWu}D_{C1}D_{V2} \\ +B_{SWdc}D_{DCu} \end{pmatrix} \end{bmatrix}_{10\times 10}, \tag{3.33}$$

$$B_{ALui} = \begin{bmatrix} B_{V1} \\ B_{C1}D_{V1} \\ B_{LCLu}D_{C1}D_{V1} \\ B_{SWu}D_{C1}D_{V1} \end{bmatrix}_{10\times 2}, \; B_{ALvi} = \begin{bmatrix} 0 \\ 0 \\ B_{LCLv}T_R^{-1} \\ 0 \end{bmatrix}_{10\times 2}, \tag{3.34}$$

$$B_{AL\omega i} = \begin{bmatrix} 0 \\ 0 \\ B_{LCL\omega} \\ 0 \end{bmatrix}_{10\times 1}, \; B_{ALdci} = \begin{bmatrix} 0 \\ 0 \\ 0 \\ B_{SWdc} \end{bmatrix}_{10\times 1}, \tag{3.35}$$

$$C_{ALci} = \begin{bmatrix} 0 & 0 & \begin{bmatrix} 0 & 0 & T_R \end{bmatrix} & 0 \end{bmatrix}, \tag{3.36}$$

$$C_{ALdci} = \begin{bmatrix} 0 & 0 & 0 & C_{SW} \end{bmatrix}. \tag{3.37}$$

3.2 Analysis of the Active Load

The properties of the active load are detailed in Table 3.1. There are two parameters detailed in Table 3.1, circuit parameters and controller parameters. The physical circuit parameters of the active load were based on the laboratory equipment such that the model could be verified.

Table 3.1: Properties of the active load

Active Load Circuit			
Parameter	***Value***	***Parameter***	***Value***
L_f	2.3 mH	r_f	0.1 Ω
L_c	0.93 mH	r_c	0.03 Ω
C_f	8.8 μH	C_{dc}	2040 μF
R_{load}	70 Ω		
Controller			
Parameter	***Value***	***Parameter***	***Value***
K_{pv}	0.5	K_{pc}	15
K_{iv}	150	K_{ic}	30,000

Table 3.2: Steady-state values of the active load

Steady State Voltages			
Parameter	***Value***	***Parameter***	***Value***
V_{gd}	381.05 V	V_{gq}	0 V
V_{cd}	381.03 V	V_{cq}	-5.5350 V
V_{id}	378.31 V	V_{iq}	-3.9930 V
V_{dc}	700 V_{dc}		
Steady State Current			
Parameter	***Value***	***Parameter***	***Value***
I_{gd}	18.833 A	I_{gq}	0.0229 A
I_{ld}	18.831 A	I_{lq}	-1.000 A
I_{dc}	10.000 A		
Steady State Power and Frequency			
Parameter	***Value***	***Parameter***	***Value***
P	7176.0 W	Q	113.00 VAr
f	50 Hz		

Gains in the controllers and subsequently the controller damping and bandwidth were chosen to provide the active load with good performance and be similar to the controller damping and bandwidth of the inverter sources. This was chosen to excite any interactions between the inverter controllers and active load controller. The properties of the inverter interfaced generation are described in [20].

Steady state values for the active load are shown in Table 3.2. These values were obtained from a time-series simulation in Matlab Simulink but could have been obtained from a load-flow calculation.

3.2.1 Participation analysis of the active load

Figure 3.4 shows the eigenvalue plot of the active load model, the values for which these were calculated from the A-matrix of the active load in Equation (3.33). A Matlab script was used to generate the eigenvalues and the eigenvalue plot. This Matlab code for Figure 3.4 is shown in Appendix A. Three groups of eigenvalues labelled 'A1', 'A2' and 'A3' were identified from Figure 3.4 and participation analysis was used to identify which states the three eigenvalue groups were associated with.

The active load used for this study had a power rating of $10kW$. Other active loads may be larger or may be smaller. If the active load were larger, then the resistance of the active load would decrease and the inductance of the active load would increase. This would cause the magnitude of the eigenvalues of the active load to decrease and the eigenvalues would move towards the positive-real axis. Moving the eigenvalues to the right would cause the dynamics of the active load to be slower. As increasing the size of the active load would cause the eigenvalues to move towards the right, decreasing the size of the active load would cause the eigenvalues to move towards the left. This is because the resistance of the active load would be larger and the inductance of the active load would be smaller. Moving the eigenvalues to the left would cause the dynamics of the active load to increase.

Figure 3.5 shows the participation analysis of the eigenvalues of the active load model in Figure 3.4. The active load model has 10 states and each state is listed on the x-axis of Figure 3.5 and described in Table 3.3. Each state will have a participation value for each eigenvalue in Figure 3.5. Therefore, each of the 10 states will have 10 participation factors that associate each of the states to each of the eigenvalues.

In Figure 3.5 the 10 states have been grouped into three groups labelled 'A1', 'A2', 'A3'. Group 'A1' contains two eigenvalues and groups 'A2' and 'A3' each contain four eigenvalues. Participation factors for each eigenvalue in each group is found for each state and then summed to create the resultant participation factor. For example, the participation factor that relates group 'A1' (which contains two eigenvalues) with state 1 is the participation factor of the first eigenvalue for state 1 summed with the participation value for the second eigenvalue for state 1.

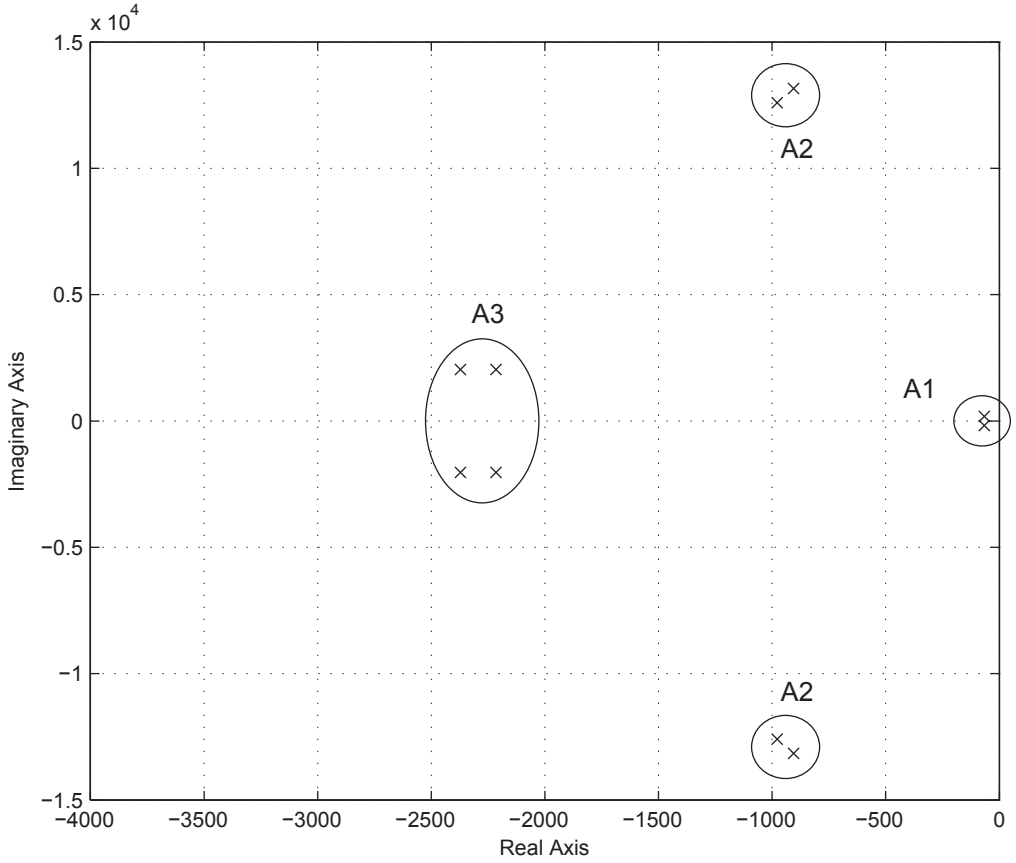

Figure 3.4: Eigenvalues of the active load indicating the three eigenvalue groups

The participation factors for each group of eigenvalues ('A1', 'A2' and 'A3') are shown in Figure 3.5. If none of the eigenvalues in a particular group do not participate in a particular state, there is no 'bar' for state in Figure 3.5. For example, none of the eigenvalues in group 'A1' participate in states 5, 6 and 7. However eigenvalues in groups 'A2' and 'A3' do participate in states 5, 6 and 7. The higher the participation from one of the three groups to a state, the more coupling there is between the eigenvalues in that group and the state. For example the eigenvalues in group 'A1' participate most with states 1 and 10.

From Figure 3.5, it may be seen that the group of eigenvalues 'A1' have high participation factors for states 1 and 10 which are the integrator of the dc-voltage controller and the states of the dc-capacitor. The group labelled 'A2' have high participation factors for states 6 to 9 which are the filter capacitor (C_f) and the coupling inductor (L_c) in the LCL filter of the active load. The group labelled 'A3' have high participation factors for states 2 to 5 which are the ac-current

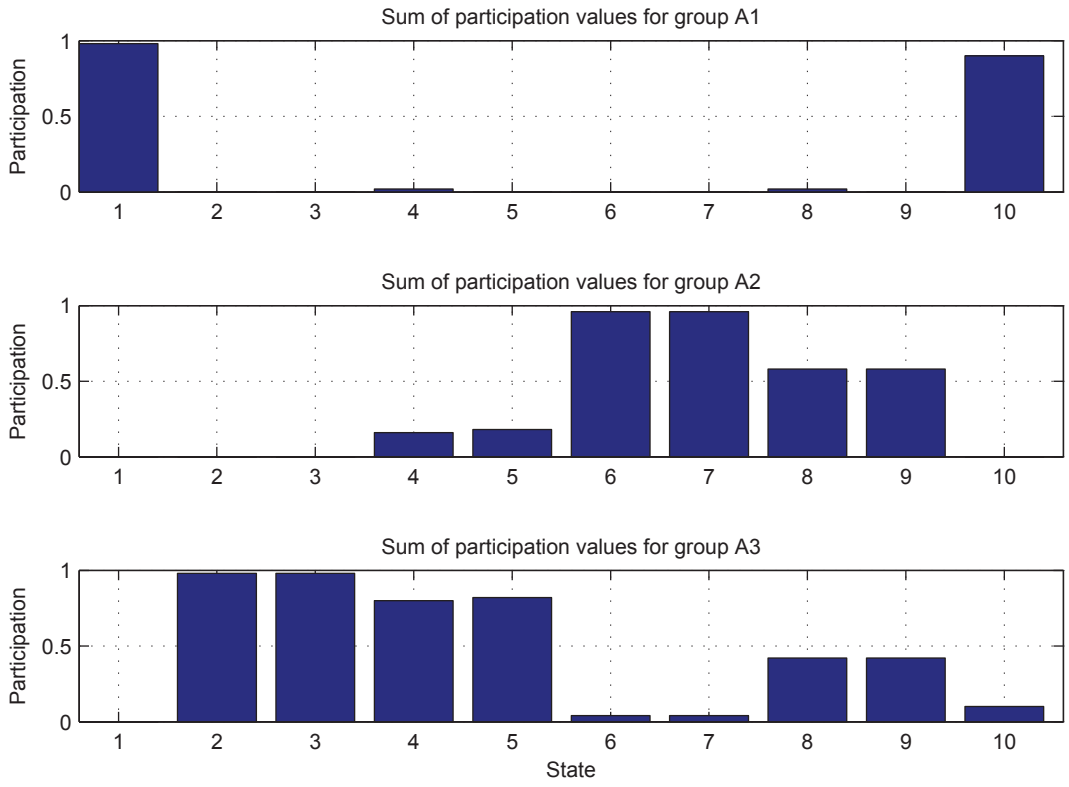

Figure 3.5: Participation values of states for the three eigenvalue groups

controller and the filter inductor (L_f) and there is also a small participation in states 8 and 9 which are the ac-current i_g within the coupling inductor L_c.

The eigenvalues in groups 'A1', 'A2' and 'A3' are the low-frequency, mid-frequency and high-frequency modes of the active load. From the participation analysis, the low-frequency modes are most sensitive to the DC-side of the active load. The mid-frequency modes are most sensitive to the filter capacitor and coupling inductor within the LCL filter. Finally, the high-frequency modes are most sensitive to the ac-current controller. Therefore changing the gains in the DC controller and ac-controller will most likely impact the low-frequency modes and high-frequency modes respectively. In terms of stability, the low frequency modes are most likely to cause the active-load to become unstable.

Table 3.3: List of the active load states

State Number	*State Name*	*State Symbol*
1	Integrator of the dc-voltage controller	$\Delta\phi_{dc}$
2	Integrator of the d-axes of the ac-current controller	$\Delta\gamma_d$
3	Integrator of the q-axes of the ac-current controller	$\Delta\gamma_q$
4	Current of the d-axes of the filter inductor	Δi_{ld}
5	Current of the q-axes of the filter inductor	Δi_{lq}
6	Voltage of the d-axes of the filter capacitor	Δv_{cd}
7	Voltage of the q-axes of the filter capacitor	Δv_{cq}
8	Current of the d-axes of the coupling inductor	Δi_{gd}
9	Current of the q-axes of the coupling inductor	Δi_{gq}
10	Voltage of the dc-capacitor	Δv_{dc}

3.2.2 Effect of the integrator gain of the dc-voltage controller on the low-frequency modes

Figure 3.6 plots the the low-frequency eigenvalues when the integrator gain of the dc-voltage controller is increased. The figure shows that when the integrator gain in increased, the eigenvalues move towards the unstable region making the active-load more oscillatory and eventually unstable. The eigenvalues are in the right-half plane and hence unstable when the integrator gain is above 2037. The low-frequency eigenvalues of the active load are very sensitive to the integrator gain of the DC voltage controller. From Figure 3.5 the low-frequency eigenvalues are highly sensitive to the states of the dc-voltage controller and dc-capacitor. Hence, in this system the dc-voltage controller and dc-capacitor is most critical for system stability.

3.2.3 Effect of the integrator gain and proportional gain of the dc-voltage controller on the modes

Figure 3.7 plots the eigenvalues when the integrator gain and proportional gain of the dc-voltage controller is increased. The ratio of the integrator gain and proportional gain is maintained at

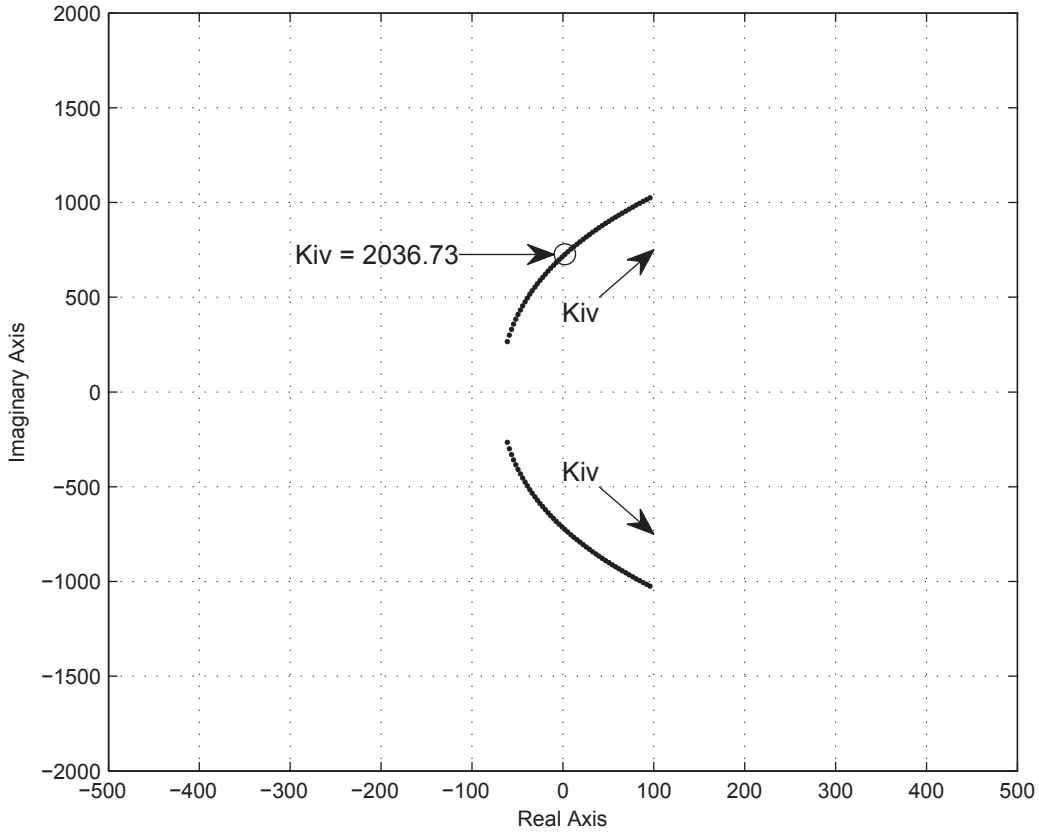

Figure 3.6: Trace of low-frequency modes as a function of dc-voltage controller integrator gain: $300 \leq K_{iv} \leq 4000$

the design value of $\frac{1}{300}$. The figure shows that when the integrator gain and proportional gain are increased, the mid-frequency eigenvalues and not the low frequency eigenvalues, move towards the unstable region making the active-load more oscillatory and eventually unstable. The eigenvalues are in the right-half plane and hence unstable when the integrator gain is 3070 and the proportional gain is 10.23. In Figure 3.5 the mid-frequency eigenvalues are sensitive to the ac-current controller of the active load. However changing the gains of the dc-voltage controller has caused an instability in the eigenvalues originally associated with the ac-current controller. This further shows that the dc-voltage controller is most critical for system stability and care must be used when choosing the gain values of the dc-voltage controller.

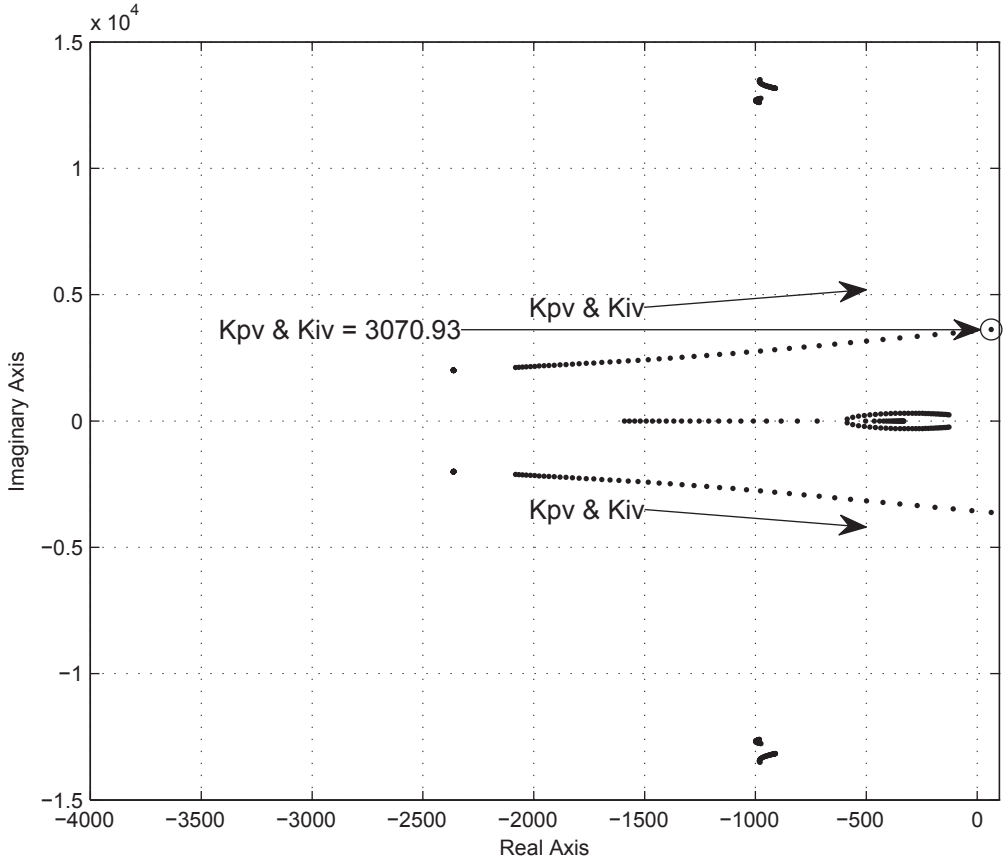

Figure 3.7: Trace of low and high frequency modes as a function of dc-voltage controller integrator and proportional gain: $300 \leq K_{iv} \leq 4000$ where $K_{pv} = \frac{1}{300} K_{iv}$

3.2.4 Effect of the integrator gain of the ac-current controller on the high-frequency modes

Figure 3.8 plots the eigenvalues when the integrator gain of the ac-current controller is increased. The figure shows that when the integrator gain is increased the mid-frequency eigenvalues move towards the unstable region and become more oscillatory. However the movement of the eigenvalues is small compared to the size of the gain change and the eigenvalues would require a significantly large gain before the active load became unstable. From this it is possible to conclude that the system is not very sensitive to changes in the integrator gain of the ac-current controller and it is not most critical for system stability. It is also noted that the increase in integrator gain does not have much influence in the low-frequency modes of the active load.

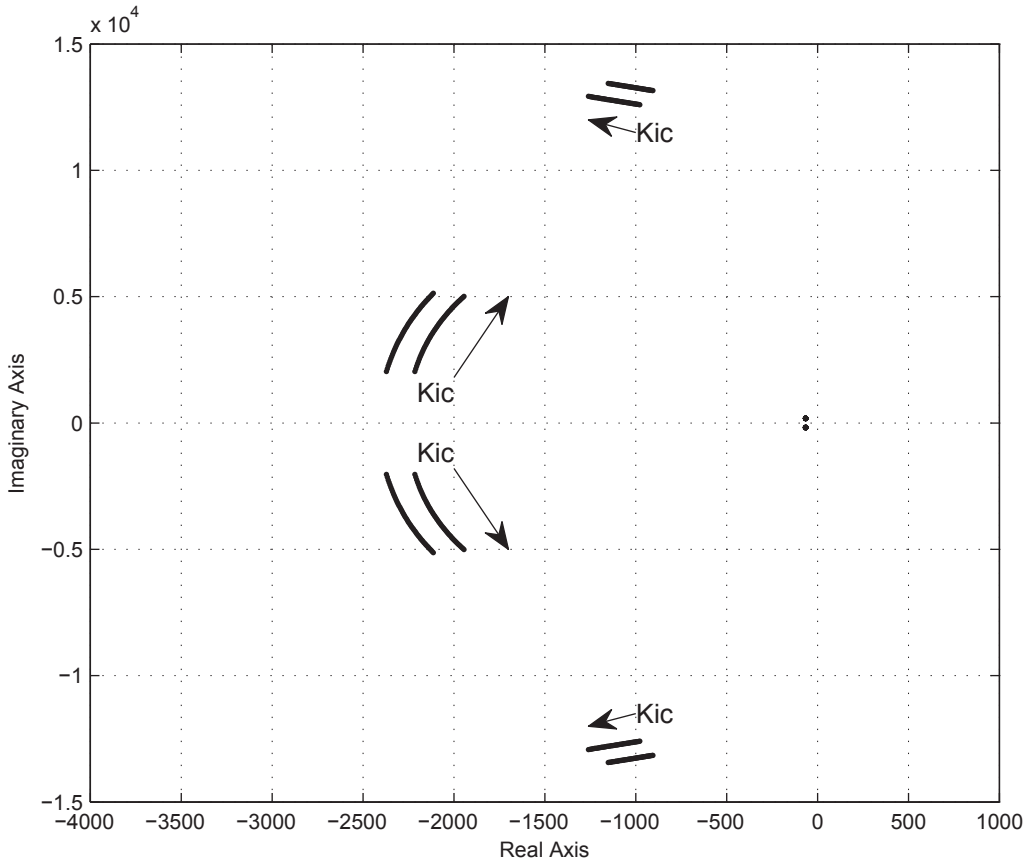

Figure 3.8: Trace of high-frequency modes as a function of ac-current controller integrator gain: $30,000 \leq K_{ic} \leq 100,000$

3.2.5 Effect of the coupling inductor on the high-frequency modes

Figure 3.9 plots the eigenvalues when the value of inductance of the coupling inductor is increased. The figure shows that the increase in inductance causes the eigenvalues at the top to become better damped and the ac-current controller eigenvalues to become more oscillatory. This suggests that the increase of inductance causes the current to become more difficult for the current controller to regulate, however the LCL filter becomes less oscillatory. A larger inductance increases the stability margin of the filter but reduces the stability margin of the ac-current controller.

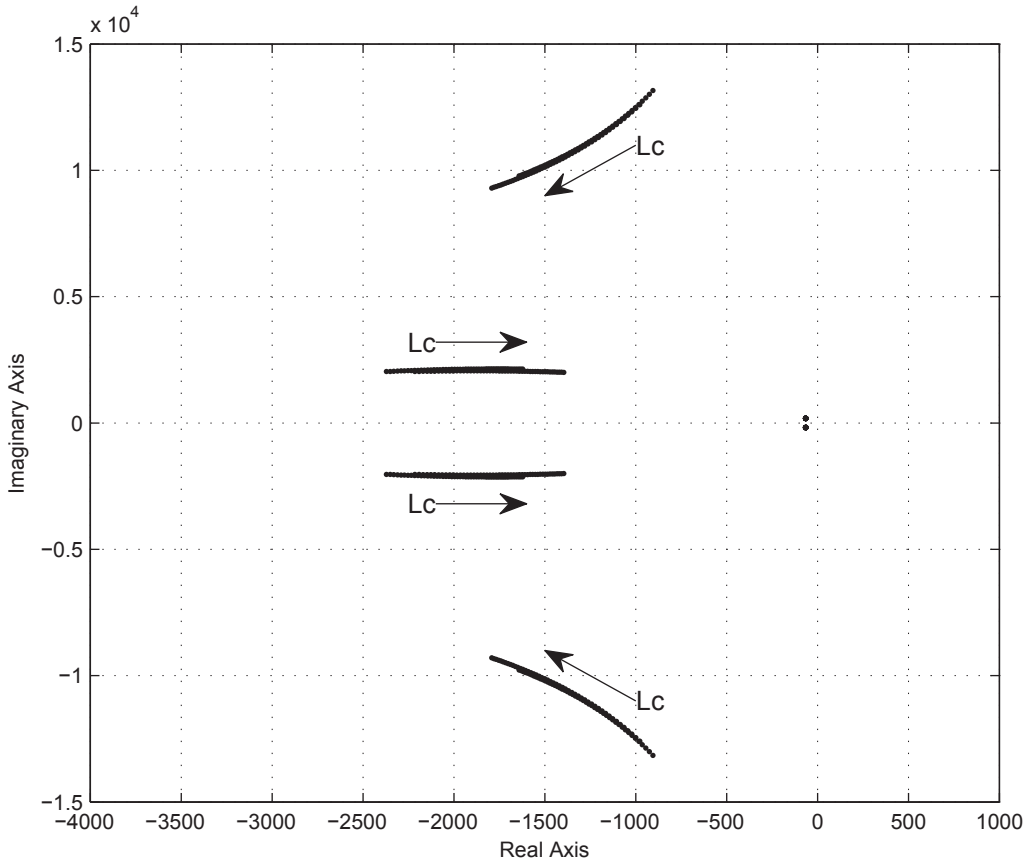

Figure 3.9: Trace of high-frequency modes as a function of the coupling inductor: $0.93mH \leq L_c \leq 2.35mH$

3.2.6 Effect of the dc-load on the low-frequency modes

Figure 3.10 plots the low-frequency eigenvalues when the dc-load is increased (resistance of the dc-load is decreased). It can be seen that the decrease in resistance has a very slight effect and causes the active-load to become a little more damped.

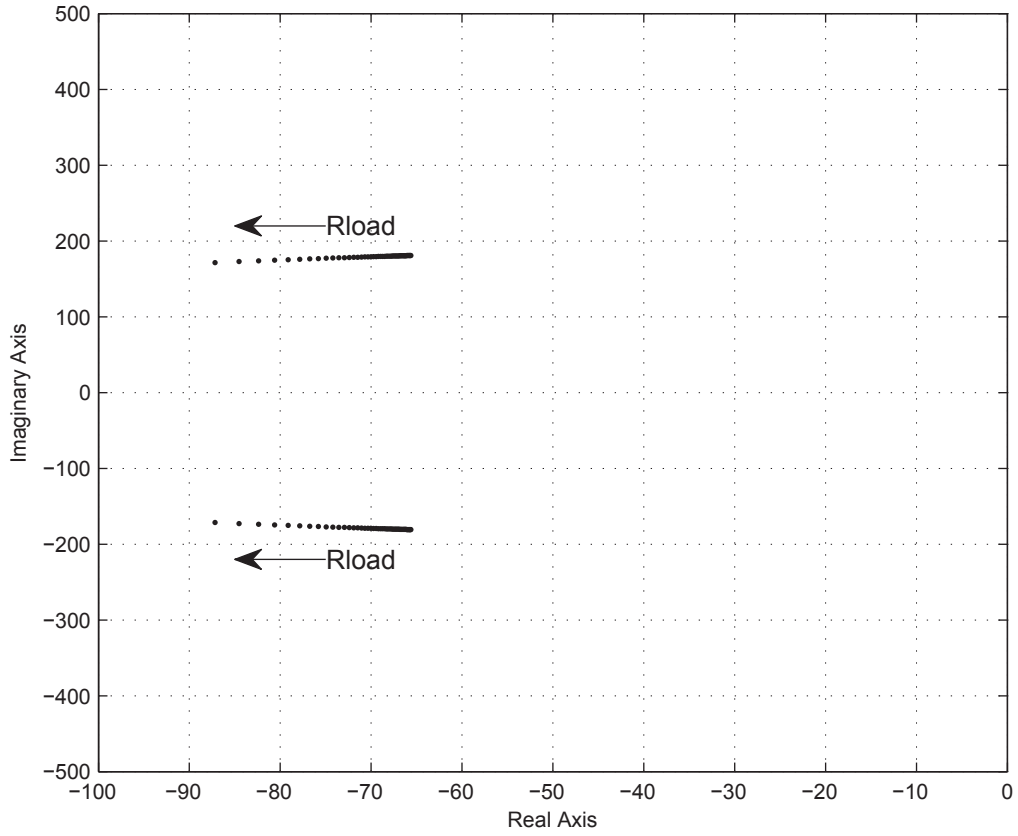

Figure 3.10: Trace of low-frequency modes as a function of the dc-load: $67\Omega \geq R_{load} \geq 10\Omega$

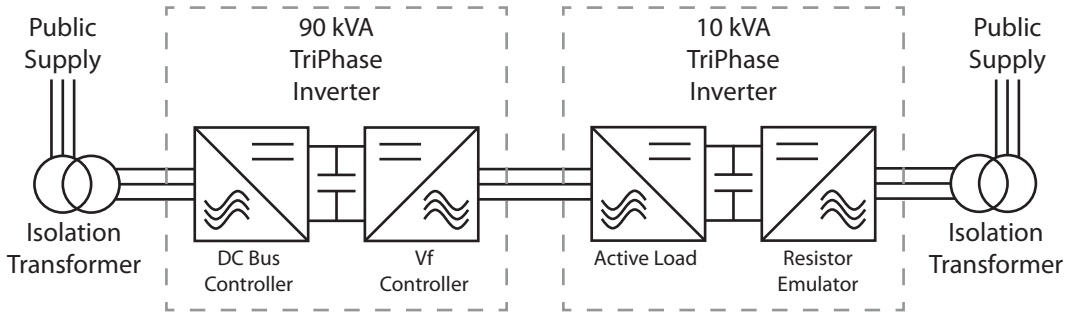

Figure 3.11: Experimental setup of the active load

3.3 Verification of the Active Load

The active load, as described in Section 3.1 and analysed in Section 3.2, was programmed on one converter that consisted of two back-to-back inverters. More information about the experimental inverter is in Appendix B. The first inverter in the back-to-back configuration was configured as the active load and the second inverter was programmed to emulate a DC resistor and used to export the power drawn from the active load back to the public supply.

There were two aims of the experiment. The first was to verify the small-signal model against an experimental set-up and show that the small-signal model is a valid representation of the active load. The second aim was to experimental identify the low frequency modes and high-frequency modes by perturbing the active load and observing the resulting output oscillations.

3.3.1 Experimental set-up

Experimental validation of the active load model was tested using an experimental inverter as shown in Figure 3.11. The ac-side of the inverter used as the active load was connected to a 90 Kilovolt Ampere (kVA) inverter that regulated the ac supply voltage. The dc-side of the inverter used as the active load was connected to an other inverter via a dc-bus. This second inverter was programmed to emulate a DC resistor and used to export the power drawn from the active load back to the public supply.

The DC resistor was emulated by programming the inverter to control the AC-grid current where the reference to the AC-grid current controller uses Equation (3.46). A PI controller

was used to control the required AC-gird current and this was the same design as the AC-current controller in the active load. Ideally, a DC resistance would have been used and no emulation would have been required, however this would have required modification to the TriPhase inverter.

To emulate R_{dc}, the inverter needs to be controlled to have an ohmic characteristic where the dc-current must be proportional to the dc-current as shown in Equation (3.38). Therefore v_{dc} or i_{dc} needs to be controlled to satisfy Equation (3.39) which links R_{dc}, v_{dc} and i_{dc}. For the active load experiment v_{dc} is being controlled by the active load. Therefore the DC emulator is only able to control i_{dc}. However, the experimental set-up does not contain an i_{dc} measurement sensor and this variable is calculated by assuming the inverter switching bridge is ideal and the power on the dc-side is equal to the power on the ac-side as in Equation (3.40).

$$\frac{di}{dv} = \frac{1}{R} \tag{3.38}$$

$$i_{dc} = \frac{v_{dc}}{R_{dc}} \tag{3.39}$$

$$P_{dc} \approx P_{ac} \tag{3.40}$$

Assuming the ac-side power (Equation (3.41)) is equal to the dc-side power (Equation (3.42)), then v_{dc} and i_{dc} may be linked to v_d, v_q, i_d and i_q. The variables v_q and i_q are assumed to be zero. The PPL in the DC emulator aligns the phase angle of the inverter to the mains frequency by controlling v_q to zero. Using the ac-current controller, the variable i_q can be controlled to zero. This reduces the power identity of the switching bridge to Equation (3.43).

$$P_{ac} = v_d i_d + v_q i_q \tag{3.41}$$

$$P_{dc} = v_{dc} i_{dc} \tag{3.42}$$

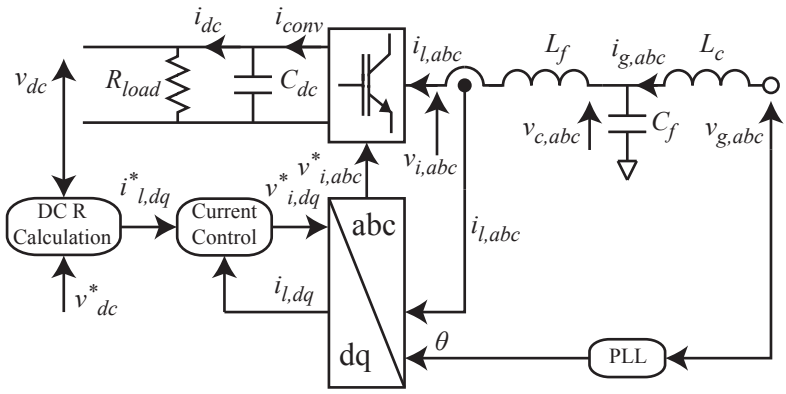

Figure 3.12: Control of the inverter that emulates the dc resistor

$$v_{dc} i_{dc} \approx v_d i_d \tag{3.43}$$

Rearranging Equation (3.43), such that it can be used at the input to the ac-current controller, the equation becomes Equation (3.45). Substituting Equation (3.39) into Equation (3.44), yields Equation (3.45) which can be simplified to Equation (3.46). Equation (3.46) is the equation used in the R_{dc} emulator block in Figure 3.12 as it measures v_{dc} and sets i_d such that the impedance of the inverter on the dc-side is approximately R_{dc}

$$i_d \approx i_{dc} \frac{v_{dc}}{v_d} \tag{3.44}$$

$$i_d \approx \frac{v_{dc}}{R_{dc}} \frac{v_{dc}}{v_d} \tag{3.45}$$

$$i_d \approx \frac{1}{R_{dc}} \frac{v_{dc}^2}{v_d} \tag{3.46}$$

3.3.2 Experimental tests

Two experimental tests were conducted. The first test perturbed the reference to R_{dc}, the dc emulator, and the second test perturbed the ac-voltage to the active load. The aim of perturbing

the reference to R_{dc} was to observe the low-frequency oscillations from the dc-controller. The aim of perturbing the reference to the ac-supply voltage was to observe the high-frequency oscillations from the ac-current controller. Both the low-frequency and high-frequency modes were analysed in Section 3.2.

Both experimental test were simulated using the small-signal model developed in Section 3.1. The aim of this was to verify the small-signal model and show that it provides a good approximation to the experimental active load.

All experimental components have tolerances and so are expected to differ from the values assumed in the model. Approximation errors may also be caused by the state-space model being a linear model of a non-linear system. The linear model is an accurate representation at the steady-state operation point. However once the model is displaced from this operating point by a large deviation, the linear model of the non-linear system is no longer a valid model. All perturbations were reasonably small such that the linear model remained a good approximation of the non-linear model.

3.3.3 Experimental results

Figure 3.13 shows the dc-bus voltage and the ac-current of the active load in response to a DC load step. The experimental results are the internal variables of the converter that were captured by using the on-board Digital-to-Analogue (D/A) converter. The experimental data shows the low-frequency modes of the active load which are in good agreement with the state-space model. Both the ac-current controller and the dc-voltage controller show the low-frequency modes but the participation analysis showed that the low-frequency modes were associated with only the dc-voltage controller. This is because the output of the dc-voltage controller is connected to the input of the ac-current controller as shown in Figure 3.1. When there is a low-frequency oscillation on the dc-bus voltage, the dc-voltage controller may only change the ac-current reference in order to damp the oscillations. The change in ac-current reference is then seen on the ac-current measurement as the ac-current controller follows the ac-current reference.

From the participation analysis in Section 3.2.1, the low-frequency modes are associated with the dc-voltage controller as indicated by circle ‘A1’ in Figure 3.4. In group ‘A1’ shown in

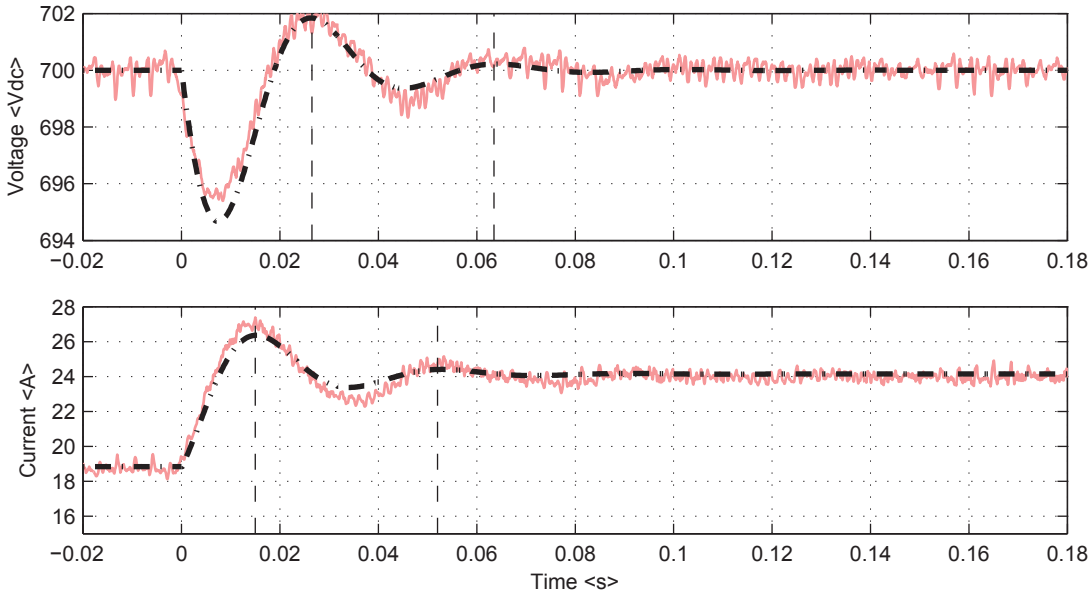

Figure 3.13: Comparison of experimental data and small signal model data for the dc-voltage and ac-current of the active load when subject to a dc-load perturbation. The small-signal model data is shown by the black dotted line and the experimental data is shown by the solid red line.

Figure 3.4, the low-frequency modes are at a frequency of 28 Hz. To measure the frequency from the experimental results of the low-frequency mode, two peaks within the oscillation (indicated by the dotted lines) are measured in Figure 3.14. These peaks have a time period of 0.037 s which corresponds to a frequency of 26.5 Hz. From this it is concluded that the low-frequency mode, as predicted by the participation analysis, of 28 Hz is a good match.

In Figure 3.14, the response of the active load to a three phase voltage perturbation of 381 V to 340 V is also shown. It is seen that when the ideal voltage is decreased, the current demand of the active load increases. This demonstrates the negative impedance characteristic of the active load. Also, from the voltage perturbation, the high-frequency response of the active load is observed within the ac-grid current which is indicated by '1' in Figure 3.14 but is not seen in the dc-bus voltage. This is because the high-frequency modes are strongly associated with the AC-current controller. The grid voltage perturbation has also excited the low-frequency modes in both the AC-current controller and the dc-voltage controller. From Figures 3.13 – 3.14, the state-space model is in good agreement with the experimental data.

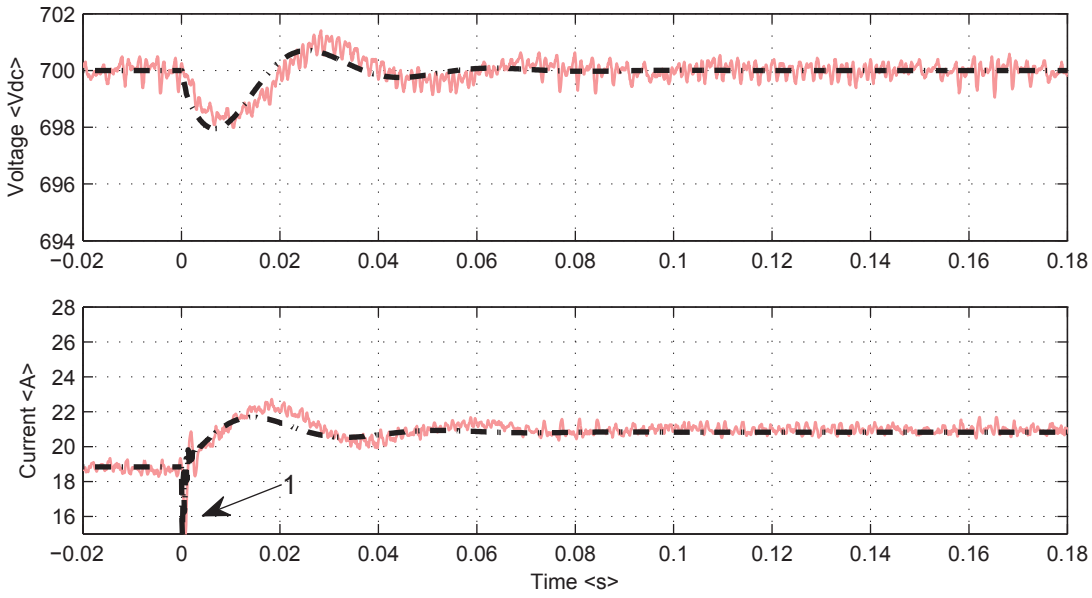

Figure 3.14: Comparison of experimental data and small signal model data for the dc-voltage and ac-current of the active load when subject to an ac-voltage perturbation. The small-signal model data is shown by the black dotted line and the experimental data is shown by the solid red line.

3.4 Modelling the Active Load in the Microgrid

When connecting the active load or any sub-system model to the microgrid model, that active load or subsystem model must follow the same rules and be in an appropriate format. Sections 3.4.1 – 3.4.6 describe the procedure and Section 3.4.7 follows this procedure described and mathematically connects the active load to the microgrid.

3.4.1 General Model Procedure

Each system, whether it be an inverter, line, load, or active load, will be referred to as a device or abbreviated to '*dev*'. All devices of a similar type (inverter, line, load, active load) will be grouped into the same set of state-space equations and will be denoted with the abbreviation '*DEV*'. This set will be referred to as a group of devices of the same type. Every device will connect to a node where the nodal voltage is calculated. Each group must be written in the format of Equation (3.47). All devices in the state-space model have current as the output and voltage as the input.

$$\begin{aligned}\frac{d}{dt}[\Delta x_{DEV}] &= A_{DEV}[\Delta x_{DEV}] + B_{DEVu}[\Delta u_{DEV}] \\ &\quad + B_{DEVv}[\Delta v_{DEV}] + B_{DEV\omega}[\Delta \omega_{COM}].\end{aligned} \tag{3.47}$$

Each matrix in Equation (3.47) is listed in Equations (3.48) – (3.53). The equations describe a group of N_i devices that are of the same type in a system of N_j nodes. Each device in the group has N_s states, N_u inputs and N_o outputs. It is noted that not all groups will have a B_{DEVu}; if this is the case, this matrix must be ignored or set to zero.

$$\Delta x_{DEV} = \begin{bmatrix} \Delta x_{dev1} \\ \Delta x_{dev2} \\ \vdots \\ \Delta x_{devN_i} \end{bmatrix}_{N_i N_s \times 1}, \; \Delta u_{DEV} = \begin{bmatrix} \Delta u_{dev1} \\ \Delta u_{dev2} \\ \vdots \\ \Delta u_{devN_i} \end{bmatrix}_{N_i N_u \times 1}, \tag{3.48}$$

$$\Delta v_{DEV} = \begin{bmatrix} \Delta v_{dev1} \\ \Delta v_{dev2} \\ \vdots \\ \Delta v_{devN_i} \end{bmatrix}_{2N_j \times 1}, \tag{3.49}$$

$$A_{DEV} = \begin{bmatrix} A_{dev1} & 0 & \cdots & 0 \\ 0 & A_{dev2} & \cdots & 0 \\ \vdots & \vdots & \ddots & \vdots \\ 0 & 0 & \cdots & A_{devN_i} \end{bmatrix}_{N_i N_s \times N_i N_s}, \tag{3.50}$$

$$B_{DEVu} = \begin{bmatrix} B_{devu1} & 0 & \cdots & 0 \\ 0 & B_{devu2} & \cdots & 0 \\ \vdots & \vdots & \ddots & \vdots \\ 0 & 0 & \cdots & B_{devuN_i} \end{bmatrix}_{N_i N_s \times N_i N_u}, \tag{3.51}$$

$$B_{DEV\omega} = \begin{bmatrix} \Delta B_{dev\omega 1} \\ \Delta B_{dev\omega 2} \\ \vdots \\ \Delta B_{dev\omega N_i} \end{bmatrix}_{N_i N_s \times 1}. \tag{3.52}$$

3.4.2 Input Voltage Mapping

Matrix B_{DEVv} is a special case since it maps the device input voltage to the correct node. For example, if an i^{th} source or i^{th} load is connected to the j^{th} node, the element $B_{DEVv}(i,j)$ will be B_{DEVvi} and all other elements in that row will be zero. Equation (3.53) shows the case when three devices ($N_i = 3$) are connected to nodes 1, 2 and 3 respectively of a three node system ($N_j = 3$).

$$B_{DEVv} = \begin{bmatrix} B_{devv1} & 0 & 0 \\ 0 & B_{devv2} & 0 \\ 0 & 0 & B_{devv3} \end{bmatrix}_{3N_s \times (2 \times 3)}. \tag{3.53}$$

If a device connects to two nodes, for example the i^{th} line is connected to ja^{th} and jb^{th} node, the matrix will have the following elements within the matrix. Element $B_{DEVv}(i, ja)$ will be B_{DEVvai}, element $B_{DEVv}(i, jb)$ will be B_{DEVvbi}, and all other elements in that row will be zero. Equation (3.54) shows the case when two lines ($N_i = 2$) are connected to nodes 1,2 and 2,3 respectively of a three node system ($N_j = 3$).

$$B_{DEVv} = \begin{bmatrix} B_{devv11} & B_{devv21} & 0 \\ 0 & B_{devv12} & B_{devv22} \end{bmatrix}_{2N_s \times (2\times 3)} . \tag{3.54}$$

3.4.3 Output Variables to Outside the Microgrid

Not all groups will need to output their variables outside the microgrid. For the groups that this is relevant to, they must follow Equation (3.55).

$$[\Delta y_{DEV}] = C_{DEV}[\Delta x_{DEV}] + D_{DEVu}[\Delta u_{DEV}]. \tag{3.55}$$

Where C_{DEV} and D_{DEV} are stated in Equation (3.56)

$$C_{DEV} = \begin{bmatrix} C_{dev1} & 0 & \cdots & 0 \\ 0 & C_{dev2} & \cdots & 0 \\ \vdots & \vdots & \ddots & \vdots \\ 0 & 0 & \cdots & C_{devi} \end{bmatrix}_{N_i N_o \times N_i N_s} , \tag{3.56}$$

$$D_{DEV} = \begin{bmatrix} D_{dev} & 0 & \cdots & 0 \\ 0 & D_{dev} & \cdots & 0 \\ \vdots & \vdots & \ddots & \vdots \\ 0 & 0 & \cdots & D_{dev} \end{bmatrix}_{N_i N_o \times N_i N_u} . \tag{3.57}$$

3.4.4 Output Current Mapping

Each group must output its current as in Equation (3.58).

$$[\Delta i_{DEV}] = \Delta C_{DEVc}[\Delta x_{DEV}]. \tag{3.58}$$

Where C_{DEV} is stated in Equation (3.59)

$$C_{DEVc} = \begin{bmatrix} C_{devc1} & 0 & \cdots & 0 \\ 0 & C_{devc2} & \cdots & 0 \\ \vdots & \vdots & \ddots & \vdots \\ 0 & 0 & \cdots & C_{devcN_i} \end{bmatrix}_{2N_i \times N_i N_s} . \tag{3.59}$$

Each group must have an output current mapping matrix, M_{DEV}, that connects the output current to a node and includes a large virtual resistance R_N, to define the voltage at the node. All devices in the microgrid will either export or import current to or from the node the device is connect to. Export current from the node is represented with a minus and import current to the node is represented with a plus. For this mode, the voltage at the *ith* node is defined by:

$$v_{gDi} = R_N \left(i_{invDi} - i_{loadDi} - i_{recDi} + i_{distDi} + i_{lineDi}\right) \tag{3.60}$$

$$v_{gQi} = R_N \left(i_{invQi} - i_{loadQi} - i_{recQi} + i_{distQi} + i_{lineQi}\right) \tag{3.61}$$

Using the matrix M, the node voltage is defined as,

$$\begin{aligned} [v_{gDQ}] \; &= M_{INV}\left[i_{invDi}\right] + M_{LOAD}\left[i_{loadDi}\right] + M_{REC}\left[i_{recDi}\right] \\ &+ M_{DIST}\left[i_{distDi}\right] + M_{NET}\left[i_{lineDi}\right] \end{aligned} \tag{3.62}$$

To follow the current definitions stated, the elements in the M matrix are either 0, R_N or $-R_N$. If an element is 0 there is no connection, if an element is R_N the current is defined to be flowing into the node, and if an element is -R_N the current is defined to be flowing out of the node. For example, if an i^{th} source providing current or i^{th} load drawing current is connected to the j^{th} node, the element $M_{DEV}\,(j,i)$ will be R_N or -R_N respectively. All other elements in that row will be zero. Equation (3.63) shows the case when two devices ($N_i = 2$) with two

states ($N_s = 2$) each are connected to nodes 1 and 3 respectively of a three node system. Each device is defined to be drawing current from the node.

$$M_{DEV} = \begin{bmatrix} \begin{bmatrix} -R_N & 0 \\ 0 & -R_N \end{bmatrix} & 0 \\ 0 & 0 \\ 0 & \begin{bmatrix} -R_N & 0 \\ 0 & -R_N \end{bmatrix} \end{bmatrix}_{(2\times3)\times3s} . \tag{3.63}$$

If a device connects two nodes, that device will have two M_{DEV} matrices. For example an i^{th} line is connected to ja^{th} and jb^{th} node, where the current is defined as flowing from the ja^{th} node to the jb^{th} node. The element $M_{DEV}\,(ja, i)$ and $M_{DEV}\,(jb, i)$ will be R_N and -R_N respectively, and all other elements in that row will be zero. Equation (3.64) shows the case when two lines ($N_i = 2$) that have two states ($N_s = 2$) each, are connected to nodes 1,2 and 2,3 respectively of a three node system. The current is defined to flow from node 1 to node 2, and from node 2 to node 3.

$$M_{DEV} = \begin{bmatrix} \begin{bmatrix} -R_N & 0 \\ 0 & -R_N \end{bmatrix} & 0 \\ \begin{bmatrix} R_N & 0 \\ 0 & R_N \end{bmatrix} & \begin{bmatrix} -R_N & 0 \\ 0 & -R_N \end{bmatrix} \\ 0 & \begin{bmatrix} R_N & 0 \\ 0 & R_N \end{bmatrix} \end{bmatrix}_{(2\times3)\times(2\times2)} . \tag{3.64}$$

3.4.5 Microgrid Reference Frequency

Only one device, in one group defines the system reference frequency. This equation is defined in Equation (3.65)

$$[\Delta\omega_{COM}] = \Delta C_{DEV\omega}[\Delta x_{DEV}]. \tag{3.65}$$

Equation (3.66) shows the case when the reference frequency is defined by the first source, in a network of three sources. Each source in this network is a device of the same type.

$$C_{DEV\omega} = \begin{bmatrix} C_{DEV\omega 1} & 0 & 0 \end{bmatrix}_{1\times 3s}. \tag{3.66}$$

3.4.6 Combined Model of All the Devices

Consider an arbitrary microgrid with N_d group of devices, where $DEV1$ contains a source that the common reference frame is aligned to. By considering the procedure in sub-Section 3.4.1 – 3.4.5, the consolidated microgrid state-space equation is given in Equations (3.67) – (3.73).

$$\frac{d}{dt}[\Delta x_{MG}] = A_{MG}[\Delta x_{MG}] + B_{MG}[\Delta u_{MG}]. \tag{3.67}$$

$$[\Delta y_{MG}] = C_{MG}[\Delta x_{MG}] + D_{MG}[\Delta u_{MG}]. \tag{3.68}$$

Where,

$$\Delta x_{MG} = \begin{bmatrix} \Delta x_{DEV1} \\ \Delta x_{DEV2} \\ \vdots \\ \Delta x_{DEVN_d} \end{bmatrix}_{N_d N_i N_s \times 1}, \Delta u_{MG} = \begin{bmatrix} \Delta u_{DIST} \\ \Delta u_{DEV1} \\ \Delta u_{DEV2} \\ \vdots \\ \Delta u_{DEVN_i} \end{bmatrix}_{2+N_d N_i N_u \times 1} \tag{3.69}$$

$$A_{MG} = \begin{bmatrix} \left(\begin{array}{c} A_{DEV1} \\ +B_{DEV1v}M_{DEV1}C_{DEV1c} \end{array}\right) & B_{DEV1v}M_{DEV2}C_{DEV2c} & \cdots & B_{DEV1v}M_{DEVN_d}C_{DEVN_dc} \\ \left(\begin{array}{c} B_{DEV1\omega}C_{DEV1\omega} \\ B_{DEV2v}M_{DEV1}C_{DEV1c} \end{array}\right) & \left(\begin{array}{c} A_{DEV2} \\ +B_{DEV2v}M_{DEV2}C_{DEV2c} \end{array}\right) & \cdots & B_{DEV2v}M_{DEVN_d}C_{DEVN_dc} \\ \vdots & \vdots & \ddots & \vdots \\ \left(\begin{array}{c} +B_{DEV2\omega}C_{DEV1\omega} \\ B_{DEVN_dv}M_{DEV1}C_{DEV1c} \end{array}\right) & B_{DEVN_dv}M_{DEV2}C_{DEV2c} & \cdots & \left(\begin{array}{c} A_{DEVN_d} \\ +B_{DEVN_dv}M_{DEVN_d}C_{DEVN_dc} \end{array}\right) \end{bmatrix}_{NdN_iN_s \times N_dN_iN_s}, \tag{3.70}$$

$$B_{MG} = \begin{bmatrix} B_{DEV1v}M_{DIST}C_{DISTc} & B_{DEV1u} & 0 & \cdots & 0 \\ B_{DEV2v}M_{DIST}C_{DISTc} & 0 & B_{DEV2u} & \cdots & 0 \\ \vdots & \vdots & \vdots & \ddots & \vdots \\ B_{DEVN_dv}M_{DIST}C_{DISTc} & 0 & 0 & \cdots & B_{DEVN_du} \end{bmatrix}_{N_dN_iN_s \times (2+N_dN_iN_u)}, \tag{3.71}$$

$$C_{MG} = \begin{bmatrix} C_{DEV1} & 0 & \cdots & 0 \\ 0 & C_{DEV2} & \cdots & 0 \\ \vdots & \vdots & \ddots & \vdots \\ 0 & 0 & \cdots & C_{DEVN_d} \end{bmatrix}_{N_d N_i N_s \times N_d N_i N_s}, \tag{3.72}$$

$$D_{MG} = \begin{bmatrix} D_{DEV1} & 0 & \cdots & 0 \\ 0 & D_{DEV2} & \cdots & 0 \\ \vdots & \vdots & \ddots & \vdots \\ 0 & 0 & \cdots & D_{DEVN_d} \end{bmatrix}_{N_d N_i N_s \times N_d N_i N_u}, \tag{3.73}$$

3.4.7 Complete Microgrid Model

Using the procedure outlined in Sections 3.4.1 – 3.4.6, the complete microgrid small-signal model including the active load is given in Equations (3.74) – (3.79). The microgrid consists of inverters 'INV', lines '$LINE$', loads '$LOADS$', and active loads 'AL'. Any group of devices that do not have an input from outside the microgrid, or output to outside the microgrid have been omitted.

$$\frac{d}{dt}\begin{bmatrix} \Delta x_{INV} \\ \Delta i_{LINE} \\ \Delta i_{LOAD} \\ \Delta x_{AL} \end{bmatrix} = A_{MG}\begin{bmatrix} \Delta x_{INV} \\ \Delta i_{LINE} \\ \Delta i_{LOAD} \\ \Delta x_{AL} \end{bmatrix} + B_{MG}\begin{bmatrix} \Delta i_{DIST} \\ \Delta u_{AL} \end{bmatrix} \tag{3.74}$$

$$\begin{bmatrix} \Delta y_{INV} \\ \Delta y_{AL} \end{bmatrix} = C_{MG}\begin{bmatrix} \Delta x_{INV} \\ \Delta i_{LINE} \\ \Delta i_{LOAD} \\ \Delta x_{AL} \end{bmatrix} \tag{3.75}$$

The complete system state-space matrices A_{MG}, B_{MG}, and C_{MG} is given in Equations (3.76) – (3.79).

$$A_{MG} = \begin{bmatrix} \left(\begin{array}{c} A_{INV} \\ +B_{INVv}M_{INV}C_{INVc} \end{array}\right) & B_{INVv}M_{NET}C_{NETc} & B_{INVv}M_{LOAD}C_{LOADc} & B_{RECv}M_{REC}C_{RECc} \\ +B_{INV\omega}C_{INV\omega} & & & \\ \left(\begin{array}{c} B_{NETv}M_{INV}C_{INVc} \\ +B_{NET\omega}C_{INV\omega} \end{array}\right) & \left(\begin{array}{c} A_{NET} \\ +B_{NETv}M_{NET}C_{NETc} \end{array}\right) & B_{NETv}M_{LOAD}C_{LOADc} & B_{NETv}M_{REC}C_{RECc} \\ \left(\begin{array}{c} B_{LOADv}M_{INV}C_{INVc} \\ +B_{LOAD\omega}C_{INV\omega} \end{array}\right) & B_{LOADv}M_{NET}C_{NETc} & \left(\begin{array}{c} A_{LOAD} \\ +B_{LOADv}M_{LOAD}C_{LOADc} \end{array}\right) & B_{LOADv}M_{REC}C_{RECc} \\ \left(\begin{array}{c} B_{RECv}M_{INV}C_{INVc} \\ +B_{REC\omega}C_{INV\omega} \end{array}\right) & B_{RECv}M_{NET}C_{NETc} & B_{RECv}M_{LOAD}C_{LOADc} & \left(\begin{array}{c} A_{REC} \\ +B_{RECv}M_{REC}C_{RECc} \end{array}\right) \end{bmatrix}. \tag{3.76}$$

$$B_{MG} = \begin{bmatrix} B_{INVv}M_{DIST}C_{DISTc} & 0 \\ B_{NETv}M_{DIST}C_{DISTc} & 0 \\ B_{LOADv}M_{DIST}C_{DISTc} & 0 \\ B_{RECv}M_{DIST}C_{DISTc} & B_{RECu} \end{bmatrix}, \tag{3.77}$$

$$C_{MG} = \begin{bmatrix} C_{INV} & 0 & 0 & 0 \\ 0 & 0 & C_{LOAD} & 0 \\ 0 & 0 & 0 & C_{REC} \\ M_{INV}C_{INVc} & M_{NET}C_{NETc} & M_{LOAD}C_{LOADc} & M_{REC}C_{RECc} \end{bmatrix}, \tag{3.78}$$

$$D_{MG} = \begin{bmatrix} 0 & 0 \\ 0 & 0 \\ 0 & 0 \\ M_{DIST}C_{DISTc} & 0 \end{bmatrix} \tag{3.79}$$

3.5 Analysis of the Active Load Connected to Node 1 in the Microgrid

The active load (AL) that was modelled in Section 3.1 and analysed in Section 3.2 was connected to the microgrid at node 1. The circuit diagram of the microgrid is shown in Figure 3.15 where the three inverters and their controllers are bounded by the bottom box and the active load and its controllers are bounded by the top box. Each inverter controller is identical. Other components in the microgrid are two lines that are modelled by an inductance and a resistance and a resistive load which is connected to node 3.

The microgrid was modelled in accordance to the procedure outlined in Section 3.4. Participation analysis is performed to identify the connection between the states of the microgrid and the eigenvalues that result from the A matrix of the small signal model. Eigenvalue trajectories are presented in order to identify the effect that the active load has on the microgrid.

3.5.1 Participation analysis of the active load in the microgrid

Figure 3.16 shows the eigenvalue plot of the active load model connected to the microgrid model. The active load is connected to node 1 of the microgrid and there is an additional resistive load

Table 3.4: Properties of the microgrid with an active load connected to node 1

Inverter Source Circuit			
Parameter	***Value***	***Parameter***	***Value***
L_f	1.35 mH	r_f	0.1 Ω
L_c	0.93 mH	r_c	0.03 Ω
C_f	50 μH	C_{dc}	680 μF
Inverter Source Controller			
Parameter	***Value***	***Parameter***	***Value***
P_{max}	10,000 W	Q_{max}	6,000 VAr
F_{droop}	0.003	V_{droop}	0.02
m_p	9.4×10^{-5}	n_q	0.0013
ω_c	31.4159 rad/s	ω_n	314.15 rad/s
V_n	[381 0]	F_v	0.75
K_{pv}	0.5	K_{pc}	10.5
K_{iv}	390	K_{ic}	16,000

Active Load Circuit			
Parameter	***Value***	***Parameter***	***Value***
L_f	2.3 mH	r_f	0.1 Ω
L_c	0.93 mH	r_c	0.03 Ω
C_f	8.8 μH	C_{dc}	2040 μF
R_{load}	67.1233 Ω		
Active Load Controller			
Parameter	***Value***	***Parameter***	***Value***
K_{pv}	0.5	K_{pc}	15
K_{iv}	150	K_{ic}	30,000

Line and Load Circuit			
Parameter	***Value***	***Parameter***	***Value***
L_{line}	[0.35, 1.85] mH	r_{line}	[0.23, 0.35] Ω
L_{load}	10 nH	r_{load}	21 Ω

which is connected to node 3 of the eigenvalue model. Five groups of eigenvalues labelled ‘A1’, ‘A2’, ‘A3’, ‘A4’, ‘A5’, were identified for analysis using participation analysis.

Figure 3.17 shows the participation analysis of the eigenvalues of the active load model connected to the microgrid model. The active load has 10 states as described in Table 3.3 and the microgrid has 45 states which is a total of 55 states for the complete model. The 55 states are listed in Table 3.6 and Table 3.7. Using the same principle that was used for the active load in Section 3.2.1 the eigenvalues have been grouped and the participation values of each eigenvalue in each group has been summed. An explanation of the algorithm is in Section 3.2.1. This created five participation values for each state that represents how each state participates

in the five groups of eigenvalues.

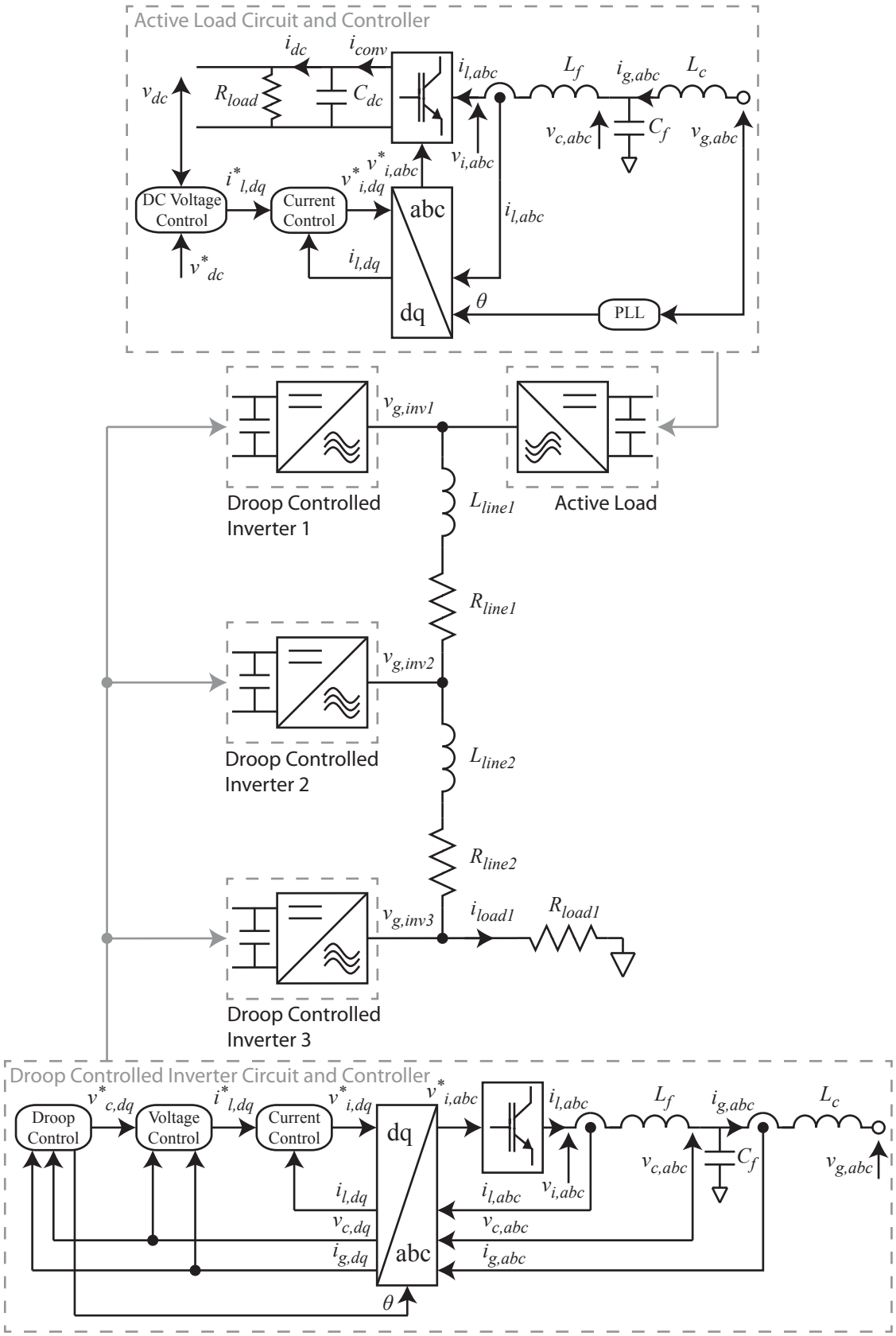

Figure 3.15: Circuit diagram of the active load connected to node 1 of the microgrid

Table 3.5: Steady-state values of the microgrid with an active load connected to node 1

Inverter Source Steady State Voltages			
Parameter	***Value***	***Parameter***	***Value***
V_{gd}	[380.39, 381.69, 380.25] V	V_{gq}	[-1.3215, -1.3823, -1.3196] V
V_{cd}	[380.71, 381.82, 380.39] V	V_{cq}	[0, 0, 0] V
V_{id}	[378.67, 378.79, 378.64] V	V_{iq}	[28.157, 28.379, 28.092] V
Inverter Source Steady State Current			
Parameter	***Value***	***Parameter***	***Value***
I_{gd}	[12.156, 12.121, 12.166] A	I_{gq}	[-0.5985, 1.6808, -1.2637] A
I_{ld}	[12.161, 12.126, 12.170] A	I_{lq}	[5.258, 7.555, 4.588] A
Inverter Source Steady State Power and Frequency			
Parameter	***Value***	***Parameter***	***Value***
P	[4627.9, 4628.0, 4627.9] W	Q	[227.86, -641.79, 480.71] VAr
f	[49.931, 49.931, 49.931] Hz		
Inverter Source Reference Frame Transformation			
Parameter	***Value***	***Parameter***	***Value***
V_{gD}	[380.39, 381.69, 380.25] V	V_{gQ}	[-1.3215, -1.3855, -1.3194] V
I_{gD}	[12.156, 12.117, 12.166] A	I_{gQ}	[-0.5985, 1.6847, -1.2636] A
δ_0	[0, 0.0023, -1.358$\times 10^{-4}$] rad		

Active Load Steady State Voltages			
Parameter	***Value***	***Parameter***	***Value***
V_{gd}	380.39 V	V_{gq}	-0.0053 V
V_{cd}	380.30 V	V_{cq}	-5.3542 V
V_{id}	377.59 V	V_{iq}	-3.4996 V
V_{dc}	700 V_{dc}		
Active Load Steady State Current			
Parameter	***Value***	***Parameter***	***Value***
I_{gd}	18.323 A	I_{gq}	0.0192 A
I_{ld}	18.319 A	I_{lq}	-1.000 A
I_{dc}	9.7143 A		
Active Load Steady State Power and Frequency			
Parameter	***Value***	***Parameter***	***Value***
P	6967.8 W	Q	105.32 VAr
f	49.931 Hz		
Active Load Reference Frame Transformation			
Parameter	***Value***	***Parameter***	***Value***
V_{gD}	379.92 V	V_{gQ}	-0.0056 V
I_{gD}	18.299 A	I_{gQ}	0.0202 A
δ_0	0.0496 rad		

Line and Load Steady State Current			
Parameter	***Value***	***Parameter***	***Value***
I_{lineD}	[-6.1669, 5.9501] A	I_{lineQ}	[-0.5550, 1.1534] A
I_{loadD}	18.1060 A	I_{loadQ}	-0.2073 A

Table 3.6: List of Inverter 1 and Inverter 2 states in the microgrid

State Number	***Device Name***	***State Name***	***State Symbol***
1	Inverter 1	Angle difference between the common reference frame and the inverter's local reference frame	$\Delta\delta_1$
2	Inverter 1	Real Power of the inverter used for the droop function	ΔP_1
3	Inverter 1	Reactive Power of the inverter used for the droop function	ΔQ_1
4	Inverter 1	Integrator of the d-axes of the ac-voltage controller	$\Delta\phi_{d1}$
5	Inverter 1	Integrator of the q-axes of the ac-voltage controller	$\Delta\phi_{q1}$
6	Inverter 1	Integrator of the d-axes of the ac-current controller	$\Delta\gamma_{d1}$
7	Inverter 1	Integrator of the q-axes of the ac-current controller	$\Delta\gamma_{q1}$
8	Inverter 1	Current of the d-axes of the filter inductor	Δi_{ld1}
9	Inverter 1	Current of the q-axes of the filter inductor	Δi_{lq1}
10	Inverter 1	Voltage of the d-axes of the filter capacitor	Δv_{cd1}
11	Inverter 1	Voltage of the q-axes of the filter capacitor	Δv_{cq1}
12	Inverter 1	Current of the d-axes of the coupling inductor	Δi_{gd1}
13	Inverter 1	Current of the q-axes of the coupling inductor	Δi_{gq1}
14	Inverter 2	Angle difference between the common reference frame and the inverter's local reference frame	$\Delta\delta_2$
⋮	⋮	⋮	⋮
26	Inverter 2	Current of the q-axes of the coupling inductor	Δi_{gq2}

Table 3.7: List of Inverter 3, line and load states in the microgrid

State Number	*Device Name*	*State Name*	*State Symbol*
27	Inverter 3	Angle difference between the common reference frame and the inverter's local reference frame	$\Delta\delta_3$
⋮	⋮	⋮	⋮
39	Inverter 3	Current of the q-axes of the coupling inductor	Δi_{gq3}
40	Line 1	Current of the d-axes of the line inductor	Δi_d
41	Line 1	Current of the q-axes of the line inductor	Δi_q
42	Line 2	Current of the d-axes of the line inductor	Δi_d
43	Line 2	Current of the q-axes of the line inductor	Δi_q
44	Passive Load	Current of the d-axes of the load inductor	Δi_d
45	Passive Load	Current of the q-axes of the load inductor	Δi_q
46	Active Load	Integrator of the dc-voltage controller	$\Delta\phi_{dc}$
47	Active Load	Integrator of the d-axes of the ac-current controller	$\Delta\gamma_d$
48	Active Load	Integrator of the q-axes of the ac-current controller	$\Delta\gamma_q$
49	Active Load	Current of the d-axes of the filter inductor	Δi_{ld}
50	Active Load	Current of the q-axes of the filter inductor	Δi_{lq}
51	Active Load	Voltage of the d-axes of the filter capacitor	Δv_{cd}
52	Active Load	Voltage of the q-axes of the filter capacitor	Δv_{cq}
53	Active Load	Current of the d-axes of the coupling inductor	Δi_{gd}
54	Active Load	Current of the q-axes of the coupling inductor	Δi_{gq}
55	Active Load	Voltage of the dc-capacitor	Δv_{dc}

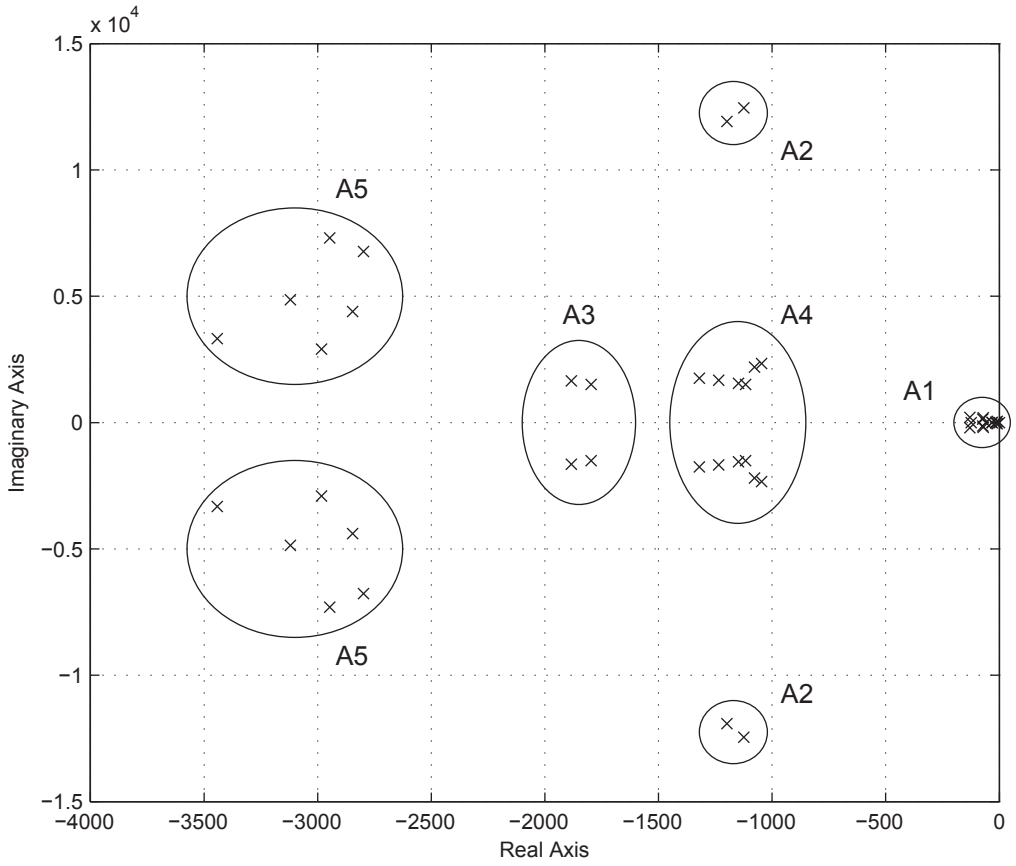

Figure 3.16: Eigenvalues of the active load in the microgrid indicating the five eigenvalue groups

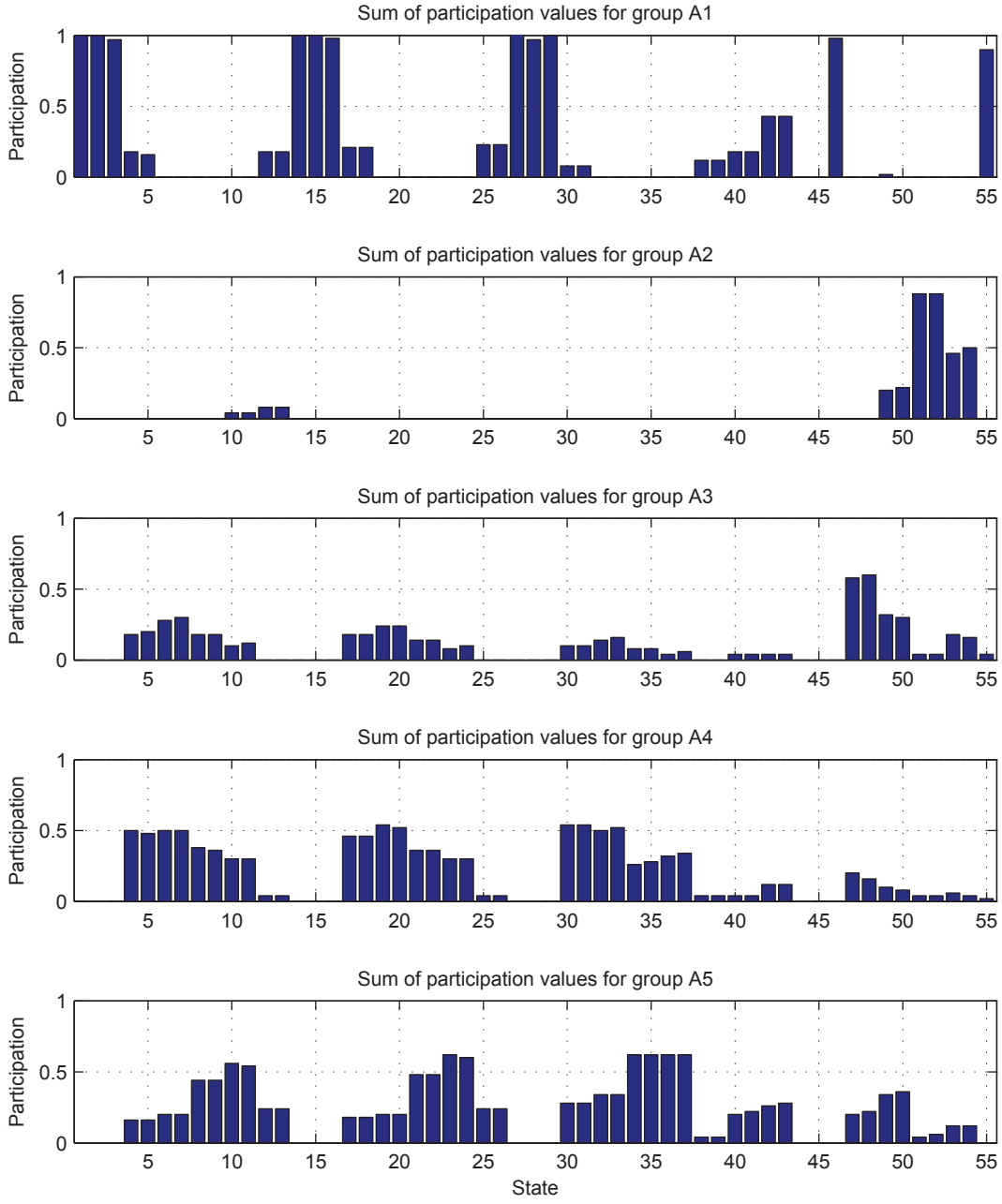

Figure 3.17: Participation values of the states for the five eigenvalue groups

From Figure 3.17, it can be seen that the group of eigenvalues labelled 'A1' have high participation factors for the three droop controller states in each of the three inverters (states 1–3, 14–16 and 27–29) and for the dc-capacitor and dc-voltage controller in the active load (states 46 and 55).

The group labelled 'A2' have high participation factors for the states of the filter capacitor and the coupling inductor in the LCL filter of the active load (states 51–54). A small participation factor can also be seen for the states of the filter capacitor and the coupling inductor in the LCL filter of Inverter 1 (states 10–13). This is expected since the two LCL filters are connected to the same node. The group 'A2' does not appear in the states of Inverter 1 and Inverter 2 (states 14–39).

The group labelled 'A3' have high participation factors for the states of the ac-current controller and filter inductor of the active load (states 47–50). The group 'A3' also have small participation factors for the ac-voltage, ac-current, filter inductor and filter capacitor in each of the three inverters (states 4–11, 17–24 and 30–37). Although the link is weak in each of the three inverters, the link is the strongest in Inverter 1 (states 4–11) and the weakest in Inverter 3 (states 30–37). A stronger link in Inverter 1 is because the active load is connected to node 1 of which Inverter 1 is also connected to.

The group 'A4' have high participation factors in the ac-voltage and ac-current controllers of the three inverters (states 4–7, 17–20 and 30–33) and a smaller participation in the LCL filter states of the inverters (states 8–13, 18–26 and 34–39). There is also a small participation in the active load ac-current controller and LCL states (states 47–54).

The group 'A5' have high participation in the filter inductor and filter capacitor of the LCL filter states of the inverters (states 8–11, 18–24 and 34–37) and a lower participation in the coupling inductor, ac-voltage and ac-current controllers of the inverters (states 4–7, 12–13, 17–20, 25–26, 30–33 and 38–39) and the ac-current controller and LCL filter of the active load (states 47–54).

As seen in Figure 3.17, the active load states show coupling to all the groups associated with the inverters. The states that have the highest participation for a particular group will be deemed to have the most influence on the eigenvalues that belong to that particular group.

The summarised relationships between the eigenvalue groups and the states are as follows. The eigenvalues in the group labelled 'A1' are the low-frequency modes and are most associated with the droop controllers of the inverters and the dc-voltage controller and the dc-capacitor of the active load. The eigenvalues in the group labelled 'A2' are the mid-frequency modes and are most associated with with the LCL filter of the active load. The group 'A3' are the high-frequency modes of the active load but are really mid-frequency modes in the microgrid with active load. This group is associated with the ac-current controller and the filter inductor of the active load. The group labelled 'A4' are the mid-frequency modes of the inverters in the microgrid and are most associated with the inverter ac-current and ac-voltage controllers. The group labelled 'A5' are the high-frequency modes of the inverters and microgrid and are most associated with the filter inductor and filter capacitor of the inverters.

By comparing Figure 3.4 and Figure 3.16, it is possible to see the effect that the microgrid has on the active load. All three groups that are associated with the active load appear in similar locations on Figure 3.4 and Figure 3.16, but groups 'A2' and 'A3' have changed slightly. As already discussed, groups 'A2' and 'A3' in Figure 3.16 are those associated with the LCL filter and the ac-current controllers of the active load. Group 3 has become better damped (with the real part of the eigenvalue changing from approximately $(-2,300$ to $-1,750)$ and group 2 has become slightly less well damped $(-1,000$ to $-1,200)$.

3.5.2 Effect of the integrator gain of the dc-voltage controller on the low-frequency modes

Figure 3.18 plots the the low-frequency eigenvalues when the integrator gain of the dc-voltage controller is increased. Comparing the plot with 3.6, it can be seen that there is no change with the low-frequency modes when the gain is increased. It is noticed that there is no displacement of the low-frequency modes that are associated with the droop controller of the inverters. From this plot, it can be seen that the low-frequency modes of the active load and the low-frequency modes of the inverters are two distinct groups.

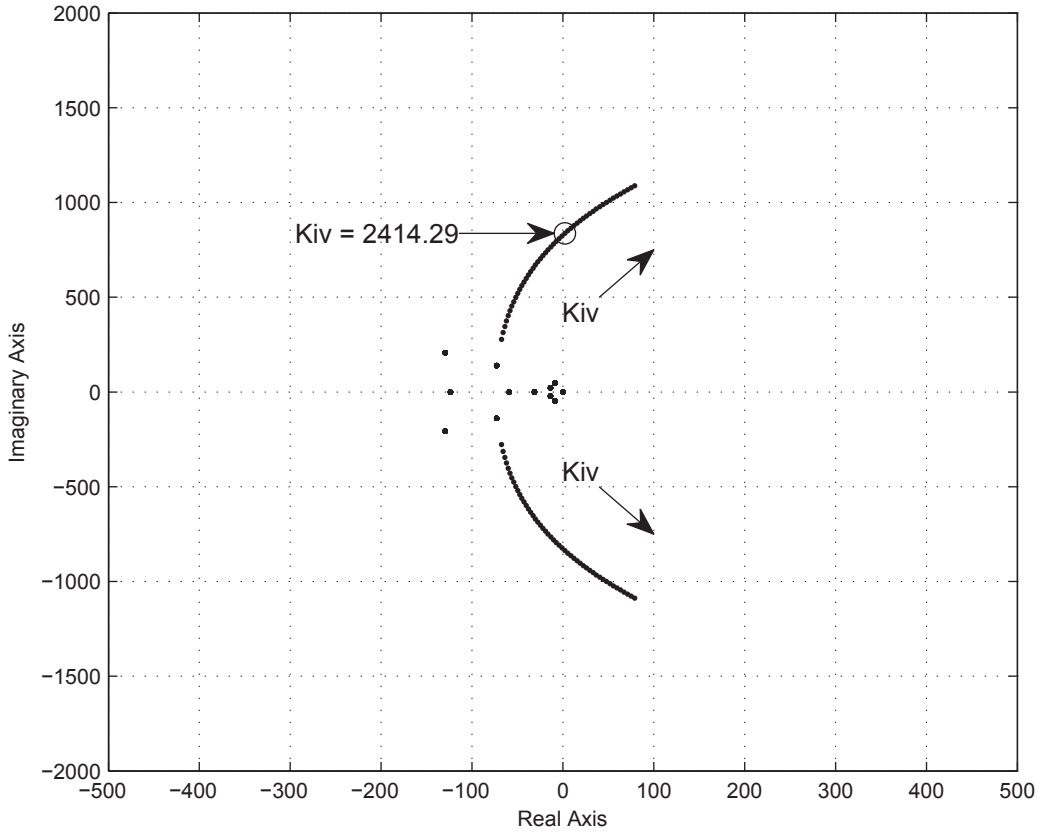

Figure 3.18: Trace of low-frequency modes as a function of dc-voltage controller integrator gain: $300 \leq K_{iv} \leq 4000$

3.5.3 Effect of the integrator gain and proportional gain of the dc-voltage controller on the modes

Figure 3.19 plots the eigenvalues when the integrator gain and proportional gain of the dc-voltage controller is increased. The ratio of the integrator gain and proportional gain is maintained at $\frac{1}{300}$. Comparing the plot with 3.7, it can be seen that the dc-controller gains of the active load still cause the eigenvalues associated with the ac-current controller of the active load to become more oscillatory. However, this change has the greatest effect on the eigenvalues that are associated with the ac-current and ac-voltage controllers of the inverters. It is these eigenvalues that have become more oscillatory and caused the microgrid to become unstable. This plot demonstrates a link between the dc-controller of the active load and the ac-current and ac-voltage controllers of the inverters.

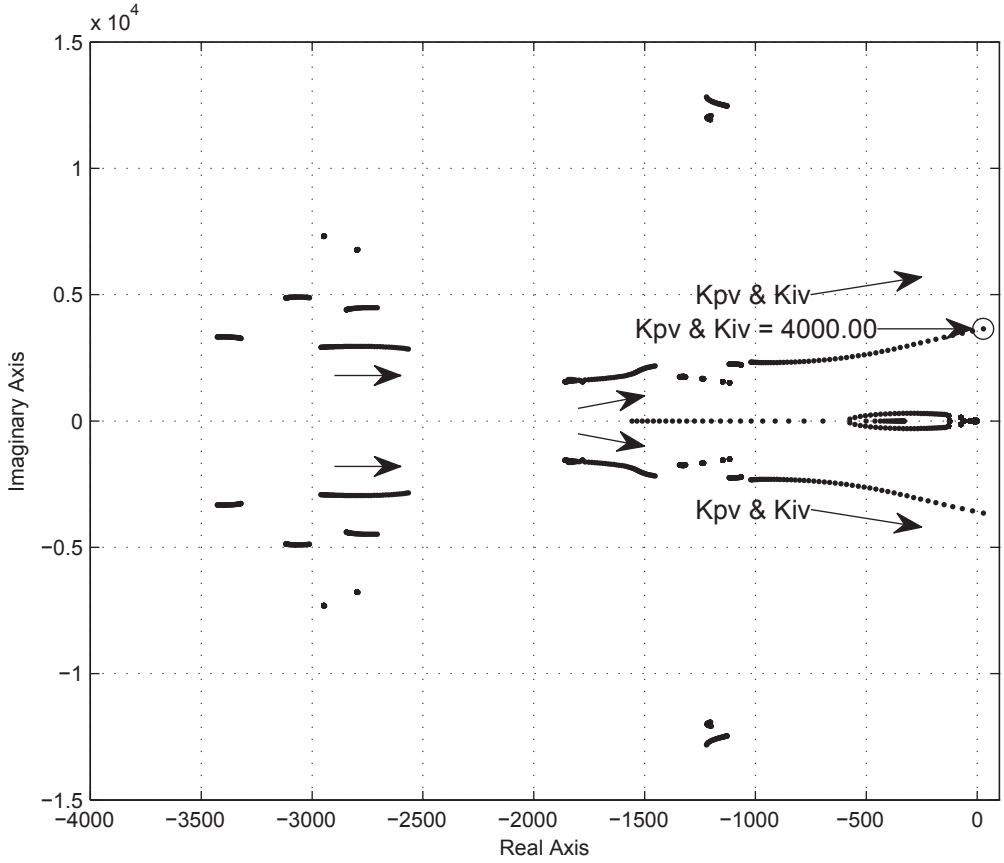

Figure 3.19: Trace of low and high frequency modes as a function of dc-voltage controller integrator and proportional gain: $300 \leq K_{iv} \leq 4000$ where $K_{pv} = \frac{1}{300} K_{iv}$

3.5.4 Effect of the integrator gain of the ac-current controller on the high-frequency modes

Figure 3.20 plots the eigenvalues when the integrator gain of the ac-current controller of the active load is increased. It can be seen that there is a large interaction between the gain and the eigenvalues that are associated with the inverters. In some cases this interaction causes the eigenvalues to become less oscillatory and in other cases this interaction causes the eigenvalues to become more oscillatory. In all cases the stability of the microgrid is not compromised.

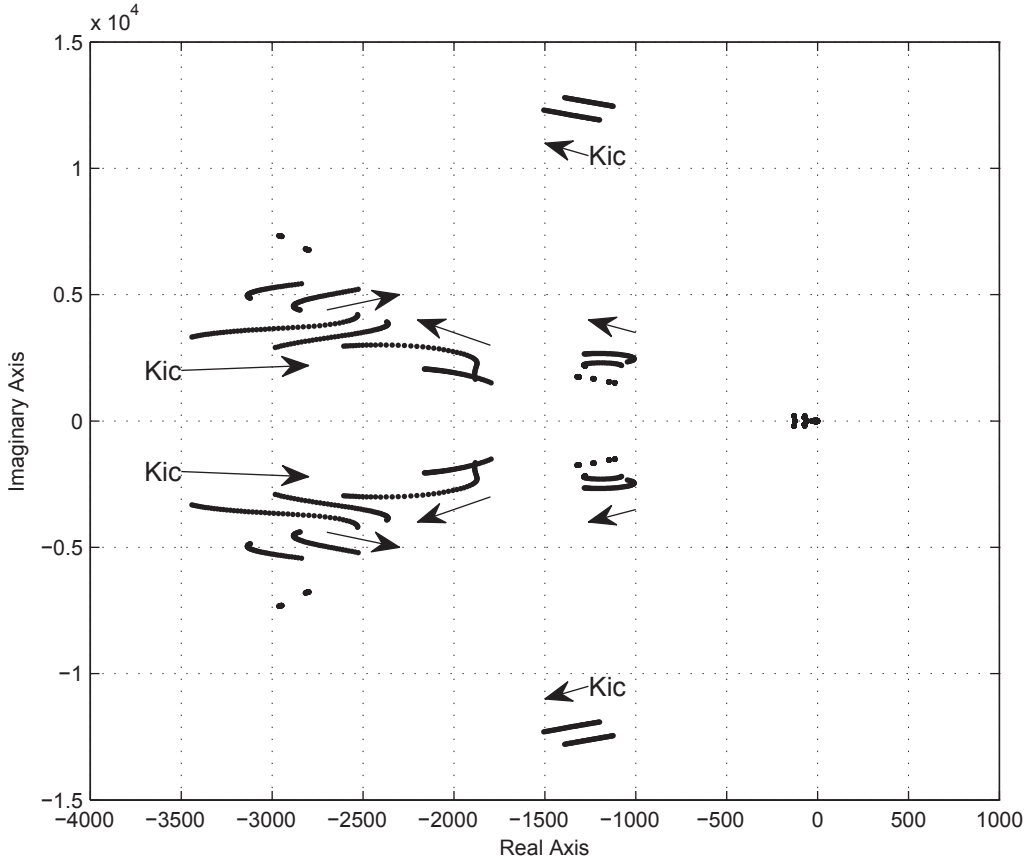

Figure 3.20: Trace of high-frequency modes as a function of ac-current controller integrator gain: $30,000 \leq K_{ic} \leq 100,000$

3.5.5 Effect of the coupling inductor on the high-frequency modes

Figure 3.21 plots the eigenvalues when the coupling inductor of the active load is increased. It can be seen that the increase in coupling inductor has a little effect on the eigenvalues associated with the active load. The increase in coupling inductor has a smaller effect on the eigenvalues associated with the inverters. It is concluded that the stability of the microgrid with an active load is not sensitive to an increase in the coupling inductance L_c.

3.5.6 Effect of the dc-load on the low-frequency modes

Figure 3.22 plots the low-frequency eigenvalues when the dc-load of the active load is increased (the resistance of the load is decreased). It can be seen that the change of load has no noticeable

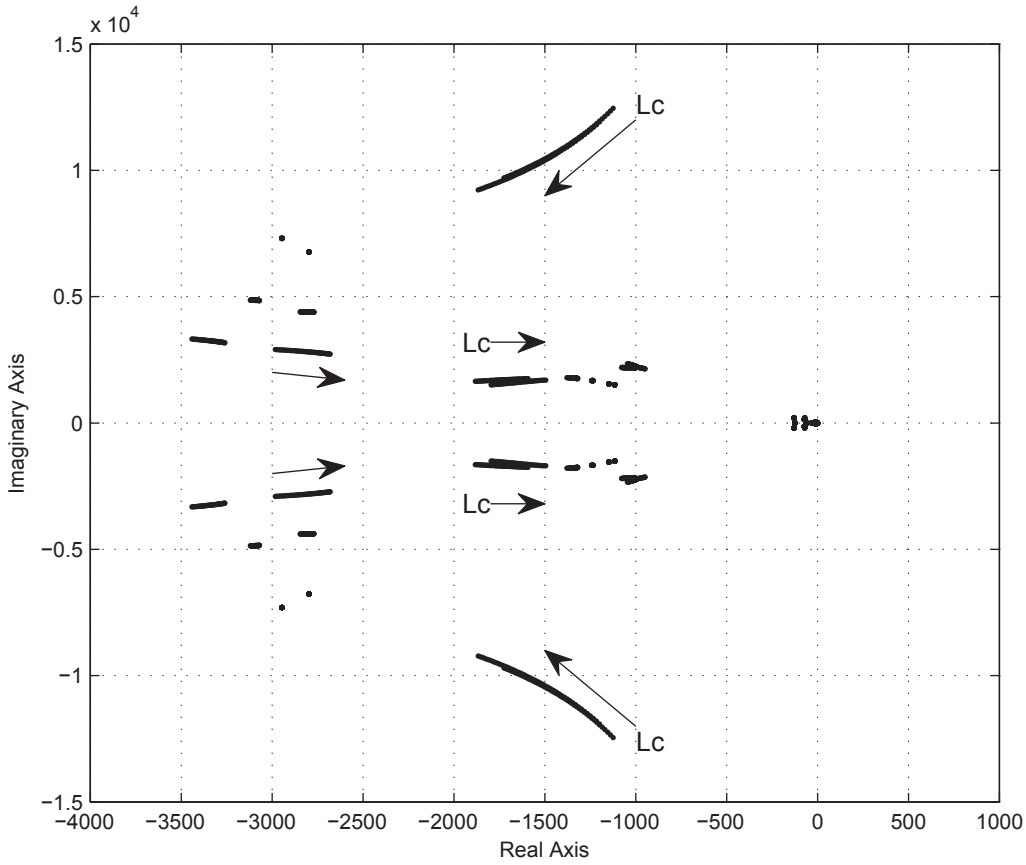

Figure 3.21: Trace of high-frequency modes as a function of the coupling inductor: $0.93mH \leq L_c \leq 2.35mH$

effect on the low-frequency eigenvalues. In this case, changing the load that the active load presents to the microgrid does not affect the stability of the microgrid. Therefore, in the experimental set-up the choice of active load resistance is not an important parameter to consider.

3.5.7 Effect of the droop gain on the low-frequency modes

Figure 3.23 plots the low-frequency eigenvalues when the droop gain of the inverters is increased. It can be seen from this plot that increasing the droop gains causes the microgrid to become unstable. However, only the eigenvalues that are associated with the inverters have become more oscillatory. The eigenvalues that are associated with the dc-voltage controller and dc-capacitor of the active load have not changed. This confirms that the microgrid is most sensitive to the gains of the droop controllers, however the stability of the active load is not sensitive to the

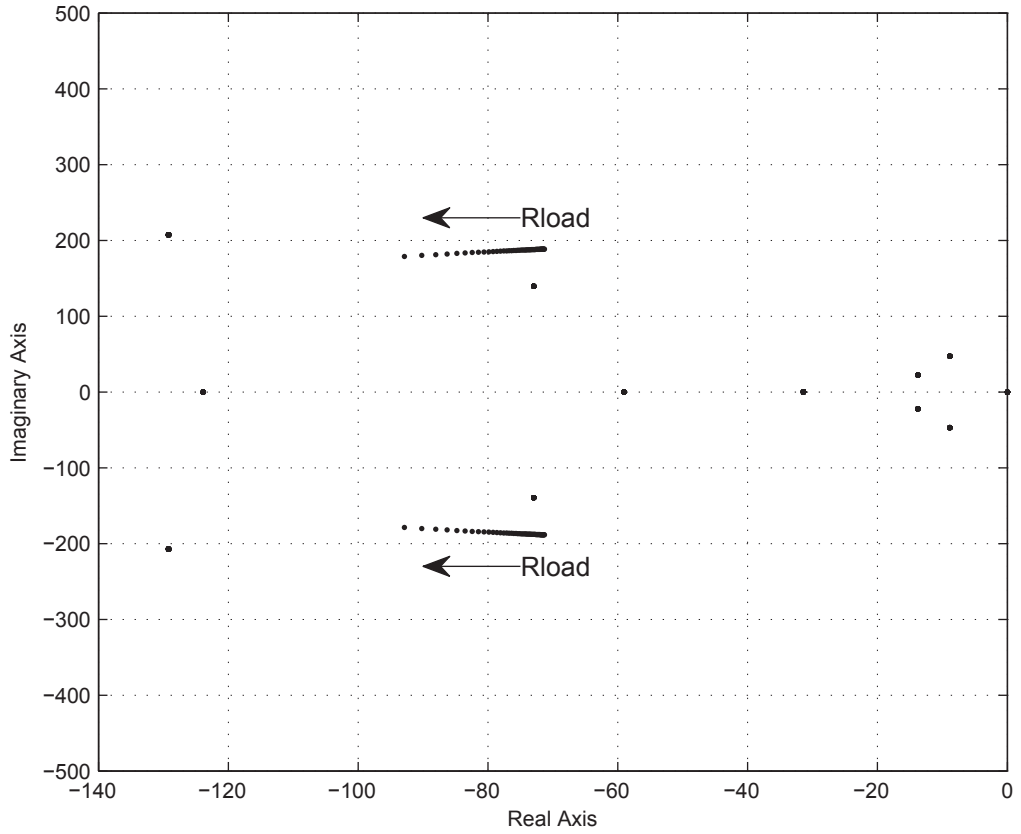

Figure 3.22: Trace of low-frequency modes as a function of the dc-load: $67\Omega \geq R_{load} \geq 10\Omega$

gains of the droop controller. It can also be seen that there is no link between the low-frequency modes of the active load and the low-frequency modes of the microgrid. These two low frequency modes can be designed independently.

3.6 Analysis of the Active Load Connected to Node 3 in the Microgrid

In Section 3.5, the active load was connected to node 1 and the resistive load was connected to node 3 of the microgrid. In this section, the loads have been swapped such that the active load is connected to node 3 and the resistive load is connected to node 1. The circuit diagram used for this section is presented in Figure 3.24.

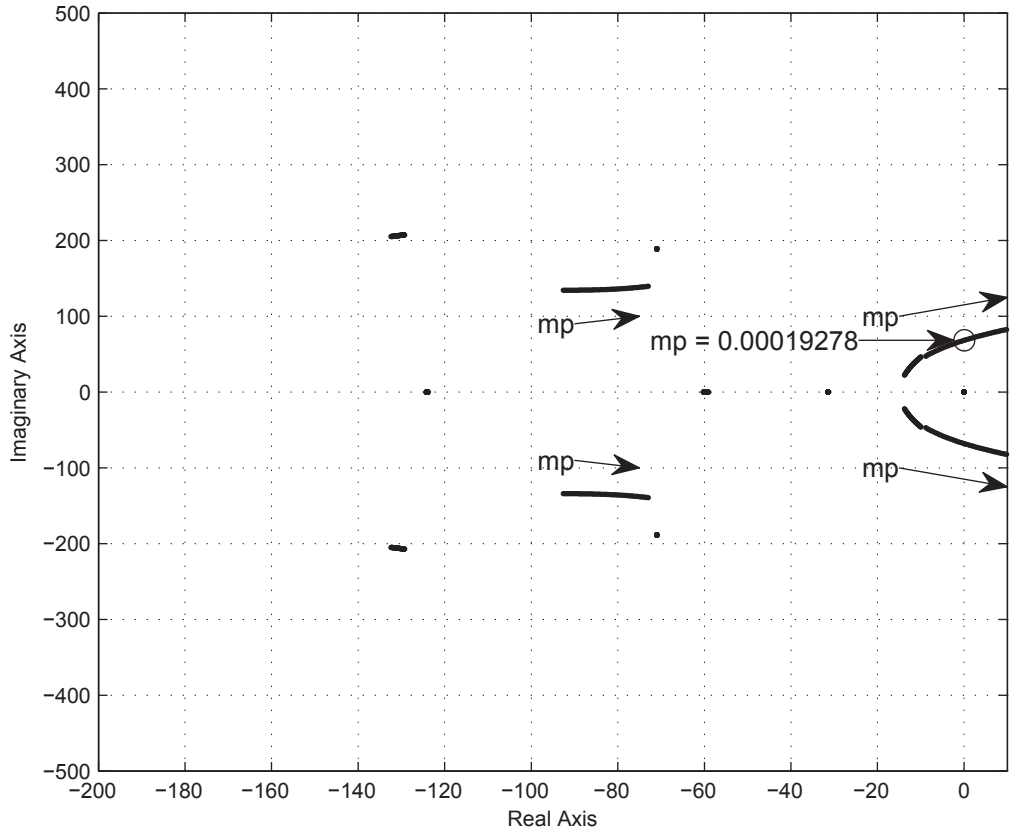

Figure 3.23: Trace of low-frequency modes as a function of the inverter droop gain: $9.4 \times 10^{-3} \leq m_p \leq 3.14 \times 10^{-4}$

The same modeling procedure that was used in Section 3.5 is used in this section which is defined in Section 3.4. This section is included with the aim of comparing if placing the active load in a different position within the microgrid has an effect on the small-signal stability of the microgrid.

3.6.1 Participation analysis of the active load in the microgrid

The same analysis as in Section 3.5 is applied and the eigenvalue plots and participation analysis are shown in Figure 3.25 and Figure 3.26 respectively.

Comparing the eigenvalue groups in Figure 3.16 and Figure 3.25 will provide information as to how the stability of the microgrid has changed when the active load was changed from

Table 3.8: Properties of the microgrid with an active load connected to node 3

Inverter Source Circuit			
Parameter	***Value***	***Parameter***	***Value***
L_f	1.35 mH	r_f	0.1 Ω
L_c	0.93 mH	r_c	0.03 Ω
C_f	50 μH	C_{dc}	680 μF
Inverter Source Controller			
Parameter	***Value***	***Parameter***	***Value***
P_{max}	10,000 W	Q_{max}	6,000 VAr
F_{droop}	0.003	V_{droop}	0.02
m_p	9.4×10^{-5}	n_q	0.0013
ω_c	31.4159 rad/s	ω_n	314.15 rad/s
V_n	[381 0]	F_v	0.75
K_{pv}	0.5	K_{pc}	10.5
K_{iv}	390	K_{ic}	16,000

Active Load Circuit			
Parameter	***Value***	***Parameter***	***Value***
L_f	2.3 mH	r_f	0.1 Ω
L_c	0.93 mH	r_c	0.03 Ω
C_f	8.8 μH	C_{dc}	2040 μF
R_{load}	72.058 Ω		
Active Load Controller			
Parameter	***Value***	***Parameter***	***Value***
K_{pv}	0.5	K_{pc}	15
K_{iv}	150	K_{ic}	30,000

Line and Load Circuit			
Parameter	***Value***	***Parameter***	***Value***
L_{line}	[0.35, 1.85] mH	r_{line}	[0.23, 0.35] Ω
L_{load}	10 nH	r_{load}	21 Ω

node 1 to node 3. Both figures have five distinct groups and the five group are in similar locations. Upon closer inspection groups in Figure 3.25 have moved marginally to the right and the microgrid is marginally more oscillatory. This has indicated that connecting the active load to node 3 has caused this slight decrease in stability. In the microgrid, node three is connected to the end of Line 2 of which Line 2 is slightly longer than Line 1. By placing the active load at the end of a longer line a slight decrease in stability has been observed.

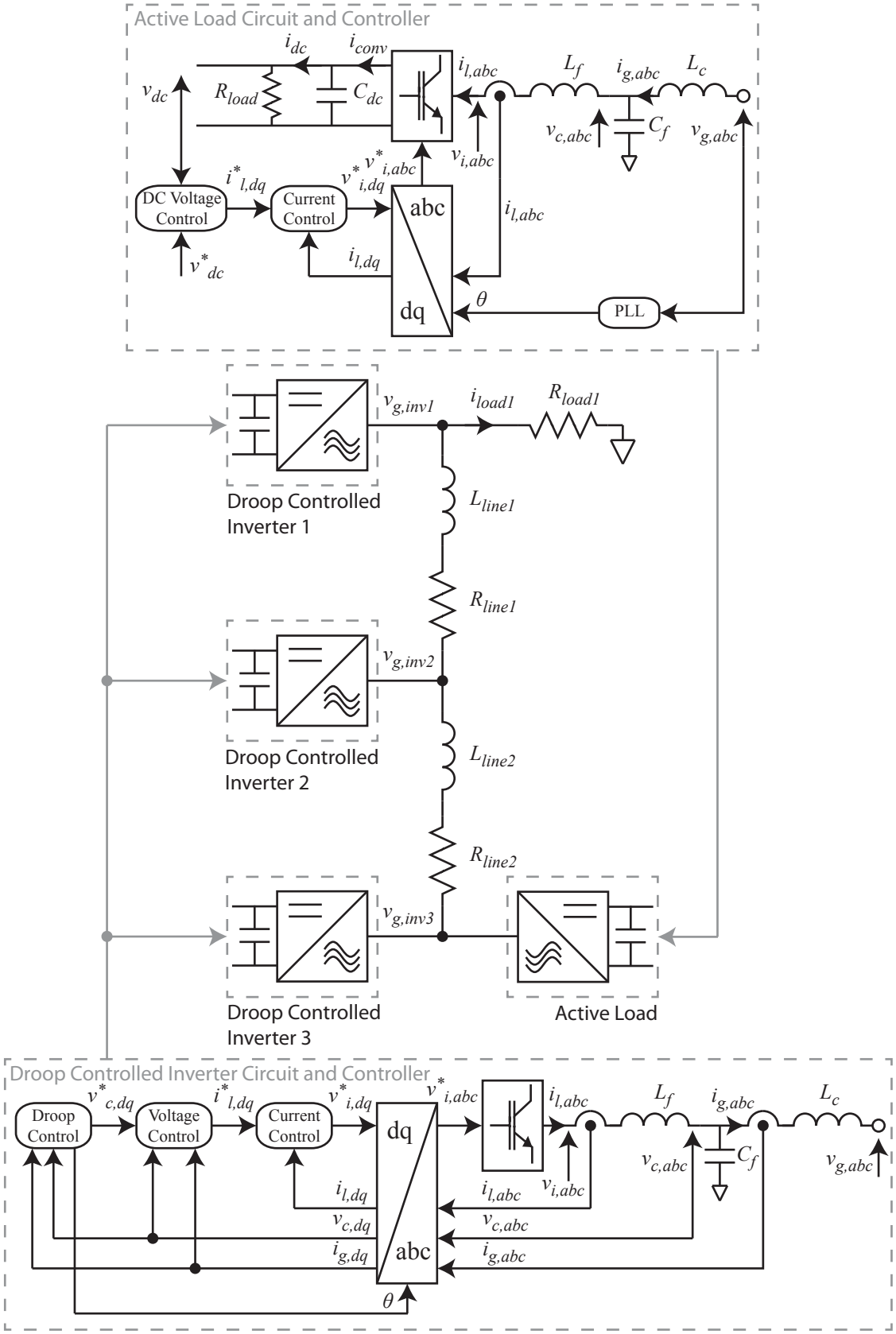

Figure 3.24: Circuit diagram of the active load connected to node 3 of the microgrid

Table 3.9: Steady-state values of the microgrid with an active load connected to node 3

Inverter Source Steady State Voltages			
Parameter	***Value***	***Parameter***	***Value***
V_{gd}	[380.32, 381.64, 380.35] V	V_{gq}	[-1.3045, -1.3756, -1.3420] V
V_{cd}	[380.74, 381.81, 380.36] V	V_{cq}	[0, 0, 0] V
V_{id}	[378.68, 378.79, 378.64] V	V_{iq}	[28.163, 28.379, 28.086] V
Inverter Source Steady State Current			
Parameter	***Value***	***Parameter***	***Value***
I_{gd}	[12.158, 12.124, 12.169] A	I_{gq}	[-0.5362, 1.6748, -1.3234] A
I_{ld}	[12.162, 12.128, 12.174] A	I_{lq}	[5.321, 7.549, 4.528] A
Inverter Source Steady State Power and Frequency			
Parameter	***Value***	***Parameter***	***Value***
P	[4629.0, 4629.0, 4628.9] W	Q	[204.14, -639.45, 503.37] VAr
f	[49.931, 49.931, 49.931] Hz		
Inverter Source Reference Frame Transformation			
Parameter	***Value***	***Parameter***	***Value***
V_{gD}	[380.32, 381.63, 380.34] V	V_{gQ}	[-1.3045, -1.3678, -1.3411] V
I_{gD}	[12.158, 12.133, 12.168] A	I_{gQ}	[-0.5362, 1.6652, -1.3225] A
δ_0	[0, -0.0057, -6.5001$\times 10^{-4}$] rad		

Active Load Steady State Voltages			
Parameter	***Value***	***Parameter***	***Value***
V_{gd}	380.35 V	V_{gq}	-0.0036 V
V_{cd}	380.23 V	V_{cq}	-5.3530 V
V_{id}	377.51 V	V_{iq}	-3.5036 V
V_{dc}	700 V_{dc}		
Active Load Steady State Current			
Parameter	***Value***	***Parameter***	***Value***
I_{gd}	18.327 A	I_{gq}	0.0197 A
I_{ld}	18.322 A	I_{lq}	-1.000 A
I_{dc}	9.7143 A		
Active Load Steady State Power and Frequency			
Parameter	***Value***	***Parameter***	***Value***
P	6968.1 W	Q	105.50 VAr
f	49.931 Hz		
Active Load Reference Frame Transformation			
Parameter	***Value***	***Parameter***	***Value***
V_{gD}	379.84 V	V_{gQ}	-0.0038 V
I_{gD}	18.3017 A	I_{gQ}	0.0207 A
δ_0	0.0515 rad		

Line and Load Steady State Current			
Parameter	***Value***	***Parameter***	***Value***
I_{lineD}	[-5.9525, 6.1675] A	I_{lineQ}	[-0.4741, 1.2270] A
I_{loadD}	18.1104 A	I_{loadQ}	-0.0621 A

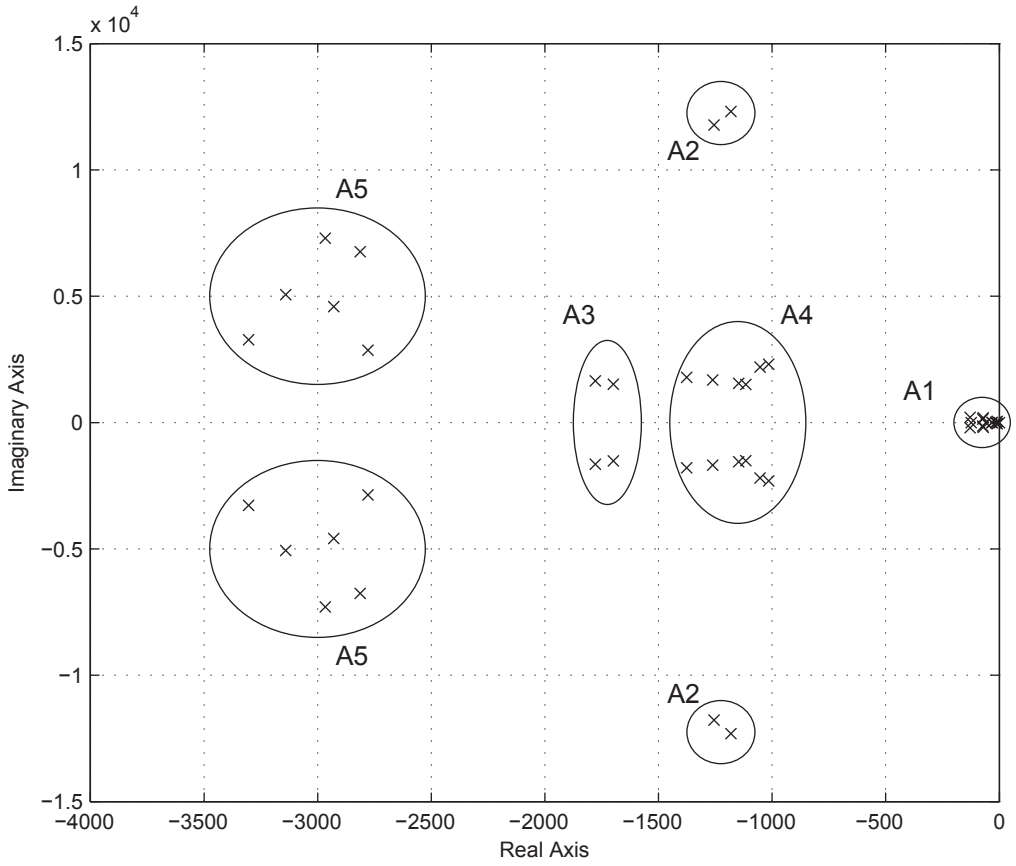

Figure 3.25: Eigenvalues of the active load in the microgrid indicating the five eigenvalue groups

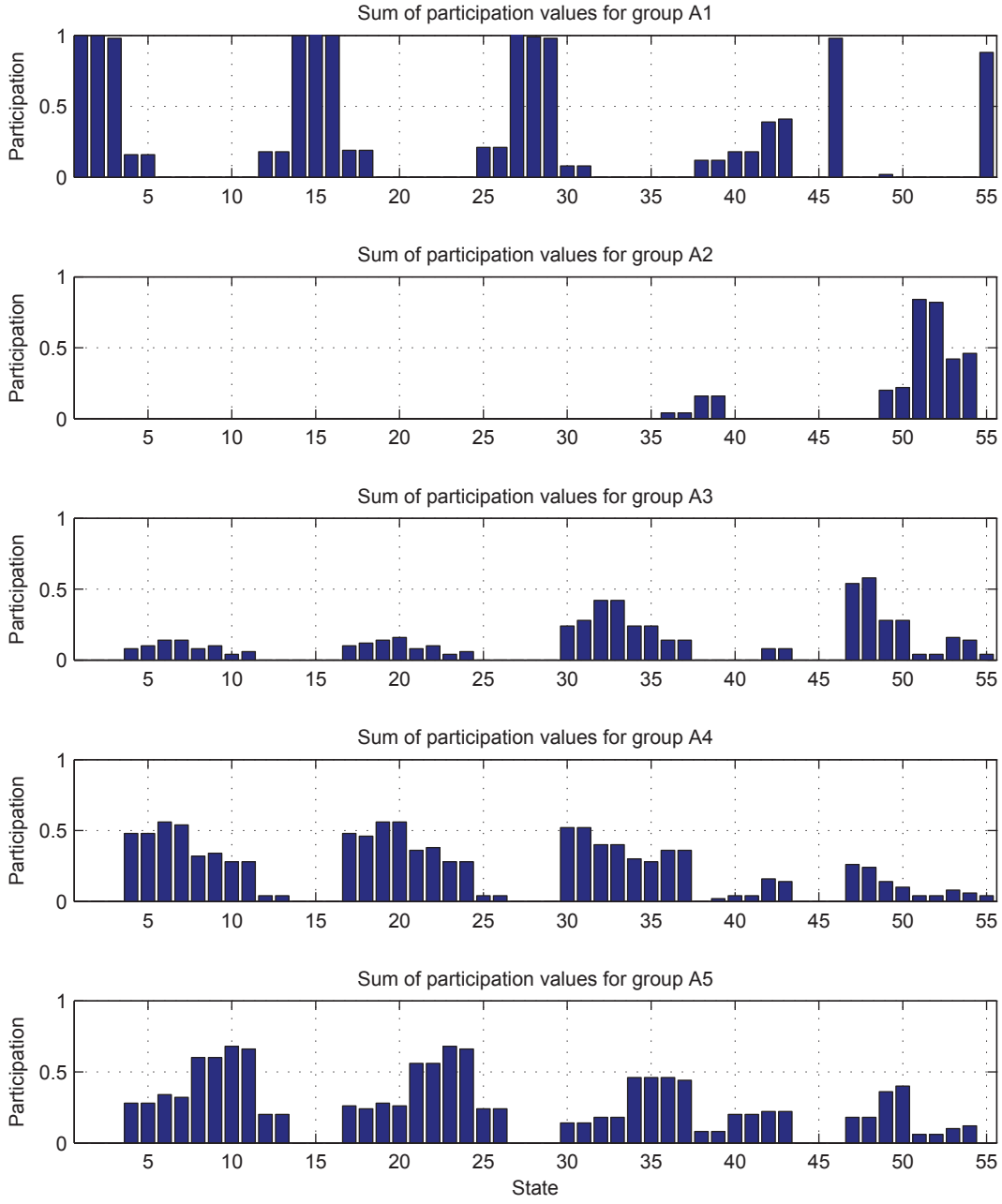

Figure 3.26: Participation values of the states for the five eigenvalue groups

The participation plot when the active load is connected to node 1 in Figure 3.17 and when connected to node 3 in Figure 3.26 share similar characteristics. In both Figure 3.17 and Figure 3.26 the group 'A1' has high participation for the droop controllers of the inverters (states 1–3, 14–16 and 27–29), group 'A2' has high participation for the filter capacitor and coupling inductor of the active load (states 51–54), group 'A3' has high participation for the ac-current controller and the filter capacitor of the active load (states 47–50), group 'A4' has high participation for the ac-voltage and ac-current controllers of the inverters (states 4–7, 17–20 and 30–33) and group 'A5' has high participation for the LCL filter of the inverters (states 8–11, 18–24 and 34–37). From these similarities, the dynamics of the microgrid has not greatly changed when the active load was moved to a different location.

However, there are differences with the small participation factors. Group 'A2' has small participation with the coupling inductor of Inverter 1 (states 12–13) in Figure 3.17 and has small participation with the coupling inductor of Inverter 3 (states 38–39) in Figure 3.26. This is expected since the active load for the participation analysis in Figure 3.17 is connect to Inverter 1 (states 12–13) and for the participation analysis in Figure 3.26, the active load is connect to Inverter 3 (states 38–39). The small participation factors have provided information about the network configuration.

It is noted that the participation of group 'A2' in Inverter 1 in Figure 3.17 is lower then the participation in Inverter 3 in Figure 3.26. From this, the active load has a greater coupling when connected to node 3 and the dynamics of the active load may greater influence the dynamics of the inverter.

3.6.2 Effect of the integrator gain of the dc-voltage controller on the low-frequency modes

Figure 3.27 plots the the low-frequency eigenvalues when the integrator gain of the dc-voltage controller is increased. Comparing the plot with Figure 3.18, it can be seen that there is no change in how the two low-frequency modes behave when the gain is increased. From the two figures, the dc-voltage controller does not affect the dynamics of the droop controllers of the

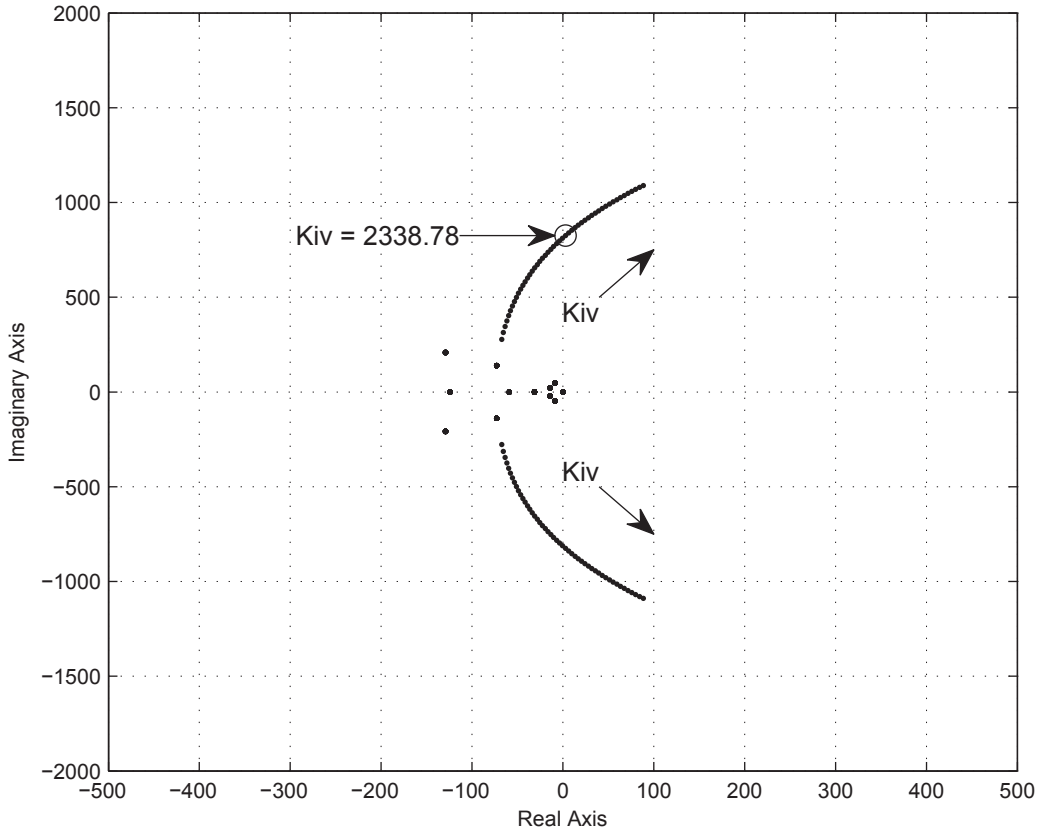

Figure 3.27: Trace of low-frequency modes as a function of dc-voltage controller integrator gain: $300 \leq K_{iv} \leq 4000$

inverters. If the active load became unstable, it would be expected that the droop controllers would remain stable.

3.6.3 Effect of the integrator gain and proportional gain of the dc-voltage controller on the modes

Figure 3.28 plots the eigenvalues when the integrator gain and proportional gain of the dc-voltage controller is increased. The ratio of the integrator gain and proportional gain is maintained at $\frac{1}{300}$, the nominal design value. Comparing the plot with Figure 3.19, the shapes are very similar and a similar dynamic response would be expected. However, because the eigenvalues in Figure 3.25 are closer to the real axis than in Figure 3.16, the microgrid experiences instability with a lower gain when the active load is connected to node 3.

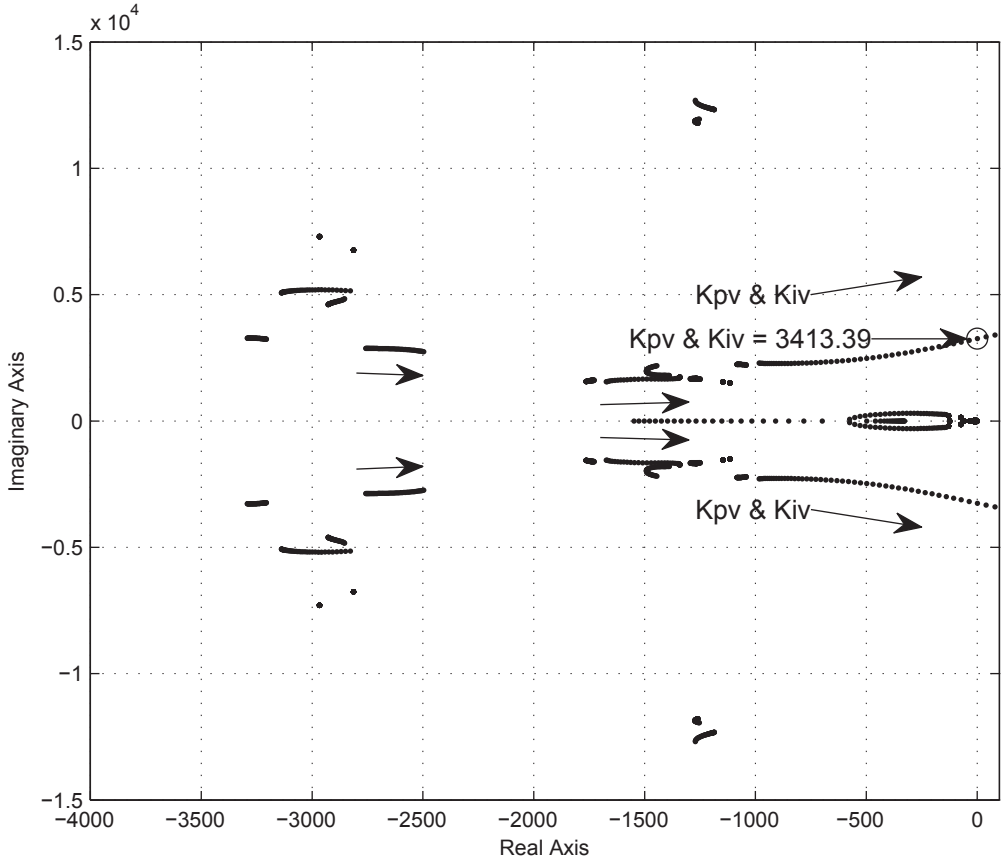

Figure 3.28: Trace of low and high frequency modes as a function of dc-voltage controller integrator and proportional gain: $300 \leq K_{iv} \leq 4000$ where $K_{pv} = \frac{1}{300} K_{iv}$

3.6.4 Effect of the droop gain on the low-frequency modes

Figure 3.23 plots the low-frequency eigenvalues when the droop gain of the inverters is increased. Comparing the plot with Figure 3.29, no change can be observed. Both plots show that the low-frequency dynamics of the droop controller are not coupled with the low-frequency dynamics of the active-load.

3.7 Verification of the active load connected to the microgrid

Experimental tests were conducted in a laboratory in order to verify the low-frequency modes and verify the result from Figure 3.28. The low-frequency modes of the microgrid are associated

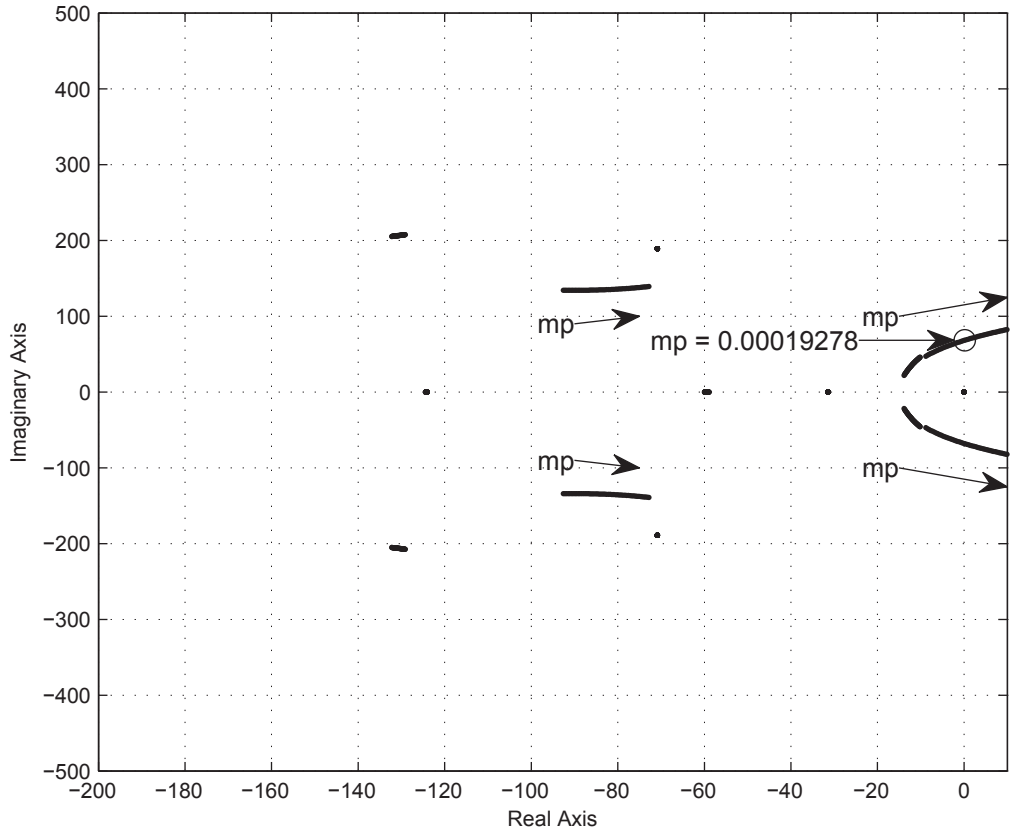

Figure 3.29: Trace of low-frequency modes as a function of the inverter droop gain: $9.4 \times 10^{-3} \leq m_p \leq 3.14 \times 10^{-4}$

with the droop controllers of the inverters and dc-side of the active load as discussed in sections 3.5.1 and 3.6.1. For every test these modes were verified by perturbing the active load and measuring the resulting oscillation from the droop controller of the inverters and the dc-bus of the active load. Figure 3.28 was verified by changing the gain of the dc-voltage controller of the active load and observing instabilities in the microgrid. The aim of the experiment was to verify the low-frequency modes and Figure 3.28 and 3.19.

If the experimental set-up successfully verifies the low-frequency modes and Figure 3.28, then it will be conduced that the model of the microgrid and active load are a good model. Thus other results obtained form this model or other microgrids modelled using the modelling technique outlined in sections 3.1 and 3.4 will not require experimental verification.

The experimental setup of the active load is discussed in Section 3.3. The operation of

Test Name	K_{iv}	K_{pv}	$\tau = \frac{K_{pv}}{K_{iv}}$
Low Gain	15	0.05	1/300
Nominal Gain	150	0.5	1/300
High Gain	600	2	1/300
Oscillatory Gain	2700	9	1/300

Table 3.10: Gains of dc- bus voltage regulator of the active load

the inverters is discussed in Appendix B.

3.7.1 Experimental test

In each of the four tests conducted, the power consumption of the active load was stepped from 7,000 W to 9,000 W and the transient responses of the load's dc- bus voltage, the inverters' output powers and the inverter's capacitor voltage was observed. The gains used, detailed in Table 3.10, correspond to the nominal gains used in the initial analysis and the extreme of the gain range used in Figure 3.18. The purpose of the experimental work is to validate the relationship between the active load and the damping of the microgrid modes that were found from the participation analysis.

3.7.2 Transient response with low, nominal and high gain

In these experiments, the low-frequency modes of the microgrid observed in the time domain are compared to the eigenvalue plot. In Figures 3.30(a), 3.31(a) and 3.32(a) two modes are identified. The modes with a frequency of 10.0 Hz, 32.1 Hz, 66.2 Hz respectively and a damping factor of 0.208, 0.351, 0.688 respectively are associated with the dc voltage controller and dc capacitor of the active load for the different gains used in the three experiments. The mode with a frequency of 4.13 Hz and a damping factor of 0.533 is associated with the droop controllers of the inverters. This does not change when the gains of the dc voltage controller for the active load are changed in the three experiments; low gain, nominal gain and high gain.

Figures 3.30(b), 3.31(b) and 3.32(b) shows that when the load is stepped, the dc voltage oscillates with a frequency of 7 Hz, 30.3 Hz, 66.2 Hz respectively and have a damping factor of 0.377, 0.250, 0.224 respectively. The envelope of the damping factor is shown by the black

long-dashed line. The experimental damping factor in all three experiments differs slightly than what the model predicts. The frequency observed is in reasonable agreement with the model.

Figures 3.30(c), 3.31(c) and 3.32(c) shows that the three inverters, which have identical droop settings, share the increased power equally when the new steady state is established. The initial increase in power is all taken by Inverter 3, which is electrically closest to the load where the power step occurred. The transient of the power output from Inverter 3 has a frequency of 7.14 Hz, 3.33 Hz, 3.17 Hz respectively and has a damping factor of 0.377, 0.500, 0.359 respectively. The damping factor envelope is shown by the black long-dashed line. The observed frequency and damping factor are in reasonable agreement with the model.

It is noted that the power output frequency of Inverter 3 in Figure 3.30(c) is greater than Figure 3.31(c) and Figure 3.32(c). This is because the inverter electrically closest to the load change will supply the current at the same rate-of-change that it is being drawn at. All three inverters will adjust their power output and converge to the new steady-state output at the nominal frequency of the droop. Within the droop controller there is a low pass filter. Any fast changing current from the inverter electrically closest to the load change will not propagate through the filter and not be seen in the power output. However, any current changing at a rate close to or slower than the power filter bandwidth will be able to propagate through the filter.

Figure 3.30(d), 3.31(d) and 3.32(d) shows the d-axis capacitor voltage of Inverter 3. The power step of the active load change has not caused a noticeable transient in the voltage trace. This figure confirms stable operation of the microgrid for the different active load gains when the active load is perturbed.

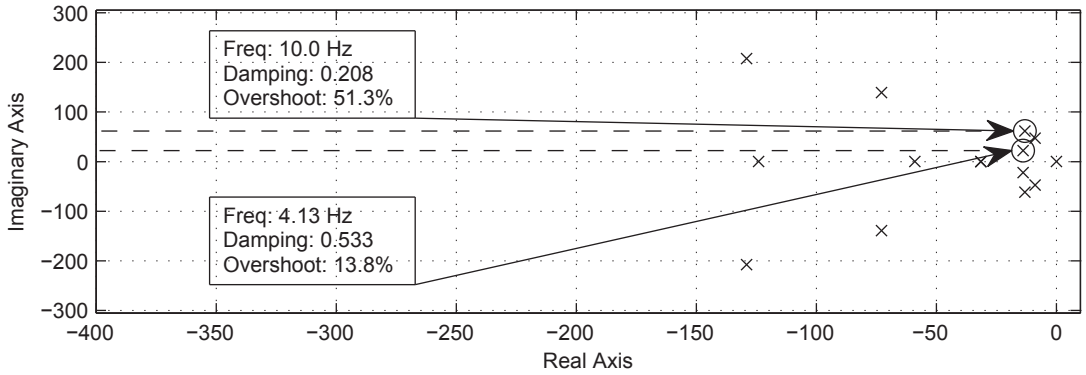

(a) Low frequency modes identified from model

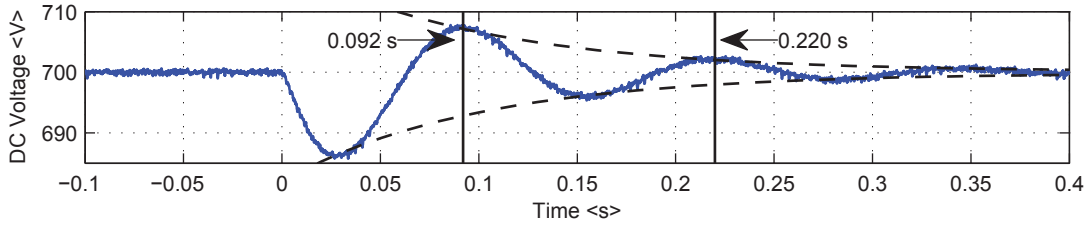

(b) The dc-voltage of active load

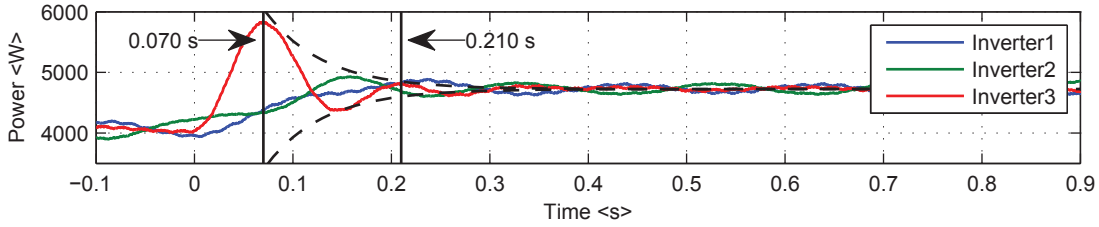

(c) Output power of inverter sources

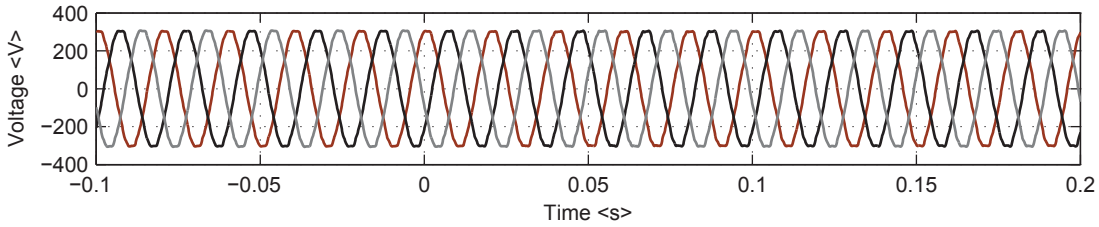

(d) Capacitor voltage of inverter sources

Figure 3.30: Experimental results with low gain

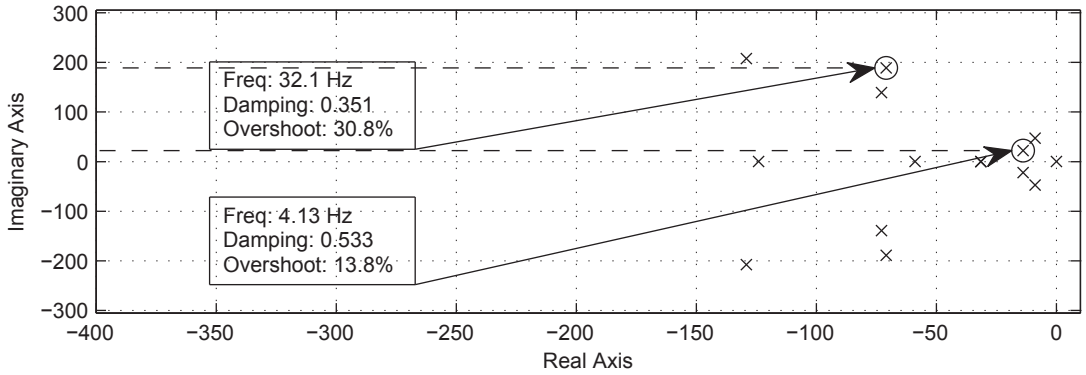

(a) Low frequency modes identified from model

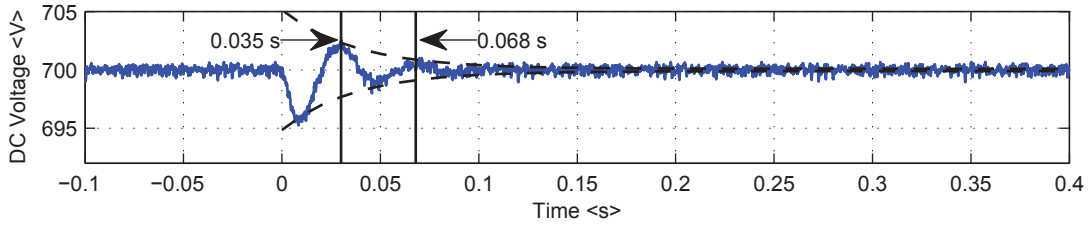

(b) The dc-voltage of active load

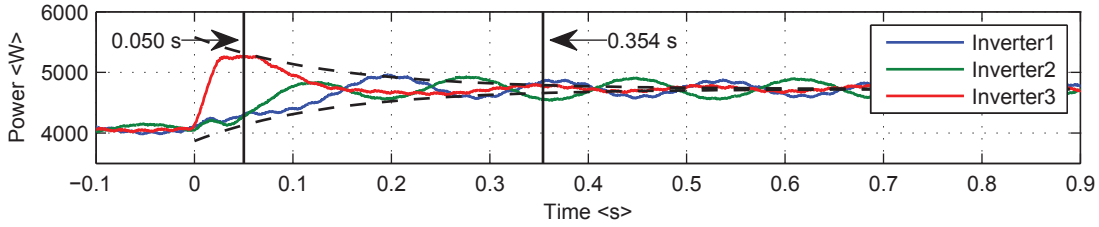

(c) Output power of inverter sources

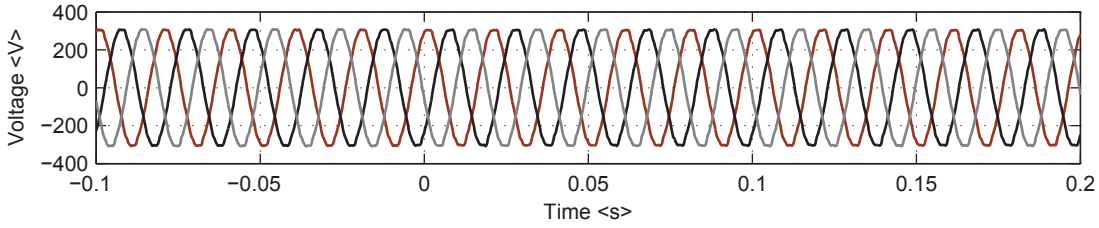

(d) Capacitor voltage of inverter sources

Figure 3.31: Experimental results with nominal gain

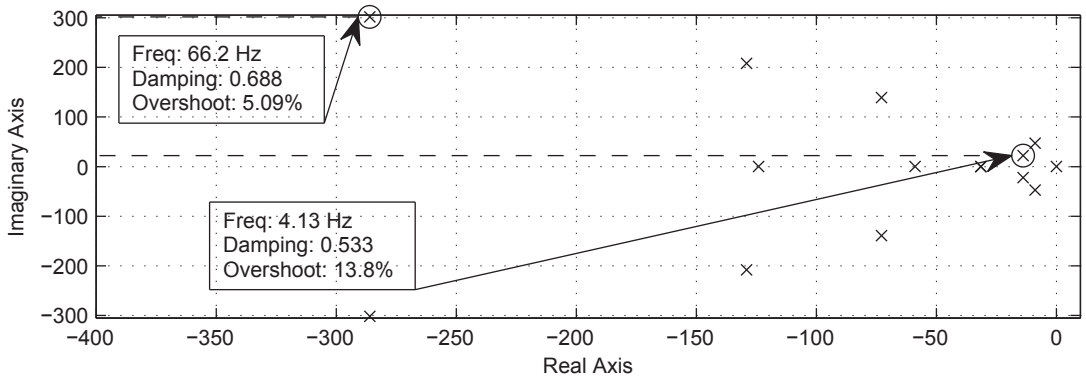

(a) Low frequency modes identified from model

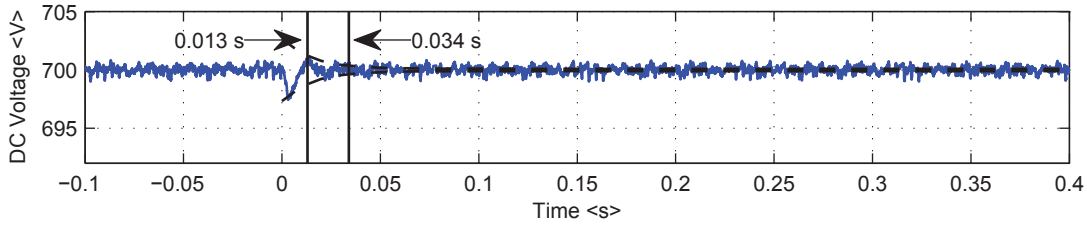

(b) The dc-voltage of active load

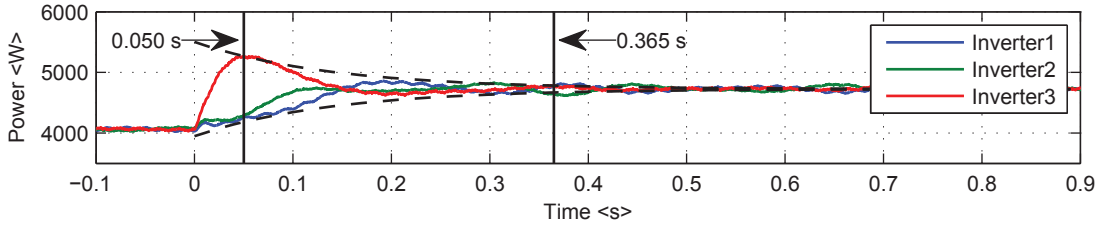

(c) Output power of inverter sources

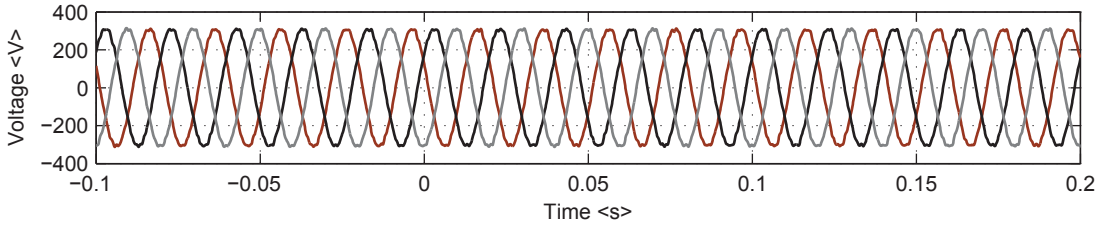

(d) Capacitor voltage of inverter sources

Figure 3.32: Experimental results with high gain

3.7.3 Transient response with oscillatory gain

The participation analysis of the microgrid with a high gain in the dc-voltage controller of the active load, showed a link between the active load dc-voltage controller and the inverters' voltage controller. The eigenvalue sweep showed that the eigenvalues, originally associated with the voltage controller of the inverter, becoming unstable and also showed the low frequency eigenvalues remaining stable.

In Figure 3.33(a) two modes are identified. The mode with a frequency of 55.1 Hz and a damping factor of 1 is associated with the dc- voltage controller and dc- capacitor of the active load. The mode with a frequency of 4.13 Hz and a damping factor of 0.688 is associated with the droop controllers of the inverters.

Figure 3.33(b) shows the dc-voltage of the active load. The dc-voltage is more oscillatory than at low, nominal or high gains. At the instant of load change, the low frequency transient is not present. However, no obvious transient in this voltage is present when the load is stepped. This absence is explained by the change in position of eigenvalue with a frequency of 55.1 Hz in Figure 3.33(a) which is seen to oscillate with a damping ratio of 1.

Figure 3.33(c) shows the power output of the inverters. The droop controllers have remained stable with a damped response at a frequency of 3.1 Hz. This is a very slight change from the output of the droop controllers in the nominal gain case. The eigenvalue plot in Figure 3.28 showed the low frequency modes, associated with the droop controllers, to be unaffected by the gain change.

Figure 3.33(d) shows the capacitor voltage of the inverters. The gains in the inverter have not altered, yet the voltage in this figure sub-plot are non-sinusoidal. An example of a sinusoidal voltage is in Figure 3.32(d). Increasing the gain in the dc- voltage controller of the load has caused the microgrid voltage to experience instabilities. This experimental test confirms the link seen in the eigenvalue trace in Figure 3.28, where the mid-frequency modes of the inverters move towards the right-hand side of the eigenvalue plot and cause the microgrid to become unstable and yet the low-frequency modes have remained stable.

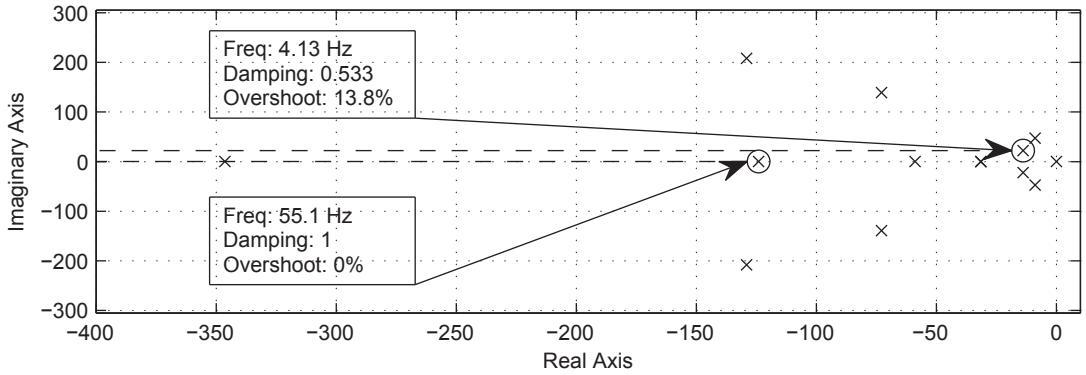

(a) Low frequency modes identified from model

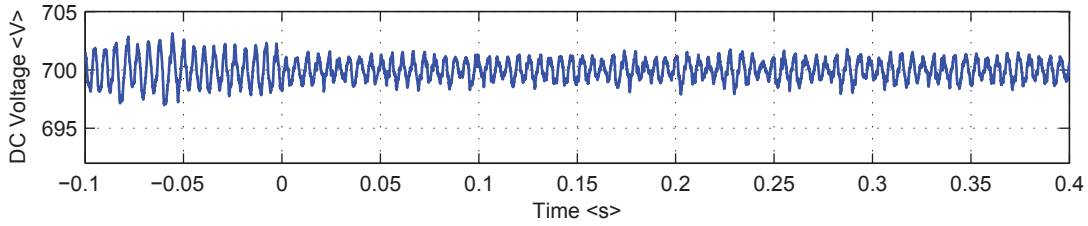

(b) The dc-voltage of active load

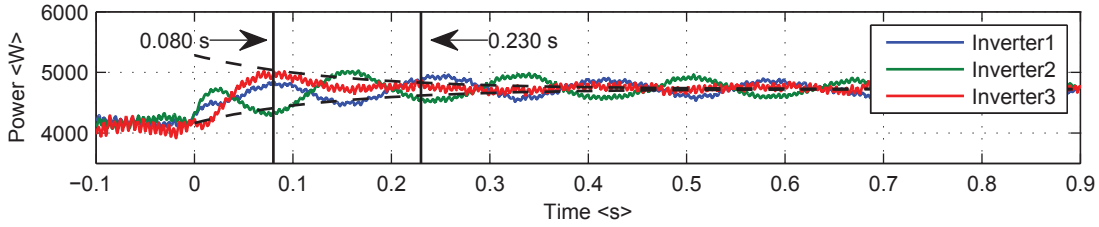

(c) Output power of inverter sources

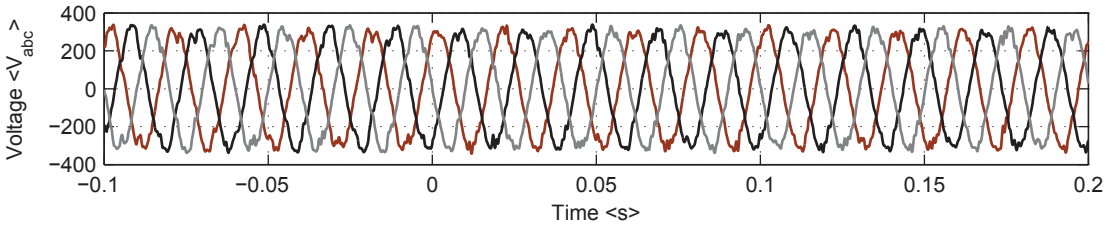

(d) Capacitor voltage of inverter sources

Figure 3.33: Experimental results with oscillatory gain

3.8 Conclusion

This chapter has presented a dynamic model of an active load which was linearised around an operating point and modelled using state-space equations. The eigenvalues of the state-space equations were calculated and participation analysis was performed to understand how the eigenvalues are linked to the states of the model. Results from the active load model have shown that the low-frequency modes are linked to the dc-voltage controller and dc-capacitor, the mid-frequency modes are linked to the coupling inductor and filter capacitor and the high frequency modes are linked to the ac-current controller and filter inductor. By increasing the gain of the dc-voltage controller, the active load experiences instabilities. The stability of the active load is most sensitive to the dc-voltage controller.

The dynamic model of the active load was integrated into the microgrid and the process was documented in this chapter. Two circuits of the microgrid were investigated where the active load was connected to node 1 and node 3. In each circuit, the eigenvalues of the linearised model were calculated and participation analysis was performed. Results showed that the low frequency modes of the active load and the inverters were in the same frequency range. All other inverter and active load eigenvalue groups did not share the same frequency and their eigenvalue groups were separate.

Participation analysis revealed that the low frequency modes of the inverter and active load did not interact with each other although they were in the same frequency range. However, the participation analysis did reveal an interaction between the low frequency modes of the active load and the mid frequency modes of the inverter. When the gain of the dc-voltage controller of the active load was increased, the modes associated with the voltage controller of the inverters became unstable. Therefore when assessing the interactions between loads and inverters, it is important to consider all control dynamics.

The interactions revealed from the participation analysis was tested using an experimental set-up. The gain of the dc-voltage controller of the active load was increased and the export power and capacitor voltage were observed. In the experiment when the gain of the dc-voltage controller of the active load is near the stability limit, the voltage controlled by the inverters

showed instability and the power oscillations, which are controlled by the inverter droop controllers, remained stable. Therefore this experimental result has supported the analysis from the participation analysis.

Chapter 4

Resetting of Inverter Limiting

The work in this chapter has been published in one conference proceeding and one journal proceeding. Specifically, sections 4.2 – 4.5 are published in [122] and Section 4.6 is published in [123].

In this chapter, methods of current limiting and current resting are explored for inverters that employ closed-loop cascaded control loops. All proposed methods are experimentally tested using a low-impedance to emulate a fault at the terminals of the inverter. The advantages and disadvantages of each method are discussed. Some proposed methods fail to correctly return back to normal operation once the fault has cleared. The methods that fail either cause the inverter to latch-up or the output of the controllers to wind-up. Reasons for this are presented within the relevant section.

All work was undertaken experimentally and no simulation results are presented. The inverters in this chapter were all designed to supply four-wire systems where there may be a requirement to supply unbalance loads. For this reason the controllers used all operation in the 'ABC' reference frame using (PR) control.

The chapter concludes with a generalised method for how to design a fault limit controller within inverters that use cascaded control structures.

4.1 Calculating RMS

In the subsequent sections, the limit and reset design requires the RMS to be calculated. This work uses a simple RMS calculation where the time series signal, as shown in Equation (4.1), is multiplied by itself which squares the signal as shown in Equation (4.2).

$$f(t) = A\sin(\omega t + \theta) \tag{4.1}$$

$$f(t) \times f(t) = A\sin(\omega t + \theta) \times A\sin(\omega t + \theta) \tag{4.2}$$

Using the sine product identity, Equation (4.2) is expanded to Equation (4.3) which is then simplified to Equation (4.6) by using the steps shown in Equation (4.4) and Equation (4.5).

$$f(t)^2 = A \times A \times \frac{\cos((\omega t + \theta) - (\omega t + \theta)) - \cos((\omega t + \theta) + (\omega t + \theta))}{2} \tag{4.3}$$

$$f(t)^2 = A^2 \times \frac{\cos(0) - \cos(2\omega t + 2\theta)}{2} \tag{4.4}$$

$$f(t)^2 = A^2 \times \frac{1 - \cos(2\omega t + 2\theta)}{2} \tag{4.5}$$

$$f(t)^2 = \frac{A^2}{2} - \frac{A^2\cos(2\omega t + 2\theta)}{2} \tag{4.6}$$

Equation (4.6) contains a dc- term and a term which is twice the frequency of the original frequency. If the dc term is square-rooted, then the equation becomes the RMS of Equation (4.1).

In the inverter controller, the signal is passed through a low-pass-filter (LPF) to separate the dc term from the $2\omega t$ term. For the ideal case, the LPF signal will only be equal to the dc-term as shown in Equation (4.7).

Figure 4.1: Implementation of Equation (4.8) for the RMS block used in the inverter controllers.

$$LPF\left(f\left(t\right)^2\right) = LPF\left(\frac{A^2}{2} - \frac{A^2\cos\left(2\omega t + 2\theta\right)}{2}\right) = \frac{A^2}{2} \tag{4.7}$$

By applying a square root function to the output of the LPF, the RMS of the input signal is calculated. Equation (4.8) shows the RMS output equation.

$$\sqrt{LPF\left(f\left(t\right)^2\right)} = \frac{A^2}{2} = \frac{A}{\sqrt{2}} \tag{4.8}$$

The implementation of Equation (4.8) inside the RMS block used in the inverter controller is shown in Figure 4.1.

4.2 Current Limiting During Fault Ride-through

Typically, inverter control designs use a cascaded structure to control current, voltage or power. The controller used within this study comprises of two control loops, as shown in Figure 4.2. The inner control loop is designed to control the current through the inductor between the switching-bridge and the filter capacitor. It has the highest bandwidth and is there to provide good power quality and to enable explicit limiting of the export current from the inverter. The outer control loop is designed to control the voltage across the capacitor. The references to the outer control loop may be fixed set-points or be varied by P/f and Q/V droop functions or a remote dispatcher. Figures 4.3 and 4.4 detail the inner current and output voltage controller respectively.

The outputs of the inner and outer control loops need to be constrained to ensure that the inverter does not operate outside of the circuits physical limits. The output of the inner controller is the voltage reference for the switching-bridge. This is limited by the modulation

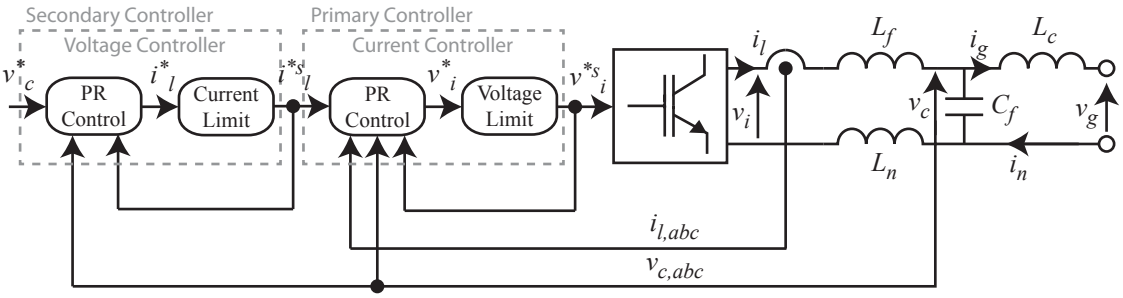

Figure 4.2: Control of the inverter source used in all studies presented in this paper. The controller has multiple control loops, of which both are closed-loop. The inverter used is operated in island and does not require a PLL. One of three phases and neutral is shown.

limit of the switching-bridge and the dc-bus voltage. The output of the outer voltage controller is the current reference for the inner current controller. The current reference is limited by the current rating of the semiconductors within the switching-bridge.

It is expected that when a low impedance fault is applied to the network, inverter output voltage will reduce. The outer voltage controller will increase the current reference to the inner controller in an attempt to maintain the system voltage. The increase in current reference will be above the maximum current allowed for the inverter and so a current limit should activate. When the fault clears, the network impedance seen by the inverter will rise suddenly and the voltage controllers will start reducing the current reference. There may be a short time-delay before the current limit of the inverter is removed and a delay in the current controllers changing the current to its new, lower reference. During this period, the voltage command of the inverter can become large (because a higher than normal current is being injected into a normal network impedance). The inverter will voltage limit naturally because of the limited dc link voltage but it is advisable to apply a limit to the command to the inverter to exercise the limit in a particular way. Three aspects of control system operation during fault ride through are of interest: the period immediately after the fault (known to power system engineers as the sub-transient period) during which the fault current should be brought under control; the steady-state fault response during which well defined sinusoidal fault currents are desired to flow that will allow the protection system to operate and the fault recovery period in which the current should rapidly return to normal levels and the voltage controllers to rapidly regain normal control over the inverter voltages.

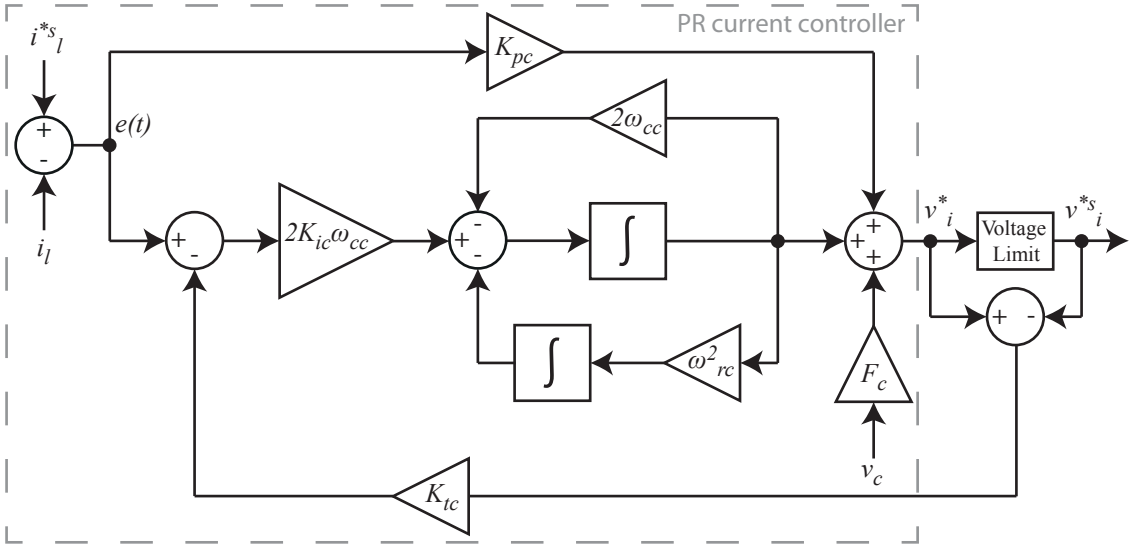

Figure 4.3: Schematic of the current controller which is indicated by the dotted-box called 'current controller' in Figure 4.2. The current controller is a non-ideal PR controller with tracking integration anti-wind-up. The anti-wind-up is designed to compensate the integrator when the limiter algorithm limits the output of the controller. The voltage limit design is dependent on the case being investigated. The reset signal of the voltage limiter is not shown because it depends on the design of the limiting strategy.

An experimental test system was built around a TriPhase 10 kVA inverter with a control structure of Figure 4.2 and parameters of Table 4.1. The limiters and anti-wind-up were added to the controller. The inverter was connected to two resistive loads rated at 3 kW each. A 63 A contactor and a 1.2 Ω impedance were arranged to close across one load to present a low impedance fault and a second 63 A contactor was arranged in series with the load to clear the fault. The second load remained connected during and after the fault. A National Instruments Compact Rio was used to control the fault which was initiated 1 s into the test and cleared at 2 s.

Results of the experiments are discussed in the subsections to follow. In each experimental plot figure, the left-hand plot shows fault inception with the controller entering current limit mode and exporting a fault current. The right-hand plot in each figure shows the controller returning from current limit mode to normal operation once the fault has been cleared.

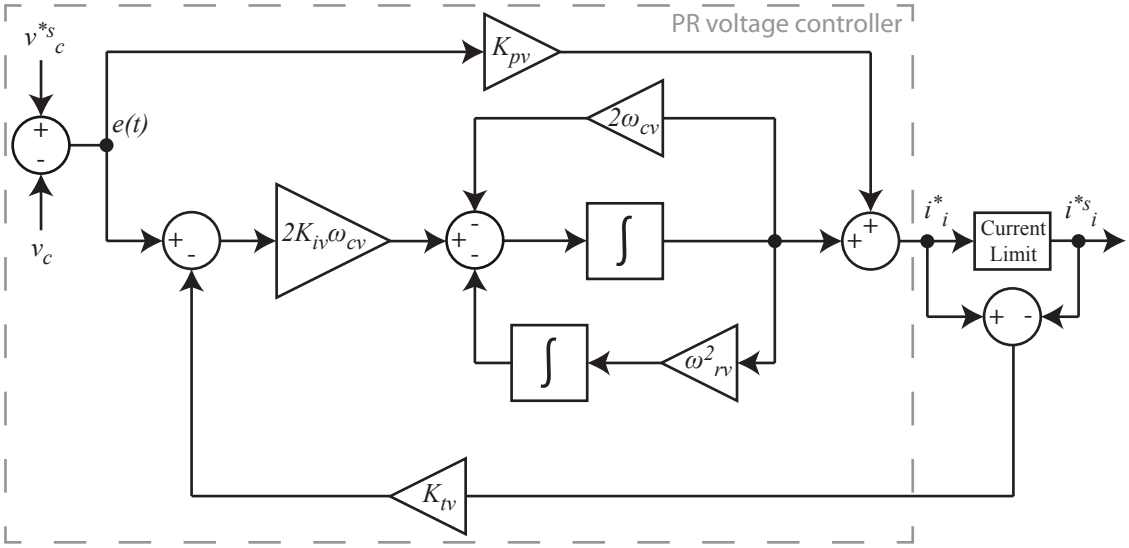

Figure 4.4: Schematic of the voltage controller which is indicated by the dotted-box called 'voltage controller' in Figure 4.2. The voltage controller is a non-ideal PR controller with tracking integration anti-wind-up. The anti-wind-up is designed to compensate the integrator when the limiter algorithm limits the output of the controller. The current limit design is dependent on the case being investigated. The reset signal of the current limiter is not shown because it depends on the design of the limiting strategy.

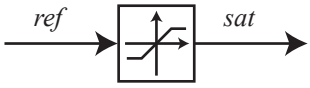

Figure 4.5: Schematic of instantaneous limit used in the current and voltage limits. Each phase is limited independently.

4.3 Instantaneous saturation limits – Case 1

Instantaneous saturation limits, as shown in Figure 4.5, were built using saturation blocks in Simulink and are only active when the reference signal is above the limit.

Examining the capacitor voltage and grid current in Figure 4.6, it can be seen that during the fault, the capacitor voltage and grid currents were distorted. The crest of the current reference was over the saturation block threshold and was subsequently limited. This caused the crest to became flat and the limited current reference to resemble a square wave.

Once the fault had been cleared, within five cycles the controller is supplying a regulated voltage to the load. Evidence of this can be seen in all three of the right-hand plots of Figure 4.6. The current-limit signal and voltage-limit signals return to false at 3.045 and 3.066 seconds

Table 4.1: Properties of the inverter source

Inverter Circuit			
Parameter	***Value***	***Parameter***	***Value***
L_f	1.35 mH	r_f	0.1 Ω
L_c	0.35 mH	r_c	0.03 Ω
L_n	0.45 mH	r_n	0.1 Ω
C_f	50 μF		
Voltage Controller			
Parameter	***Value***	***Parameter***	***Value***
K_{pv}	0.05	ω_{cv}	2π0.1 rad/s
K_{iv}	46.8	ω_{rv}	2π50 rad/s
K_{tv}	1.5		
Current Controller			
Parameter	***Value***	***Parameter***	***Value***
K_{pc}	5	ω_{cc}	2π0.1 rad/s
K_{ic}	4,000	ω_{rc}	2π50 rad/s
K_{tc}	0.1	F_c	0.5
Maximum Operating Conditions			
Parameter	***Value***	***Parameter***	***Value***
Phase Current Limit	30 Arms	Phase Voltage Limit	229 Vrms
Nominal Operating Conditions			
Parameter	***Value***	***Parameter***	***Value***
Nominal Phase Voltage	220 Vrms	Nominal Frequency	50 Hz

retrospectively and the error signal in the voltage controller, shown by the blue line in Figure 4.6 returns back to zero at 3.112 seconds. As expected and explained in Section 4.2, there is an over voltage which causes the voltage limiter to trigger after the fault had been cleared. The voltage limiter was triggered at 3 seconds until 3.066 seconds.

The advantage of using instantaneous saturation limiting is that it is simple, easy to implement and not computational intensive. The main disadvantage is that the fault current is distorted. Another disadvantage is that it is not possible to supply a lower or higher fault current once the current limiter has been triggered. For example, in a fault constrained network it may be necessary for the inverters to limit the output at 1 pu current but supply 0.5 pu of

fault current. Or in a network where the fault level is low, it may be necessary to limit at 1 pu current but supply 2 pu of fault current.

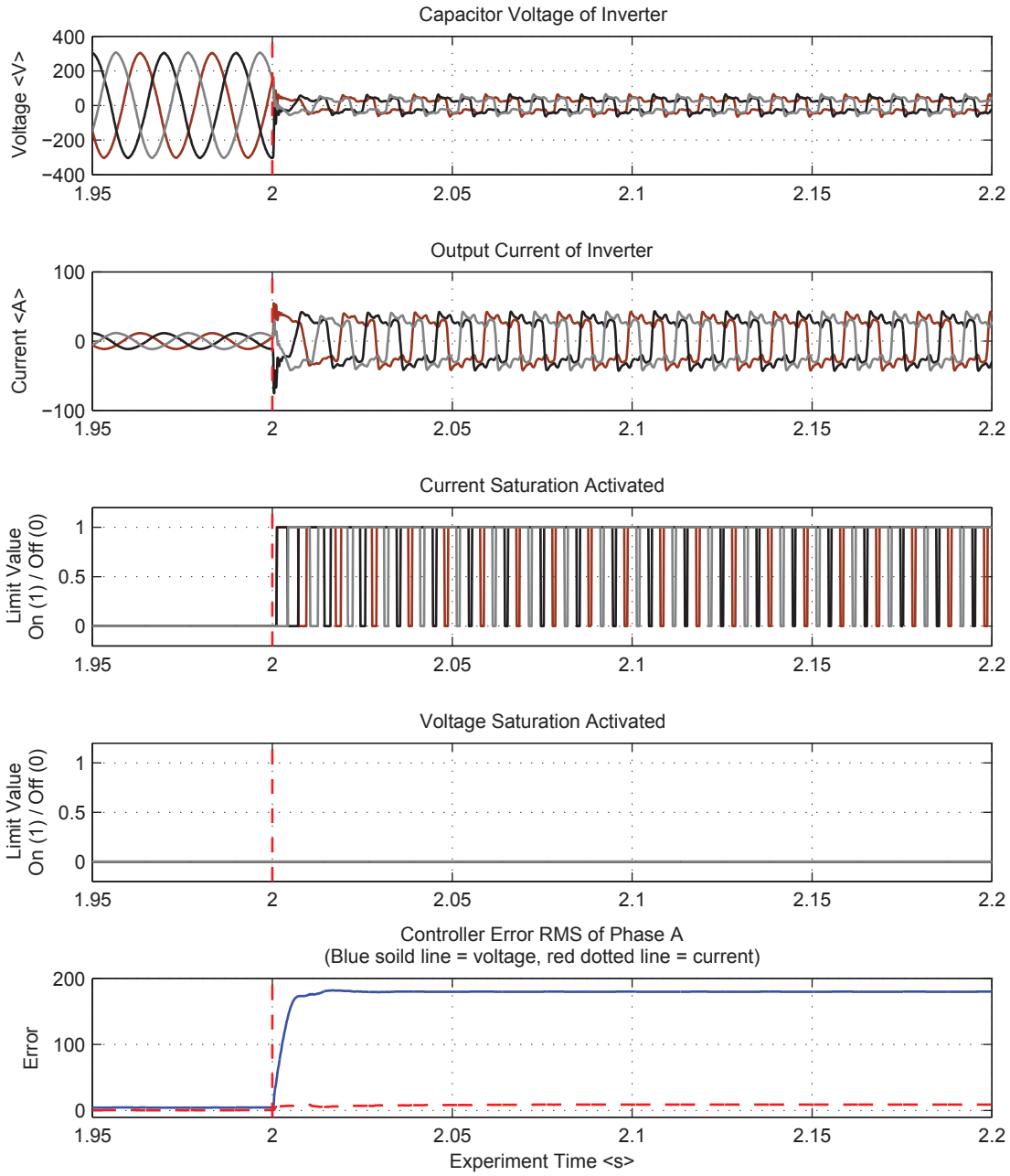

Figure 4.6: Experimental results of case 1 (instantaneous) for when the fault is applied at t = 2s. Plots show the state of the limiting circuits, the error in the controllers, the capacitor voltage and the grid current.

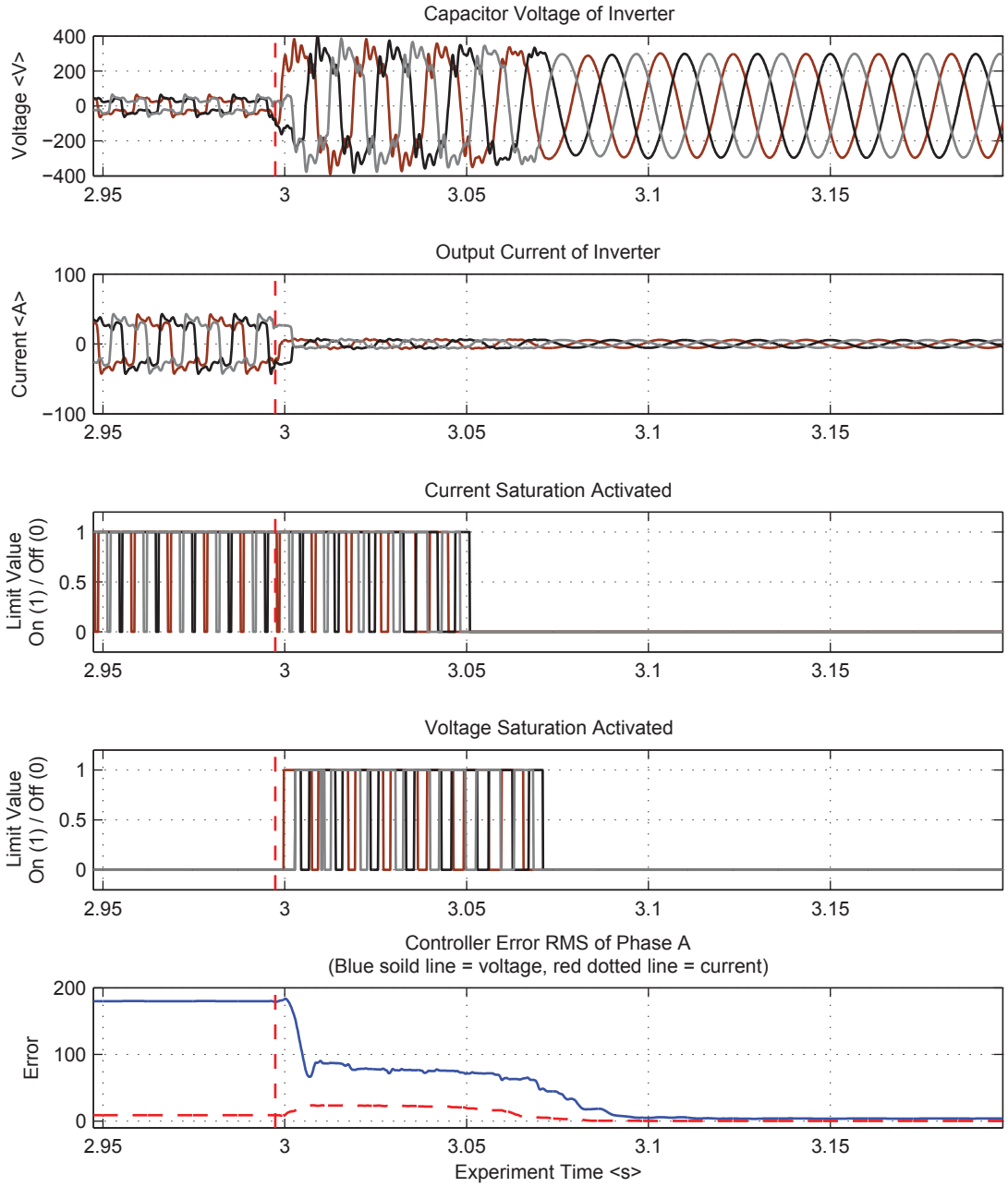

Figure 4.7: Experimental results of case 1 (instantaneous) for when the fault clears at t = 3s.

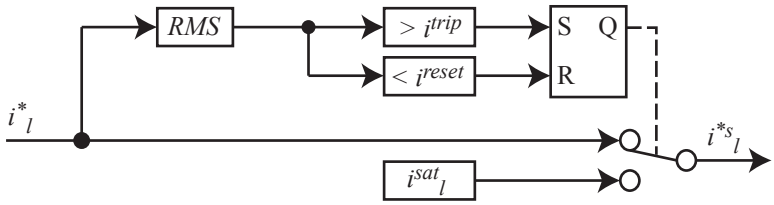

Figure 4.8: Schematic of Current-Trip Current-Reset limit used in the current limit. Each phase is limited independently.

4.4 Current-Trip and Current-Reset (CTCR) Current Limiter – Case 2

The previous section demonstrated that using instantaneous limits allowed the inverter to trip when the fault current demand was greater than the physical limit of the inverter and for the inverter to return from fault to normal control when the fault had been cleared. However, during the fault the current were very distorted. This would not be allowed to operate in a DNO's network. To provide a less distorted fault current, a current latch limit will be used.

The current latch-limit will trip when the RMS value of the current reference signal from the output of the voltage controller increases above the phase current limit defined in Table 4.1. The limiter will reset when the RMS value of the current reference signal from the output of the voltage controller decreases below 90% of the phase current limit. The operation of the RMS block is explained in Section 4.1.

To begin with, the voltage limit will remain the same as the previous test and an instantaneous voltage limit will be used.

4.4.1 Instantaneous Voltage limiter – Case 2a

When the system voltage was above the limit threshold, as seen in the voltage limit signal in Figure 4.9, the output voltage from the inverter became distorted due to the instantaneous limit clipping of the crest of the PWM reference RMS voltage. The distortion can be seen in the capacitor-voltage plot of Figure 4.9.

It can be seen from the right-hand-plots of Figure 4.9 that the current limiter never reset after the fault had been cleared. This is because the output of the voltage controller (input to the current limiter) remained greater than the reset threshold of the current limiter. An explanation for this is that the feedback from the tracking integration kept the output of the integrator, within the voltage controller, above the current limit threshold. This feedback prevents the limiter from resetting and thus the current-limiter has experienced latch-up. For the inverter to supply the fault current across the non-fault load, the inverter would need to increase the output voltage to beyond the voltage limit. For this reason the output of the current controller (input to the voltage limiter) was limited.

Neither the current controller or the voltage controller regain control (error returns to zero in the right-hand side of Figure 4.9) of the inverter once the fault had been cleared.

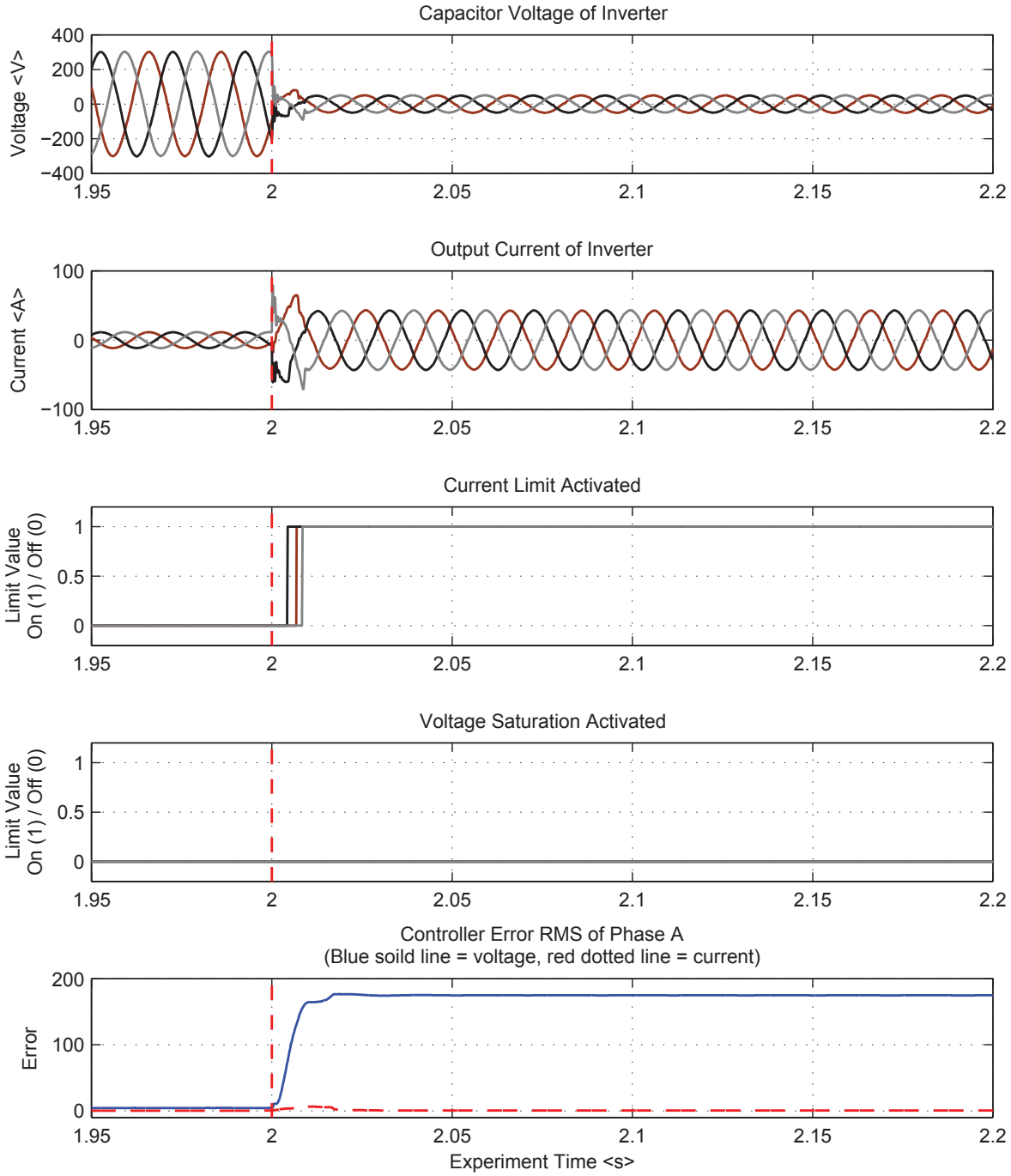

Figure 4.9: Case 2a Trip: Current-trip, current-reset current limit and instantaneous voltage limit

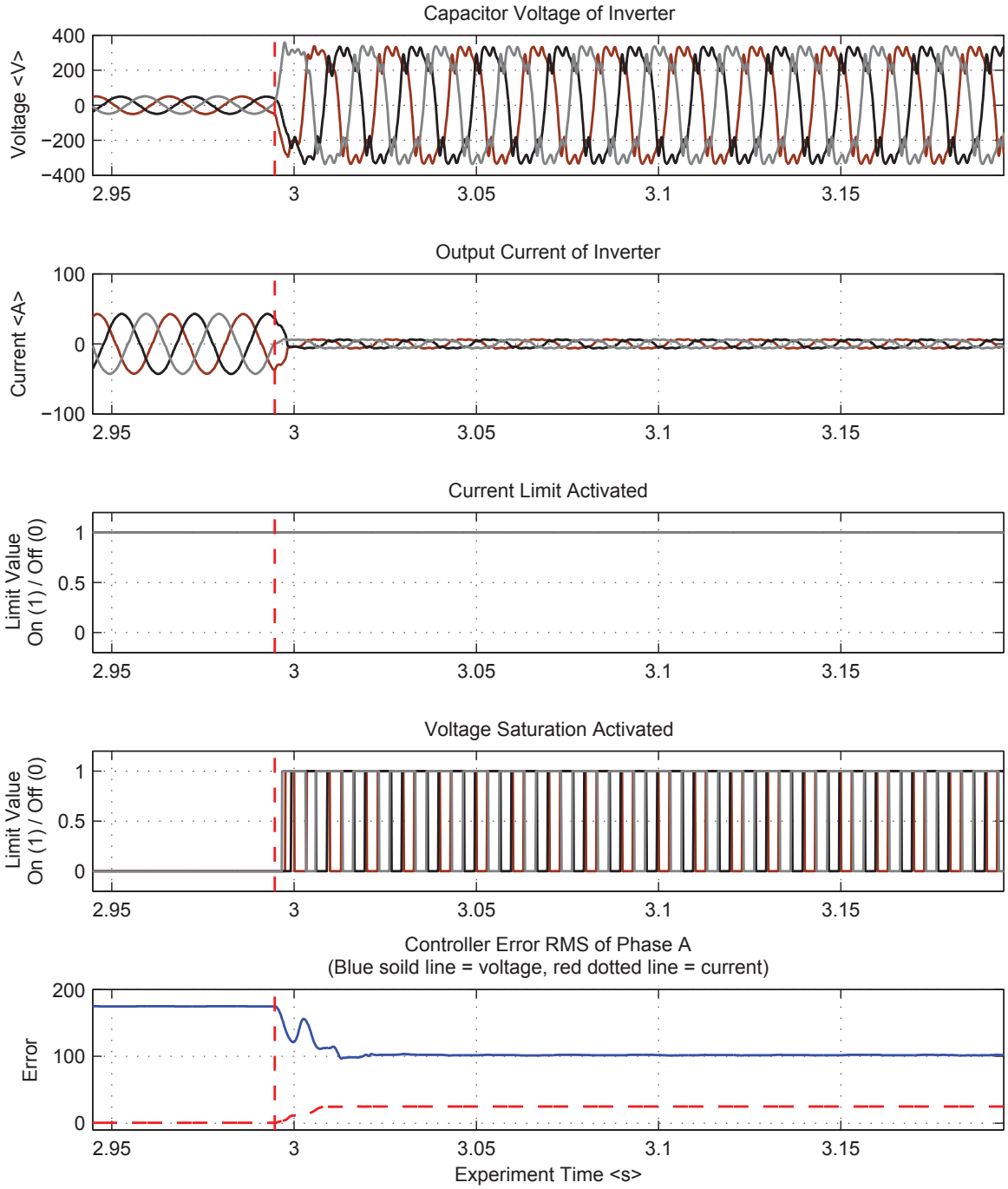

Figure 4.10: Case 2a Reset: Current-trip, current-reset current limit and instantaneous voltage limit

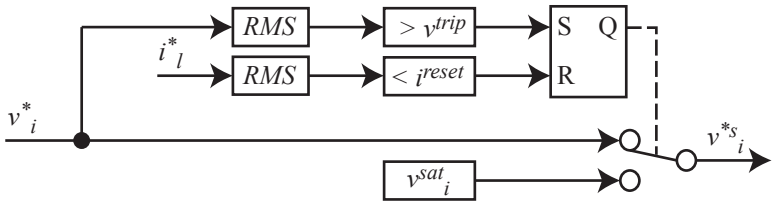

Figure 4.11: Schematic of Voltage-Trip Current-Reset limit used in the voltage limit. Each phase is limited independently.

4.4.2 Voltage-trip and current-reset (VTCR) Voltage limiter – Case 2b

In the previous case, the current limit failed to reset and the inverter continued to supply fault current once the fault had been cleared. Consequently, the capacitor voltage became distorted because the inverter was being limited by the instantaneous voltage limit. To improve the voltage distortion of the inverter once the fault has been cleared, the voltage limit will be changed to a voltage-trip and current-reset limit as shown in Figure 4.11.

The voltage limit will trip when the RMS value of the PWM voltage reference signal from the output of the current controller increases above the phase voltage limit as defined in Table 4.1. This will produce an undistorted voltage and thus improving the power quality compared to the instantaneous voltage limit. The voltage limit will reset using the same signal as the current limiter. Resetting the voltage controller at the same time as the current controller will prevent the situation where the output of the current controller is in limit and the output of the voltage controller is not in limit. This situation may cause wind-up of the voltage controller because the integrator of the voltage controller will no longer be protected by the anti-wind-up feedback provided when there is a difference between the output of the voltage controller and the output of the current limit.

In Figure 4.12 after the fault had been cleared, as with case 2a, the current limiter did not reset. The explanation for this is identical to case 2a. The feedback from the tracking anti-wind-up is preventing the current limiter from resetting and the current limiter has latched-up.

Since the output of the voltage controller (input to the current limiter) remained high, the current reset was never activated and the voltage limit was inhibited from resetting. If the voltage limiter were to be reset from the measurement of output current, then in this case

the voltage limiter would have reset. However, the inverter is physically limited by the dc bus voltage and the output would be similar to when the PWM voltage reference was limited by an instantaneous saturation limit. Also, since the tracking integration for the current controller would no longer be active, the current controller may experience wind-up.

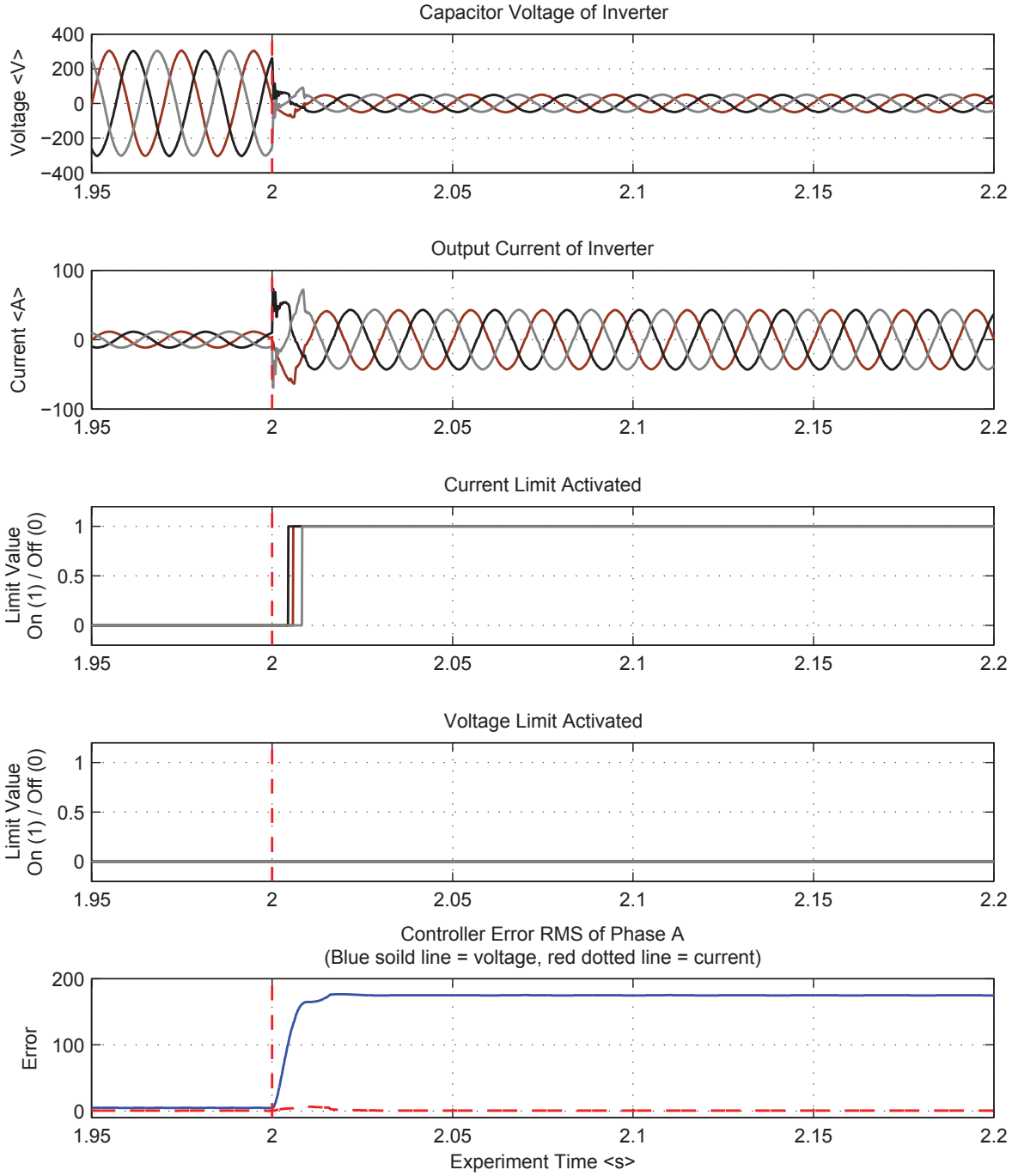

Figure 4.12: Case 2b Trip: Current-trip, current-reset current limit and voltage-trip, current-reset voltage limit

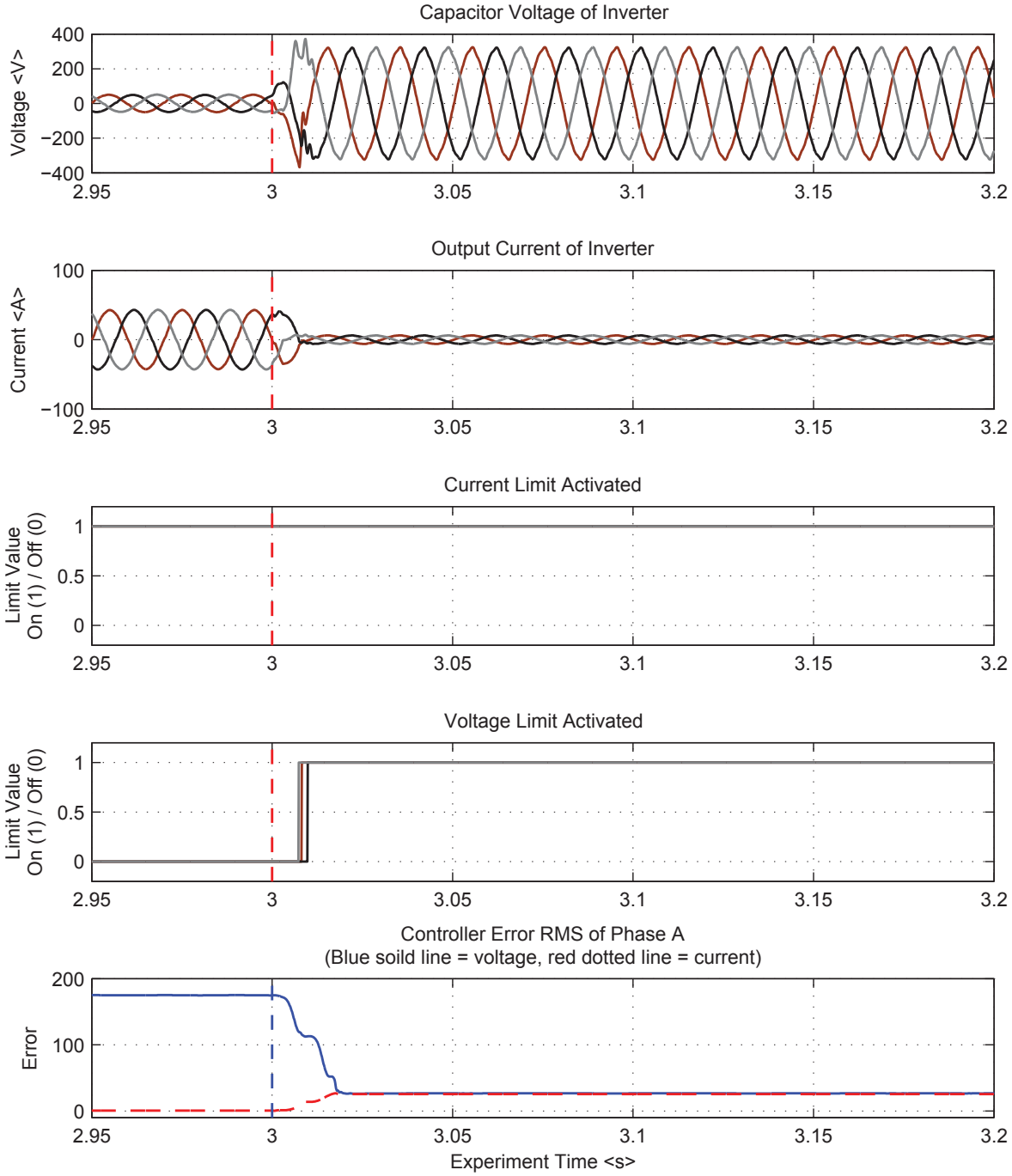

Figure 4.13: Case 2b Reset: Current-trip, current-reset current limit and voltage-trip, current-reset voltage limit

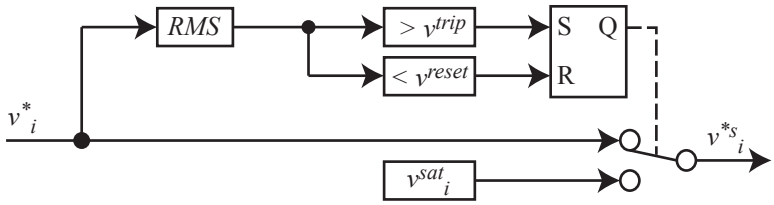

Figure 4.14: Schematic of Voltage-Trip Voltage-Reset limit used in the voltage limit. Each phase is limited independently.

4.4.3 Voltage-trip and voltage-reset (VTVR) Voltage limiter – Case 2c

Since the current limiter was not reset with either an instantaneous voltage limit or a VTCR voltage limit, it is unlikely that changing the design of the voltage limit will work. This test was conducted to determine if this change would have any impact on the current limiter. The design of the voltage limiter was changed such that it reset from the RMS value of the PWM voltage reference signal from the output of the current controller when the RMS value increases above the phase voltage limit as defined in Table 4.1 as shown in Figure 4.14. No hysteresis was added to the voltage limit because the limit is only 9 Vrms above the nominal nominal voltage of 220 Vrms.

As expected this case did not reset once the fault had cleared. For the same reason as the previous two cases (cases 2a and 2b) with a current-trip and current-reset current-limiter, the tracking integration inhibited the limiter from resetting. Since the current limiter did not reset, the reference to the current controller was much higher and this caused the output of the current controller, the PWM voltage reference, to remain high and prevent the voltage limiter from resetting.

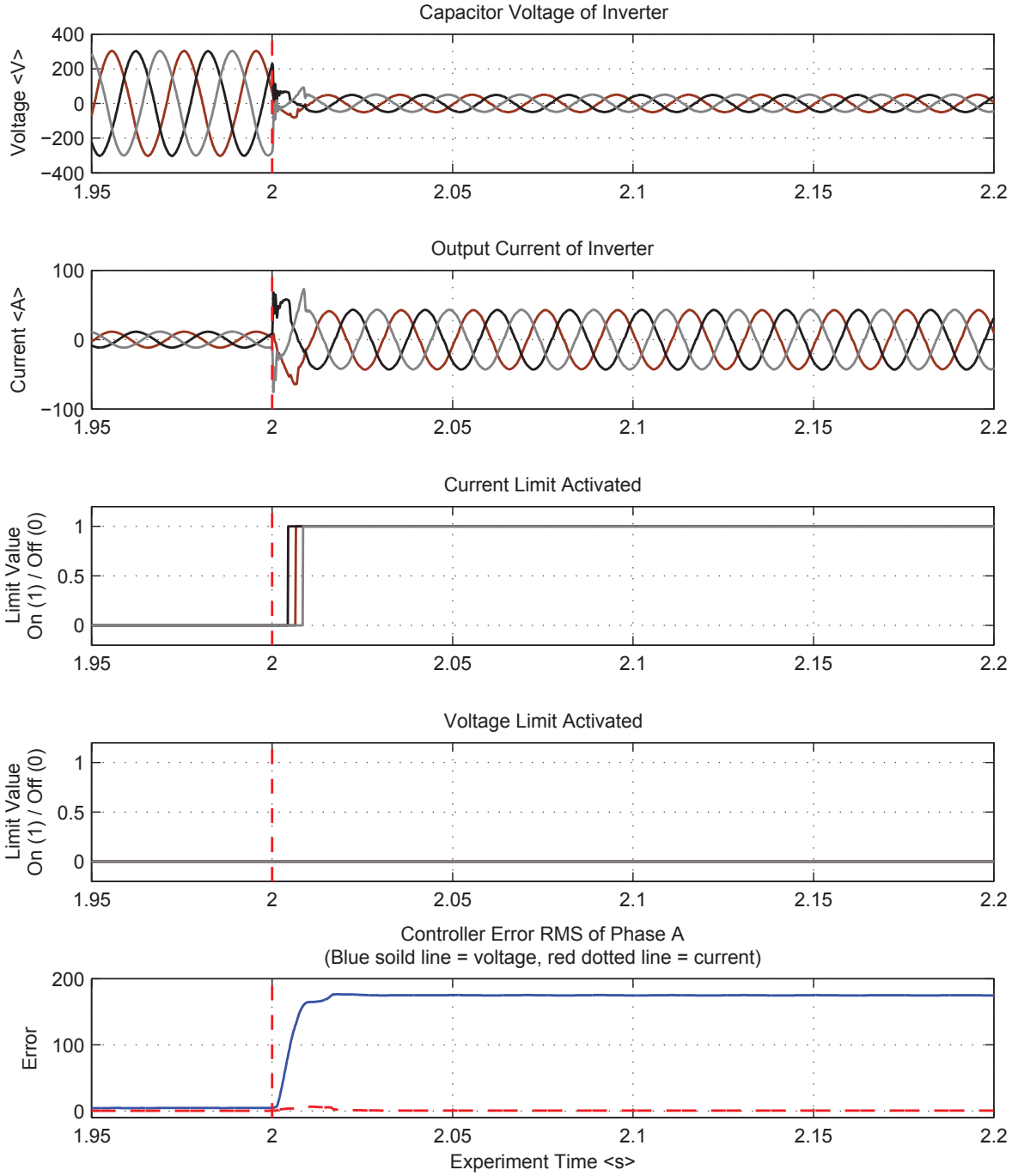

Figure 4.15: Case 2c Trip: Current-trip, current-reset current limit and voltage-trip, voltage-reset voltage limit

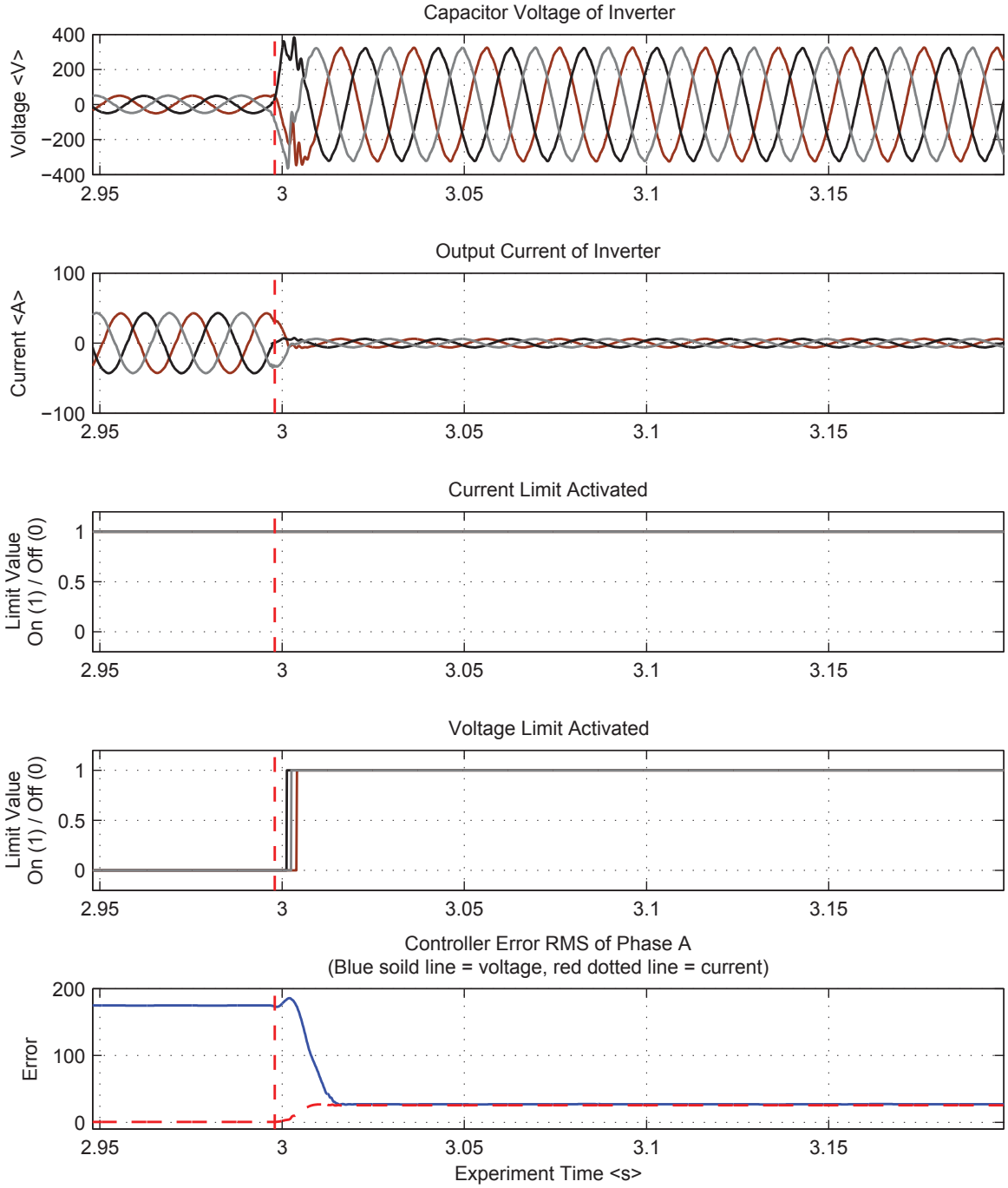

Figure 4.16: Case 2c Reset: Current-trip, current-reset current limit and voltage-trip, voltage-reset voltage limit

4.4.4 Current-trip and current-reset (CTCR) conclusion

In all cases, the current limiter experienced latch-up because the output of the voltage controller was kept high from the feedback of the tracking integration anti-wind-up. The design of the voltage limit did not assist the reset of the current limit.

A possible solution to allow the current limiter to reset would be to increase the gain of the tracking integration. This would decrease the output of the integrator and allow the reduction of the error signal once the fault had been cleared to lower the output of the voltage controller (current reference) to a level that is below the reset threshold of the limiter. However, an increase in gain may cause the integrator to become unstable.

Another possible solution to allow the current limiter to reset could be to change the anti-wind-up strategy and use conditional integration. However, if the output of the proportional gain was much lower than the threshold of the limit for both during and after the fault, then the current limiter would reset once the output of the integration had been forced to zero. Next the current output of the inverter would increase, because of the fault impedance, until the limiter was activated again. This limit oscillation would continue until the fault had been cleared.

When the outer controller uses integrators within the design, this set of experiments has shown that the limiter to the output of the outer controller should not be reset from the output of the outer controller. This then allows for the limiter to successfully reset once the fault has cleared and that either tracking integration or conditional integration could be used for the anti-wind-up strategy of the outer controller.

4.5 Current-Trip and Voltage-Reset (CTVR) Current Limiter – Case 3

As in the cases 2a – 2c that use a current-trip and current-reset current-limit, the fault current, as seen in Figure 4.9 – 4.15, was not distorted. From this it is clear that the design is a good limiting strategy. However, the limit never reset and a new reset strategy must be designed.

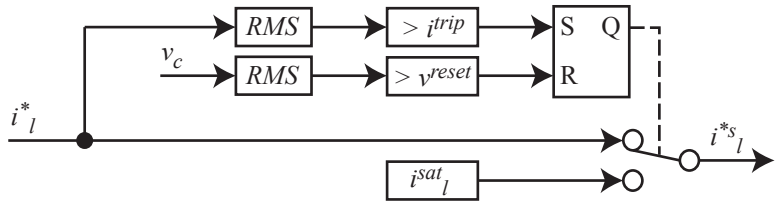

Figure 4.17: Schematic of Current-Trip Voltage-Reset limit used in the current limit. Each phase is limited independently.

Once the fault has been cleared, the voltage will increase if the inverter continues to supply fault current. Therefore when the voltage rises after the current limit has been activated, it would be a reasonable to assume that the fault has been cleared and the inverter should return from current-limit to normal-operation. To comply with this logic, the current-limiter in cases 3a – 3c will be tripped when the output of the voltage controller (current reference) is above a pre-defined threshold and will be reset when the measured capacitor voltage has increased above a pre-defined threshold, as shown in Figure 4.17.

As in the case of the Current-Trip Current-Reset limiter, the Current-Trip Voltage-Reset limiter will trip when the RMS value of the current reference signal from the output of the voltage controller increases above the phase current limit defined in Table 4.1. The Current-Trip Voltage-Reset limiter will reset when the measured RMS value of the filter capacitor voltage is above the nominal phase voltage, as defined in Table 4.1.

The Current-Trip Current-Reset limiter will be first tested with instantaneous voltage limits.

4.5.1 Instantaneous Voltage limiter (Case 3a)

As expected, the instantaneous limit at the output of the current-controller triggered because there was a small time between the current limit resetting and the controllers returning to steady-state. This event is seen in the right hand plot of Figure 4.18. There was no latch-up or wind-up and the controller operated correctly once the fault had been cleared shown by the controller error signal returning to zero. However, the transition time for the voltage controller to re-establish an undistorted voltage was 6 cycles as seen in the capacitor-voltage of Figure

4.18. This is caused by the output of the voltage controller having to decrease from the tracking integration anti-wind-up. A reduction in time from the fault clearing to the controller returning to steady-state could be achieved by resetting the integrator in the voltage controller once the current limit reset is operated, or by using condition integration anti-wind-up instead of tracking integration anti-wind-up.

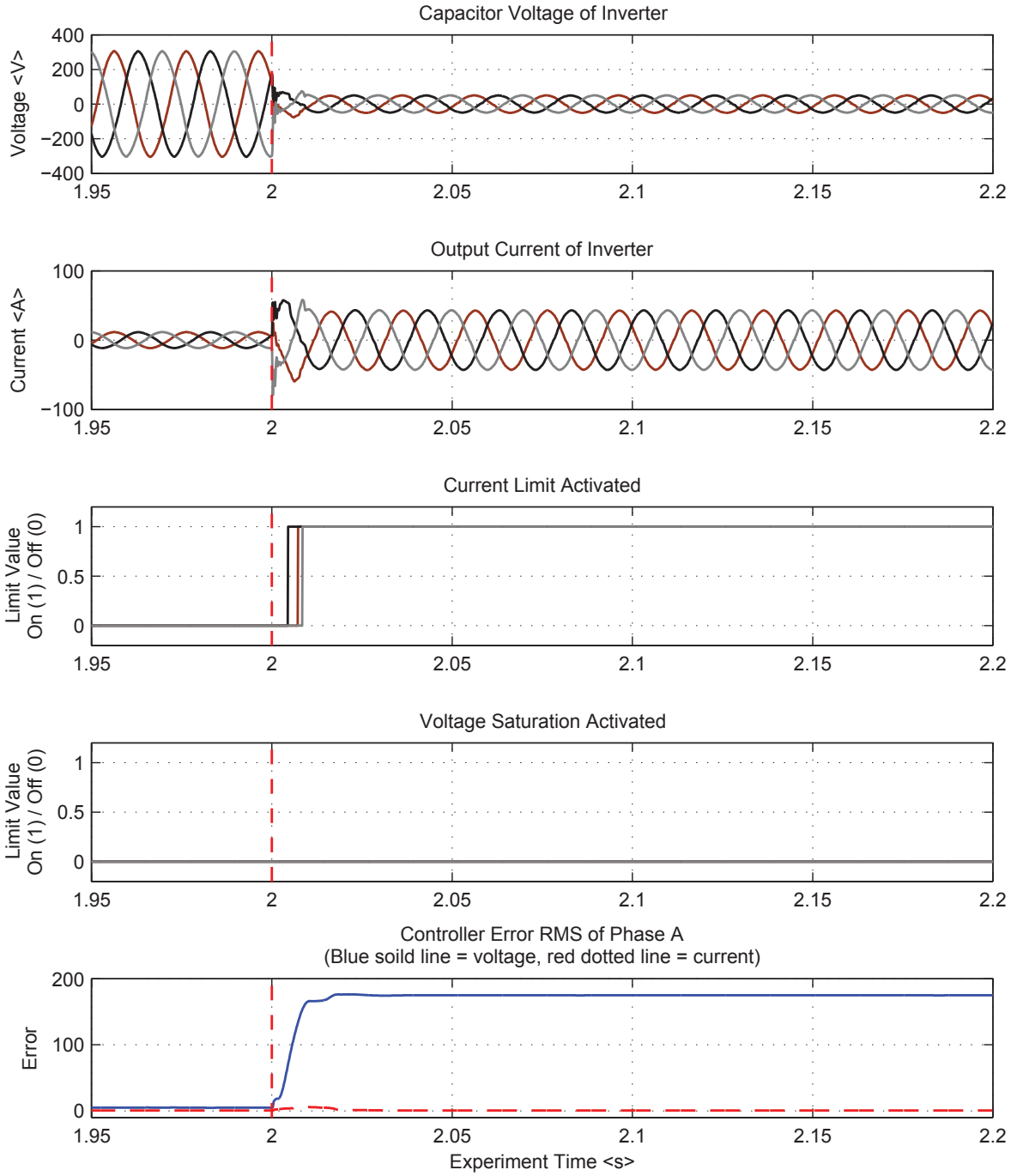

Figure 4.18: Case 3a Trip: Current-trip, voltage-reset current limit and instantaneous voltage limit

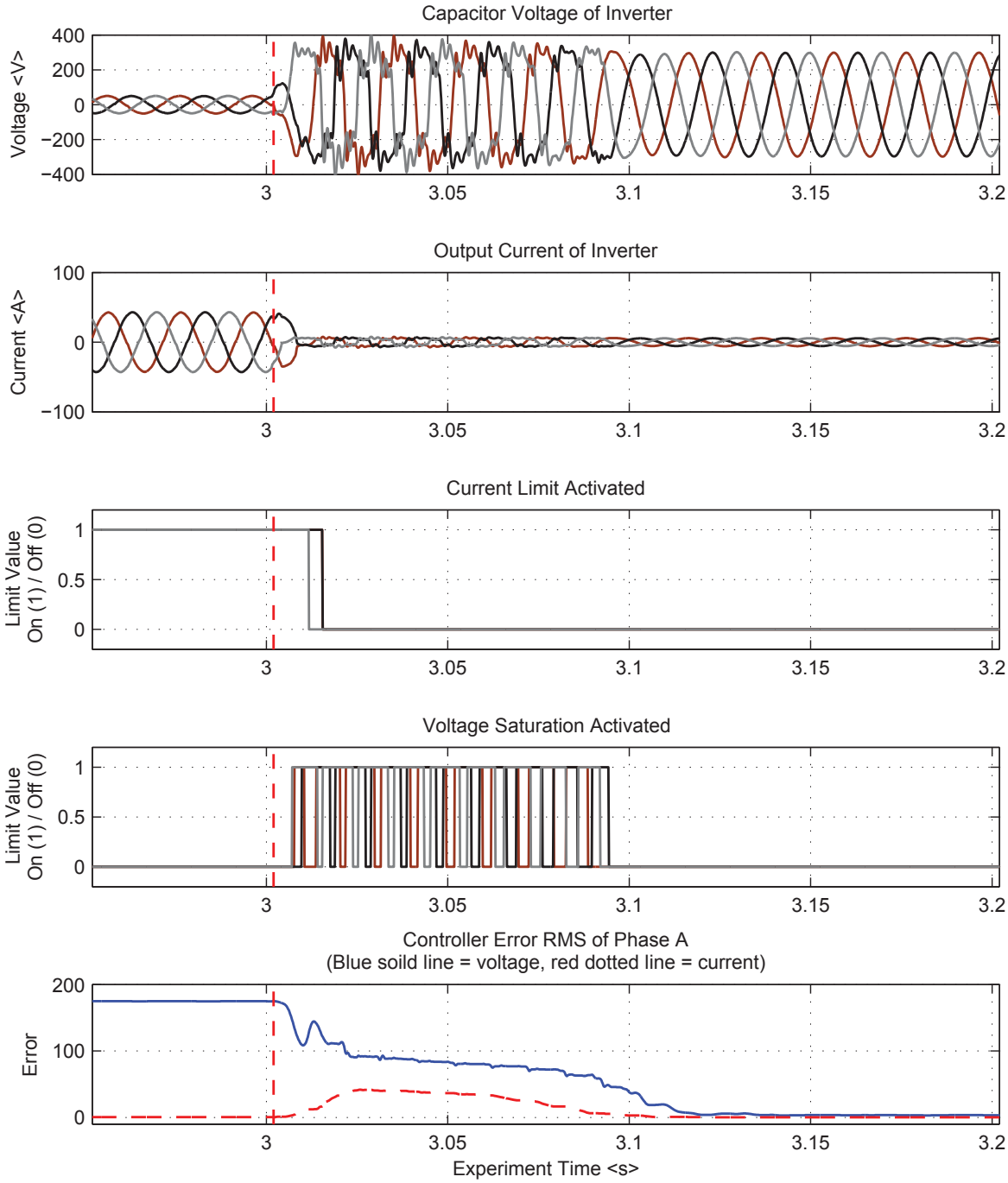

Figure 4.19: Case 3a Reset: Current-trip, voltage-reset current limit and instantaneous voltage limit

4.5.2 Voltage-trip and current-reset (VTCR) Voltage limiter (Case 3b)

Once the voltage limit is triggered, it does not reset as seen in the voltage limit signal of Figure 4.20. After the current limit reset, the voltage controller wound-up because the output of the current controller was being held by the voltage limit as seen in the limit signals of Figure 4.20. The wind-up of the voltage controller causes the input to the current controller to increase which is seen by the increasing current-error plot in Figure 4.20. Since the limiter is deactivated, the output of the limiter is equal to the input to the limiter (output of the voltage controller). This did not happen when the voltage limiter used was of the instantaneous saturation limit design. An explanation is because the voltage limiter only clipped the output and did not hold the output constant. This allowed the controller to regain 'control' of the inverter. A positive comment is that the transient of the current and voltage of the inverter once the fault had cleared in Figure 4.20 was less-distorted than when the voltage limiter was using saturation limits as in case 3a and seen in Figure 4.18.

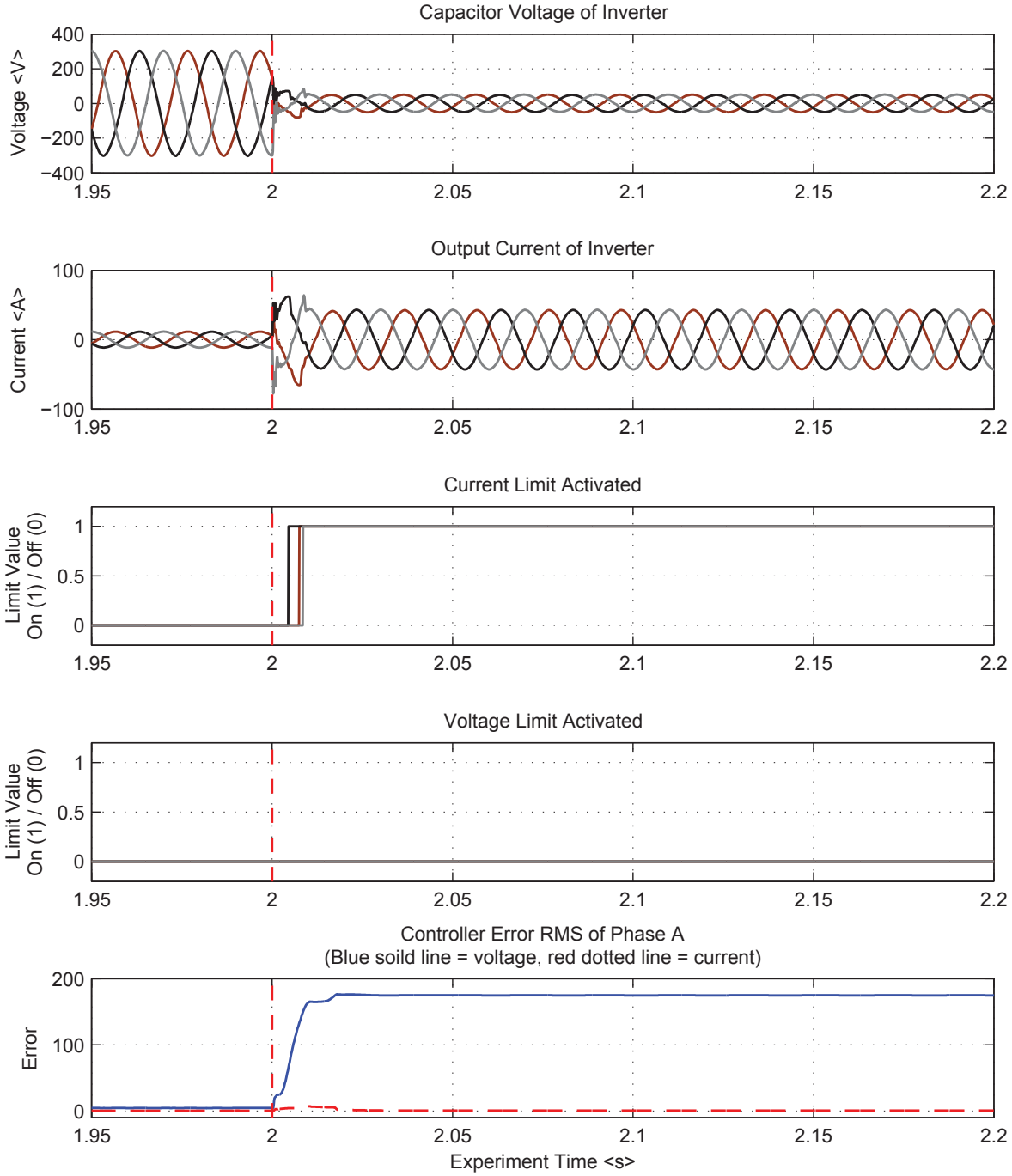

Figure 4.20: Case 3b Trip: Current-trip, voltage-reset current limit and current-trip, voltage-reset voltage limit

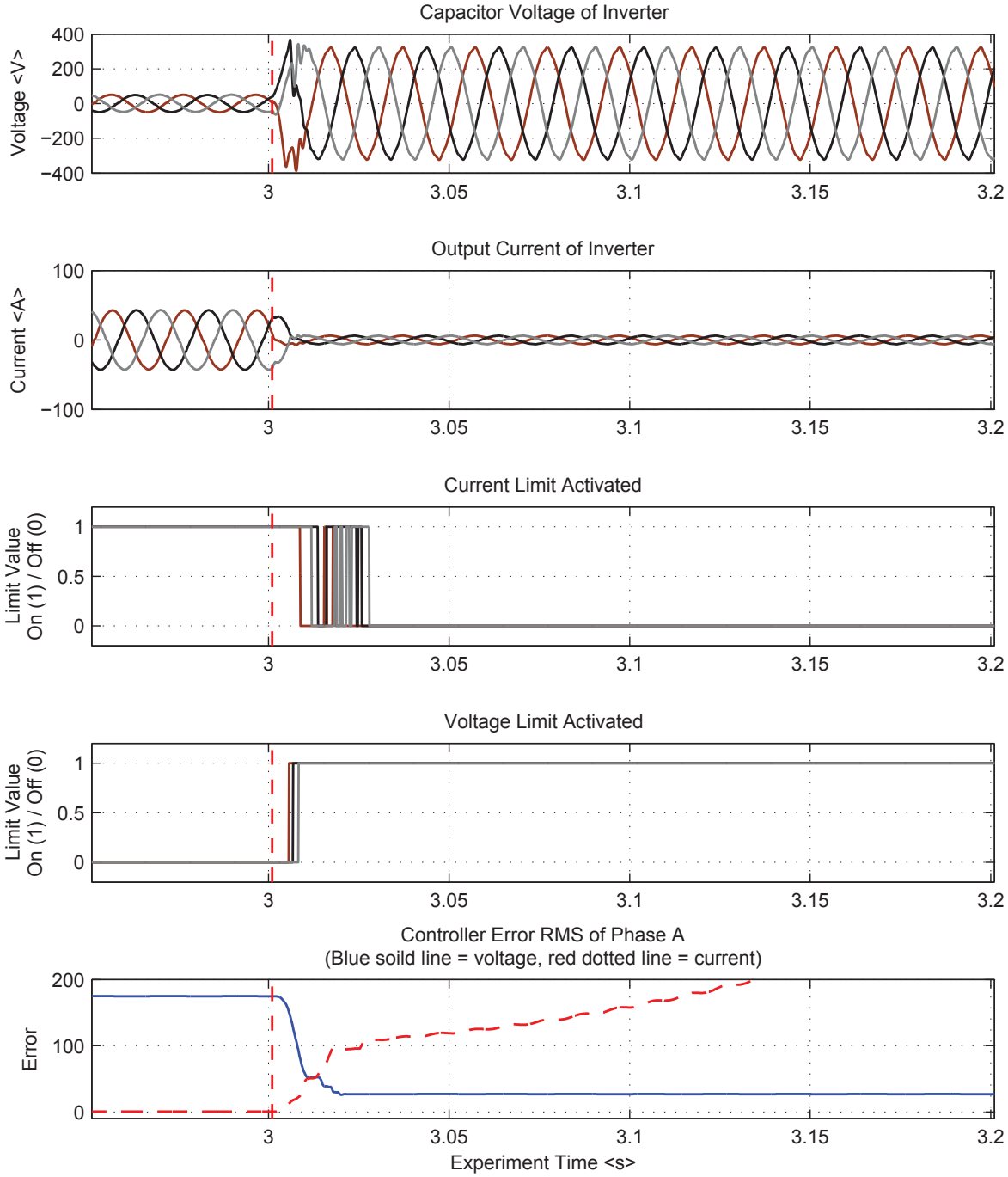

Figure 4.21: Case 3b Reset: Current-trip, voltage-reset current limit and current-trip, voltage-reset voltage limit

4.5.3 Voltage-trip and voltage-reset (VTVR) Voltage limiter (Case 3c)

As with the previous case, this case presented in Figure 4.22 does not distort the capacitor voltage after the fault had cleared. However, the strategy failed for the same reason as case 3b. Again, when the current limiter was reset, the output of the voltage controller experienced wind-up as shown by the increasing current-error signal in the right-hand plot of Figure 4.22.

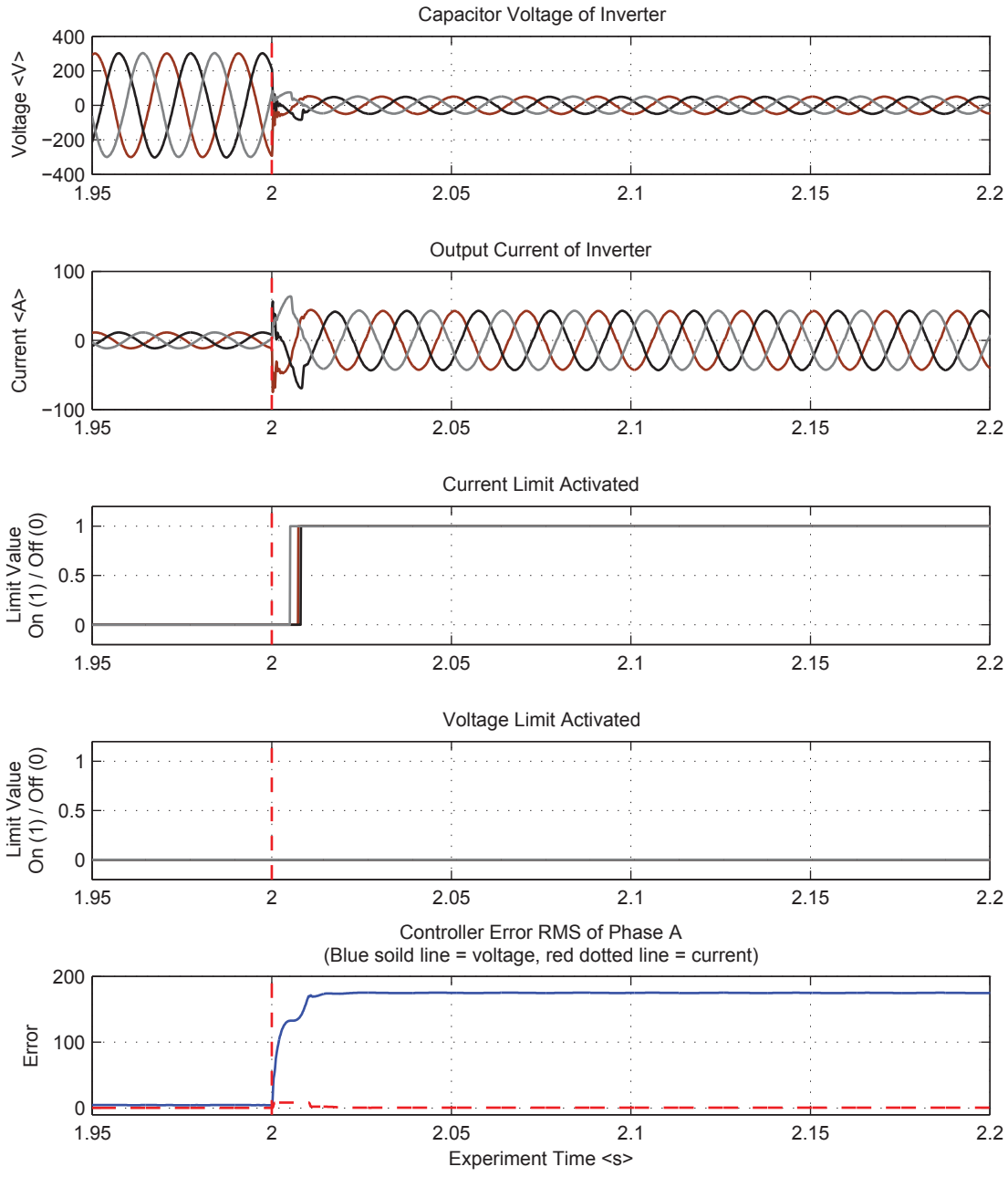

Figure 4.22: Case 3c Trip: Current-trip, voltage-reset current limit and voltage-trip, voltage-reset voltage limit

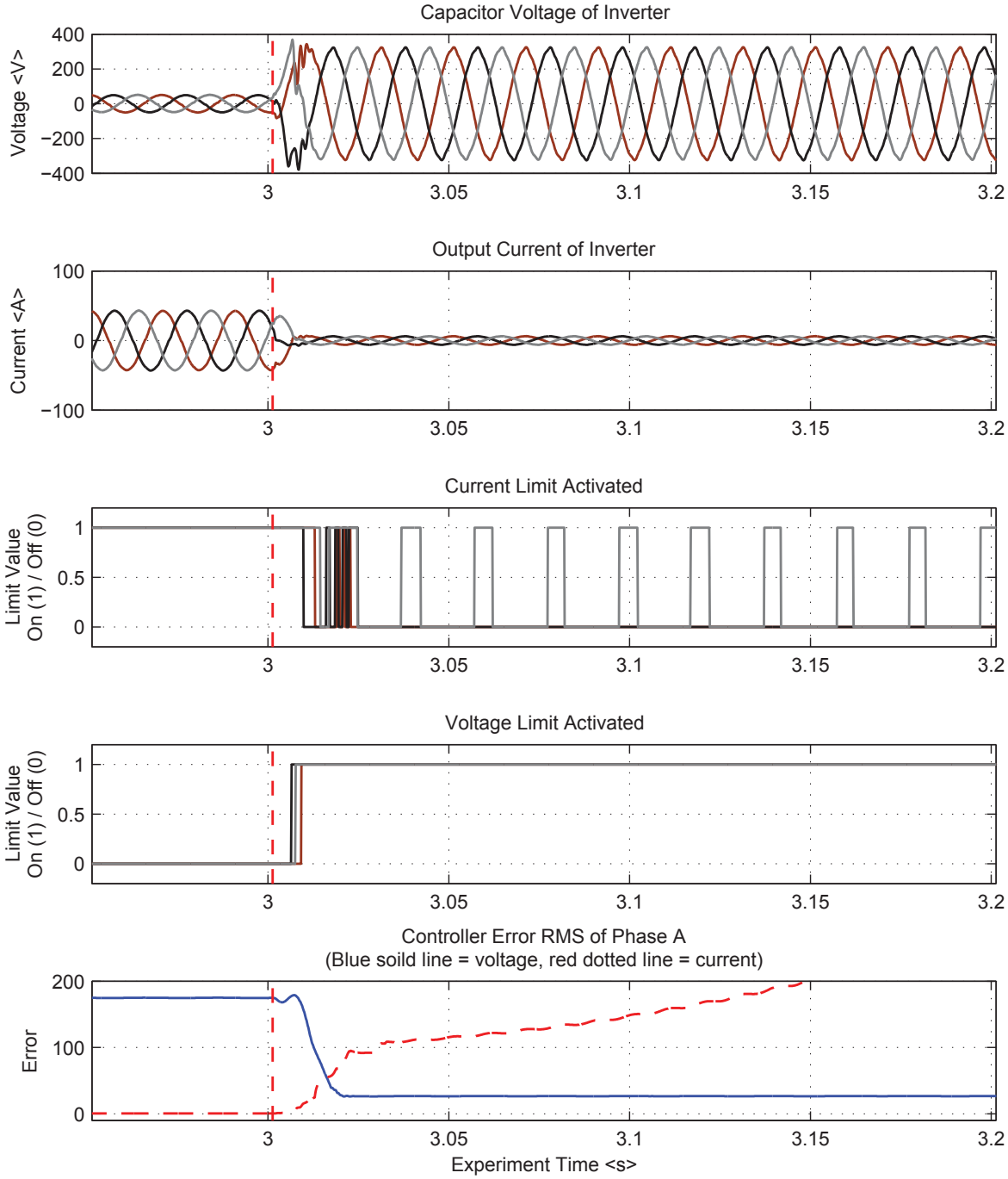

Figure 4.23: Case 3c Reset: Current-trip, voltage-reset current limit and voltage-trip, voltage-reset voltage limit

4.5.4 Current-trip and voltage-reset (CTVR) conclusion

When the output of the current-controller (limited by the voltage limit) used instantaneous saturation limiting, the controller successfully returned to normal operation after the fault had cleared as shown by the right-hand side plots in Figure 4.18. Cases 3b and 3c both failed because the output of the current-controller (voltage limit) remained in limit-mode when the output of the voltage-controller had reset. Therefore, it is concluded that the voltage-limiter should not be designed to latch and a saturation limit with anti-wind-up should be used.

In all current-trip and voltage-reset current limit, cases 3a – 3c, the current during the fault has low distortion and the current limiter reset after the fault had been cleared. To ensure the current limit resets correctly when the outer controller (voltage controller) uses an integrator, the reset signal for the current limiter should not be the output of the voltage-controller to ensure that the limiter correctly resets after the fault has cleared.

4.6 Impedance Current Limiter – Case 4

As with Cases 2 and 3, a latch limiter is used, however the set and reset signal are based on the ratio of the measured voltage and current (impedance). The limiter is operated when the impedance, calculated from the capacitor voltage and output current, decreases below the over-current or fault thresholds. When the limiter has detected a fault, the fault current will be exported. If the fault is not cleared within a pre-determined period of time, the limiter will revert to over-current mode in which, generally, a lower magnitude current than the fault current is allowed but for a longer period. A fault current will only be exported again if the limiter has detected that the network has returned to normal operation. As soon as the network returns to normal operation, the limiter will reset. The diagram for the limiter is shown in Figure 4.24 and the settings of the limiter are in Table 4.2.

An experimental test system was built around a TriPhase 10 kVA inverter with the control structure of Figure 4.24 and parameters of Table 4.2. The TriPhase inverters use a data acquisition system that provide voltage and current measurements for plotting in Matlab. The

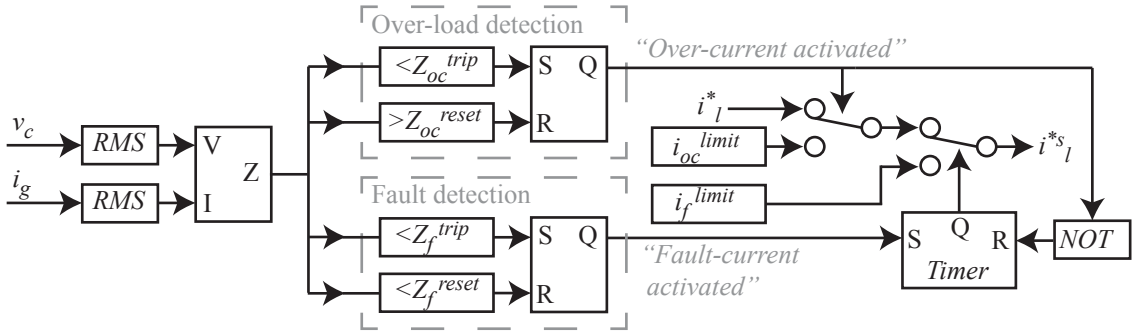

Figure 4.24: Schematic of the impedance limit used in the current limit. Each phase is limited independently.

Table 4.2: Impedance Limiter Values

Parameter	***Value***	***Parameter***	***Value***
Z_{oc}^{limit}	220/15 = 14.67 Ω	i_{oc}^{limit}	15 A
Z_{oc}^{reset}	220/13.5 = 16.30 Ω	f_{oc}^{limit}	30 A
Z_f^{limit}	220/30 = 7.33 Ω	Time out	2 s
Z_f^{reset}	220/27 = 8.15 Ω		

inverter was connected to two resistive loads that are each able to provide a load between 168 Ω and 16.8 Ω.

To verify the operation of the inverter controller for both overloads and faults, three experiments are presented in this paper. The first experiment decreases the load resistance in regular intervals from 84 Ω to 8.4 Ω. The second experiment places a 1.2 Ω fault across all phases of the load for 1 s. The third experiment places a 1.2 Ω single-phase fault across phase c of the load for 1 s.

4.6.1 Gradual increase of load experiment

The inverter was connected to a resistive load where the resistance was decreased from 84 Ω to 8.4 Ω. The purpose of this experiment was to demonstrate that the inverter is able to supply an overload current when the load impedance is between Z_{oc}^{limit} (14.67 Ω) and Z_f^{limit} (8.80 Ω) and a fault current when the load impedance less than Z_f^{limit}.

Figure 4.25 shows the response of the inverter when the load is gradually changed. It can be seen that the inverter regulates the capacitor voltage until the measured output impedance is below that of the over load limit which happens at t = 9 s. At this time the load impedance as measured by the inverter was 13.7 Ω and as measured at the load, was 14 Ω. This is a good match and the impedance calculation within the inverter is functioning correctly. Once the over load limit is reached, the inverter regulates the output current and the voltage decreases until the measured output impedance is below that of the fault limit which happens at t = 17 s. At this time, the load impedance measured by the inverter was the same as that measured at the load which was 8.4 Ω. When the measured impedance is below the fault limit, the inverter exports a fault current for two seconds before returning back to the over load limit. In this experiment, the end of the two second period happens at t = 19 s. As expected, the export current decreases, the capacitor voltage increases and the measured impedance remains constant. These changes indicate the change in output from the inverter was not caused by a load change, but caused from the timer changing the export current from a fault current to an over-load current.

It is noted that between t = 17 s and t = 19 s, both the over-current activated and fault activated signals are true. This is because the fault impedance is below both the over load limit and the fault limit. In this situation the fault limit overrides the over load limit and the inverter proceeds to export fault current.

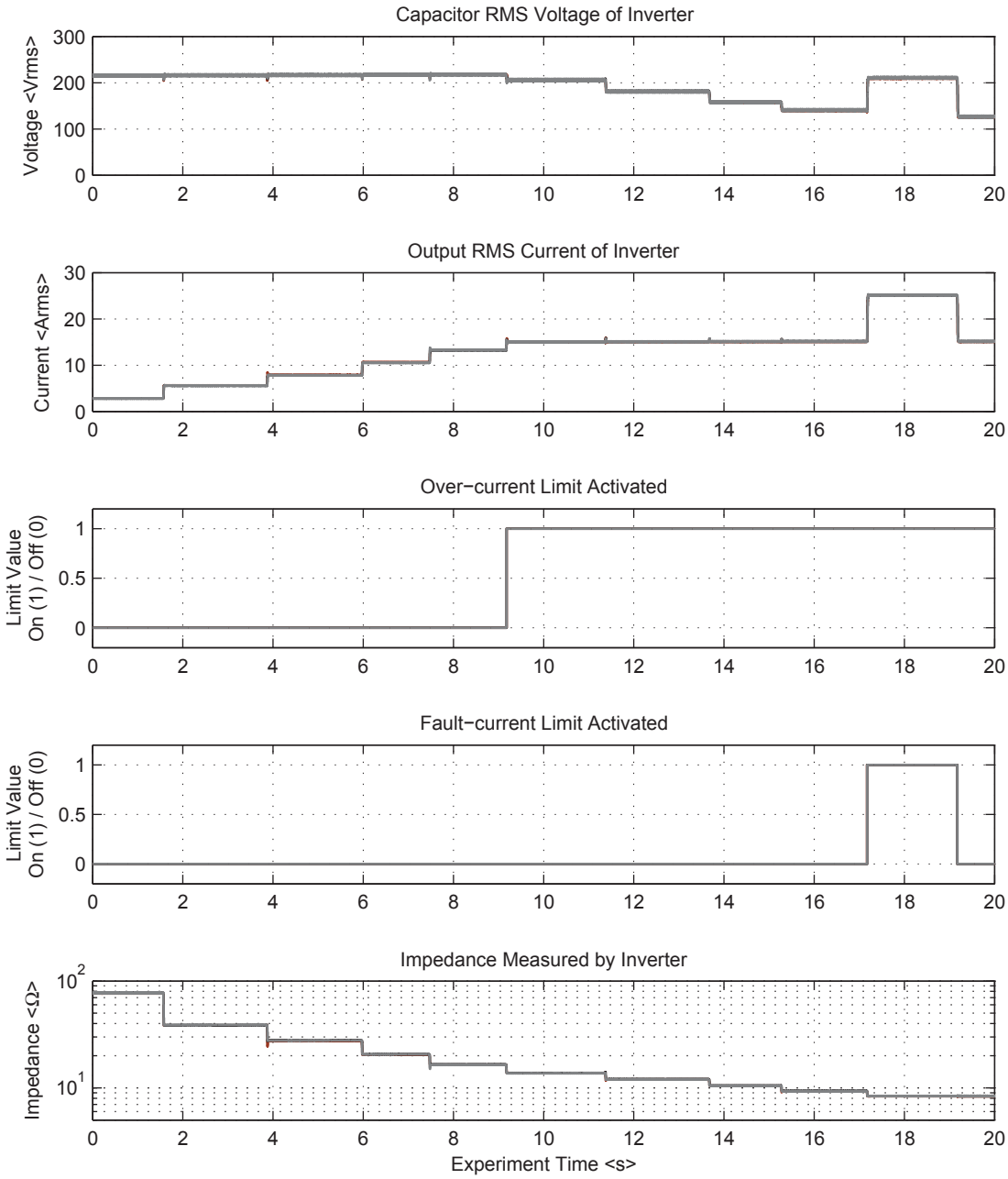

Figure 4.25: Case 4: The capacitor voltage and output current of the inverter transient from normal to exporting a fault current.

4.6.2 Three phase fault experiment

The inverter was connected to a single load of 16.8 Ω per phase. A three-phase fault with an impedance of 1.2 Ω per phase was applied in parallel with the load. The three-phase fault impedance was connected via a 63 A contactor that was able to switch the fault in and out. A National Instruments Compact Rio was used to control the fault which was initiated t = 1 s into the test and cleared at t = 2 s.

Figure 4.26 shows the transition of the inverter from normal operation to fault current mode. The red dotted line indicates the time the fault was applied. It can be seen that there is a small over-current immediately following the fault and before the current controller establishes control of the fault current. The transient arises from the inverter and current controller design and not the limit circuit design. Had the limit circuit design not detected the fault, the voltage controller would still be regulating the voltage and the over-current would be much greater. There is a short time delay of 0.01 seconds for the inverter to correctly calculate the fault impedance and this causes a delay in the inverter detecting the fault as seen in the fault activated signal. This is not a problem because the over-load circuit triggered quickly and protected the converter before the fault current activated.

Figure 4.27 shows the transition from fault current mode back to normal operation. The red dotted line indicates the time the fault cleared. In this figure four distinct periods can be seen. The dotted lines indicate the change from one period to another and are collected with respect to the phase colour. Each period change has three dotted lines, one for phase a, one for phase b and one for phase c. The only exception is from period 1 to period 2 where this happens at the same time and is indicated by a red dotted line.

The first period is between 1 s and 1.9995 s. This is when the inverter is exporting fault current and the output voltage is small due to the low impedance of the three-phase fault. Then the second period is between 1.9995 s and 2.014 s for phase a, 2.0133 s for phase b, 2.0095 s for phase c. This is when the fault has cleared but the inverter has not yet detected this and continues to export the fault current, and then over load current, which causes the network voltage to rise. In this period, the fault current exported causes an over voltage which causes the voltage limiter to operate and the voltage waveform to be clipped. The length of this period

depends on the speed of the impedance calculation which is determined by the filter used within the RMS calculation. A slow impedance calculation will cause a longer period of over-voltage and a faster impedance calculation will allow the inverter to return to normal operation quicker. The third period is between the end of the second period and 2.0377 s for phase a, 2.0343 s for phase b, 2.031 s for phase c. This is when the current limiter has returned to normal operation and voltage control is re-established in the controller loop. In this period the voltage controller is yet to fully regulate the voltage. There may still be an over-voltage in this section if the voltage controller requires a long time to settle. In this implementation the voltage controller is reset just after the inverter has detected that the fault has been cleared. The resetting of the voltage controller causes a slightly lower voltage at the end of period 2. Finally, the fourth period is when the voltage controller is regulating the output voltage and the inverter has returned back to normal operation.

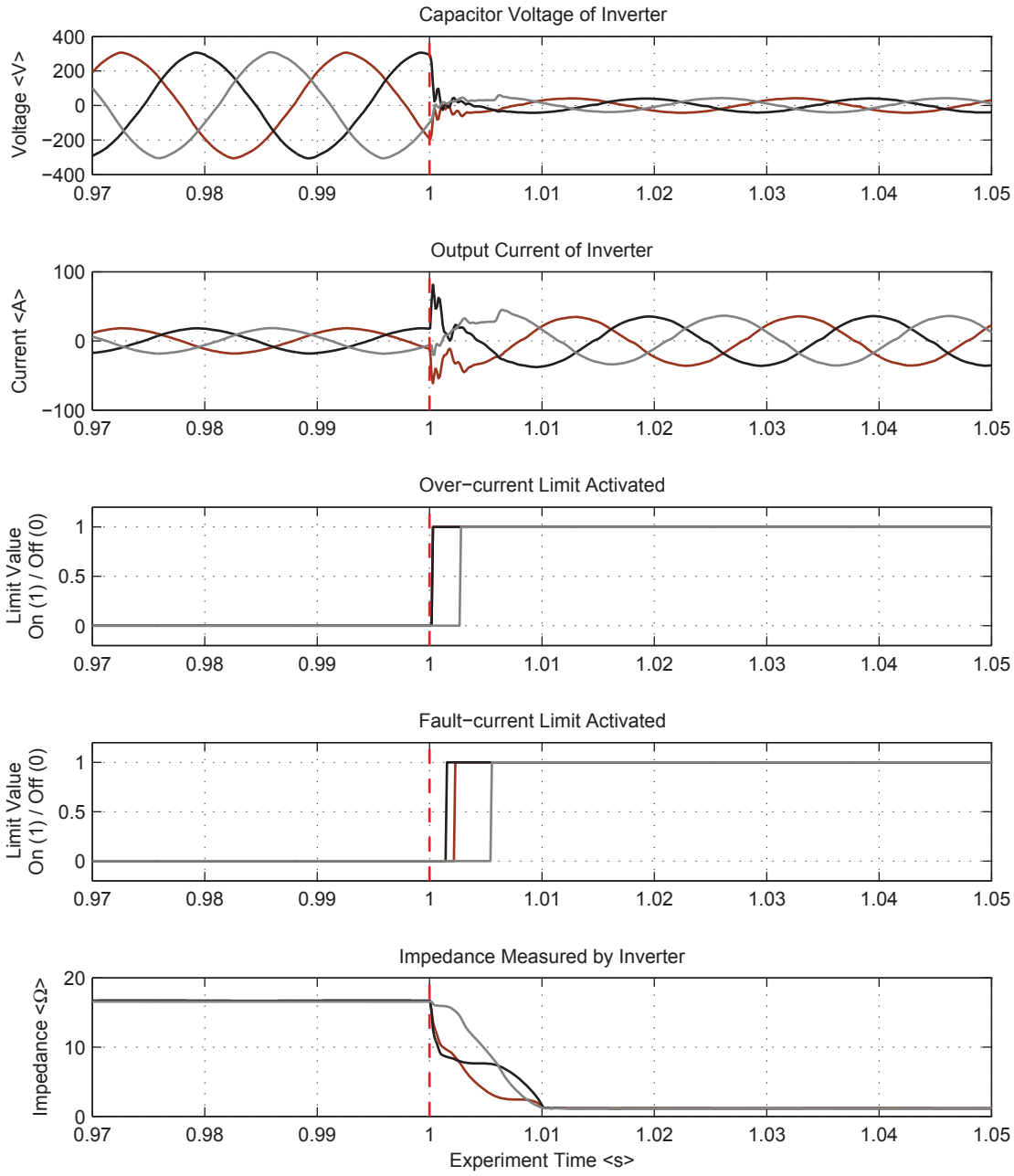

Figure 4.26: Case 4: The capacitor voltage and output current of the inverter transient from normal to exporting a fault current.

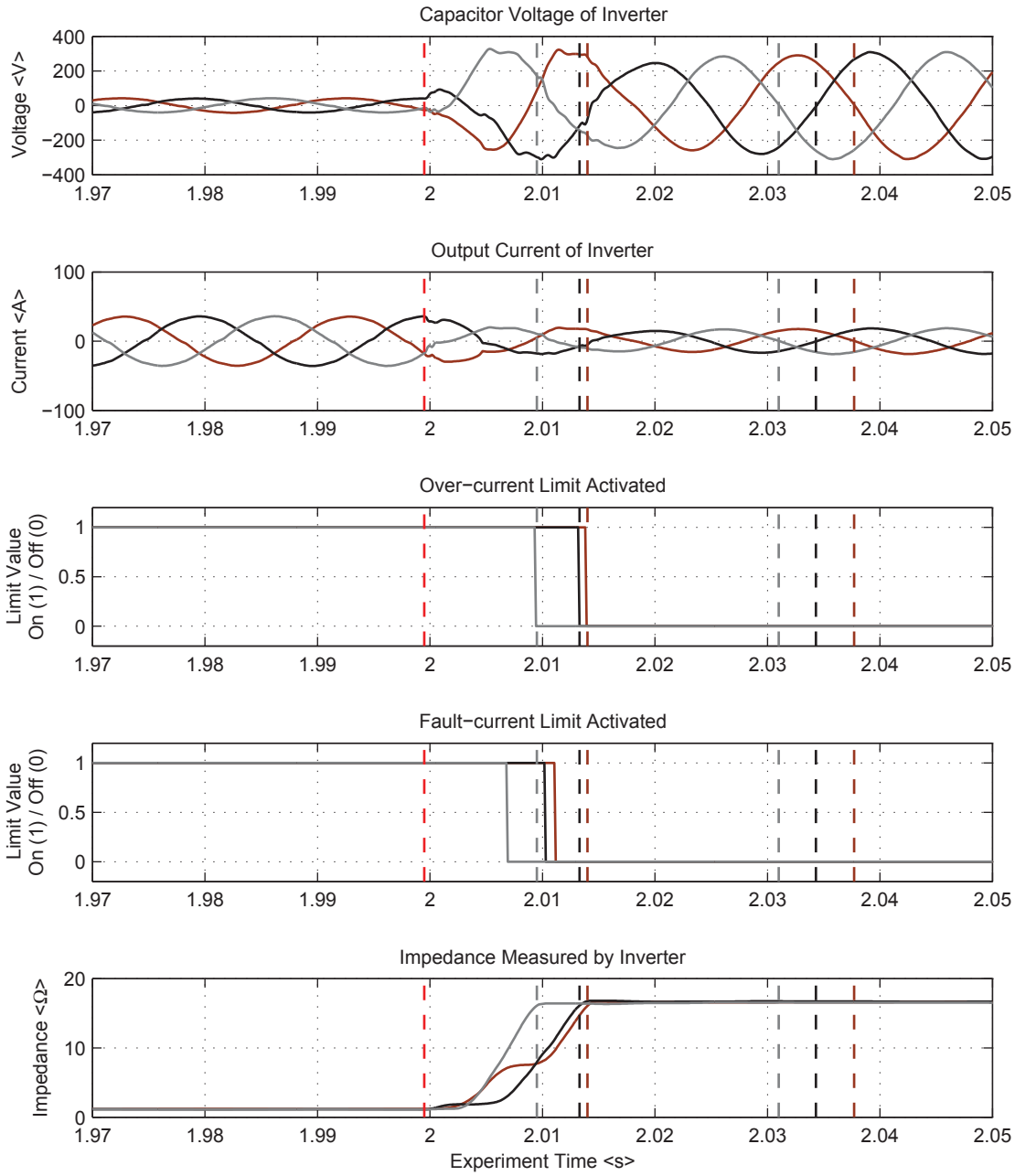

Figure 4.27: Case 4: The capacitor voltage and output current of the inverter transient exporting a fault current to normal operation.

4.6.3 Single phase fault experiment

This experiment uses the same set-up as the three-phase experiment, except that the fault is only applied to the phase c. Figure 4.28 shows the transient when the fault is applied, it can be seen that the voltage on the faulted phase decreases and the current on the faulted phase increases to the fault current limit. The voltage on the un-faulted phases is maintained however there is a slight distortion during the fault. Figure 4.29 shows the transient when the fault is cleared. It can be seen that the same four periods of recovery are present in the faulted phase as has been described in the three-phase fault experiment. These periods are shown in Figure 4.29 with dotted lines to indicate the period changes.

4.7 Conclusion

Four different strategies are investigated for inverters to be able to supply current into a faulted network and reset once the fault has been cleared. Each strategy was tested by placing a low impedance fault at the terminal of the inverter for a duration of 1 second. Key measurements of each strategy were observed to determine if the strategy successfully reset or failed to reset once the fault had been cleared and the load of the inverter returned within normal operating limits.

The first case used instantaneous limits to prevent the current and voltage reference signals from exceeding design parameters. This strategy successfully operated after the low impedance fault had been removed. However, due to control in the natural reference frame and the saturation limits, the output of the inverter was very distorted when the output of the controllers was limited.

The second case used a set-and-reset design for the outer limiter (output of the outer controller) where the reset was from the output of the output controller. Different inner limiting strategies were also tested. In every instance the second case failed because the outer limiter (output of the outer controller) did not reset and the outer controller latched-up. The different inner limiting strategies failed to aid the outer limiter.

The third case again used a set-and-reset design for the outer limiter, however the reset signal was from an external source and not from the output of the outer controller. In the test where the inner limiter was an instantaneous limit, the limiter successfully reset and returned the inverter back to normal operation after the fault. In the tests where a set-and-reset design for the inner limiter was used, the outer controller wound-up once the outer limiter reset and these tests failed to reset. From this set of experiments, it was concluded that the inner limiter should be of an instantaneous design and the outer limiter should be a set-and-reset design where the reset signal is from an external measurement and not an output of the controller.

The fourth case further developed the conclusions from the third case and designed a limiter to be set and reset from the impedance as measured by the inverter. Extra functionality was included by adding a section trip and this allowed the inverter to detect both simple over loads and faults. This design proved to be successful and was tested for an overload, a single phase and a three phase fault.

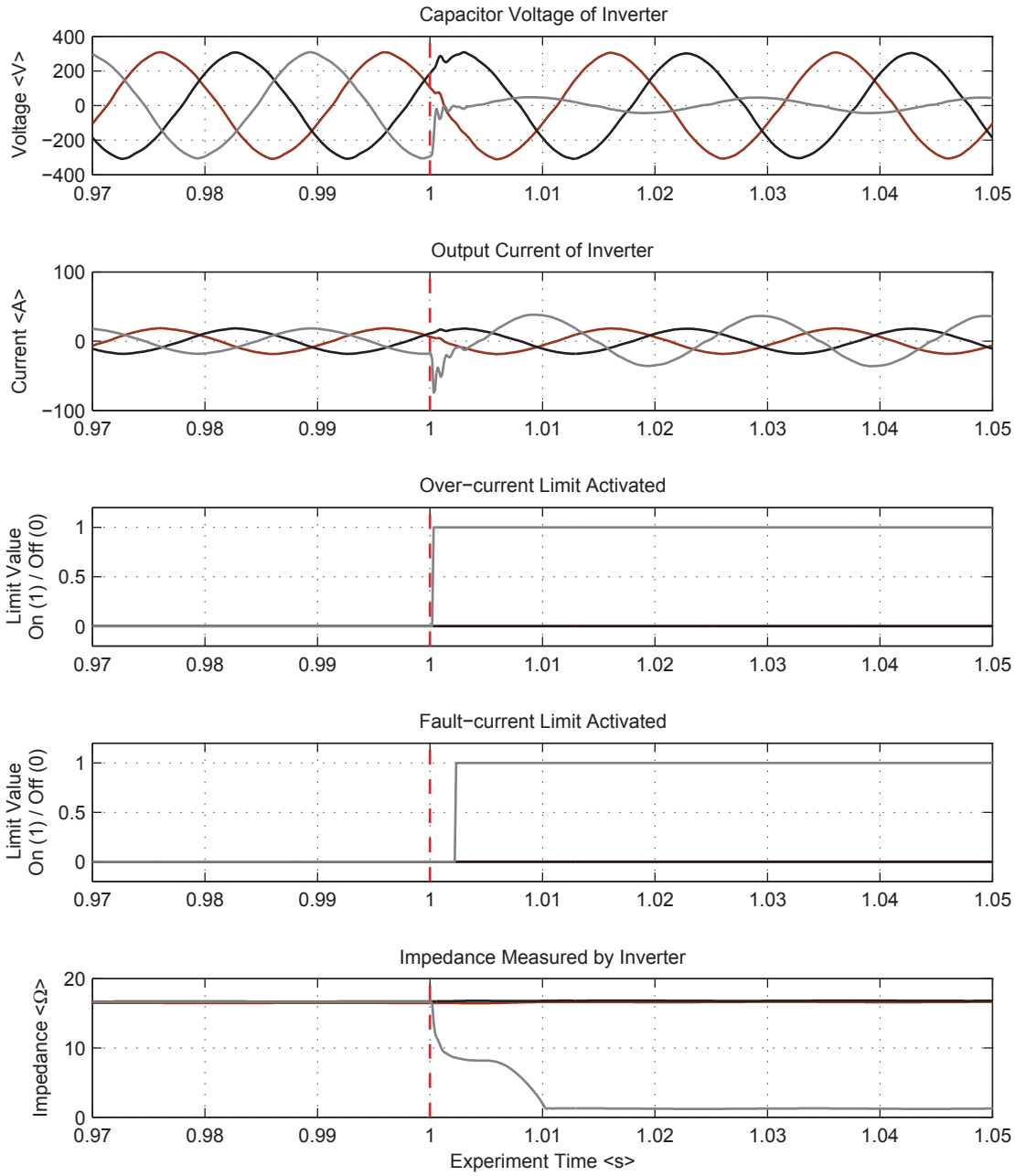

Figure 4.28: Case 4: The capacitor voltage and output current of the inverter transient from normal to exporting a fault current.

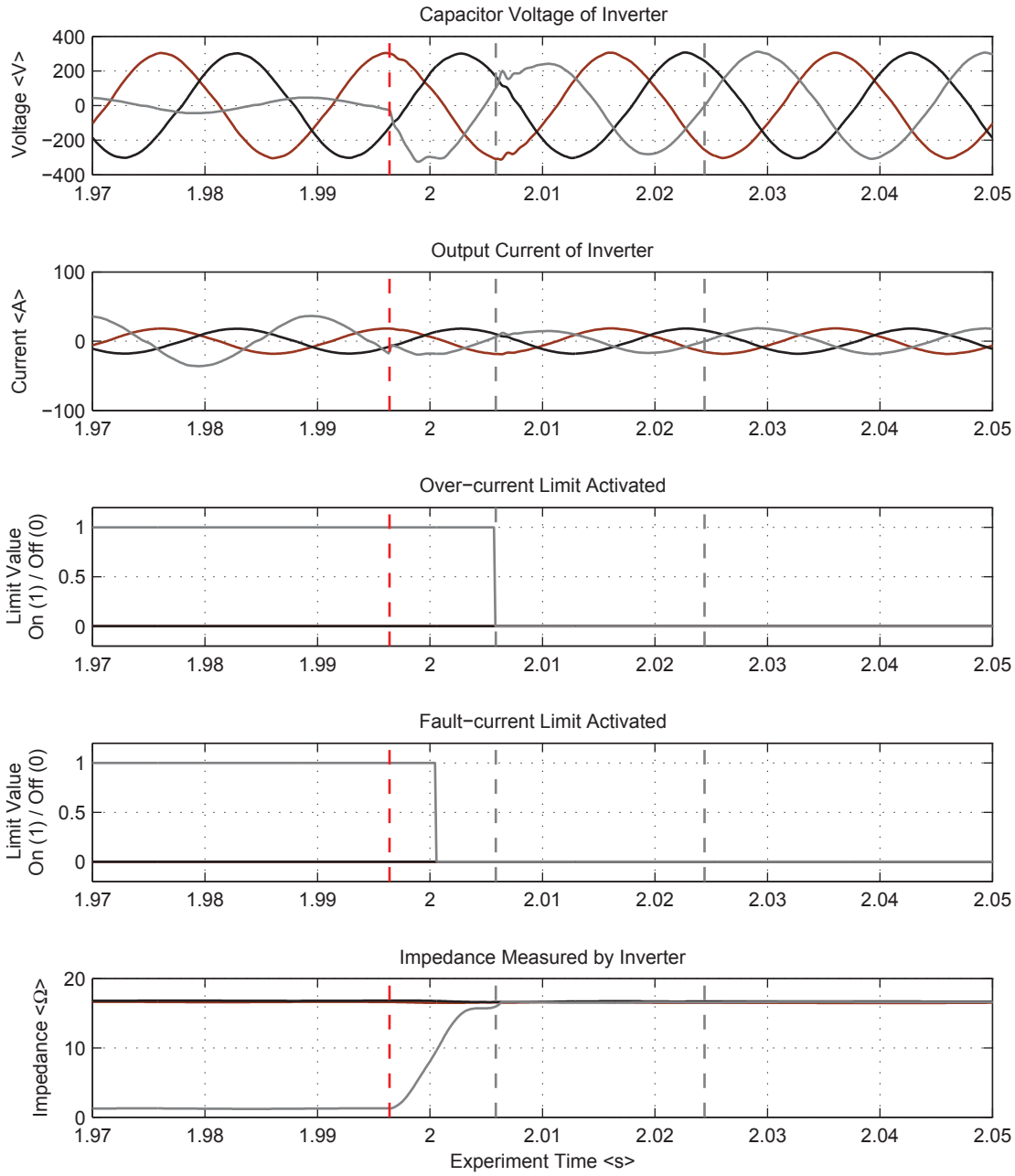

Figure 4.29: Case 4: The capacitor voltage and output current of the inverter transient exporting a fault current to normal operation.

Chapter 5

Large Signal Stability of Inverter Networks

This chapter explores the large-signal stability of a simple two inverter network that uses droop controllers to share the load between the inverters. The aim is to understand the factors that cause the two inverter network to enter a limit-cycle oscillation or become unstable once the fault within the network has been cleared.

The chapter opens with an example of a single droop controller inverter. It is noted that an inverter microgrid would probably not only use one inverter. However, it is important to understand the operation of a single device before exploring more complicated networks. A single droop-controlled inverter is presented and a analysis is undertaken to explain the results.

Upon understanding the single droop-controller inverter, the transient of a two droop inverter is presented. Analysis is undertaken in order to develop an understanding of the parameters that effect whether the inverter becomes unstable once a fault has been cleared. Upon understanding these parameters, simplified calculations are presented in order to approximate the parameters that will determine the stability of the transient of the two droop microgrid.

Once the understanding is developed, the parameters that effect the transient stability are perturb without a fault in the network. Thus providing more evidence that the initial analysis on the two droop microgrid is correct. Before the chapter conclusion, the length of the line is explored to determine how this would effect the transient stability of the microgrid.

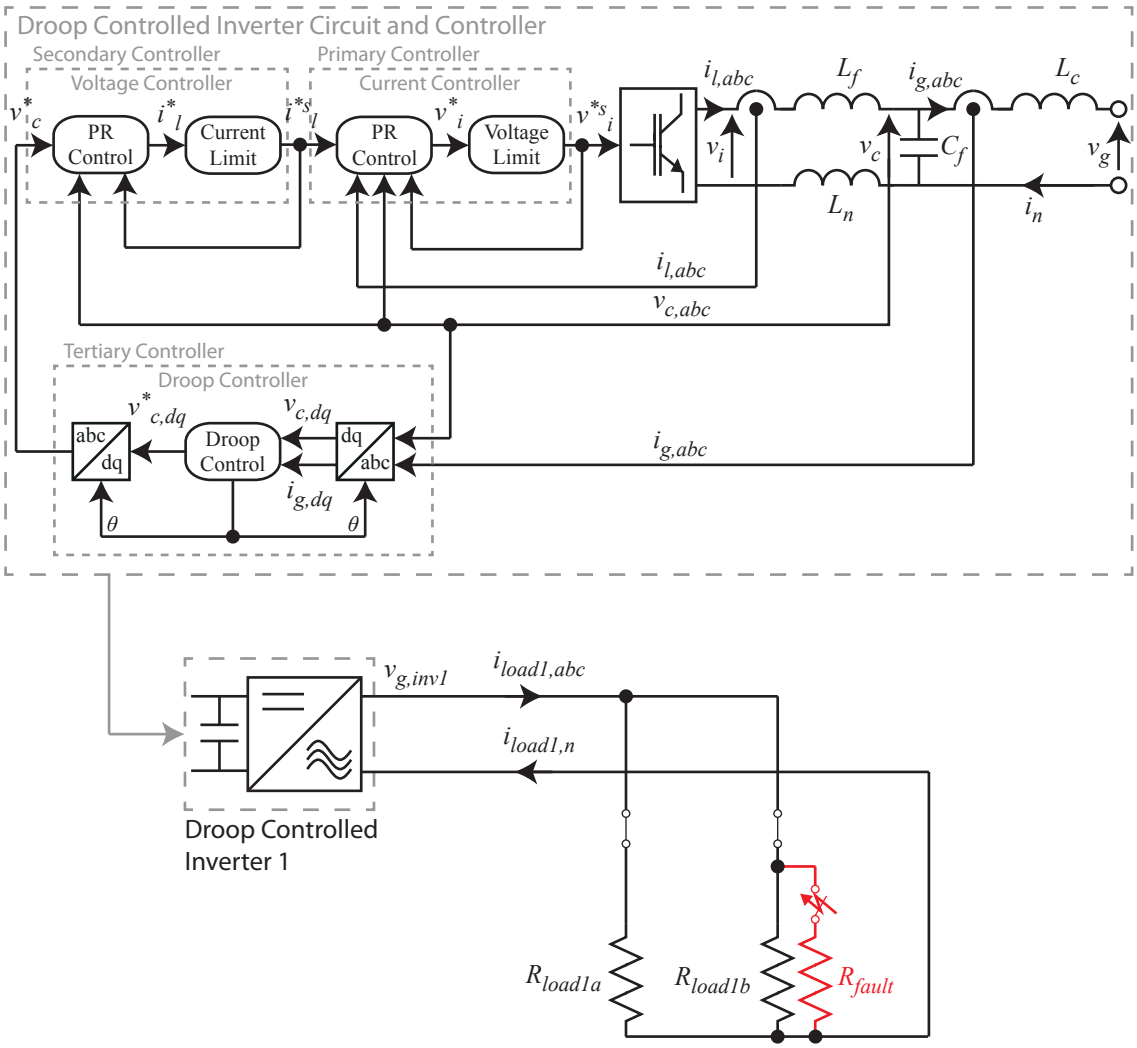

Figure 5.1: The circuit of the single droop controlled inverter

All results presented in this chapter are from Matlab simulations, none of this work has been experimentally verified.

5.1 Fault Ride-Through of a Single Droop Controller Inverter

To help gain an understanding of how a droop-controlled inverter will behave in a microgrid environment, a single droop controlled inverter was studied. The droop controlled inverter was connected to two balanced loads that are equal and controlled by independent circuit-breakers. A low impedance of 1 Ω was paralleled across one of the loads to cause a low impedance fault. This configuration is shown in Figure 5.1.

A fault was applied at t = 1 seconds and removed at t = 2 seconds. Figures 5.2 and 5.3 show the transient of the droop-controlled inverter from normal operation to current-limit operation and current-limit operation to normal operation respectively.

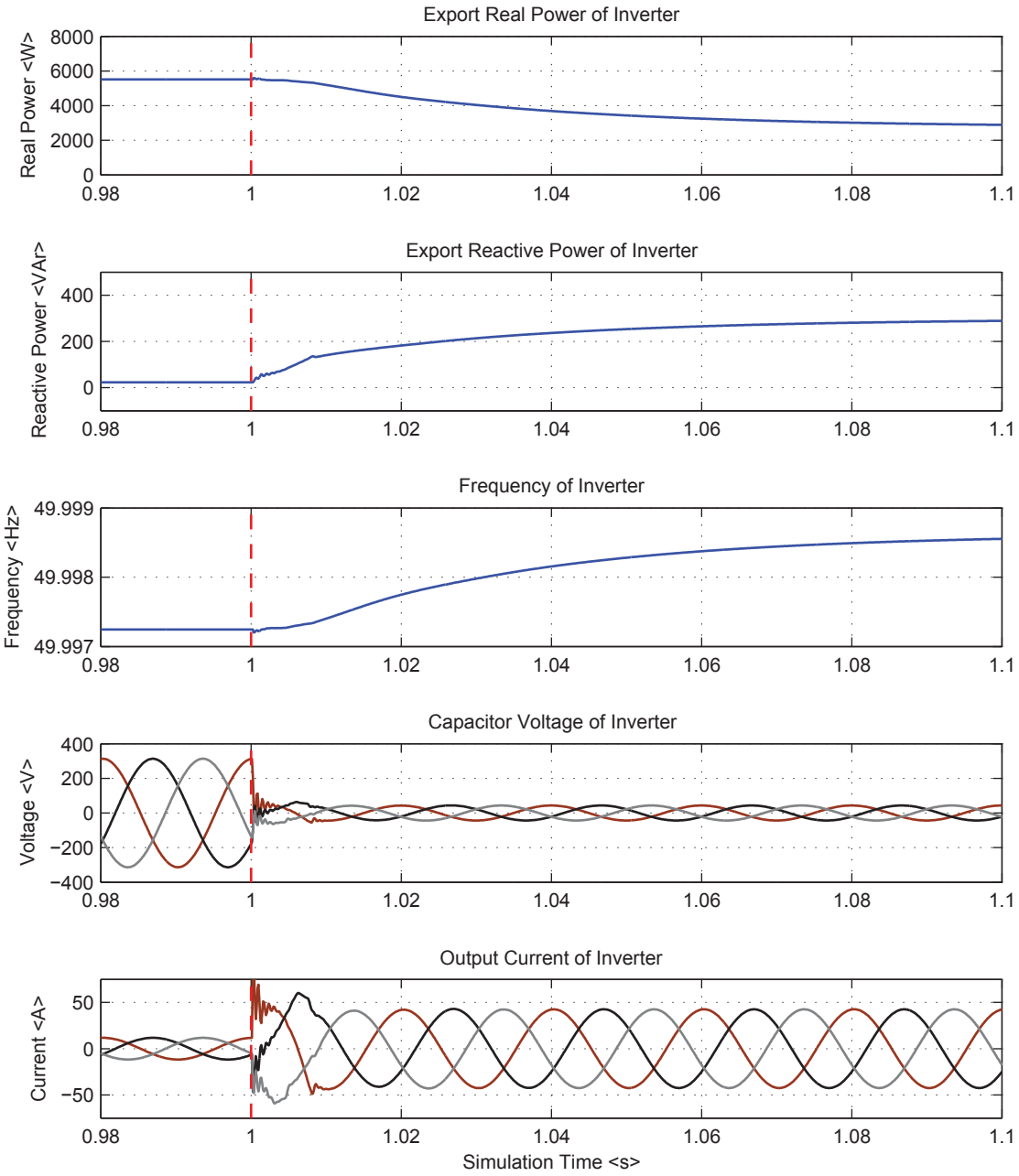

Figure 5.2: The transient from normal operation to current-limit operation of a single droop controlled inverter with Current-Trip and Voltage-Reset current limit.

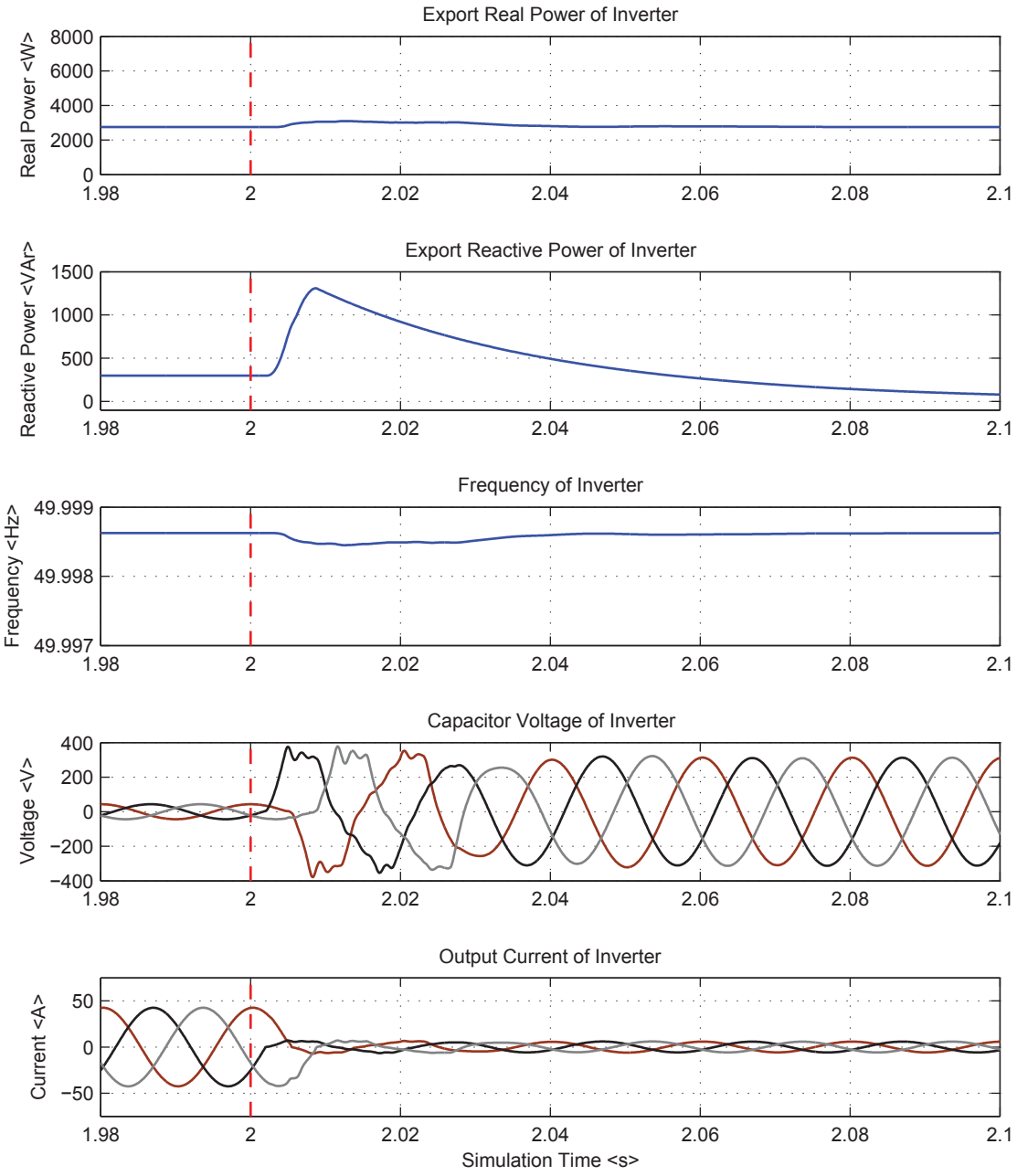

Figure 5.3: The transient from current-limit operation to normal operation of a single droop controlled inverter with Current-Trip and Voltage-Reset current limit.

5.2 Discussion of normal operation to current-limit operation

5.2.1 Real power export of the inverter

When the fault is applied at the load (which is at the output of the inverter) the real power as calculated by the inverter does not step instantaneously. From Figure 5.2, the power decreases with a first order decay. This is because the power plotted is the average power which is averaged by a low-pass filter, which in this example has a bandwidth of 5 Hz. The change in power can be calculated by using Equation (5.1) where P is the average power as calculated by the inverter, P_0 is the export power before the fault, P_{fault} is the power export during the fault, ω_p is the bandwidth of the first-order power filter and t is the time.

$$P = P_0 + (P_{fault} - P_0)\left(1 - e^{-\omega_p t}\right) \tag{5.1}$$

5.2.2 Reactive power export of the inverter

The reactive power export as measured by the inverter uses the same technique that is used for real power and the same low-pass filter is used to calculate the average reactive power. Again, the low-pass filter has a bandwidth of 5 Hz, and the measured reactive power is calculated using Equation (5.2) where Q is the average reactive power as calculated by the inverter, Q_0 is the export reactive power before the fault, Q_{fault} is the reactive power export during the fault, ω_q is the bandwidth of the first-order power filter and t is the time.

$$Q = Q_0 + (Q_{fault} - Q_0)\left(1 - e^{-\omega_q t}\right) \tag{5.2}$$

5.2.3 Analysis of the real and reactive power export

During normal operation and before the fault, the steady-state power is calculated by the voltage at the capacitor and the impedance of the load and network to which the inverter is connected. The magnitude and angle of the voltage at the capacitor is controlled by the voltage controller

and the angle of the reference frame of the controller. The set-points of these controllers are determined by the reactive-power and real power droop gradients. During the fault and if the current limiter has activated, the fault steady-state power is calculated by the export current and the impedance of the faulted network. The calculation of these values is possible by using a load-flow method or from a time-step simulation of the inverter model and network.

From Figure 5.2, the power exported by the inverter is less than the power exported during normal operation. This is because of the current limit. For all faults that trigger the inverter to enter into current limit mode, the current export will be constant. In these cases, the smaller the impedance of the network, the smaller the power export from the inverter and the lower the output voltage of the inverter.

5.2.4 Frequency of the inverter

The frequency of the inverter depends on the real power exported by the inverter and the droop-gains using the equation,

$$\omega = \omega_n - P\omega_n \frac{F_{droop}}{P_{max}} \tag{5.3}$$

where $\omega_n \frac{F_{droop}}{P_{max}}$ is the droop gain labelled m_p in the small-signal work presented in Chapter 3.

The frequency change is so small that it might be treated as constant in some fault studies. However, the small frequency change may have a significance in the transient stability of the droop controlled inverter. Until the small change in frequency is shown to be not important, the frequency will not be assumed to be constant.

5.3 Discussion of current-limit operation to normal operation

5.3.1 Real power export of the inverter

The real power did not change significantly in Figure 5.3 after the fault had cleared. In this example, the network impedance and current limit were such that the power export of the inverter is similar for both fault operation and post-fault.

5.3.2 Reactive power export of the inverter

Figure 5.3 shows that a large reactive power demand is placed on the inverter after the fault had been cleared. The reactive power demand is required to support the voltage rise. Once the voltage has returned to the pre-fault level and the voltage controller is regulating the voltage, the reactive power demand decreases to the pre-fault level. The decay of reactive power follows Equation (5.2) which is due to the low-pass filter used to calculate the average reactive power.

5.3.3 Frequency of the inverter

The frequency of the inverter follows the real power demand and the frequency reference is set by Equation (5.3).

5.4 Overview of the Single Droop Inverter

The current export of a droop-controlled inverter is determined by the current limit used within the controller. As the current export is fixed, the voltage at the terminals of the inverter is determined by the impedance of the network that the inverter is connected to. In an inverter, the current limit is fast acting in order to protect the inverter. This causes the response of the inverter to be in the millisecond time frame and for the purpose of a transient analysis could be considered to be instantaneous.

The frequency of the droop-controlled inverter is determined by the power export and the transient of the frequency is determined by the power as measured by the inverter. Power as measured by the inverter is determined by the power calculation which uses a filter. A filter is required in order for effective control. If the droop references were to use the instantaneous power measurement, the reference signal to the voltage controller would be rapidly changing and could cause the inverter to exhibit instabilities. By using average power, the high frequency changes in demand are ignored and a network with multiple inverters is able to effectively share the average power and each inverter is able to track its droop reference signal. Therefore it is important for the filter to be present within the droop-controlled inverter and the effect of the

filter on the frequency and voltage reference signals needs to be considered within a transient stability analysis.

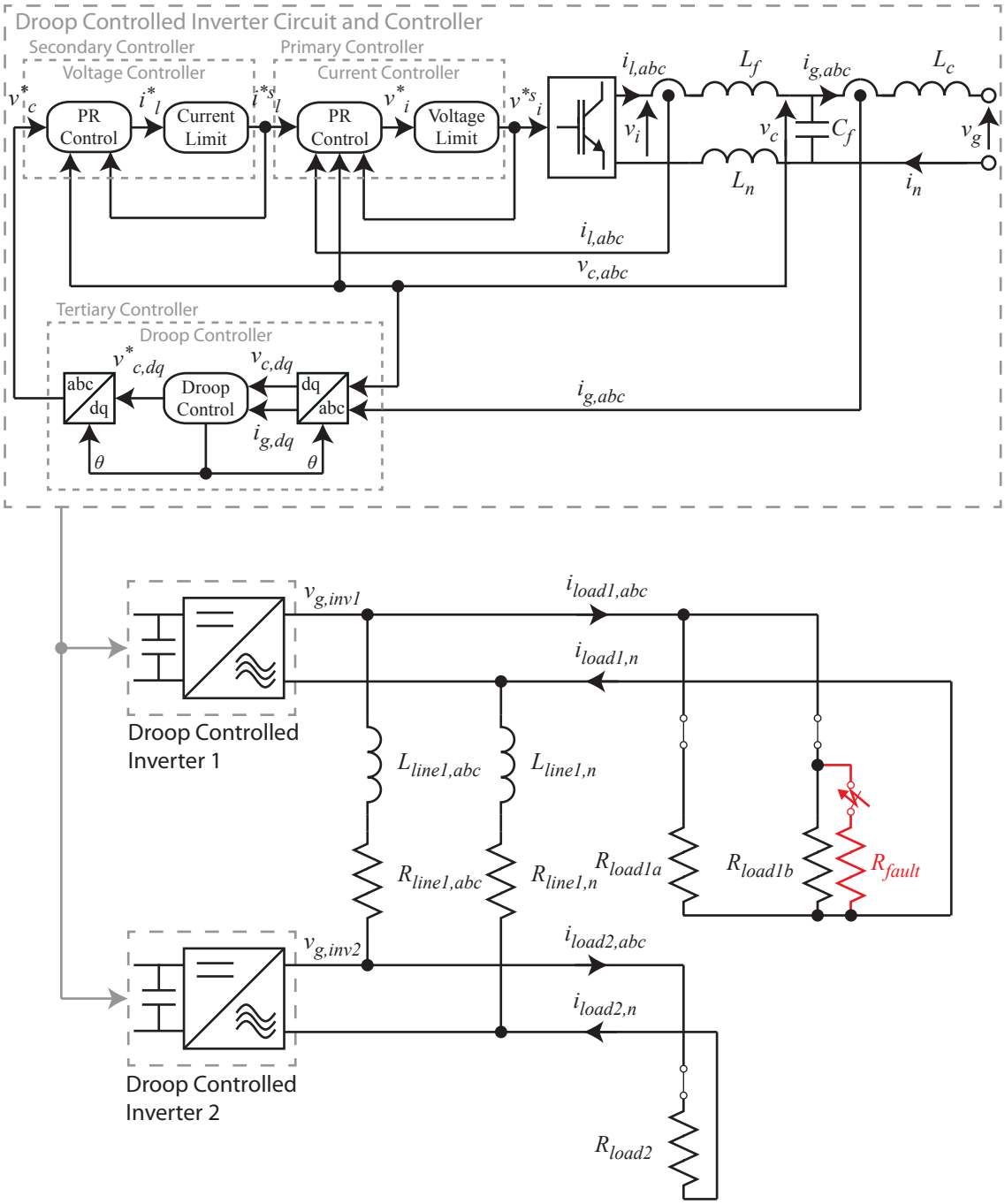

Figure 5.4: The circuit of the two droop controllers

5.5 Fault Ride-Through of Two Droop Inverters

The two droop controllers were connected to a line and two resistive loads as shown in Figure 5.4. The parameters of each inverter are identical and are listed in Table 4.1. The parameters of the droop controller are listed in Table 5.1 and the parameters of the line are listed in Table 5.2

Table 5.1: Properties of the droop controller used for the two droop inverters

Parameter	**Value**
Nominal Frequency	50 Hz
Frequency Droop	0.1×10^{-3}
Nominal Voltage	$[381,\ 0]\ V_{dq}$
Voltage Droop	0.002
Real Power Max	10 kW
Reactive Power Max	6 kVAr
Power Filter Frequency	5 Hz

Table 5.2: Properties of the line used for the two droop inverters

Parameter	**Value**
Line Inductance	0.7 mH
Line Resistance	0.46 Ω

During each of the fault simulations, a fault impedance is placed across Load 1 and once the fault has been cleared, the impedance of Load 1 is doubled (load halved). Table 5.3 provides the impedance of the loads for both pre-fault and post-fault, and the impedance of the fault.

Table 5.3: Properties of the load and fault used for the two droop inverters

Parameter	**Pre-fault Value**	**During Fault Value**	**Post-fault Value**
Load 1	26.67 Ω	26.67 Ω	53.34 Ω
Load 2	20 Ω	20 Ω	20 Ω
Fault Impedance	0 Ω	1 Ω	0 Ω

In all the simulation cases, there will be two steady-state operating points. The first will be pre-fault and the second will be post-fault. A time-step simulation was run to obtain these values and the results are listed in Table 5.4.

Previously, the limits were set only on the constraints of the inverter and no consideration was given to the network the inverters were connected to. Before any investigation is conducted a discussion of the choice of limits is required.

Table 5.4: Steady-state values of the two droop inverters

Parameter	**Pre-fault Value** [Inverter 1, Inverter 2]	**Post-fault Value** [Inverter 1, Inverter 2]
P	[6.4173, 6.4175] kW	[5.0285, 5.0296] kW
Q	[376.8, -314.0] VAr	[-1.0481, 1.0969] kVAr
$Freq$	[49.9969, 49.9969]	[49.9975, 49.9975]
V_c	[215, 214] Vrms	[210, 205]
V_g	[215, 214] Vrms	[206, 204]
I_l	[9.8, 10.1] Arms	[9.1, 7.5]
I_g	[9.4, 9.4] Arms	[7.4, 7.0]
$I_{neutral}$	[3.13×10^{-10}, -7.79×10^{-10}] A	[-4.64×10^{-9}, -4.01×10^{-8}]
δ_{12}	0.0428 deg	0.2906 deg
I_{Line}	1.4 A	3.77 A
$I_{Line,neutral}$	5.5 μA	0.16 μA
I_{load1}	8.1 A	3.9 A
I_{load2}	10.7 A	10.2 A

5.5.1 Setting the current limit using Current-Trip Voltage-Reset

The inverters used have a nominal current rating of 15 A and a peak current rating of 30 A. The peak current rating will be chosen for the fault current since the microgrid is not fault-current constrained and a higher fault current will aid in the detection of the fault. There are two choices of when to limit the current of the inverter. The first is to limit at 15 A and then export 30 A, however this may cause the inverter to export a fault current for a small over-load and this could cause an over-voltage in the microgrid. The second option is to limit at 30 A, however this may cause the inverter to export a higher than nominal current for long periods of time. Both choices will be simulated with the aim of understanding what would happen to the microgrid for both fault limit settings.

5.5.2 Setting the voltage reset when using Current-Trip Voltage-Reset

To prevent the limiter from latch-up, the reset function must over-rule the trip function. This means that if the voltage-reset is satisfied then even if the current-trip is satisfied, the limiter will not operate. For the limiter to trip correctly, the voltage-reset must be set higher than the nominal voltage or maximum permitted operating voltage. For the voltage-reset to reset, the value must also be lower than the maximum voltage that the inverter is able to generate.

In this case the maximum operating voltage is defined by the reactive-droop controller and governed by Equation (5.4).

$$v_{cd} = V_n - V_n Q \frac{V_{droop}}{Q_{max}} \tag{5.4}$$

The maximum operating voltage is when the reactive power export is equal to the negative of the maximum reactive power export ($Q = -Q_{max}$). Using the droop settings in 5.4, the maximum operating voltage can be calulated which is $v_{cd} = 382V$ and is equal to 221 Vrms. The maximum voltage that the inverter is able to generate is 229 Vrms which is equal to $v_{cd} = 397V$ when $v_{cq} = 0V$. Choosing a voltage reset in-between these two voltages is a good compromise and thus the voltage reset will be 225 Vrms.

5.5.3 Response of two inverters for a fault of one second

Figure 5.5 show the response of a two inverter network where the two inverters are controlled by a droop controller with identical parameters. It can be seen that when the two inverters enter current limit mode, the inverters no longer share the power according to the droop parameters. When the inverters are in current limit mode, their export current is identical and in phase with the internal reference frame. However, the voltage of the inverter is determined by the network impedance as measured by the inverter. The closer the inverter is electrically to the fault, the lower the voltage of that inverter is. If the two inverters are exporting the same fault current but one inverter has a lower voltage at its terminals, then the power export will be less than the inverter with the higher terminal voltage. If the power export is less, the frequency of the inverter will be greater. From the network, Inverter 1 is electrically closer to the fault and as explained, the power export from Inverter 1 is lower than the power export from Inverter 2.

The two inverters have different frequencies during the fault. The frequency of Inverter 1 is 49.9974 Hz and the frequency of Inverter 2 is 49.9969 Hz. From the difference in frequency it is possible to calculate the angle difference of the two inverters after one second by using Equation (5.5). It is noted that this small frequency difference would be difficult to measure in a real application and the controller of the droop inverter may not have a high-enough precision to

control the inverter at these frequencies. Since this is in a simulation environment, the analysis will continue.

$$\Theta_{12} = (\omega_1 - \omega_2)\, t \tag{5.5}$$

Before the fault, the output of the droop controller sends set points to the voltage controller and the voltage controller is in phase with the internal angle of the inverter. Using Equation (5.5), the expected angle difference after 1 second is $(49.9974 - 49.9969) \times 2\pi \times 1$ which is 0.00314 radians (0.18 degrees). This is such a small angle change from the beginning of the fault to the end of the fault and for this reason it is not visible in Figure 5.5.

There are large changes in the angle of the capacitor voltage and the grid current. This is not related to the difference in frequency but related to the structure of the inverter controller. Before the fault the voltage controller is in phase with the angle of the droop controller and the angle of the current is determined by the impedance of the network as seen by the inverter. During the fault, the angle of the current through the filter inductor is in phase with the angle of the droop controller and the angle of the grid current and capacitor voltage is determined by the impedance of the LCL filter and impedance of the network as measured by the inverter.

To understand the angle differences between the two droop controllers Figure 5.6 is plotted. The top graph is the difference between the two inverter angles which is set by the droop controller. In this plot it can be seen that during the fault the angle between the two inverters increases at the rate as calculated by Equation (5.5). The second plot is the angle between the current of the filter inductors L_f with the droop angle difference in the top plot shown by the green dotted line. Although the scale is too large to see the small changes in the droop angle difference, it can be seen that the current angle difference is the same as the droop angle difference for the duration of the fault. The third plot shows the angle difference between the capacitor voltages of the two inverters. Again the green dotted line is the droop angle difference as shown in the top plot. From this plot it can be seen that the angle difference between the capacitor voltage is the same as the droop angle differences when the inverters are not in current limit. As expected, during the fault the voltage angle is different from the droop angle.

From Figure 5.5 and Figure 5.6 it can be seen that a small change in the droop angle during the fault has caused a large power swing as the inverters return to normal once the fault is cleared.

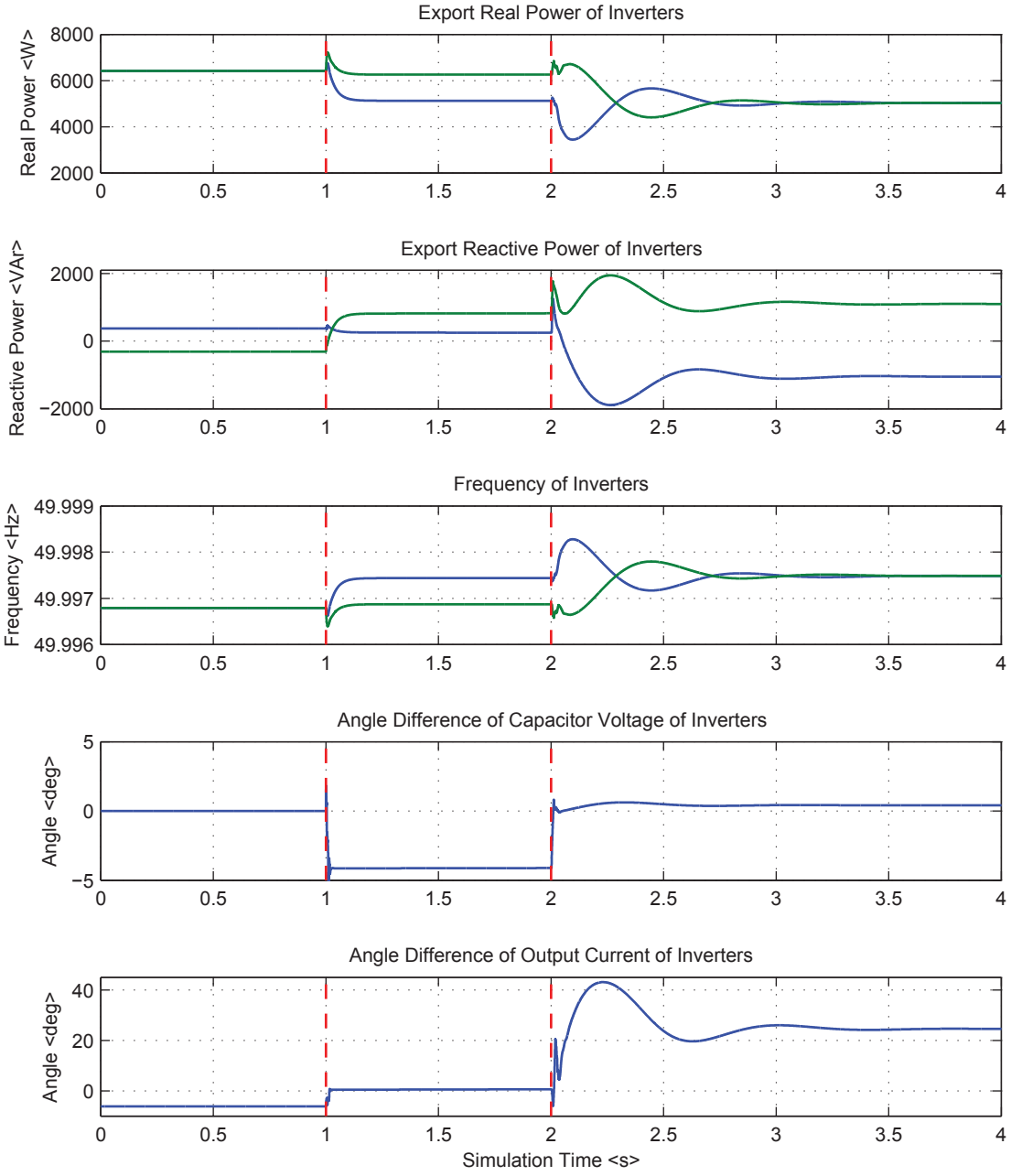

Figure 5.5: The transient of a two droop inverter network when a fault is applied at 1 second and released at 2 seconds.

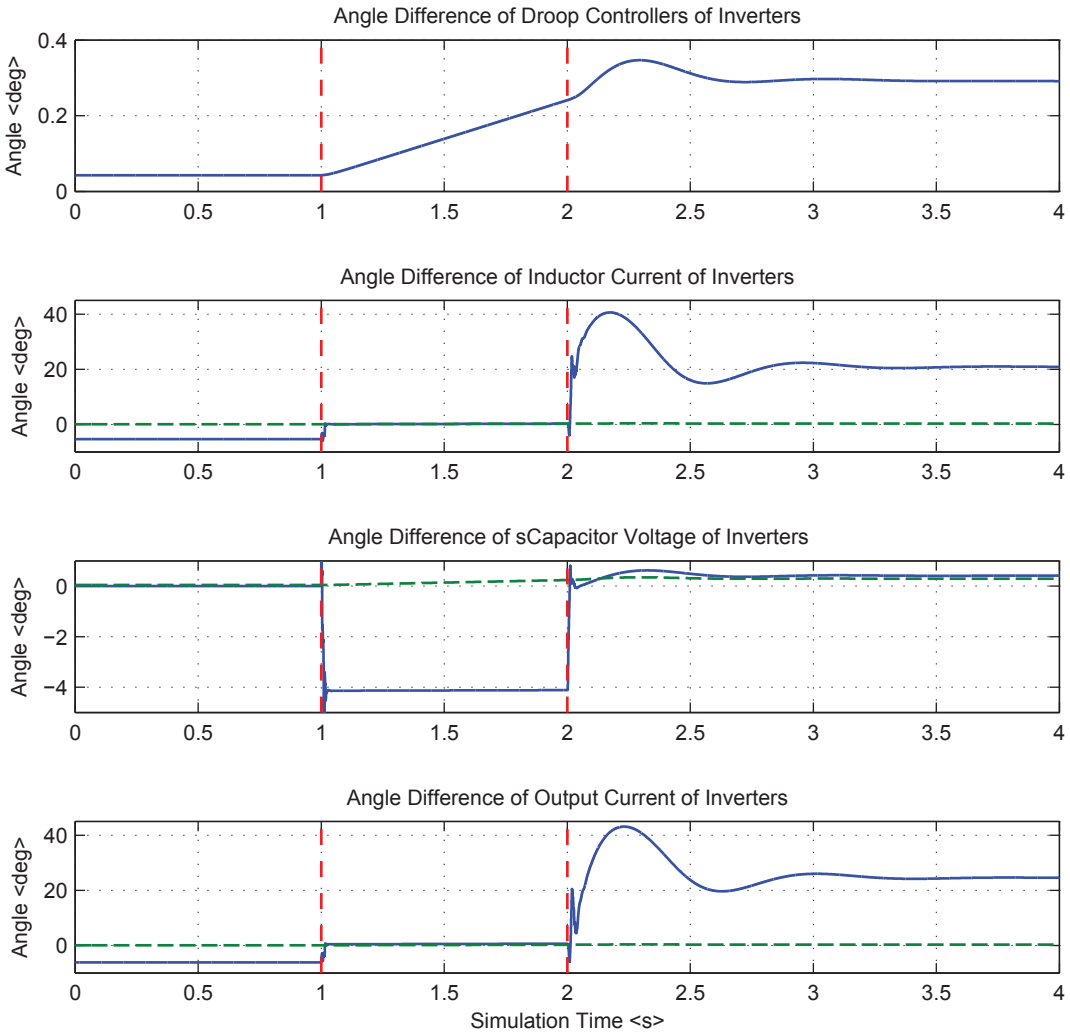

Figure 5.6: The angles of a two droop inverter network when a fault is applied at 1 second and released at 2 seconds. The green dotted line is the top graph placed for comparison.

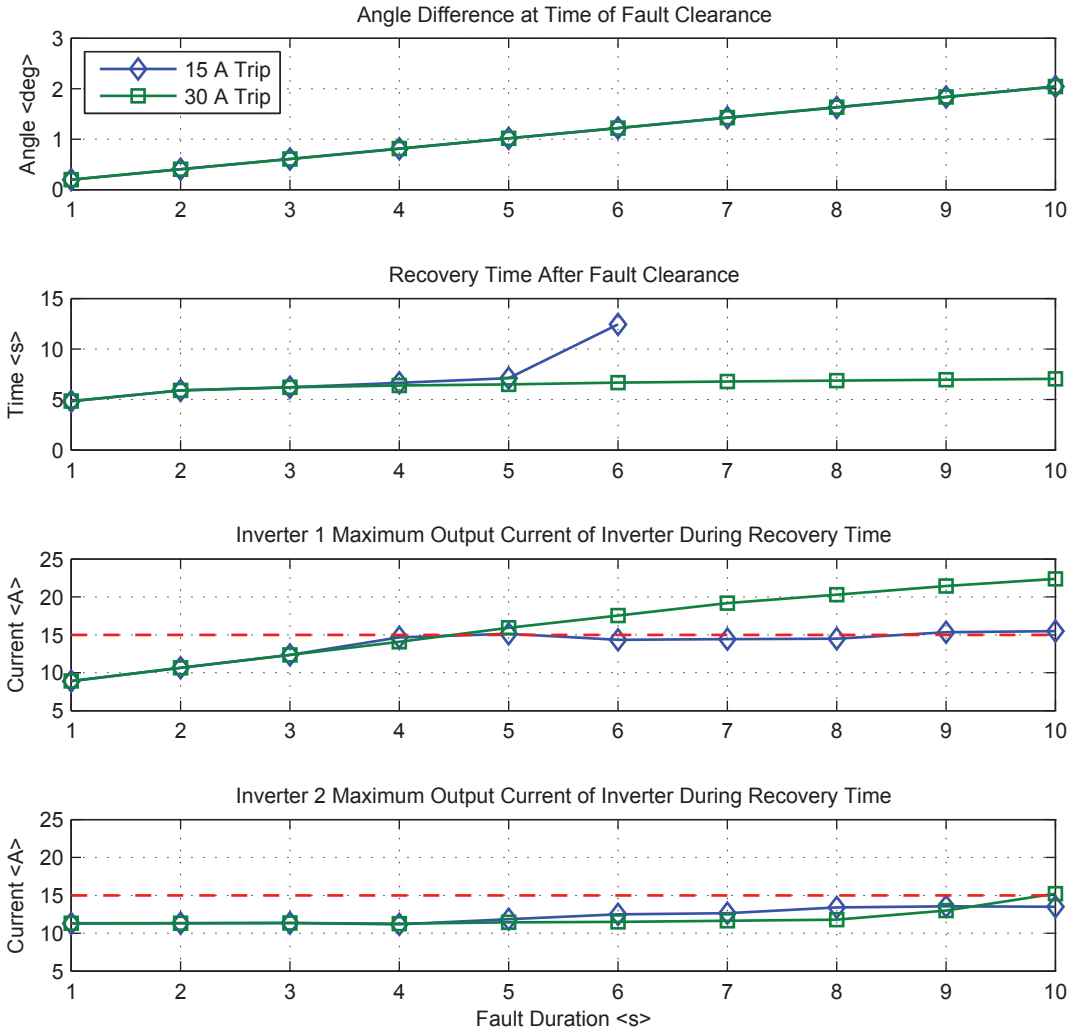

Figure 5.7: Recovery time of the inverters when the fault duration is increased. The inverter is set to trip at 15 A for the first recovery time test and 30 A for the second recovery time test.

5.6 Increasing the Duration of the Fault for the Two Droop Inverters

The duration of the fault was increased from 1 s to 10 s in one second intervals. The aim of the simulation was to study the recovery of the two droop inverters.

5.6.1 Angle Difference

The plot labelled 'Angle Difference' in Figure 5.7 shows the angle difference at the end of the fault. The difference is the droop angle of Inverter 2 minus the droop angle of Inverter 1. For the case when the fault duration is 1 s, the angle difference during the fault is shown in the plot labelled 'Inverter Droop Angle Difference' in Figure 5.6. The angle difference reported in Figure 5.7 is the angle measured at the time that the fault is removed from the network.

The angle difference in Figure 5.7 shows that as the fault duration increased, the angle difference between the two inverters also increased. During the fault the power export of each inverter and hence the frequency of each inverter is the same for every fault duration. For the fault duration of 1 second, the power and frequency of the inverter is shown in Figure 5.5. The power export of Inverter 1 is 5120 W with a frequency of 49.9974 Hz and the power export of Inverter 2 is 6260 W with a frequency of 49.9969 Hz. The difference in frequency causes the angle to increase. The longer the fault duration, the longer the frequencies are different and thus the greater the angle difference. This is explained in Section 5.5.3 and modelled using Equation (5.5). It is noted that if the power exports of the inverters were greater than in this case, then the frequency difference would be greater, and thus the angle difference would increase at a greater rate.

5.6.2 Recovery Time

The time in seconds that the inverters require to return to steady-state once the fault has been cleared is shown in the plot labelled 'Recovery Time' in Figure 5.7. The network is deemed to be in steady-state when the change in angle difference between Inverter 1 and Inverter 2 is less than 10^{-5} degrees in a 0.03 s window.

It can be seen that when the inverters trip at 15 A and 30 A, the recovery time is identical until t = 4 s. After this time the network did not recover for faults of duration 7 s to 10 s when the limit was set to trigger above 15 A. The simulation did not test when the duration of the fault was greater than 10 seconds, but it would be sensible to assume that an inverter would not be required to generate a fault current for more than 10 seconds and if the fault was longer, the inverter would disconnect.

When the current limit was set to trigger above 30 A, the network always recovered. The longer the duration of the fault, the longer the inverters took to return to steady-state. It would be reasonable to conclude that the longer the fault, the greater the angle difference and thus the longer the inverter required to return to steady-state.

5.6.3 Maximum current during the transient

Between the time the fault was cleared and when the inverter recovered or the simulation finished, the maximum current for Inverter 1 and Inverter 2 was recorded and is plotted in Figure 5.7. The trip setting of the 15 A case is shown as a red dotted line.

It can be seen that for the fault durations between 1 seconds and 4 seconds, the maximum currents exported by the inverters during between the fault being cleared and the inverters converging to a new stead-state for a 15 A and 30 A trip are identical. However, for faults of a duration greater than 4 s the maximum current diverges. It is noted that for faults of a duration of 4 seconds, the maximum current exported by Inverter 1 is just below 15 A. For the 30 A case, the maximum current exported by Inverter 1 continues to increase but never reaches the trip limit of 30 A. For the 15 A case, the maximum current exported by Inverter 1 does not continue to increase and is not greater than the trip limit of 15 A.

For the 15 A case, three of the 10 cases are studied in detail and plotted in Figure 5.8. The first is when the fault duration is 3 s, the second is when the fault duration is 5 s and the third is when the fault duration is 7 s. The same results are shown for the 30 A case in Figure 5.9 in order to compare between the two current trip settings.

When the fault duration is 3 seconds in Figures 5.8 and 5.9, the two inverters return to a steady-state. After the fault has cleared at t = 4 s, the angle difference starts to return to 0.3 degrees which is the steady-state angle difference for the post-fault network. It can be seen that the current limit is quick to reset and there is a small over voltage. This is expected and explained in Section 4.5. When the two droop controlled inverters are swinging against each other, the RMS voltage and RMS current have no distortion or high frequency oscillations. These signals converge to the new steady-state operating condition. It is also noted that the RMS current in Figure 5.8 does not exceed the 15 A current trip. The plots for the 30 A current

trip, in Figure 5.9, and 15 A current trip for 3 seconds, in Figure 5.8, are identical. This is expected as there is no difference between the 15 A and 30 A trip results for 3 seconds in Figure 5.7.

When the fault duration is 5 seconds the angle difference is greater at the end of the fault then for the 3 second fault duration. After the fault has been cleared for the 15 A trip, there are a number of limit oscillation cycles. These in Figure 5.8 occur in the RMS current and RMS voltage before the inverters converge to the new steady-state operating condition.

An explanation for the limit oscillation cycles is as follows. As soon as the fault is cleared and the current trip is reset, the current RMS falls to 5 A before it starts to increase. The RMS current continues to increase until the current limit is triggered. It can be seen that when the current trip is set to 30 A as in Figure 5.9, the RMS current passes through 15 A before reaching the maximum.

For the 15 A trip in Figure 5.8, the tripping of the current limiter causes the inverter to attempt to export the fault current into a non-faulted network. This causes the voltage to rise and the voltage saturation limit to clip the peak of the voltage waveform. This is seen in Figure 5.8 where the current reaches the blue dotted line and a spike in the 'Current Limit Activated' and 'Voltage Saturation Activated' signals appear. This suggests the voltage rise is sufficient to reset the current limiter. The resetting of the current limiter causes the RMS current to fall and then start to rise again as the two droop inverter attempt to return to their steady-state. This cycle continues until the angle difference between the two inverters is small enough such that the droop inverter can return to their steady state without setting their current limiting circuits.

When the current trip is activated, the current does not export a fault current of 30 A. This is explained by the voltage limit activating. After the fault and when the current limit is activated during the limit oscillation cycles, if the inverter were to export 30 A of current, the voltage would exceed the voltage limit.

When the fault duration is 7 seconds and the current trip is 15 A, the larger angle difference causes the current to remain in a limit oscillation cycle and not regain stability. The angle difference continues to increase after the fault has cleared as seen in Figure 5.8. When

the current trip is set to 30 A, the RMS current exceeds 15 A, but does not exceed 30 A before the angle difference starts to return to the post fault steady-state condition. There is a small discontinuity in the the RMS current and the voltage saturation is activated. This is because when the current export increases, the voltage at the reference to the inverter PWM has also increase and causes the voltage saturation to activate. The activation of this limit has not caused an instability.

5.6.4 Conclusion

In conclusion a large fault duration causes a greater angle displacement. The greater angle displacement causes a larger power swing on the recovery. The voltage is kept constant during the recovery and the current swing is similar to the power swing. The large current swing causes the current limiter to activate and when the current limit is activated during the transient, the microgrid enters into a limit oscillation cycle.

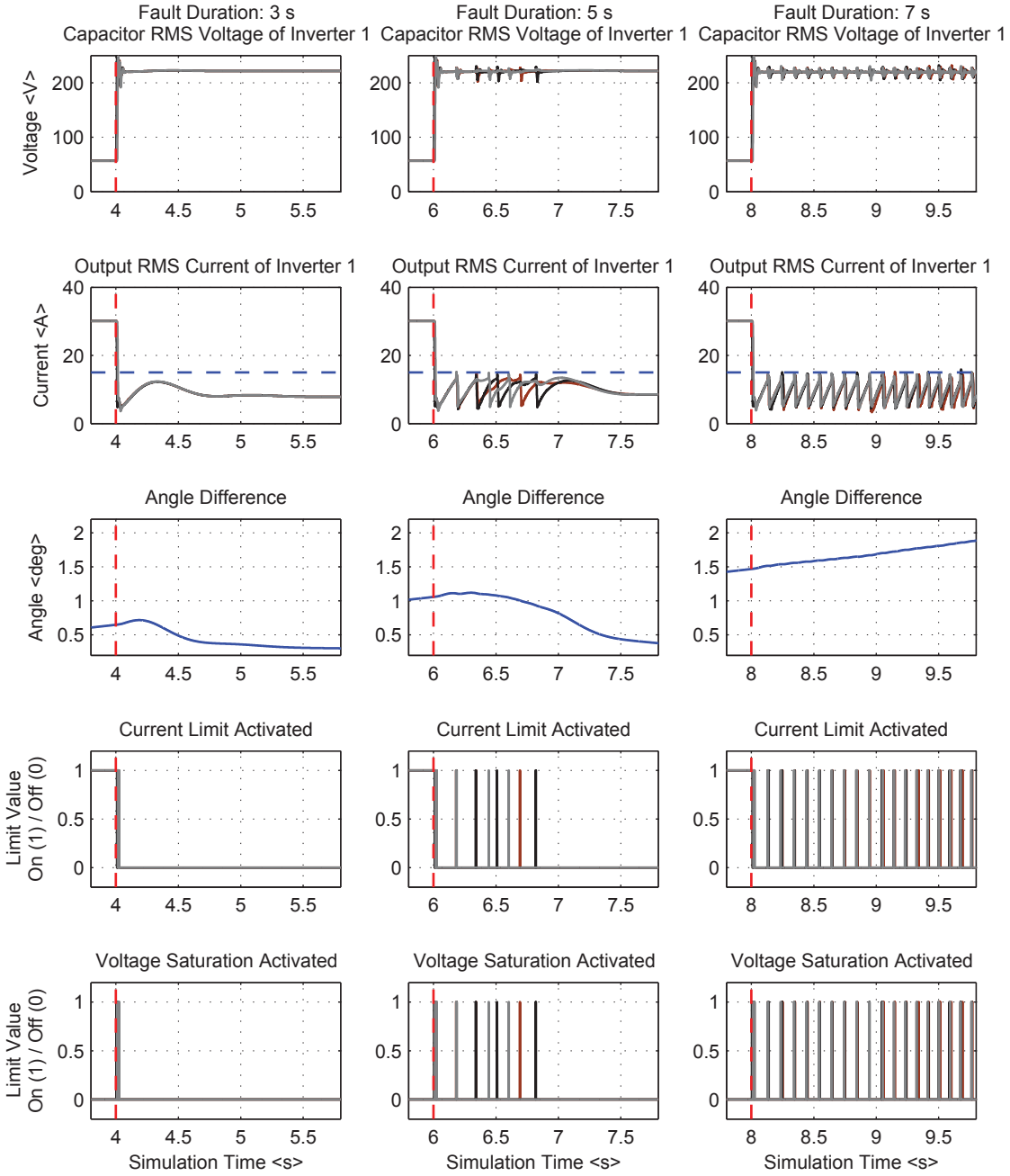

Figure 5.8: The outputs of Inverter 1 in the two droop inverter set-up for a fault duration of 3 seconds, 5 seconds and 7 seconds. The current limiter is set to trip at 15 A. The red dotted line indicates the time that the fault is cleared and the blue dotted line is the current trip.

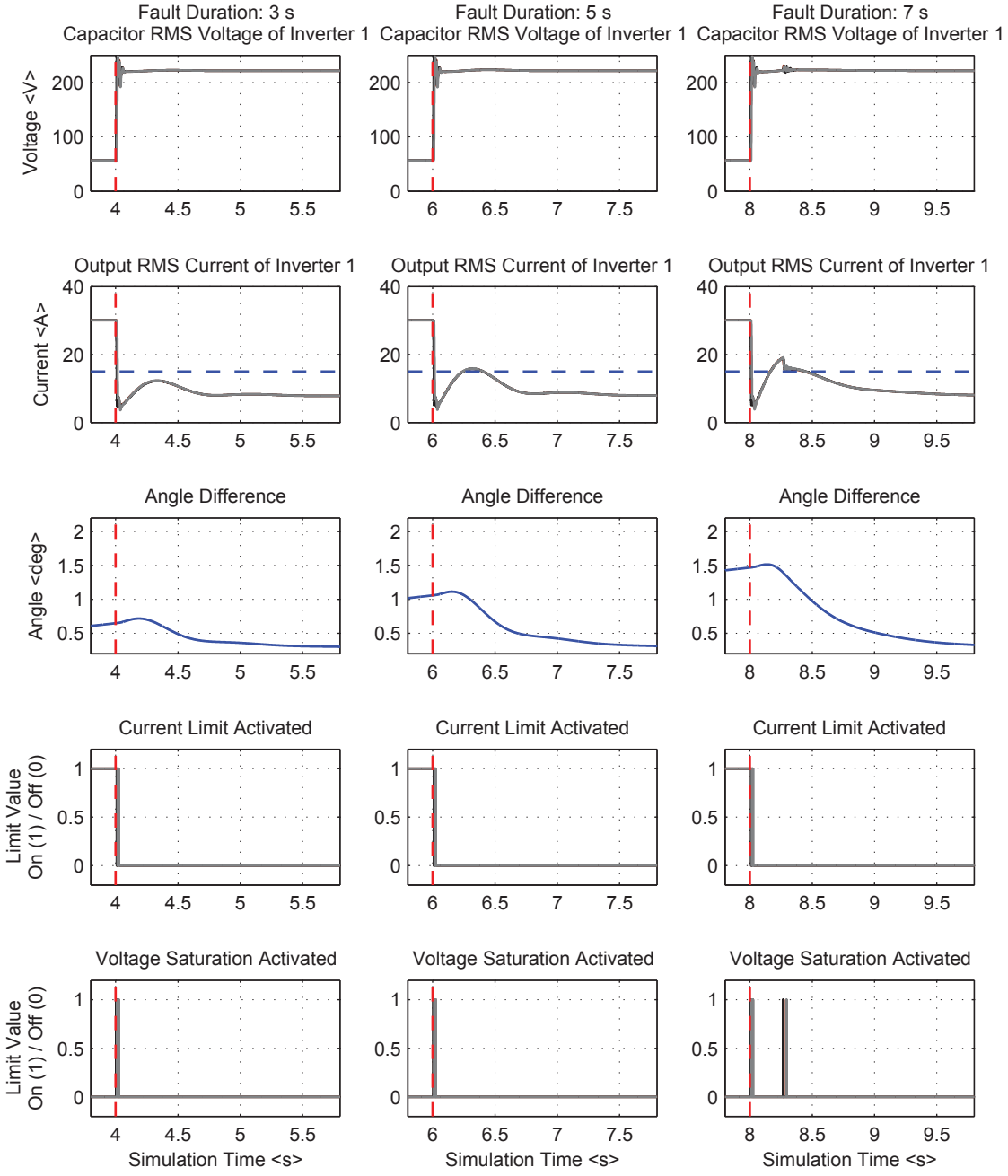

Figure 5.9: The outputs of Inverter 1 in the two droop inverter set-up for a fault duration of 3 seconds, 5 seconds and 7 seconds. The current limiter is set to trip at 30 A. The red dotted line indicates the time that the fault is cleared and the blue dotted line is the current trip for the 15 A trip.

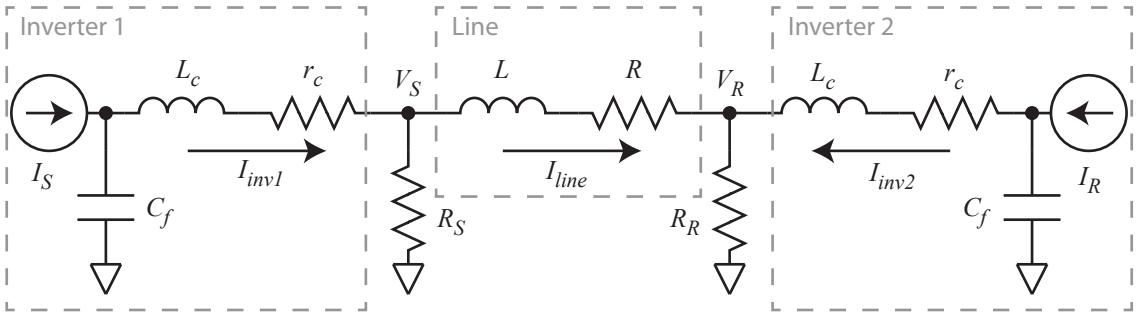

Figure 5.10: Inverter droop model during the fault

5.7 Analysis of the Fault Response of the Two-droop Microgrid

In the previous section, there are two distinct regions of the droop controller when under faulted conditions. These two regions introduce two important quantities that will allow an analysis to determine if the droop circuit will return to steady-state once the fault has been cleared. The first quantity is the angle between the inverter sources when the fault is cleared. The second quantity is the maximum current flow in the circuit when presented with an angle between the inverter sources. From the calculation of the angle difference, it is possible to calculate the maximum current flow and determine if a current limit will be exceeded.

5.7.1 Calculating the angle between the inverter sources during the fault

To calculate the angle between the inverter sources, knowledge of controller is required such that an equivalent circuit can be derived. When the inverter is operating in droop-control mode, it may be modelled as a voltage control source and when the inverter is operating in current-limit, it may be modelled as a current controlled source. A load-flow analysis should be conducted to determine when the network has a fault if the inverter current drawn when the inverter is in droop-control mode will cause the current limit to activate. For the purpose of this analysis, the assumption will be made that both inverters enter into current-limiting and that the current limiting will happen instantaneously.

When the inverter sources enter into current-limiting mode, they become a controlled current-source with an initial angle between them that is equal to the steady-state angle before

the fault was introduced to the network. An approximation of the droop controlled circuit will be as in Figure 5.10.

To calculate the angle difference at the end of the fault, how the angle changes during the fault must be considered. Two angle differences are chosen and simulated using the circuit in Figure 5.10. An arbitrary angle of 10 degrees and an arbitrary angle difference of 0.0001 Hz, which is approximately 0 Hz, are chosen.

5.7.2 Assumed angle difference of 10 Hz during the fault

If the frequency difference between the droop-controlled inverter sources has the possibility of being large, for example 10 Hz difference, then the angle between the two inverters will change quickly. A frequency difference of 10 Hz with an initial angle separation of 0.0462 degrees, where the frequency of Inverter 1 is 50 Hz and the frequency of Inverter 2 is 40 Hz, will cause the angle difference to rotate every 0.1 seconds. This is shown in Figure 5.11.

The first two graphs in Figure 5.11, show the real and reactive power oscillation from Inverter 1 of 2 kW and 1.5 Kilovolt Ampere Reactive (kVAr). This power oscillation during the fault would be caused by a 10 Hz difference in frequency between the two droop-controlled inverters. The third plot shows the capacitor RMS voltage of Inverter 1, and it can also be seen to be oscillating. During the fault, the current limiter is controlling the fault current which is being held constant. The last graph shows the angle difference between the two inverter which is also oscillating.

The aim of Figure 5.11 is to demonstrate that when there is a frequency difference of a relatively low frequency compared to the transient analysis of synchronous machines, the oscillations seen in a droop-controller microgrid could be large during the fault. This will make the calculation difficult and require a time-step simulation to calculate the angle difference at the end of the fault.

If the current sources were given a frequency reference from a droop source, then the frequency of the two sources would also be changing. When calculating the angle at the end of the fault, the changing frequency and the changing angle would need to be taken into consideration. This would make the calculation very complex and outside the scope of this thesis.

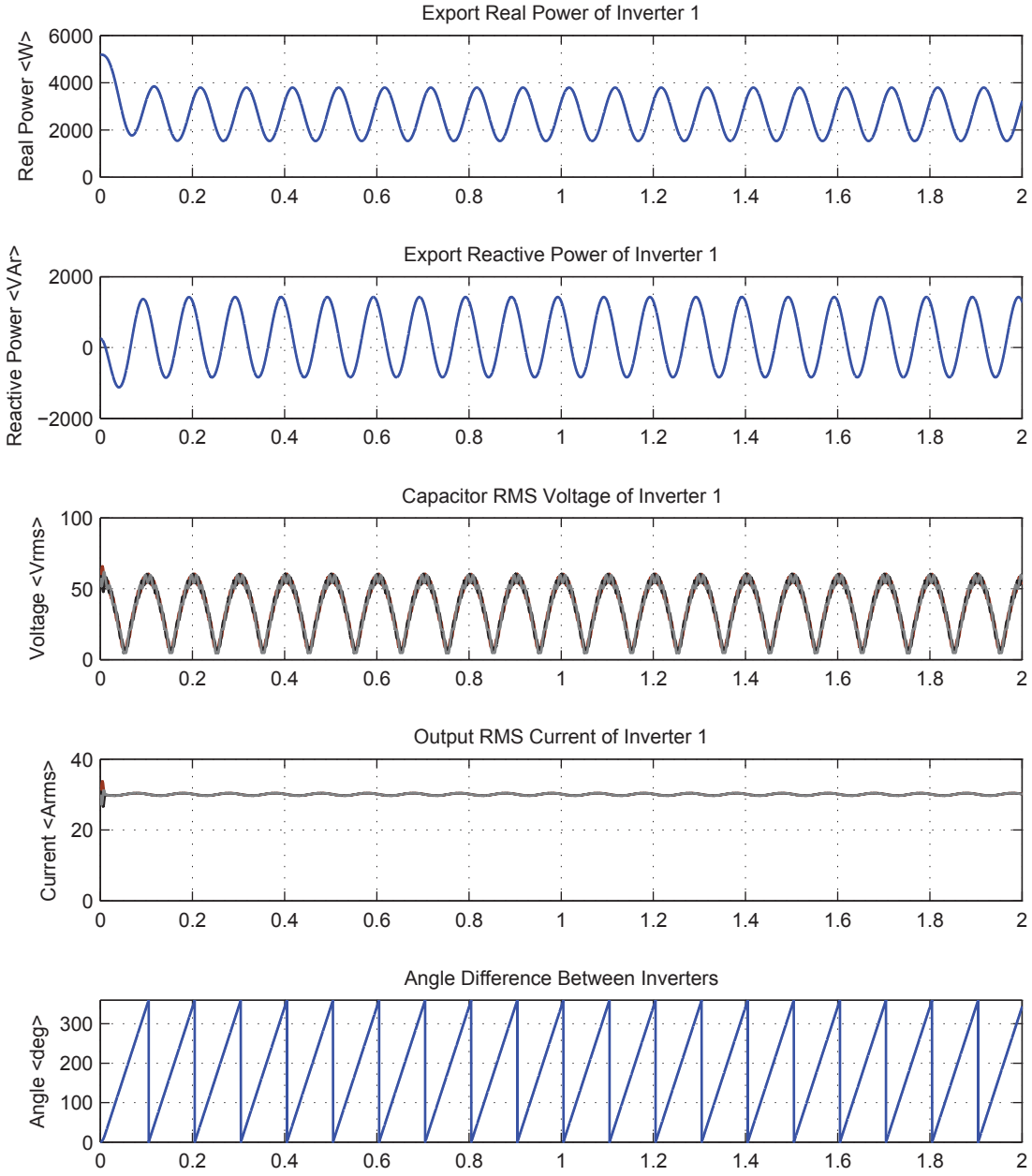

Figure 5.11: Frequency difference of 10 Hz

5.7.3 Assumed angle difference of 0.0001 Hz during the fault

It is noted that the difference in frequency between the two inverters during a fault is small. This is shown in Figure 5.5. When running the simulation in Figure 5.10 with a frequency difference that is similar to the response in Figure 5.5, the angle difference takes a long time to transient from 1 degree to 360 degrees and this is shown in Figure 5.12.

For the four seconds of simulation time, the power changes by 2 W. This can be approximated as constant for the duration of the fault. The power will oscillate as seen in Figure 5.11, however the period of oscillation will be much longer because the frequency difference is less.

The frequency of Inverter 1 is 49.997 Hz and the frequency of Inverter 2 is 49.9969 Hz which is a difference of 0.0001 Hz. The phase difference of two sources with a frequency difference of 0.0001 Hz will be in-phase every 10,000 seconds or every 2.8 hours. This is calculated using the equation in Equation (5.6). This can be checked by looking at the rate in which the angle changes. The rate of change in angle will be constant because the frequency is fixed and thus the difference in frequency is fixed. In four seconds, the angle changed by 0.144 degrees. This is a difference of 0.04 percent. Four seconds as a percentage of 10,000 seconds is also 0.04 percent, this is because the rate of change of frequency is assumed linear.

$$t = \frac{1}{|\omega_1 - \omega_2|} \tag{5.6}$$

The aim of Figure 5.12 is to demonstrate that when there is a small angle difference between the two droop controlled inverters, the power export during the fault and angle difference between the two inverter may be considered constant. However, this is not the case when the angle difference between the two inverters is 10 degrees as seen in Figure 5.11. A suitable equation for the calculation when the angle difference can be approximated as constant is Equation (5.5).

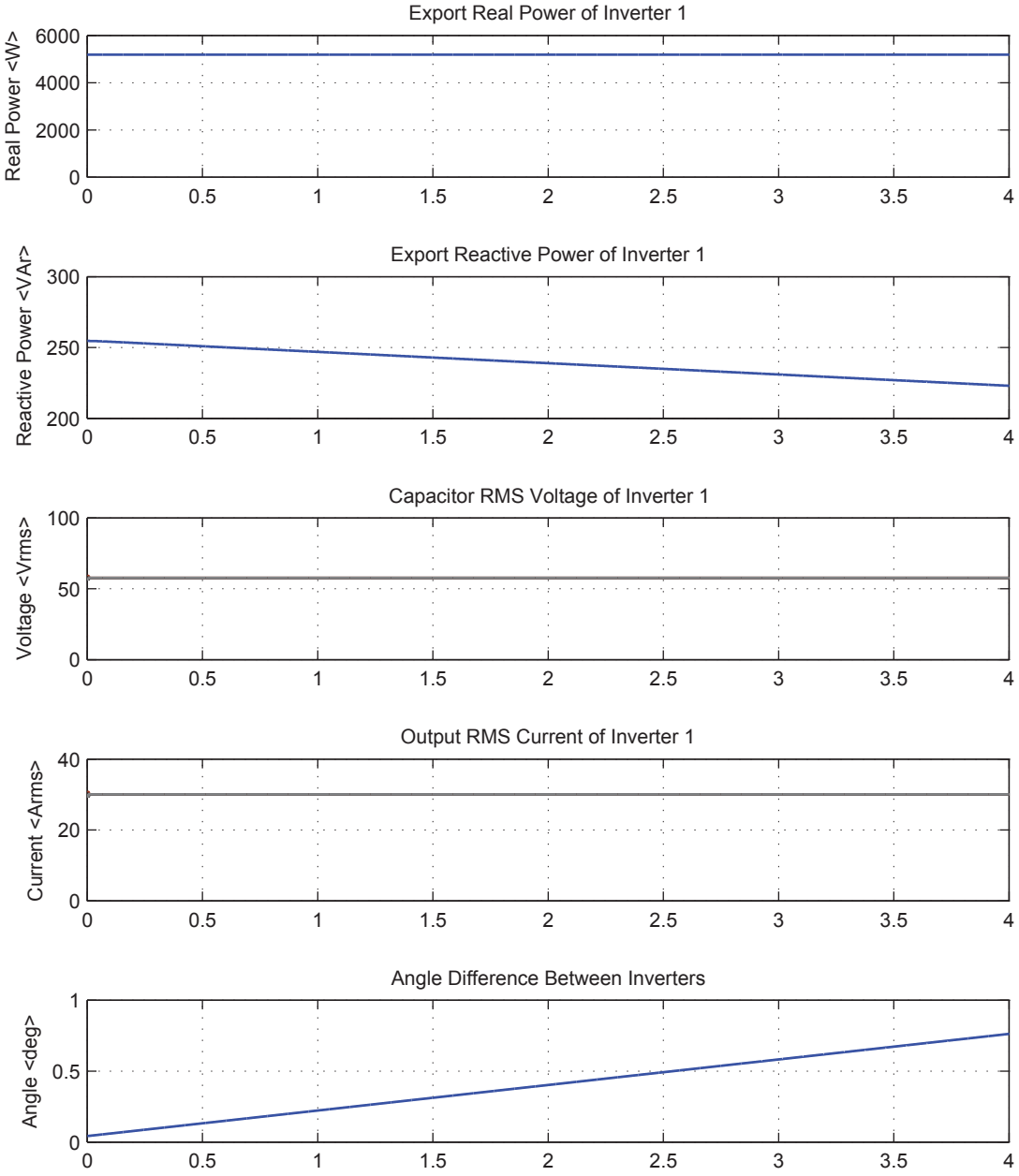

Figure 5.12: Frequency difference of 0.0001 Hz

5.7.4 Testing the calculation of the angle between the inverter sources during the fault

The frequency of the droop controlled inverter can be calculated by Equation (5.3). The maximum frequency is when the droop controller is exporting zero power and the minimum frequency is when the inverter is exporting maximum power. Maximum power may be when the inverter is exporting fault current into a node that has a high voltage which would be around twice the nominal power export. This power export is unlikely as in fault condition the voltage at the node will most likely be depressed. However, the purpose of this calculation is to calculate the minimum possible frequency and therefore a power export to twice nominal will be used in the calculation.

To calculate if the frequency difference can be approximated as constant or not, the worst case much be considered. Using parameters presented in Table 5.1 for the circuit in Figure 5.4, the maximum frequency is 50 Hz and the minimum frequency is 49.999 Hz which is a frequency difference of 0.001 Hz. Using this frequency difference, the two frequencies will be in phase every 1000 seconds or every 16.67 minutes. Therefore, for a fault which is under 10 seconds, the power that is exported from the inverters can be approximated as constant. With this frequency difference, the angle should increase by 0.36 degrees every second. The angle increase is calculated using Equation (5.5). Therefore for any frequency difference that is below the maximum frequency difference, the rate of change of angle for the duration of the fault may be assumed linear.

The approximation that the rate of change of angle for the duration of the fault is linear will be tested on the two droop inverter circuit presented in Figure 5.4 where the operating conditions are listed in Tables 5.1 – 5.4. For this circuit, the transient for a fault duration of 1 second is shown in Figure 5.5. In the simulation presented in this section, the fault will be applied at 1 second and the fault will remain connected for a duration of 10 seconds. Every second during the fault, the angle difference between the inverter will be recorded. The angle difference will also be calculated with Equation (5.5) and compared.

The aim of this simulation is to test if Equation (5.5) is a valid approximation. It was calculated that for the circuit in Figure 5.4, the worst case angle difference was 0.36 degrees

every second. In the simulation presented in Section 5.5.3 and used here, the frequencies of the two inverters as shown in Figure 5.5 are 49.9974 Hz and 49.9969 Hz. Using Equation (5.5), this is an angle difference of 0.18 degrees every second. The results of this calculation compared with the simulation are shown in table 5.5.

Table 5.5: Approximation of the angle from simulation data

Fault Time (seconds)	**Initial Angle** (degrees)	**Angle Calculated After Fault Time** (degrees)	**Angle Measured From Simulation** (degrees)
1	0.0428	0.2228	0.1972
2	0.0428	0.4028	0.4014
3	0.0428	0.5828	0.6057
4	0.0428	0.7628	0.8101
5	0.0428	0.9428	1.0147
6	0.0428	1.1228	1.2195
7	0.0428	1.3028	1.4244
8	0.0428	1.4828	1.6294
9	0.0428	1.6628	1.8346
10	0.0428	1.8428	2.04

From Table 5.5 it can be seen that this is a good and valid approximation for the small fault durations. However, as the fault duration increases the error of the approximation increases. This is because as the fault time increases the angle difference increase. This causes the power export to change. When the power export changes, the frequency of the inverter will change. An accelerating or decelerating frequency will cause the rate-of-change of angle to to change. It is these changes that cause the linear angle approximation to deviate from the measured value.

5.7.5 Maximum current flow once the fault has been cleared

After the fault has been cleared, the current limiting circuits in the inverter will reset and the inverter source will return back to a voltage controlled source. For the purpose of this study, the resetting of the inverter is assumed to be instantaneous. For the inverters to correctly converge back to a steady-state operating point, the current export during the droop oscillations must remain with the current limits of the inverter as shown in Section 5.6.3. This part aims to approximately calculate the maximum current during the droop oscillation and determine if this current will cause the inverter current limit to trip. It was shown in Figure 5.8 that when

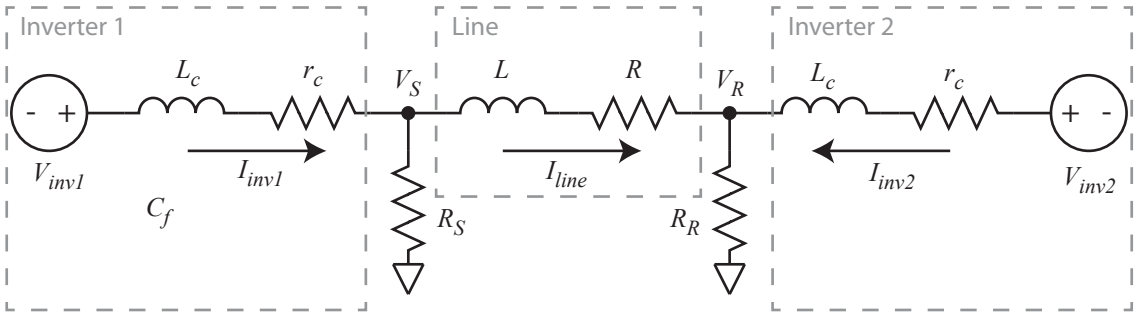

Figure 5.13: Inverter droop model after the fault

the current limit of the inverter is tripped, the microgrid becomes unstable and the angle between the two inverters diverges.

When the fault is cleared there will be an angle difference between the inverter sources that are connected to the network. The longer the duration of the fault and the greater the frequency difference between the inverters, the larger the angle difference between the two inverters. The larger the angle between the two inverters at the time that the inverter returns to droop-controlled mode, the greater the current that will be demanded from the inverters during the droop-oscillations. To calculate the magnitude of the maximum current, a load-flow of the inverter circuit will be performed. The initial parameters of the inverters are assumed to be at nominal voltage and at an angle difference equal to the angle difference at the end of the fault. The approximate circuit for the two droop-case once the fault has been cleared is shown in Figure 5.13.

A load-flow analysis using the circuit in Figure 5.13 was simulated for every measured angle which is listed in Table 5.5. The results of the current from Inverter 1 using the load-flow are compared with the measured maximum current of Inverter 1 during the transient. The measured current was from the case where the current trip was set to 30 A. This was used because every fault duration tested converged. Table 5.6 presents these results.

These results may not match, but they share an increasing trend. This suggests that increasing the angle difference when the droop controllers switch from fault current to normal operation does increase the maximum current. Further work is required to more accurately calculate the maximum current from the angle difference experienced at the time the fault is

Table 5.6: Approximation of the maximum current from simulation data

Fault Duration seconds	**Angle Difference** degrees	**Measured Maximum Current of Inverter 1** Amps	**Calculated Maximum Current of Inverter 1** Amps
1	0.198	8.92	5.96
2	0.4021	10.65	6.925
3	0.6064	12.36	7.941
4	0.8109	14.08	8.992
5	1.0155	15.91	10.07
6	1.2202	17.55	11.16
7	1.4251	19.19	12.26
8	1.6302	20.28	13.38
9	1.8354	21.44	14.5
10	2.0407	22.39	15.63

cleared.

5.8 Perturbing the droop-angle without a fault

Section 5.6 has argued that the magnitude of angle difference at the time that the fault is cleared determines the magnitude of the current during the transient after the current limiters of the droop controller are reset. To test this theory, the droop controller is modified such that the internal angle of the droop controller was perturbed. This is to show that when the internal angle is perturbed, the microgrid will enter into a limit oscillation if the angle perturbation causes the current-limit to be exceeded during the recovery from the angle perturbation.

The internal angle of the droop-controller of Inverter 1 is perturbed by five angle magnitudes which are presented in two different groups. The first group consists of three small perturbations and the second group consists of three larger perturbations. The post-fault network as presented in Table 5.4 for the circuit in Figure 5.4 is used in order to provide a comparasion between the measured angle at the end of the fault and the maximum current observed during the resulting transient.

Figure 5.14 shows the output of Inverter 1 and the angle difference when the internal angle of Inverter 1 is perturbed by 0.3 degrees, 0.5 degrees and 0.7 degrees. The perturbation happens at t = 1. In all three of these perturbations, the two droop controllers return to steady-state. The red dotted line indicates when the perturbation was applied.

From the capacitor RMS voltage graph, it can be seen that the voltage remains constant across the load. From the output current, there is a current oscillation which is caused by the perturbation. The magnitude of the current oscillation increases as the angle difference increases. The angle perturbation is seen in the angle difference graph. At t = 1 s there is a step increase in angle from the perturbation and before the droop controllers respond. The response of the two droop controllers is to return the angle difference back to the magnitude before the angle perturbation.

When the angle was perturbed by 0.7 degrees the current oscillation reaches the current trip of 15 A. The current causes the current limit to respond and a spike is seen in the 'Fault-Current Activated' plot. The transition of the inverter into constant current mode causes the voltage to rise. The voltage rise is seen by the spike in the 'Voltage Limit Activated' plot. The rise in voltage causes the current limit to reset and the droop controller returns to regulating the voltage. When the voltage limit is activated, the export current of the inverter drops as seen in the 'Output RMS current' graph. After the drop of export current, the current oscillation start and the two inverters return to steady-state. When the second current increase occurs, the angle difference has decreased enough and thus prevents the current oscillation from causing the current limit to trip.

Figure 5.15 shows the output of Inverter 1 and the angle difference when the internal angle of Inverter 1 is perturbed by 0.5 degrees, 1.0 degrees and 1.5 degrees. The perturbation of 0.5 degrees is shown as a reference and is identical to the 0.5 degree perturbation presented in Figure 5.14. In the 1.0 degree case and the 1.5 degree case, the current and voltage limiter is triggered during the current oscillation. The 1.0 degree case converges after the time shown, however the 1.5 degree case does not converge.

For the 1.0 degree case, it can be seen from the angle plot that the angle slowly decreases as the inverter returns to steady-state. As the angle is decreasing, the frequency at which the current limiter is tripped is also decreasing. As with the 0.7 degree perturbation in Figure 5.14, the tripping of fault current causes the voltage to rise which then causes the voltage limit to trip. The rise in voltage then resets the current limit. Every time the current limit and then voltage limit is tripped, the output current decreases. Once both limits have reset, the current

starts to rise which then causes the current limit to trip again. The repetition of this cycle is know as a limit oscillation.

When the droop controller of Inverter 1 is perturbed by 1.5 degrees, it can be seen that the angle difference continues to increase and the frequency of the limit oscillation cycle increases. This suggests that the two droop inverters will not converge back to the steady-state operating point and the network is no longer stable.

The perturbation of the droop-angle in Inverter 1 has confirmed that the greater the magnitude of angle difference once the fault has been cleared, the greater the current oscillation as the droop inverters return to a steady-state operating point. If the current oscillation causes the current limit to be triggered, the inverters may not converge and the inverters enter into a limit oscillation. It is noted that a small difference in angle is able to cause a limit oscillation cycle in the droop inverters.

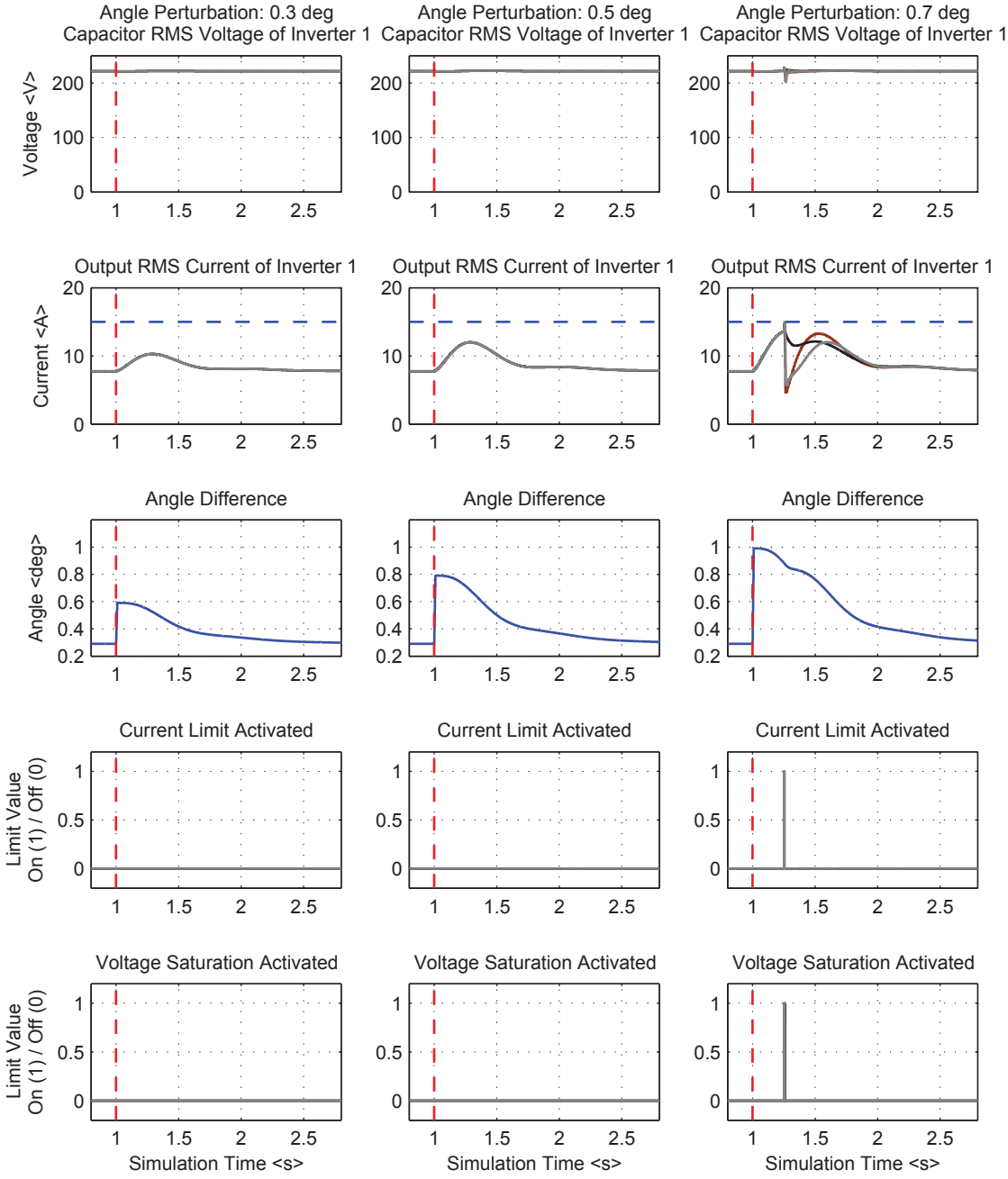

Figure 5.14: Small angle perturbation in the droop controller.

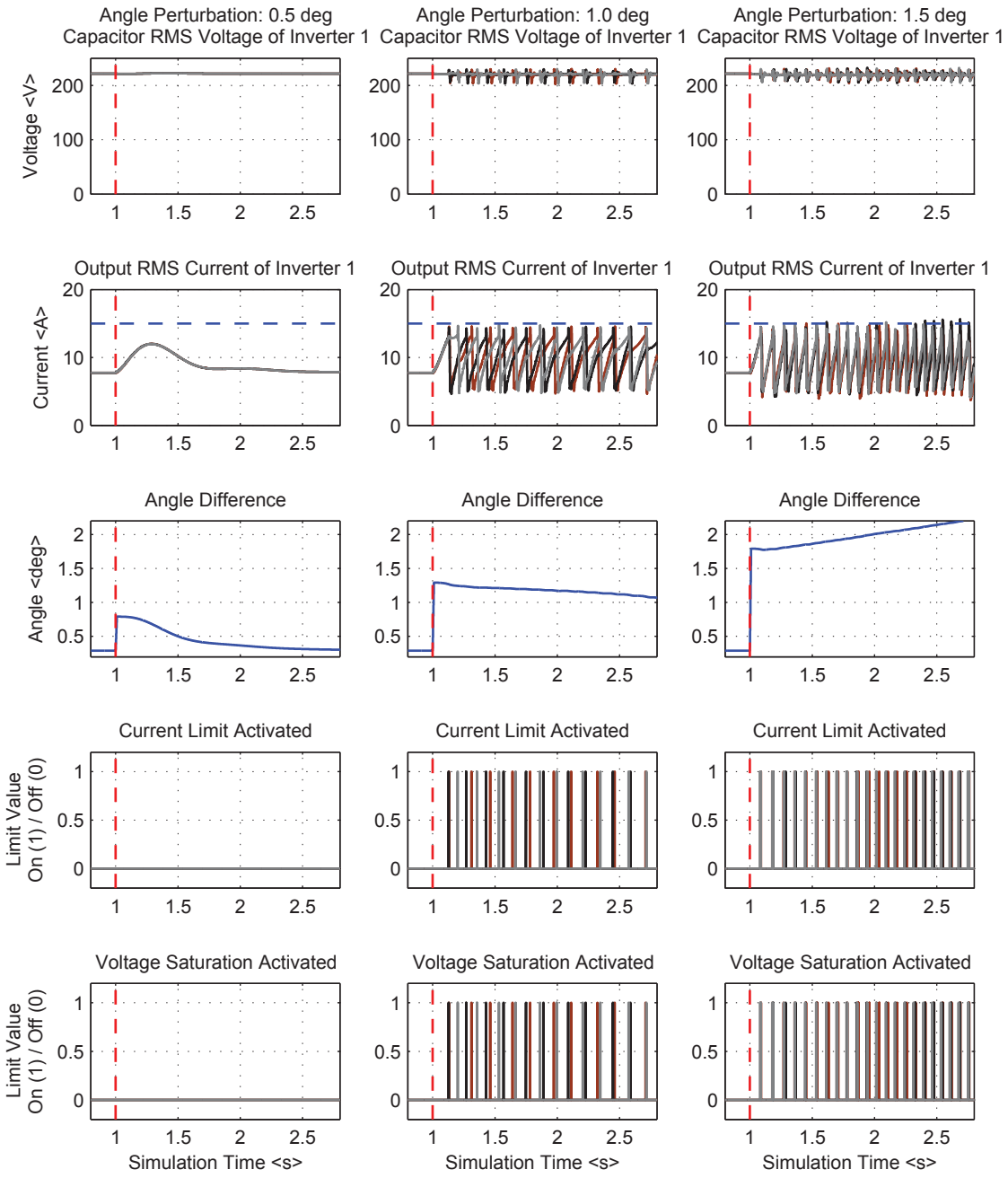

Figure 5.15: Large angle perturbation in the droop controller.

5.9 Changing the line length

A shorter line has a lower inductance and a longer line has a greater inductance. The current through an inductor with a voltage difference across the inductor's terminals is given by Equation (5.7).

$$I = \frac{V_1 - V_2}{R + j\omega L} \tag{5.7}$$

For a fixed voltage difference across the inductor, an increase in inductance will cause a smaller current to flow for the same voltage angle and a decrease in inductance will cause a larger current to flow. At the end of a fault when the angle difference is a function of the fault duration and the frequency of each inverter during the fault, the value of inductance will determine the maximum current flow through the line during the transient after the current limiters have reset. For a longer line, the voltage angle difference will cause a smaller current to flow. For a given line difference, it will be possible to calculate the maximum voltage difference between the inverters. Therefore, calculating the maximum voltage difference, will allow the calculation of the maximum angle difference and subsequently this allows the maximum duration of fault to be calculated. If a fault were to exceed the maximum duration, it would be reasonable to expect the inverter to become unstable after the fault has cleared.

It is reasonable to expect that a longer line will have a greater inductance and thus the current for a given voltage angle difference will be smaller. Therefore it is expected that a longer long line will allow for the permitted fault duration to be greater.

5.9.1 Calculation of the approximate maximum and approximate minimum impedance between the inverters

For a fixed current through the inductor, an increase in inductance will require a large voltage angle and a decrease in inductance will require a smaller voltage angle. If the line is very long, then the 90 degree stability criterion may be reached for normal operation. The maximum inductance of a line is set by the nominal current flow and the minimum inductance of the line is set by the maximum fault duration.

To approximately calculate the maximum impedance between the inverters, the following assumptions will be used. The maximum voltage angle will be assumed to be 90 degrees, although when the line has resistance, the maximum angle for the voltage will be different from 90 degrees. The current angle will be assumed to be in phase with the voltage of Inverter 1. It is noted that the current angle is dependent on the line impedance and load impedance. The voltage at Inverter 1 will be assumed to be at a phase of zero degrees and the voltage at Inverter 2 will be assumed to be at a phase of -90 degrees with respect to Inverter 1. The voltage magnitude will be assumed to be the nominal voltage of 220 V and the maximum current through the line will be assumed to be the nominal current of a single inverter which is 15 A. Since this calculation is not aiming to provide an exact line impedance and only an approximate line impedance, these assumptions are reasonable. If a more exact calculation were required, then the line inductance and resistance would be measured and the maximum current would be plotted over a range of voltages to ensure that the line was able to carry the current that the inverters require for the network to reach a steady-state operating point.

Using the approximations stated in the paragraph above, the maximum line impedance is calculated in Equation (5.8) and Equation (5.9).

$$Z = \frac{V_1 - V_2}{I} \tag{5.8}$$

$$Z = \frac{220 + 220j}{15} = 14.667 + 14.667j \tag{5.9}$$

The maximum resistance is 14.667 Ω and the maximum inductance at 50 Hz for an impedance of 14.667 Ω is 46.685 mH. To put these numbers into context, these numbers will be compared with the data sheet for Prysmain Waveform Cable. The resistance per kilometre for 185 mm^2 cable is 0.164 Ω. For this maximum resistance calculation in Equation (5.9) and ignoring the inductance, this equates to 89.43 meters of cable. The inductance per kilometre at 50 Hz for 185 mm^2 cable is 0.0725 Ω. For this maximum inductance calculation in Equation (5.9) and ignoring the resistance, this equates to 202.30 meters of cable. In this case, the resistance of the cable is the limiting factor at 89.43 meters.

To approximately calculate the minimum impedance between the inverters the same assumptions as were used for the maximum line calculation will be used, except for the assumption of voltage angle. The voltage angle will be assumed to be the maximum permitted angle between the two inverters once the fault has been cleared. For the purpose of this calculation this is assumed to be 90 degrees. Using these approximations, the minimum line impedance is calculated in Equation (5.10) and Equation (5.11).

$$Z = \frac{V_1 - V_2}{I} \tag{5.10}$$

$$Z = \frac{220 - (219.966 - 3.83953j)}{15} = 0.0022 + 0.2560j \tag{5.11}$$

The minimum resistance is 0.0022 Ω and the minimum inductance is 0.81477 mH.

5.9.2 Changing the line length for a fault duration of 1 second

As argued in Section 5.9.1, a longer line or greater coupling inductance in the inverters is expected to create a smaller current oscillation during the fault recovery. To test this theory, three line lengths were simulated for the two inverter network as presented in Section 5.5. This network is exposed to a 1 second fault and the line lengths chosen are within the constraints presented in Section 5.9.1. The choice of line lengths are presented in Table 5.7.

Table 5.7: Properties of the three lines used for the two droop inverters

Line Number	**Inductance** mH	**Resistance** Ω
1	0.7	0.46
2	2.2	0.46
3	4.9	0.56

Figure 5.16 shows the output of Inverter 1 when the line parameters were changed as listed in Table 5.7. Investigating the maximum current during the transient which is after the fault has been cleared at t = 2 s in the plot 'Output RMS Current of Inverter 1'. It can be seen that as the line length and impedance increases, the maximum current during the transient

is reduced. It is also noted, that changing the line lenght also changes the frequency of the oscillation of output current (after t = 2 s). From this, it is expected that the eigenvalues of the microgrid are changing. The analysis presented in Chapter 3 would be required to determine the change in eigenvalues.

It is also interesting to comment on the angle difference which is shown in the third graph from the top in Figure 5.16. Before the fault at t = 1 s, the steady-state angle difference between the two inverters increases as the inductance of the line increases but the RMS current before the fault does not increase. This is because, as the inductance increases, a greater voltage angle difference is required for the same current to flow through the inductor. The droop controllers when not in current limiting mode are voltage source controllers and the angle difference between the inverters should be the same as the voltage angle difference between the inverters. The current export from the inverter before the fault is determined by the load within the microgrid and the loses of the lines.

When the inverters are in current-limit mode, the increase in angle is is 0.196 for Line 1, 0.213 for Line 2 and 0.309 for line 3. The increase in angle difference between when the fault is activated and when the fault is cleared increases when the inductance is increased. This is because the increase in inductance will cause a different voltage to be at the output of the inverter when the inverters are in current limit mode and exporting a controlled current. If the two inverters have a different output voltage but the same current export, then their power export will be different. Two inverters with a difference in export power will cause their frequency to differ. A difference in frequency will cause the angle between the inverters to change with respect to time.

After the fault has been cleared, the steady-state angle increases as the inductance increases. This is again because the increased inductance in the line causes an increase in voltage angle for the same steady-state current. After the fault has been cleared the inverters are again voltage controlled sources and the difference between the internal angles of the inverters is proportional to the angle difference across the line.

The voltage limit and current limit signals are shown to demonstrate that the inverters correctly reset once the fault has been cleared.

If the protection requires a large delay before the fault is cleared, then the inverters should have a greater inductance to ensure transient stability once the fault has been cleared. However care should be taken to ensure that the 90 degree stability criterion is not reached when the maximum current flows through the inductance.

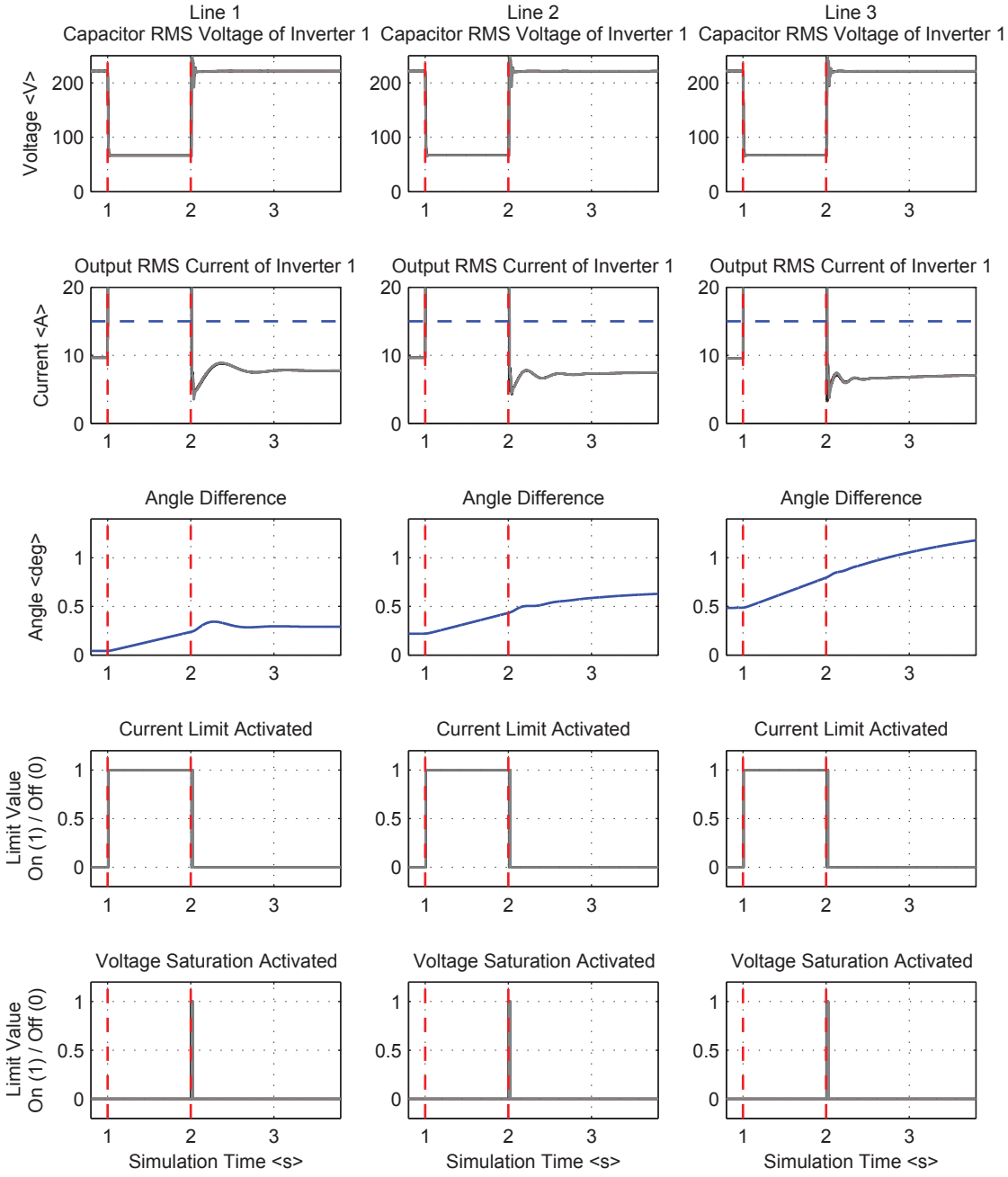

Figure 5.16: Fault for a duration of one second for a three different line parameters

5.10 Conclusion

Large signal stability of a two-droop controlled inverter network with passive loads was investigated. Results determined that the transient stability of the network is related to the change in angle of the inverter when they are operating in current-limit. The greater the change in angle, the greater the peak current of the transient after the current limiters have reset. The peak of the current causes the inverters to limit and this results in the droop controllers failing to converge to a post-fault steady-state which may lead to the controllers entering in to a limit oscillation.

Chapter 6

Conclusions and Future Work

6.1 Conclusions

This thesis has presented a dynamic model of an active load and used that model as part of an overall dynamic model of a 3-node microgrid. The controllers within the droop-controlled inverter were then further developed to be able to current limit in the event of a network fault and successfully reset upon the fault being cleared by network protection. An investigation of the large-signal stability of the microgrid was undertaken to determine the required fault clearance time of the microgrid and the factors affecting that fault clearance time.

6.1.1 Small-signal stability of a microgrid with an active load

The active load was modelled as a non-linear state-space model with the intention of being used for analysis within microgrid or distribution network analysis. The model was linearised about an operating point and participation analysis was used to identify which state variables were associated with which eigenvalues and subsequently revealed information about the high frequency and low frequency modes. The high frequency modes were largely sensitive to the states of the LCL filter and the ac-current controller. The low frequency modes were largely sensitive to the states of the dc voltage capacitor and the dc voltage controller. It was possible to observe both the high and low frequency modes through experimentation. The high frequency

modes could be observed by grid-side perturbations and the low frequency modes could be observed by dc-side perturbations.

When the active load model was joined to a microgrid, further key results were identified. The microgrid used models of droop-controlled inverters and a network, all of which were modelled on a common reference frame. The addition of the active load within the microgrid caused the damping of the microgrid to very slightly decrease. Upon further inspection, the low frequency eigenvalues, that are associated with either the inverter droop controllers or the dc-voltage controller of the active load, had little interaction with each other. In contrast, the medium-frequency eigenvalues of the microgrid, that were initially associated with the AC-voltage controller of the inverters, became much less damped when the gain of the active load dc-voltage controller was increased.

The system model was verified against an experimental system with three 10 kVA inverters, one passive load and one active load. Step changes of load were used to excite low-frequency modes and allow observation of frequency and damping factors for different controller gain conditions. Despite initial concerns that the negative resistance property of active load would destabilise the power-sharing (droop) controllers, no significant reduction of damping of the low frequency modes was observed for a range of active load voltage control parameters. However, the eigenvalue analysis showed that eigenvalues associated with the dc-voltage controller of the active load moved away from the imaginary axis and the eigenvalues associated with the inverter ac-voltage controller moved towards the imaginary axis as the gain of the rectifier dc-voltage controller was varied.

Although some inverter—active–load coupling has been identified, it was not in the low-frequency power sharing eigenvalues as anticipated. In the example experimental system, unstable operation did occur for very large gains in the dc voltage loop but these were beyond the gains needed to achieve good steady-state voltage regulation. Therefore it is possible to design the rectifier controller by using conventional frequency domain analysis and independently of the inverter controllers, provided the design is suitably conservative.

6.1.2 Resetting of inverter limiting

The thesis investigated how current and voltage limiting should be implemented in inverters with cascaded control loops with particular reference to preventing latch-up of the limiters and wind-up of the controllers. A further consideration was the desire to avoid high levels of distortion of current and voltage waveforms during the fault.

The results of this study show that to avoid high levels of distortion of current and voltage waveforms during the fault the current limit (applied to the current reference at the output voltage controller) should be a set and reset function. The set and reset limiting of the current reference preserves sinusoidal current references during the majority of the fault and recovery period and avoids high levels of harmonic distortion.

Providing the current limiter correctly resets after the fault has been cleared, the results show that the best transient stability performance is obtained when the voltage limit (applied to the inverter voltage command at the output of the current controller) is an instantaneous (saturation) function. Although the instantaneous limit is shown to cause high levels of distortion for sinusoidal references when in limit, the instantaneous limiting of the inverter voltage command helped prevent wind-up of the outer controllers once the current limit is reset. In this study the outer controller was a voltage controller and this is the middle controller in the droop controlled inverters. As expected this does cause distorted voltage waveforms to appear for a short period after fault clearance as the voltage controller establishes control of the capacitor voltage. If the current limit (output of the voltage controller) is reset and the voltage limit (output of the current controller) is set, the experimental results presented in this thesis have shown the outer voltage controller to experience wind-up and hence this would not be acceptable in a microgrid application.

For avoiding latch-up of the set and reset current limit, it is important that the reset signal is not derived from the output of the outer controller. The experimental results presented in Chapter 4 have also shown that using a set and reset voltage limiter at the output of the inner controller did not assist in the resetting of the current limiter at the output of the outer controller. The set and reset design which used the current reference (output of the voltage controller) to initiate a set and the measured inverter capacitor voltage to initiate a reset was

the only latched current limiter to reset when used in conjunction with an instantaneous voltage limiter. For this design to function correctly in other networks, the capacitor voltage would only recover (and cause a reset) provided the network impedance seen when the fault clears is sufficiently high. For a microgrid, this will be true if the total post-fault load power demand is within the capacity of the generators remaining on the system.

A further development for the set and reset design was to introduce a second trip such that the inverter could export a particular current for over-loads and export a different current for network faults. The multi-trip design used an impedance method for the detection of over-loads and network faults. Experimental results have shown this method to be successful for detecting over-loads and faults for a microgrid application and also successfully resetting once the over-load or fault had been removed.

6.1.3 Large-signal stability of the microgrid network

The large-signal stability of a two-inverter microgrid with each inverter using droop-control was analytically investigated. The chapter started by investigating a single droop-controlled inverter connected to a single load where a fault was applied. A discussion was made about the real power, reactive power and frequency output of the inverter. A limiting strategy was used that would not wind-up the controllers or latch-up once the fault had been disconnected. The inverter would current limit as expected and the voltage at the output would collapse, again as expected. However, the droop controller would continue to control the frequency of the inverter. The frequency transient would be first-order decay function which is because the calculated power is filtered before being applied to the droop function.

A microgrid was formed of two droop-controlled inverters, a single line and two loads. This simplistic model was chosen to understand the interactions between the controllers during a fault. It was discovered that the steady-state output frequency of the inverter during the fault was dependent on the real power export of the inverter and that the rate of change of frequency from the previous steady-state to the steady-state during the fault was dependent on the filter used to calculate the power reference for the droop functions. During the transient period from the fault being cleared to the post-fault steady-state operating point, the magnitude of the

current exported from the inverter was dependent on the duration of the fault, the impedance of the line that was used to connect the two inverters and the impedance of the coupling inductance of the inverter.

The magnitude of the current when the two droop-controlled inverters were transitioning from fault to normal operation was critical to the recovery of the inverters. If the magnitude of the current activated a current limit of one of the two inverters, then the two droop-inverters would not return to a steady-state operating mode and the two inverters would enter a limit oscillation. The large-signal transient stability of the droop controlled microgrid is dependent on the limiting approached used in the inverters. The droop-controlled microgrid will return to a steady-state after a fault event if the peak of the current during the transient period does not trigger a limit event in the controllers of the inverters.

6.2 Authors Contribution

The end of the introduction in Chapter 1 set out three questions of research that are not covered in the literature and are documented in Chapters 3 – 5. Chapter 3 answered how an active load interacted within a microgrid. Chapter 4 answered how inverters should reset their limiters after a network fault or disturbance. Chapter 5 answered if a microgrid would settle to a new steady-state or loose stability after a network disturbance.

It was identified in Chapter 1 that existing work in the small-signal stability of microgrids models the loads as a passive impedance. However this is not true for all loads and many active loads exhibit constant power characteristics. This thesis contributed to the literature by identifying that the low frequency dynamics of the active loads do not cause the droop controllers of the microgrid to exhibit instabilities. However, it was identified that the active load did interact with the voltage controllers of the inverters and instabilities were observed in the inverter voltage controllers when the gain of the dc-voltage controller of the active load was increased.

There is much litreature on characterising the fault impedance of an inverter and designing limiting circuits for inverters. However, this work has not considered how the inverters should

reset from the limit state and return to normal operation after the fault has cleared. This thesis has contributed an understanding of the factors that may cause an inverter to fail to correctly reset from a limit state and has recommended a design to ensure an inverter in a microgrid always resets.

There has been a lot of work in understanding the small-signal stability of microgrids, however the large-signal stability is also important and must be considered. There has been a little research in this area and the existing literature has not considered the factors that cause large-signal instabilities. This thesis has sought to understand this, investigated the droop-controlled inverter and concluded that the microgrid will become unstable if the limiters are enter limit while the droop controllers are transiting from the steady-state during the fault to the steady-state after the fault.

6.3 Future Work

For every inverter that was presented in this thesis, it was assumed that there is a constant dc-bus voltage. Whilst this is a reasonable assumption if there were a constant energy source, for example sufficient battery storage or if there were advanced power electronics controlling and regulating the dc-bus voltage. However, the dc-bus voltage may not be constant and may not have a negligible supply impedance. In a practical microgrid there may be many different types of energy sources, each with a different supply characteristic and some of which may not be able to supply a constant dc voltage. Therefore, in these microgrids it would be essential to model the energy source and any power electronics that is used to regulate or filter the dc voltage source. This thesis could be extended by modelling the prime-mover and seeing the effect that the "prime-mover" has on the results that are presented.

The load model used in the small-signal work presented in Chapter 3 was an active load with a constant power characteristic and previous work had investigated constant impedance load. However in many microgrids, there may be a proportion of induction motor loads that are connected without any motor-drive or soft-start power electronics. When these types of loads start they have a large in-rush current and may cause the inverter to current limit. If the inverter were to current limit, then the voltage at the motor may be depressed. A reduction in

voltage could cause the motor to stall and this may cause a voltage collapse at the node. Also, if the motor were to start and the in-rush current reduced to the operating current, then the resetting of the inverter limiter could cause the microgrid to become unstable. Therefore, for a comprehensive microgrid small-signal and large-signal model, it may be necessary to model induction motor loads.

For the analysis undertaken in Chapter 3, the equilibrium point which the linear model was linearised around, was found by using a time-domain simulation. It would also be possible to obtain these steady-state operating values by the use of a load-flow algorithm. However, a conventional load-flow does not allow for the droop algorithm and assumes that the network has a fixed frequency. Therefore, for the steady-state parameters to be calculated by a load-flow algorithm, a load-flow algorithm that considers a changing frequency and the droop algorithm would need to be developed.

Author's Publications

6.4 Papers published from the work in Chapter 3

- N. Bottrell, M. Prodanovic, and T. Green, "*Dynamic stability of a microgrid with an active load,*" Power Electronics, IEEE Transactions on, vol. 28, no. 11, pp. 5107–5119, 2013.
- N. Bottrell and T. Green, "*Modeling microgrids with active loads,*" in Control and Modeling for Power Electronics (COMPEL), 2012 IEEE 13th Workshop on, pp. 1–8, 2012.
- N. Bottrell, M. Prodanovic, and T. Green, "*Analysed small signal state-space model of an active rectifier,*" in Universities Power Engineering Conference (UPEC), 2010 45th International, pp. 1–6, 2010.

6.5 Papers published from the work in Chapter 4

- N. Bottrell and T. Green, "*An impedance-based method for the detection of over-load and network faults in inverter interfaced distributed generation,*" in Power Electronics and Applications, 2012 European Conference on, pp. 1–1, 2013.
- N. Bottrell and T. Green, "*Comparison of current limiting strategies during fault ride-through of inverters to prevent latch-up and wind-up,*" Power Electronics, IEEE Transactions on, vol. PP, no. 99, pp. 1–1, 2013.

Appendix A

Matlab Script Used for the Active Load

This appendix provides the Matlab scrips used to generate the eigenvalue plot in Figure 3.4 and the participation graphs in Figure 3.5.

A.1 Active Load Model

```
%startMicrogrid

%Select data file with parameters and initial values
load('RectifierSteadyState1');

%Build state space model
[Rectifier] = modelRectifier(RecData);
```

```
function [Rectifier] = modelRectifier(RecData)
%modelRectifier The state-space equations for the rectifier
%model used with the microgrid work.
%   This script creates rectifier model
%   By Nathaniel Bottrell
```

```
6
% Declare a structure to save the Rectifier model
8 Rectifier = struct(...
    'A', [], ...
10  'B', [], ...
    'C', [], ...
12  'D', [], ...
    'SystemName', {'Rectifier'},...
14  'StateNames', {{'CtrlVdc'; 'CtrlId'; 'CtrlIq'; 'ild'; 'ilq'; 'vcd'; 'vcq'; '
    igd'; 'igq'; 'vdc'}},...
    'InputNames', {{'Vdcref'; 'Ildref'; 'vgD'; 'vgQ'; 'wcom'; 'idc'}},...
16  'OutputNames', {{'igD'; 'igQ'; 'vdc'}},...
    'OutputSteadyState', [RecData.IgD; RecData.IgQ; RecData.Vdc]);
18
%% Rectifier Matrices
20
% Define DC voltage controller
22
Rectifier.DCVoltageController = struct(...
24  'A', 0,...
    'B1', [1,0],...
26  'B2', -1,...
    'C', [RecData.Kiv;0],...
28  'D1', [RecData.Kpv, 0;...
           0, 1],...
30  'D2', [-RecData.Kpv;...
           0]);
32
% Define AC current controller
34
Rectifier.ACCurrentController = struct(...
36  'A', [0;0],...
    'B1', [1,0;...
38         0,1],...
    'B2', [-1,0,0,0,0,0;...
40         0,-1,0,0,0,0],...
    'C', [-RecData.Kic,0;...
```

```
42              0,-RecData.Kic],...
    'D1', [-RecData.Kpc,0;...
44              0,-RecData.Kpc],...
    'D2', [RecData.Kpc,RecData.wn*RecData.Lf,0,0,0,0;...
46              -RecData.wn*RecData.Lf,RecData.Kpc,0,0,0,0]);

48 % Define switching block

50 Rectifier.SwitchingBlock = struct(...
    'A', -(RecData.Vid*RecData.Ild+RecData.Viq*RecData.Ilq)/(RecData.Cdc*RecData.
    Vdc^2),...
52  'B', [RecData.Vid/(RecData.Cdc*RecData.Vdc), RecData.Viq/(RecData.Cdc*RecData.
    Vdc), 0, 0, 0, 0],...
    'Bu', [RecData.Ild/(RecData.Cdc*RecData.Vdc), RecData.Ilq/(RecData.Cdc*RecData
    .Vdc)],...
54  'Bdc', -1/RecData.Cdc,...
    'C', 1);
56

% Define DC load
58

Rectifier.DCLoad = struct(...
60  'A', 0,...
    'Bu', 0,...
62  'Bdist', 0,...
    'C', 0,...
64  'Du', 1/RecData.Rload,...
    'Ddist', 1);
66

% Define LCL filter
68

Rectifier.LCLFilter = struct(...
70  'A', [-RecData.rf/RecData.Lf, RecData.w0, 1/RecData.Lf, 0, 0, 0;...
        -RecData.w0, -RecData.rf/RecData.Lf, 0, 1/RecData.Lf, 0, 0;...
72      -1/RecData.Cf, 0, 0, RecData.w0, 1/RecData.Cf, 0;...
        0, -1/RecData.Cf, -RecData.w0, 0, 0, 1/RecData.Cf;...
74      0, 0, -1/RecData.Lc, 0, -RecData.rc/RecData.Lc, RecData.w0;...
        0, 0, 0, -1/RecData.Lc, -RecData.w0, -RecData.rc/RecData.Lc],...
```

```
76      'Bu', [-1/RecData.Lf, 0;...
            0, -1/RecData.Lf;...
78          zeros(4,2)],...
        'Bv', [zeros(4,2);...
80          1/RecData.Lc, 0;...
            0, 1/RecData.Lc],...
82      'Bw', [RecData.Ilq;...
            -RecData.Ild;...
84          RecData.Vcq;...
            -RecData.Vcd;...
86          RecData.Igq;...
            -RecData.Igd],...
88      'C', 0,...
        'D', 0);
90
% Define reference frame
92
Rectifier.ReferenceFrame = struct(...
94      'Tr', [cos(RecData.delta0), -sin(RecData.delta0);...
            sin(RecData.delta0), cos(RecData.delta0)]);
96
% Build rectifier model
98
Rectifier.A = [0, zeros(1,2), zeros(1,6), Rectifier.DCVoltageController.B2;
100     Rectifier.ACCurrentController.B1*Rectifier.DCVoltageController.C, zeros(2,2),
        Rectifier.ACCurrentController.B2, Rectifier.ACCurrentController.B1*Rectifier.
        DCVoltageController.D2;
        Rectifier.LCLFilter.Bu*Rectifier.ACCurrentController.D1*Rectifier.
        DCVoltageController.C, Rectifier.LCLFilter.Bu*Rectifier.ACCurrentController.C,
         Rectifier.LCLFilter.A+Rectifier.LCLFilter.Bu*Rectifier.ACCurrentController.D2
        , Rectifier.LCLFilter.Bu*Rectifier.ACCurrentController.D1*Rectifier.
        DCVoltageController.D2;
102     Rectifier.SwitchingBlock.Bu*Rectifier.ACCurrentController.D1*Rectifier.
        DCVoltageController.C, Rectifier.SwitchingBlock.Bu*Rectifier.
        ACCurrentController.C, Rectifier.SwitchingBlock.B+Rectifier.SwitchingBlock.Bu*
        Rectifier.ACCurrentController.D2, Rectifier.SwitchingBlock.A+Rectifier.
        SwitchingBlock.Bu*Rectifier.ACCurrentController.D1*Rectifier.
```

```
    DCVoltageController.D2+Rectifier.SwitchingBlock.Bdc*Rectifier.DCLoad.Du];

Rectifier.Bu = [Rectifier.DCVoltageController.B1;
    Rectifier.ACCurrentController.B1*Rectifier.DCVoltageController.D1;
    Rectifier.LCLFilter.Bu*Rectifier.ACCurrentController.D1*Rectifier.
    DCVoltageController.D1;
    Rectifier.SwitchingBlock.Bu*Rectifier.ACCurrentController.D1*Rectifier.
    DCVoltageController.D1];

Rectifier.Bv = [zeros(1,2);
    zeros(2,2);
    Rectifier.LCLFilter.Bv*(Rectifier.ReferenceFrame.Tr^-1);
    zeros(1,2)];

Rectifier.Bw = [0;
    zeros(2,1);
    Rectifier.LCLFilter.Bw;
    0];

Rectifier.Bdc = [0;
    zeros(2,1);
    zeros(6,1);
    Rectifier.SwitchingBlock.Bdc*Rectifier.DCLoad.Ddist];

Rectifier.B = [Rectifier.Bu, Rectifier.Bv, Rectifier.Bw, Rectifier.Bdc];

Rectifier.Cc = [zeros(2,1), zeros(2,2), [zeros(2,2), zeros(2,2), Rectifier.
    ReferenceFrame.Tr], zeros(2,1)];

Rectifier.Cdc = [0, zeros(1,2), zeros(1,6), Rectifier.SwitchingBlock.C];

Rectifier.C = [Rectifier.Cc; Rectifier.Cdc];

sizeB = size(Rectifier.B);
sizeC = size(Rectifier.C);
Rectifier.D = zeros(sizeC(1), sizeB(2));
```

```
Rectifier.M = RecData.rn*eye(2);


%%
disp('Finished')
```

A.2 Eigenvalue Plot

```
Eigenvalues = struct(...
    'SystemName', 'Rectifier',...
    'SystemAmatrix', Rectifier.A,...
    'FigureNumber', 1,...
    'xAxisLimits', [-4000, 0],...
    'yAxisLimits', [-15000, 15000],...
    'Grid', {'on'},...
    'DataPointType', {'kx'},...
    'PlotFigure', true,...
    'SaveFigure', true,...
    'PrintFigureName', {'Fig'});

Eigenvalues = plotEigenvalues(Eigenvalues);
```

```
function [Eigenvalues] = plotEigenvalues(eigenvalueParameters)
%PLOTEIGENVALUES Plots the eigenvalues of an A Matrix
%   Results from the scrip are used within the thesis
%   By Nathaniel Bottrell

% Declare a structure to save the eigenvalues
Eigenvalues = struct(...
    'SystemName', eigenvalueParameters.SystemName,...
    'SystemAmatrix', eigenvalueParameters.SystemAmatrix,...
    'SystemEigenvalues', {''},...
    'FigureNumber', eigenvalueParameters.FigureNumber,...
    'EigenValues', {''},...
```

```
    'xAxisLimits', eigenvalueParameters.xAxisLimits,...
    'yAxisLimits', eigenvalueParameters.yAxisLimits,...
    'Grid', eigenvalueParameters.Grid,...
    'DataPointType', eigenvalueParameters.DataPointType,...
    'PlotFigure', eigenvalueParameters.PlotFigure,...
    'SaveFigure', eigenvalueParameters.SaveFigure,...
    'PrintFigureName', eigenvalueParameters.PrintFigureName);


% Calculate eigenvalues
Eigenvalues.SystemEigenvalues = eig(Eigenvalues.SystemAmatrix);

% Plot eigenvalues
if Eigenvalues.PlotFigure
    figure(Eigenvalues.FigureNumber)
    plot(Eigenvalues.SystemEigenvalues, Eigenvalues.DataPointType);
    title(sprintf('Eigenvalues of %s', Eigenvalues.SystemName));
    xlim(Eigenvalues.xAxisLimits);
    ylim(Eigenvalues.yAxisLimits);
    xlabel('Real Axis');
    ylabel('Imaginary Axis');
    grid(Eigenvalues.Grid);
    disp('Eigenvalues Plotted');
end

% Print eigenvalues plot
if Eigenvalues.SaveFigure
    papersize = [5,4];
    border = 0;
    set(gcf,'PaperUnits','inches','PaperPositionMode','Manual','PaperSize',
    papersize,'PaperPosition',[border,border,papersize(1)-border,papersize(2)-
    border])
    print(gcf,'-deps2',sprintf('%s_%sEigenvalues', Eigenvalues.PrintFigureName,
    Eigenvalues.SystemName))
    disp('Eigenvalues Saved to File');
end
```

A.3 Participation Graphs

```
EigenParticipation = struct(...
    'SystemName', Rectifier.SystemName,...
    'SystemAmatrix', Rectifier.A,...
    'ParticipationFactor', 0,...
    'FigureNumber', 3,...
    'OnlyEigenvalueFigure', true,...
    'xAxisLimits', [-4000, 0],...
    'yAxisLimits', [-15000, 15000],...
    'Grid', {'on'},...
    'DataPointType', {'k.'},...
    'PlotFigure', true,...
    'PrintFigure', false,...
    'PrintType', {'-dpdf'},...
    'PrintFigureName', 'Fig');

EigenParticipation = calcEigenvalueParticipation_v2(EigenParticipation);

EigenParticipation.StateNames = Rectifier.StateNames;

EigenParticipation.Eigen = {5:1:6, 1:1:4, 7:1:10};

ParticipationState = plotStateParticipation_v3(EigenParticipation);
```

```
function [EigenParticipation] = calcEigenvalueParticipation_v2(
    eigenvalueParameters)
%CALCEIGENVALUES Calculates eigen values and state participation values
%   By Nathaniel Bottrell

% Declare a structure to save the eigenvalues
EigenParticipation = struct(...
    'SystemName', eigenvalueParameters.SystemName,...
    'SystemAmatrix', eigenvalueParameters.SystemAmatrix,...
    'ParticipationFactor',{eigenvalueParameters.ParticipationFactor},...
    'FigureNumber', eigenvalueParameters.FigureNumber,...
    'OnlyEigenvalueFigure', eigenvalueParameters.OnlyEigenvalueFigure,...
```

```
    'RightEigenvalues', {''},...
    'RightEigenvectors', {''},...
    'LeftEigenvalues', {''},...
    'LeftEigenvectors', {''},...
    'Eigenvalues', {''},...
    'ParticipationMatrix', {''},...
    'ParticipationMatrixMag', {''},...
    'xAxisLimits', eigenvalueParameters.xAxisLimits,...
    'yAxisLimits', eigenvalueParameters.yAxisLimits,...
    'Grid', eigenvalueParameters.Grid,...
    'DataPointType', eigenvalueParameters.DataPointType,...
    'PlotFigure', eigenvalueParameters.PlotFigure,...
    'PrintFigure', eigenvalueParameters.PrintFigure,...
    'PrintType', eigenvalueParameters.PrintType,...
    'PrintFigureName', eigenvalueParameters.PrintFigureName);

% Calculate the left and right eigenvalues
% and eigenvectors from the A matrix.

[EigenParticipation.RightEigenvectors, EigenParticipation.RightEigenvalues] = eig(
    EigenParticipation.SystemAmatrix);

EigenParticipation.LeftEigenvectors = inv(EigenParticipation.RightEigenvectors);

% Calculate eigenvalues from diagional matrix
EigenParticipation.Eigenvalues = diag(EigenParticipation.RightEigenvalues);

% Calculate the Participation Matrix

% Uses formular pij = (|vij|*|wji|)/sum[k=1 to n](|vik|*|wki|)
% where:
% i = state variable
% j = eigenvalue
% p = participation value
% w = left eigenvectors
% v = right eigenvectors

```

```
% calculate size of Eigenvector matrix
[il jl] = size(EigenParticipation.LeftEigenvectors);

% initilise p
EigenParticipation.ParticipationMatrix = zeros(il,jl);

% calculate participation matrix
for i = 1:il
    wv = abs(EigenParticipation.RightEigenvectors(i,:))*abs(EigenParticipation.
    LeftEigenvectors(:,i));
    for j = 1:jl
        EigenParticipation.ParticipationMatrix(i,j) = abs(EigenParticipation.
    RightEigenvectors(i,j)) * abs(EigenParticipation.LeftEigenvectors(j,i))/wv;
    end
end

% calculate the magnitude of the participation matrix
EigenParticipation.ParticipationMatrixMag = round(100*abs(EigenParticipation.
    ParticipationMatrix))/100;


disp('Eigenvalue Participtation Calculation Done')

end
```

```
function [Participation] = plotStateParticipation_v3(EigenvalueData)
%plotStateParticipation_v2 plots the states and highlights the
%state participation of the eigenvalues
%   By Nathaniel Bottrell

%The code assumes the participation matrix supplied is in the form of:
%pij
% where:
% i = state variable
% j = eigenvalue
% p = participation value
```

```
13 EigenvaluePlotSequence = {'b*', 'g*', 'r*'};
   EigenvalueStemSequence = {'b', 'g', 'r'};
15
   % Set up the date struct to save the participation values for each eigenvalue.
17 %find the number of itterations the user has requested for investigation
   noItterations = max(size(EigenvalueData.Eigen));
19
   %calculate the number of states
21 noStates = max(size(EigenvalueData.Eigenvalues));

23 ParticipationStemPlot = zeros(noStates,noItterations);

25 for itteration = 1:noItterations


27
    %find the number of eigenvalues the user has requested for investigation
29  noEigenvalues = max(size(EigenvalueData.Eigen{itteration}));
    %for each eigenvalue create a blank data structure
31  Participation = cell(noEigenvalues,1);

33  %put data into the structure - we're now ready to start the analysis
    for k = 1:noEigenvalues
35      Participation{k} = struct(...
            'Eigenvalue', EigenvalueData.Eigenvalues(EigenvalueData.Eigen{
    itteration}(k)),...
37          'StatesAssociated', {''},...
            'ParticipationValues', []);
39  end

41  % Participation Analysis
    %go through all states in an eigenvalues and save them if they have a
43  %participation value higher than 0.
    %to set the loop, the script needs to know how many states there are
45  %the script already knows how many eigenvalues that need looking at.

47  for jl = 1:noEigenvalues
```

```
49        for il = 1:noStates
              %go through each states in the eigenvalue and check to see if the
51            %states participates in the eigenvalue.
              if EigenvalueData.ParticipationMatrixMag(il, EigenvalueData.Eigen{
    itteration}(jl)) ~= 0;
53                %if the participation of the state for the eigenvalue does not
                  %equal zero, it is important and needs to be saved.
55                %the data needs to be saved in order, the next section of code
                  %sorts the data by the participation value
57
                  %first a check need to be made to see if there is any data, if
59                %there is no data there is nothing to sort.

61                %first the code needs to calculate the size of the data
                  %structure
63                sizeSavedData = max(size(Participation{jl}.ParticipationValues));

65                if sizeSavedData == 0
                      %this section is run if there is NO data in the
67                    %Participation structure
                      Participation{jl}.StatesAssociated = EigenvalueData.StateNames
    (il);
69                    Participation{jl}.ParticipationValues = EigenvalueData.
    ParticipationMatrixMag(il, EigenvalueData.Eigen{itteration}(jl));
                  else
71                    %this section is run if there is data in the Participation
                      %structure
73
                      %to sort the data the algorithm is going to go through
75                    %every entry until the entry is placed. This isn't the most
                      %efficient way, but it will still work. The sorting will go
77                    %from the heighest to the lowest

79                    %before the loop begins a flag varible needs to be set to
                      %indicate that the values has not been placed in the
81                    %structure. Another variable needs to be set that keeps
```

```
                    %count of the loops and knows which saved data the loop is
                    %pointing to.

                    dataSorted = false;
                    dataPointer = 1;

                    %if the last data sample is greater to or equal to the data
                    %sample wanting to be saved, the data wanting to be saved
                    %needs to be placed at the begining of the sequence and
                    %the flag set so that the loop doesn't start.
                    if Participation{jl}.ParticipationValues(sizeSavedData) >=
EigenvalueData.ParticipationMatrixMag(il, EigenvalueData.Eigen{itteration}(jl)
)
                        %Participation{jl}.ParticipationValues(sizeSavedData)
                        %EigenvalueData.ParticipationMatrixMag(il, EigenvalueData.
Eigen{itteration}(jl))
                        Participation{jl}.StatesAssociated = [Participation{jl}.
StatesAssociated, EigenvalueData.StateNames(il)];
                        Participation{jl}.ParticipationValues = [Participation{jl
}.ParticipationValues, EigenvalueData.ParticipationMatrixMag(il,
EigenvalueData.Eigen{itteration}(jl))];
                        dataSorted = true;
                    end

                    %if the first data sample is less than the data
                    %sample wanting to be saved, the data wanting to be saved
                    %needs to be placed at the begining of the sequence and
                    %the flag set so that the loop doesn't start.
                    if Participation{jl}.ParticipationValues(1) < EigenvalueData.
ParticipationMatrixMag(il, EigenvalueData.Eigen{itteration}(jl))
                        Participation{jl}.StatesAssociated = [EigenvalueData.
StateNames(il), Participation{jl}.StatesAssociated];
                        Participation{jl}.ParticipationValues = [EigenvalueData.
ParticipationMatrixMag(il, EigenvalueData.Eigen{itteration}(jl)),
Participation{jl}.ParticipationValues];
                        dataSorted = true;
                    end
```

```
109
                while and(not(dataSorted), not(dataPointer == sizeSavedData))
111                 %this loop will run if the data has not been placed at
                    %the beginning of the sequence. On each itteration the
113                 %loop will check to see if the data wanting to be saved
                    %is less than the data being pointed at by the loop.
115
                    %the data pointer needs to be incremented so that it
117                 %points to the correct data
                    dataPointer = dataPointer + 1;
119
                    if Participation{jl}.ParticipationValues(dataPointer) <
EigenvalueData.ParticipationMatrixMag(il, EigenvalueData.Eigen{itteration}(jl)
)
121                     Participation{jl}.StatesAssociated = [Participation{jl
}.StatesAssociated(1:dataPointer-1), EigenvalueData.StateNames(il),
Participation{jl}.StatesAssociated(dataPointer:sizeSavedData)];
                        Participation{jl}.ParticipationValues = [Participation
{jl}.ParticipationValues(1:dataPointer-1), EigenvalueData.
ParticipationMatrixMag(il, EigenvalueData.Eigen{itteration}(jl)),
Participation{jl}.ParticipationValues(dataPointer:sizeSavedData)];
123                     dataSorted = true;
                    end
125
                end
127
            end
129
        end
131
    end
133
end
135
%Display the Participation Analysis
137 %go through the saved data and display it on the screen.
```

```
139     %print the header on the screen
        fprintf('\n*********************************************\n');
141     fprintf('*          State Participation Analysis        *\n');
        fprintf('*          Itteration %i of %i                   *\n',itteration,
    noItterations);
143     fprintf('*********************************************\n\n');

145     %loop through the saved data to display it on the screen
        for jl = 1:noEigenvalues
147         %display header for the eigenvalue being displayed
            fprintf('Analysis for eigenvalue: %8.1f%+8.1fj\n', real(Participation{jl}.
    Eigenvalue), imag(Participation{jl}.Eigenvalue));
149         fprintf('*********************************************\n');
            fprintf('                State -|- Participation\n');
151         fprintf('═══════════════════════╪═══════════════════════\n');

153         %compute the amount of saved data for each state in the analysis
            sizeSavedData = max(size(Participation{jl}.ParticipationValues));
155
            %if there is no saved date, there must be no eigenvalues associated
157         %with the state. Unlikly case but probably good to tell the user.
            if sizeSavedData == 0
159             disp('----------NO EIGENVALUES ASSOCIATED----------');
            else
161             %loop through all the saved data and display it
                for ip = 1:sizeSavedData
163                 fprintf('%20s  | %5.2f\n', Participation{jl}.StatesAssociated{ip},
     Participation{jl}.ParticipationValues(ip));
                end
165         end

167         %display footer
            fprintf('═══════════════════════════════════════════════\n');
169
            %now sum up the participation values to check they add to 1.
171         fprintf('Sum of participation values: %2.2f\n\n', sum(Participation{jl}.
    ParticipationValues));
```

```
173     end

175     %if requested by the initial options, plot the eigenvales that's bring
        %investigated
177     if EigenvalueData.PlotFigure
            %setup a figure with the figure number requested
179         figure(EigenvalueData.FigureNumber);
            %plot all the eigenvalues of the system
181         if itteration == 1
                hold off
183             plot(EigenvalueData.Eigenvalues, 'blackx');
                hold all
185             LegendText = {'Eigenvalue', 'Itteration 1'};
            else
187             LegendText = {LegendText{:,:}, sprintf('Itteration %i',itteration)};
            end
189         %plot all the eigenvalues that have been investigated.

191         %Look through all the saved data to extract the eigenvalues that have
            %been used in the analysis. The code will look from the top to the
193         %bottom of the saved data and store it in a new variable. This new
            %variable will be used to plot the data.
195
            %create the variables for the plot data
197         ParticipationPlotData = zeros(noEigenvalues, 1);

199         for jl = 1:noEigenvalues
                %read every entry in the saved data and extrat the eigenvalues
201             %investigated
                ParticipationPlotData(jl) = Participation{jl}.Eigenvalue;
203         end

205         %plot the saved date the the high participation
            if mod(itteration,max(size(EigenvaluePlotSequence))) == 0
207             EigenvaluePlotNumber = max(size(EigenvaluePlotSequence));
            else
```

```
209             EigenvaluePlotNumber = mod(itteration,max(size(EigenvaluePlotSequence)
    ));
        end
211
        plot(real(ParticipationPlotData), imag(ParticipationPlotData),
    EigenvaluePlotSequence{EigenvaluePlotNumber});
213
        %sort out all the plot processing stuff that is an option
215     %title(sprintf('Eigenvalues Investigated in Analysis of %s',EigenvalueData
    .SystemName));
        xlim(EigenvalueData.xAxisLimits);
217     ylim(EigenvalueData.yAxisLimits);
        xlabel('Real Axis');
219     ylabel('Imaginary Axis');
        legend(LegendText);
221     %legend('Eigenvalue', 'Eigenvalues Investigated');
        legend('Location','NorthWest')
223     grid(EigenvalueData.Grid);
        disp('Poles and Zeros Plotted');
225
    end
227
229
    for jl = 1:noEigenvalues
231     ParticipationStemPlot(:,itteration) = ParticipationStemPlot(:,itteration)+
    EigenvalueData.ParticipationMatrixMag(:, EigenvalueData.Eigen{itteration}(jl))
    ;
    end
233
    if EigenvalueData.OnlyEigenvalueFigure
235     %define initial variable
        %ParticipationStemPlot = zeros(noStates,1);
237     %add all the participations values of the eigenvalues that are being
        %analysied into a new variable
239     %for jl = 1:noEigenvalues
```

```
        %   ParticipationStemPlot = ParticipationStemPlot+EigenvalueData.
    ParticipationMatrixMag(:, EigenvalueData.Eigen{itteration}(jl));
241         %end
                %setup a figure with the figure number requested
243         figure(EigenvalueData.FigureNumber+1)
            %plot all the eigenvalues of the system
245
            subplot(noItterations,1,itteration)
247         bar(ParticipationStemPlot(:,itteration))
            xlabel('State');
249         ylabel('Participation');
            title(sprintf('Sum of participation values for group A%i',itteration))
251         grid('on')
            xlim([0.6 noStates+0.6]);
253         ylim([0, 1]);

255     end

257 end

259     if EigenvalueData.PrintFigure
            papersize = [5,4];
261         border = 0;
            set(gcf,'PaperUnits','inches','PaperPositionMode','Manual','PaperSize',
    papersize,'PaperPosition',[border,border,papersize(1)-border,papersize(2)-
    border])
263         print(gcf,EigenvalueData.PrintType,sprintf('%s_%sStateParticipation',
    EigenvalueData.PrintFigureName, EigenvalueData.SystemName))
            disp('Eigenvalues Saved to File');
265     end

267 end
```

Appendix B

TriPhase Inverter System

All the experimental tests in this thesis are undertaken using rapid prototyping inverter manufactured from a company called TriPhase. Each power converter station is controlled in real time by a host computer which executes the control algorithms. The PWM and gate driver circuits of the inverter bridge are controlled from an FPGA which receives the modulation reference set-point from the host computer.

The control algorithms are programmed in SIMULINK and then complied to the host computer via a C complier in Matlab from any workstation computer. When the inverter is being operated, the real time data from the sensors in the inverter are sent from the host computer to the workstation computer using the laboratory local area network. Figure B.1 diagrammatically shows this representation.

Two types of power converter station are available. One power converter station consists of three four-leg 10 kVA inverters, where each dc link is independently supplied from separate passive rectifiers. These passive rectifiers are fed from the public supply network via an isolation transformer. The other type of power converter station is composed of a three-leg 10 kVA inverter, and a four-leg 10 kVA inverter. These two inverters have an option of connecting the dc buses back-to-back. In this configuration one converter maybe used to control the dc bus voltage, and the other converter used to export or import power on the AC-side. Either side of this back-to-back pair can be connected to the lab private network or public supply

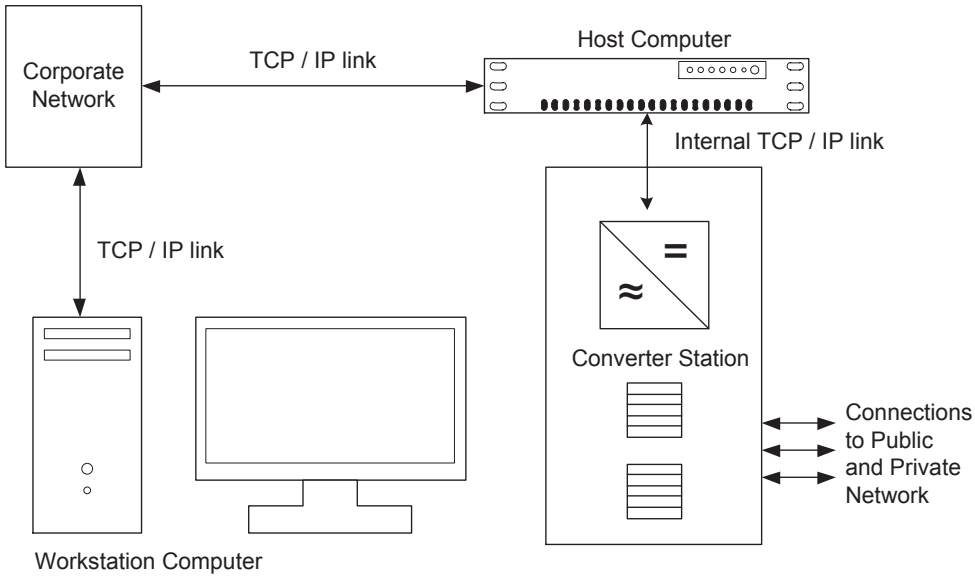

Figure B.1: Laboratory hardware

network. This enables the power converter station to be used as a power sink or source and have bi-directional power flows.

An image of the TriPhase inverter used for the experimental active load in chapter 3 is shown in Figure B.2.

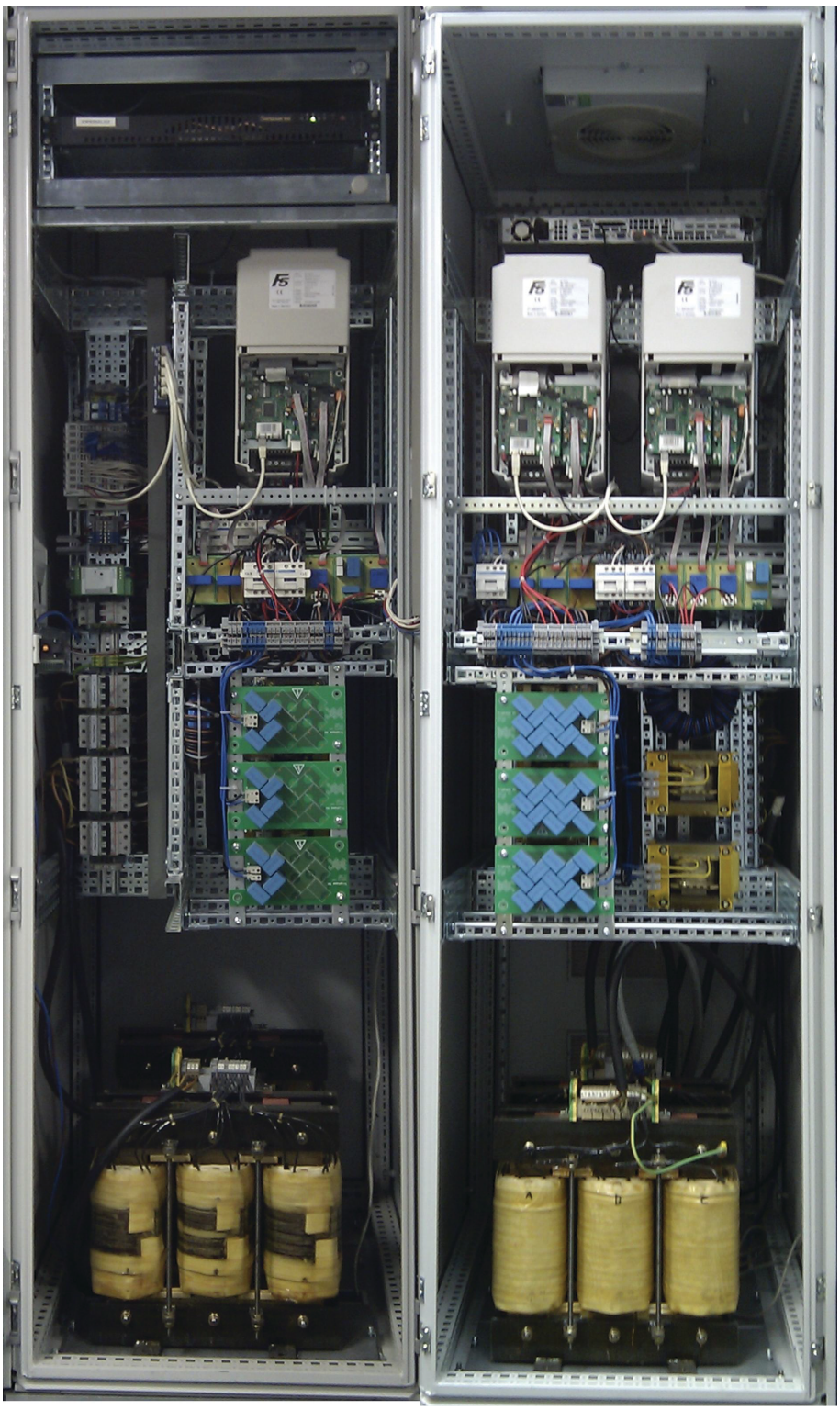

Figure B.2: Laboratory hardware

Bibliography

[1] Legislation, "Climate Change Act." UK Government, 2008.

[2] Policy, "The Carbon Plan: Delivering our Low Carbon Future." Department of Energy and Climate Change, 2011.

[3] Policy, "Reducing demand for energy from industry, businesses and the public sector." Department of Energy and Climate Change, 2012.

[4] Website, "Getting started with renewables." Energy Saving Trust, 2013.

[5] O. Anaya-Lara, N. Jenkins, J. Ekanayake, P. Cartwright, and M. Hughes, *Wind Energy Generation: Modelling and Control*. Wiley, 2011.

[6] T. Ackermann, *Wind Power in Power Systems*. Wiley, 2005.

[7] C. Solanki, *Solar Photovoltaics : Fundamentals, Technologies and Applications*. PHI Learning, 2011.

[8] N. Mohan, T. Undeland, and W. Robbins, *Power Electronics: Converters, Applications and Design, Media Enhanced*. John Wiley & Sons Australia, Limited, 2003.

[9] T. Ackermann, *Wind Power in Power Systems*. Wiley, 2012.

[10] T. Ackermann, "Distributed generation: a definition," *Electric Power Systems Research*, vol. 57, pp. 195–204, Apr. 2001.

[11] F. Iov and F. Blaabjerg, *Power electronics for renewable energy systems*. IEEE, Mar. 2009.

[12] L. L. Freris and D. Infield, *Renewable energy in power systems.* Wiley-Blackwell Press, 2008.

[13] N. Nimpitiwan, G. T. Heydt, R. Ayyanar, and S. Suryanarayanan, "Fault Current Contribution From Synchronous Machine and Inverter Based Distributed Generators," *IEEE Transactions on Power Delivery*, vol. 22, pp. 634–641, Jan. 2007.

[14] M. Prodanovic and T. Green, "Control of inverter-based micro-grids," *Electric Power Systems Research*, vol. 77, no. 9, pp. 1204 – 1213, 2007.

[15] M. Prodanovic and T. Green, "High-quality power generation through distributed control of a power park microgrid," *Industrial Electronics, IEEE Transactions on*, vol. 53, no. 5, pp. 1471–1482, 2006.

[16] M. Prodanovic and T. Green, *Control of power quality in inverter-based distributed generation.* IEEE, 2002.

[17] Z. Jiang and X. Yu, *Active power: Voltage control scheme for islanding operation of inverter-interfaced microgrids.* IEEE, July 2009.

[18] L. Amuda, B. Cardoso Filho, S. Silva, S. Silva, and A. Diniz, *Wide bandwidth single and three-phase PLL structures for grid-tied PV systems.* IEEE, 2000.

[19] P. Piagi and R. Lasseter, *Autonomous control of microgrids.* IEEE, 2006.

[20] N. Pogaku, M. Prodanovic, and T. Green, "Modeling, analysis and testing of autonomous operation of an inverter-based microgrid," *Power Electronics, IEEE Transactions on*, vol. 22, no. 2, pp. 613–625, 2007.

[21] G. M. Shafiullah, A. Oo, D. Jarvis, A. Ali, and P. Wolfs, "Potential challenges: Integrating renewable energy with the smart grid," in *Universities Power Engineering Conference (AUPEC), 2010 20th Australasian*, pp. 1–6, 2010.

[22] Policy, "Increasing the use of low-carbon technologies." Department of Energy and Climate Change, 2012.

[23] I. Burdon, "Implementation of a medium-scale CHP scheme," *Power Engineering Journal*, vol. 8, no. 6, pp. 265–271, 1994.

[24] C. Williams, "CHP systems," *Distributed Energy*, pp. 57–59, 2003.

[25] P. Chiradeja, "Benefit of distributed generation: A line loss reduction analysis," in *Transmission and Distribution Conference and Exhibition: Asia and Pacific, 2005 IEEE/PES*, pp. 1–5, 2005.

[26] T. McDermott and R. Dugan, *Distributed generation impact on reliability and power quality indices*. IEEE, 2002.

[27] A. Dyso, G. Burt, S. Galloway, C. Booth, and J. McDonald, "UK distribution system protection issues," *IET Generation, Transmission & Distribution*, vol. 1, no. 4, p. 679, 2007.

[28] N. Mithulananthan, C. Canizares, and J. Reeve, "Tuning, performance and interactions of pss and facts controllers," in *Power Engineering Society Summer Meeting, 2002 IEEE*, vol. 2, pp. 981–987 vol.2, 2002.

[29] E. Haesen, C. Bastiaensen, J. Driesen, and R. Belmans, "A probabilistic formulation of load margins in power systems with stochastic generation," *Power Systems, IEEE Transactions on*, vol. 24, no. 2, pp. 951–958, 2009.

[30] P. M. S. Carvalho, P. F. Correia, and L. Ferreira, "Distributed reactive power generation control for voltage rise mitigation in distribution networks," *Power Systems, IEEE Transactions on*, vol. 23, no. 2, pp. 766–772, 2008.

[31] S. Salman and I. Rida, "Investigating the impact of embedded generation on relay settings of utilities electrical feeders," *Power Delivery, IEEE Transactions on*, vol. 16, no. 2, pp. 246–251, 2001.

[32] A. Girgis and S. Brahma, "Effect of distributed generation on protective device coordination in distribution system," in *Power Engineering, 2001. LESCOPE '01. 2001 Large Engineering Systems Conference on*, pp. 115–119, 2001.

[33] A. Massoud, S. Ahmed, S. Finney, and B. Williams, "Inverter-based versus synchronous-based distributed generation; fault current limitation and protection issues," in *Energy Conversion Congress and Exposition (ECCE), 2010 IEEE*, pp. 58–63, 2010.

[34] H. R. Baghaee, M. Mirsalim, M. J. Sanjari, and G. Gharehpetian, "Effect of type and interconnection of dg units in the fault current level of distribution networks," in *Power Electronics and Motion Control Conference, 2008. EPE-PEMC 2008. 13th*, pp. 313–319, 2008.

[35] T. Aziz, T. Saha, and N. Mithulananthan, "A study of fault ride through with widespread grid integration of distributed generation," in *Electrical Computer Engineering (ICECE), 2012 7th International Conference on*, pp. 603–606, 2012.

[36] S. Salman, "Investigation of the effect of load magnitude and characteristics on the detection of islanding condition," *32nd Universities Power Engineering Conference*, 1997.

[37] M. Redfern, J. I. Barrett, and O. Usta, "A new loss of grid protection based on power measurements," in *Developments in Power System Protection, Sixth International Conference on (Conf. Publ. No. 434)*, pp. 91–94, 1997.

[38] J. Kim and J. Hwang, "Islanding detection method of distributed generation units connected to power distribution system," in *Power System Technology, 2000. Proceedings. PowerCon 2000. International Conference on*, vol. 2, pp. 643–647 vol.2, 2000.

[39] S. Salman, "Detection of embedded generator islanding condition using elliptical trajectory technique," in *Developments in Power System Protection, Sixth International Conference on (Conf. Publ. No. 434)*, pp. 103–106, 1997.

[40] S. Salman, D. King, and G. Weller, "New loss of mains detection algorithm for embedded generation using rate of change of voltage and changes in power factors," in *Developments in Power System Protection, 2001, Seventh International Conference on (IEE)*, pp. 82–85, 2001.

[41] C. Bright, "Corocof: comparison of rate of change of frequency protection. a solution to the detection of loss of mains," in *Developments in Power System Protection, 2001, Seventh International Conference on (IEE)*, pp. 70–73, 2001.

[42] M. Guillot, C. Collombet, P. Bertrand, and B. Gotzig, "Protection of embedded generation connected to a distribution network and loss of mains detection," in *Electricity Distribu-*

tion, 2001. Part 1: Contributions. CIRED. 16th International Conference and Exhibition on (IEE Conf. Publ No. 482), vol. Summaries, pp. 254–254, 2001.

[43] J. Motohashi, T. Ichinose, T. Ishikawa, C. Nakazawa, H. Fukai, and I. Chihara, "Comparison of digital simulation and field test results of islanding detection system for synchronous generators," in *Power Engineering Society 1999 Winter Meeting, IEEE*, vol. 2, pp. 931–936 vol.2, 1999.

[44] P. O'Kane and B. Fox, "Loss of mains detection for embedded generation by system impedance monitoring," in *Developments in Power System Protection, Sixth International Conference on (Conf. Publ. No. 434)*, pp. 95–98, 1997.

[45] H. Zeineldin, T. Abdel-Galil, E. El-Saadany, and M. Salama, "Islanding detection of grid connected distributed generators using tls-esprit," in *Electrical Power Systems Research*, vol. 77, pp. 155–62, 2007.

[46] M. Ropp, K. Aaker, J. Haigh, and N. Sabbah, "Using power line carrier communications to prevent islanding [of pv power systems]," in *Photovoltaic Specialists Conference, 2000. Conference Record of the Twenty-Eighth IEEE*, pp. 1675–1678, 2000.

[47] M. Ropp, M. Begovic, and A. Rohatgi, "Analysis and performance assessment of the active frequency drift method of islanding prevention," *Energy Conversion, IEEE Transactions on*, vol. 14, no. 3, pp. 810–816, 1999.

[48] H. Zeineldin, E. El-Saadany, and M. Salama, "Islanding detection of inverter-based distributed generation," *Generation, Transmission and Distribution, IEE Proceedings-*, vol. 153, no. 6, pp. 644–652, 2006.

[49] BSi, *BS EN 50160:2010 - Voltage characteristics of electricity supplied by public electricity networks.* BSI, 2010.

[50] F. Katiraei, C. Abbey, S. Tang, and M. Gauthier, *Planned islanding on rural feeders, utility perspective.* IEEE, July 2008.

[51] T. Ostrem, W. Sulkowski, L. Norum, and C. Wang, "Grid connected photovoltaic (pv) inverter with robust phase-locked loop (pll)," in *Transmission Distribution Conference and Exposition: Latin America, 2006. TDC '06. IEEE/PES*, pp. 1–7, 2006.

[52] S. D. G. Jayasinghe, D. Vilathgamuwa, and U. Madawala, "Connecting two wind turbine generators to the grid using only one three level npc inverter," in *IECON 2010 - 36th Annual Conference on IEEE Industrial Electronics Society*, pp. 3263–3268, 2010.

[53] S. D. G. Jayasinghe, D. Vilathgamuwa, and U. Madawala, "Dual inverter based battery energy storage system for grid connected photovoltaic systems," in *IECON 2010 - 36th Annual Conference on IEEE Industrial Electronics Society*, pp. 3275–3280, 2010.

[54] H. Karegar and A. Shabani, "Effects of inverter modulation index on the stability of grid connected micro-turbines," in *Power and Energy Conference, 2008. PECon 2008. IEEE 2nd International*, pp. 1623–1627, 2008.

[55] M. Sough, D. Depernet, F. Dubas, G. Gaultier, B. Boualem, and C. Espanet, "High frequency pmsm and inverter losses analysis-application to flywheel system on real cycle operation," in *Vehicle Power and Propulsion Conference (VPPC), 2011 IEEE*, pp. 1–5, 2011.

[56] R. Lasseter, *MicroGrids*. IEEE, 2002.

[57] Centre for Alternative Technology, *Zero Carbon Britain 2030*. CAT Publications, a division of the Centre for Alternative Technology Charity Limited, first edit ed., 2010.

[58] D. Cornforth, T. Moore, and S. Sayeef, "Challenges and opportunities for inverters in microgrids," in *IECON 2011 - 37th Annual Conference on IEEE Industrial Electronics Society*, pp. 3111–3116, 2011.

[59] S. Chowdhury, S.P. Chowdhury, and P. Crossley, *Microgrids and Active Distribution Networks*. The Institute of Engineering and Technology, 2009.

[60] R. Digra and R. Pandey, "Multi-agent control coordination of microgrid," in *Engineering and Systems (SCES), 2013 Students Conference on*, pp. 1–5, 2013.

[61] I. Hiskens and J. Milanovic, "Load modelling in studies of power system damping," *IEEE Transactions on Power Systems*, vol. 10, no. 4, pp. 1781–1788, 1995.

[62] M. Kent, W. Schmus, F. McCrackin, and L. Wheeler, "Dynamic Modeling of Loads in Stability Studies," *IEEE Transactions on Power Apparatus and Systems*, vol. PAS-88, pp. 756–763, May 1969.

[63] E. Kyriakides and R. G. Farmer, "Modeling of Damping for Power System Stability Analysis," *Electric Power Components and Systems*, vol. 32, pp. 827–837, Aug. 2004.

[64] K. Qian, C. Zhou, M. Allan, and Y. Yuan, *Load modelling in distributed generation planning*. IEEE, Apr. 2009.

[65] F. J. Meyer and K. Y. Lee, "Improved Dynamic Load Model for Power System Stability Studies," *IEEE Power Engineering Review*, vol. PER-2, pp. 49–50, Sept. 1982.

[66] P. Kundur, J. Paserba, V. Ajjarapu, G. Andersson, A. Bose, C. Canizares, N. Hatziargyriou, D. Hill, A. Stankovic, C. Taylor, T. Van Cutsem, and V. Vittal, "Definition and classification of power system stability ieee/cigre joint task force on stability terms and definitions," *Power Systems, IEEE Transactions on*, vol. 19, no. 3, pp. 1387–1401, 2004.

[67] J. Machowski, J. Bialek, and J. Bumby, *Power System Dynamics: Stability and Control*. Wiley, 2011.

[68] P. Kundur, N. Balu, and M. Lauby, *Power system stability and control*. EPRI power system engineering series, McGraw-Hill, 1994.

[69] P. Anderson, A. Fouad, I. of Electrical, and E. Engineers, *Power system control and stability*. IEEE Press power engineering series, IEEE Press, 2003.

[70] J. Machowski, J. W. Bialek, and J. R. Bumby, *Power System Dymanics: Stability and Control*. John Wiley and Sons, second edi ed., 2008.

[71] O. E. Dictionary, "Oxford: Oxford university press, 2013," *Oed. com*, 2013.

[72] E. W. Weisstein, "Eigenvector." From MathWorld–A Wolfram Web Resource, 2014.

[73] S. Leeb, J. Kirtley, and G. C. Verghese, "Recognition of dynamic patterns in dc-dc switching converters," *Power Electronics, IEEE Transactions on*, vol. 6, no. 2, pp. 296–302, 1991.

[74] R. Majumder, "Some aspects of stability in microgrids," *Power Systems, IEEE Transactions on*, vol. 28, no. 3, pp. 3243–3252, 2013.

[75] N. Pogaku, M. Prodanovic, and T. Green, "Inverter-based microgrids: Small-signal modelling and testing," in *Power Electronics, Machines and Drives, 2006. The 3rd IET International Conference on*, pp. 499–504, 2006.

[76] Y. Zhang, Z. Jiang, and X. Yu, "Small-signal modeling and analysis of parallel-connected voltage source inverters," in *Power Electronics and Motion Control Conference, 2009. IPEMC '09. IEEE 6th International*, pp. 377–383, 2009.

[77] C. Rowey, T. Summers, R. Betz, and D. Cornforth, "Small signal stability analysis of arctan power frequency droop," in *Power Electronics and Drive Systems (PEDS), 2011 IEEE Ninth International Conference on*, pp. 787–792, 2011.

[78] Y. A. R. I. Mohamed and E. El-Saadany, "Adaptive decentralized droop controller to preserve power sharing stability of paralleled inverters in distributed generation microgrids," *Power Electronics, IEEE Transactions on*, vol. 23, no. 6, pp. 2806–2816, 2008.

[79] J. Guerrero, J. Vasquez, J. Matas, M. Castilla, and L. de Vicuna, "Control strategy for flexible microgrid based on parallel line-interactive ups systems," *Industrial Electronics, IEEE Transactions on*, vol. 56, no. 3, pp. 726–736, 2009.

[80] G. Diaz, C. Gonzalez-Moran, J. Gomez-Aleixandre, and A. Diez, "Complex-valued state matrices for simple representation of large autonomous microgrids supplied by and generation," *Power Systems, IEEE Transactions on*, vol. 24, no. 4, pp. 1720–1730, 2009.

[81] G. Venkataramanan and M. Illindala, "Small signal dynamics of inverter interfaced distributed generation in a chain-microgrid," in *Power Engineering Society General Meeting, 2007. IEEE*, pp. 1–6, 2007.

[82] J. Ma, X. Wang, and X. Lan, "Small-signal stability analysis of microgrid based on perturbation theory," in *Power and Energy Engineering Conference (APPEEC), 2012 Asia-Pacific*, pp. 1–4, 2012.

[83] E. Barklund, N. Pogaku, M. Prodanovic, C. Hernandez-Aramburo, and T. Green, "Energy management system with stability constraints for stand-alone autonomous microgrid," in *System of Systems Engineering, 2007. SoSE '07. IEEE International Conference on*, pp. 1–6, 2007.

[84] E. Barklund, N. Pogaku, M. Prodanovic, C. Hernandez-Aramburo, and T. Green, "Energy management in autonomous microgrid using stability-constrained droop control of inverters," *Power Electronics, IEEE Transactions on*, vol. 23, no. 5, pp. 2346–2352, 2008.

[85] M. Kohansal, G. Gharehpetian, M. Rahmatian, M. Abedi, and M. J. Sanjari, "The effect of load condition on stability in isolated microgrids," in *Renewable Energy and Distributed Generation (ICREDG), 2012 Second Iranian Conference on*, pp. 28–32, 2012.

[86] D. Ariyasinghe and D. Vilathgamuwa, "Stability analysis of microgrids with constant power loads," in *Sustainable Energy Technologies, 2008. ICSET 2008. IEEE International Conference on*, pp. 279–284, 2008.

[87] N. Jayawarna, X. Wu, Y. Zhang, N. Jenkins, and M. Barnes, "Stability of a microgrid," in *Power Electronics, Machines and Drives, 2006. The 3rd IET International Conference on*, pp. 316–320, 2006.

[88] X. Chen, W. Pei, and X. Tang, "Transient stability analyses of micro-grids with multiple distributed generations," in *Power System Technology (POWERCON), 2010 International Conference on*, pp. 1–8, 2010.

[89] F. Andrade, J. Cusido, and L. Romeral, "Transient stability analysis of inverter-interfaced distributed generators in a microgrid system," in *Power Electronics and Applications (EPE 2011), Proceedings of the 2011-14th European Conference on*, pp. 1–10, 2011.

[90] R. Park, "Two-reaction theory of synchronous machines generalized method of analysis-part I," *American Institute of Electrical Engineers, Transactions of the*, vol. 48, no. 3, pp. 716–727, 1929.

[91] N. Kroutikova, C. Hernandez-Aramburo, and T. Green, "State-space model of grid-connected inverters under current control mode," *Electric Power Applications, IET*, vol. 1, pp. 329 –338, may 2007.

[92] L. Yaohua, D. Xiaoli, M. Fanrong, and Y. Jiang, "High performance repetitive controller for eliminating periodic disturbance of inverter with unbalance load," in *Power and Energy Engineering Conference (APPEEC), 2012 Asia-Pacific*, pp. 1 –4, march 2012.

[93] M. Brucoli, T. Green, and J. McDonald, "Modelling and analysis of fault behaviour of inverter microgrids to aid future fault detection," in *System of Systems Engineering, 2007. SoSE '07. IEEE International Conference on*, pp. 1 –6, april 2007.

[94] C. Plet and T. Green, "A method of voltage limiting and distortion avoidance for islanded inverter-fed networks under fault," in *Power Electronics and Applications (EPE 2011), Proceedings of the 2011-14th European Conference on*, pp. 1 –8, 30 2011-sept. 1 2011.

[95] G. Zeng and T. W. Rasmussen, "Design of current-controller with pr-regulator for lcl-filter based grid-connected converter," in *Power Electronics for Distributed Generation Systems (PEDG), 2010 2nd IEEE International Symposium on*, pp. 490 –494, june 2010.

[96] R. Teodorescu, F. Blaabjerg, M. Liserre, and P. Loh, "Proportional-resonant controllers and filters for grid-connected voltage-source converters," *Electric Power Applications, IEE Proceedings* -, vol. 153, pp. 750 –762, september 2006.

[97] A. Bhalla, S. Shekhawat, J. Gladish, J. Yedinak, and G. Dolny, "Igbt behavior during desat detection and short circuit fault protection," in *Power Semiconductor Devices and ICs, 1998. ISPSD 98. Proceedings of the 10th International Symposium on*, pp. 245–248, 1998.

[98] H. Wang, X. Yue, X. Pei, and Y. Kang, "A current-limiting protection strategy for the combined three-phase inverter," in *Electrical Machines and Systems, 2008. ICEMS 2008. International Conference on*, pp. 1267–1271, 2008.

[99] X. Yu and Z. Jiang, "Dynamic current limiting control of voltage source inverters," in *Electric Machines and Drives Conference, 2009. IEMDC '09. IEEE International*, pp. 1664–1668, 2009.

[100] F. Peng, Y. W. Li, and L. Tolbert, "Control and protection of power electronics interfaced distributed generation systems in a customer-driven microgrid," in *Power Energy Society General Meeting, 2009. PES '09. IEEE*, pp. 1–8, 2009.

[101] H. Wang, X. Yue, X. Pei, and Y. Kang, "Improved software current-limiting protection strategy for starting the high-power motor," in *Electrical Machines and Systems, 2009. ICEMS 2009. International Conference on*, pp. 1–4, 2009.

[102] M. Dewadasa, R. Majumder, A. Ghosh, and G. Ledwich, "Control and protection of a microgrid with converter interfaced micro sources," in *Power Systems, 2009. ICPS '09. International Conference on*, pp. 1–6, 2009.

[103] F. Salha, F. Colas, and X. Guillaud, "Virtual resistance principle for the overcurrent protection of pwm voltage source inverter," in *Innovative Smart Grid Technologies Conference Europe (ISGT Europe), 2010 IEEE PES*, pp. 1–6, 2010.

[104] M. Brucoli and T. C. Green, "Fault behaviour in islanded microgrids," in *19th International Conference on Electricity Distribution*, pp. 1–4, 2007.

[105] M. Castilla, J. Miret, A. Camacho, J. Matas, and L. Garcia de Vicuna, "Voltage support control strategies for static synchronous compensators under unbalanced voltage sags," *Industrial Electronics, IEEE Transactions on*, vol. 61, no. 2, pp. 808–820, 2014.

[106] P. Rodriguez, G. Medeiros, A. Luna, M. Cavalcanti, and R. Teodorescu, "Safe current injection strategies for a statcom under asymmetrical grid faults," in *Energy Conversion Congress and Exposition (ECCE), 2010 IEEE*, pp. 3929–3935, 2010.

[107] IEEE, "Load representation for dynamic performance analysis (of power systems)," *IEEE Transactions on Power Systems*, vol. 8, pp. 472–482, May 1993.

[108] IEEE, "Standard load models for power flow and dynamic performance simulation," *IEEE Transactions on Power Systems*, vol. 10, no. 3, pp. 1302–1313, 1995.

[109] J. Acero, J. Burdio, L. Barragan, and R. Alonso, *A model of the equivalent impedance of the coupled winding-load system for a domestic induction heating application.* IEEE, June 2007.

[110] D. F. Shankle, C. M. Murphy, R. W. Long, and E. L. Harder, "Transient-Stability Studies - I Synchronous and Induction Machines," *Transactions of the American Institute of Electrical Engineers. Part III: Power Apparatus and Systems*, vol. 73, pp. 1563–1580, Jan. 1954.

[111] E. B. Makram, V. O. Zambrano, R. G. Harley, and J. C. Balda, "Three-Phase Modeling for Transient Stability of Large Scale Unbalanced Distribution Systems," *IEEE Power Engineering Review*, vol. 9, no. 5, pp. 47–47, 1989.

[112] G. T. Heydt and W. M. Grady, "Distributed Rectifier Loads in Electric Power Systems," *IEEE Power Engineering Review*, vol. PER-4, pp. 57–58, Sept. 1984.

[113] Q. Ai, D. Gu, and C. Chen, "New Load Modeling Approaches Based on Field Tests for Fast Transient Stability Calculations," *IEEE Transactions on Power Systems*, vol. 21, pp. 1864–1873, Nov. 2006.

[114] V. Boscaino, G. Capponi, P. Livreri, and F. Marino, *Measurement-based load modelling for power supply system design.* IEEE, Aug. 2008.

[115] P. Ju, F. Wu, Z.-Y. Shao, X.-P. Zhang, H.-J. Fu, P.-F. Zhang, N.-Q. He, and J.-D. Han, "Composite load models based on field measurements and their applications in dynamic analysis," *IET Generation, Transmission & Distribution*, vol. 1, no. 5, p. 724, 2007.

[116] Z. Dong, *Uncertainty analysis of load models in small signal stability.* IEEE, Apr. 2009.

[117] D.-Q. Ma and P. Ju, "A novel approach to dynamic load modelling," *Power Systems, IEEE Transactions on*, vol. 4, no. 2, pp. 396–402, 1989.

[118] O. Abdalla, M. Bahgat, A. Serag, and M. El-Sharkawi, "Dynamic load modelling and aggregation in power system simulation studies," *Power System Conference, 2008. MEPCON 2008. 12th International Middle-East*, pp. 270–276, 2008.

[119] N. Bottrell, M. Prodanovic, and T. Green, "Analysed small signal state-space model of an active rectifier," in *Universities Power Engineering Conference (UPEC), 2010 45th International*, pp. 1–6, 2010.

[120] N. Bottrell and T. Green, "Modeling microgrids with active loads," in *Control and Modeling for Power Electronics (COMPEL), 2012 IEEE 13th Workshop on*, pp. 1–8, 2012.

[121] N. Bottrell, M. Prodanovic, and T. Green, "Dynamic stability of a microgrid with an active load," *Power Electronics, IEEE Transactions on*, vol. 28, no. 11, pp. 5107–5119, 2013.

[122] N. Bottrell and T. Green, "Comparison of current limiting strategies during fault ride-through of inverters to prevent latch-up and wind-up," *Power Electronics, IEEE Transactions on*, vol. PP, no. 99, pp. 1–1, 2013.

[123] N. Bottrell and T. Green, "An impedance-based method for the detection of over-load and network faults in inverter interfaced distributed generation," in *Power Electronics and Applications, 2012 European Conference on*, pp. 1–1, 2013.